PHOTODESORPTION AND HIGHER-ORDER ASSEMBLIES OF POTASSIUM POLYTITANATE FOR WATER TREATMENT

Submitted by

Mohammad Shahid

A thesis submitted in fulfilment of the requirements for the degree of

Doctor of Philosophy

University of Technology Sydney
FACULTY OF ENGINEERING

2015

Certificate of Authorship

I certify that the work in this thesis has not previously been submitted for a degree nor has it been submitted as part of requirements for a degree except as fully acknowledged within the text.

I also certify that the thesis has been written by me. Any help that I have received in my research work and the preparation of the thesis itself has been acknowledged. In addition, I certify that all information sources and literature used are indicated in the thesis.

Production Note:
Signature removed prior to publication.

Signature of Student:

Date: 07/07/2015

Acknowledgments

Foremost, I would like to express my sincere gratitude to my principal supervisor A/Prof. Ho Kyong Shon for his continuous support, encouragement and guidance throughout my journey at UTS. I will always remember your invaluable mentorship which helped me to achieve my goals. I would also like to thank my co-supervisor Dr Andrew McDonagh for his advice, motivation and immense knowledge. His wisdom and guidance helped me to deal with several issues during my doctoral candidature.

Moreover, I would like to acknowledge Dr Ibrahim El Saliby and Dr Leonard D. Tijing for their help in the design, implementation and revision of this research thesis. Their kind support helped me bring this research to its end. I would also like to express my appreciation to faculty members Prof. Saravanmuthu Vigneswaran, Prof. Huu Hao Ngo, A/Prof Jaya Khandaswamy and Dr Robert McLaughlan for their support and engagement in the CTWW.

I am also grateful to UTS research fellows Dr Sherub Phuntsho, Dr Tien Than, and Dr Ghausul Hussain for their assistance concerning several issues. Special thanks must go to all my colleagues and beloved friends, Johir, Laura, Tahir, Aaron, Soleyman, Fouzy for their friendship and help during the last four years.

Lastly, I also would like to thank UTS-IRS and APA-LP for providing scholarship and financial support that made for the completion of my thesis possible.

List of Abbreviations

AFM	:	Atomic Force Microscopy
AOPs	:	Advanced Oxidation Processes
BET	:	Brunauer, Emmet and Teller
BJH	:	Barret Joyner Halender
CB	:	Conduction Band
CNTs	:	Carbon Nanotubes
CV	:	Crystal Violet
DO	:	Dissolved Oxygen
DOC	:	Dissolved Organic Carbon
DOM	:	Dissolved Organic Matter
EDS	:	Energy Dispersive X-ray Spectroscopy
EDX	:	Energy Dispersive X-ray
FTIR	:	Fourier Transform Infrared Spectroscopy
HDTMA	:	Hexadecyltrimethylammonium
HMW	:	High Molecular Weight
HOC	:	Hydrophilic Organic Carbon
HP-SEC	:	High Performance Size Exclusion Chromatography
LC-OCD	:	Liquid Chromatography - Organic Carbon Detection
LMW	:	Low Molecular Weight
MB	:	Methylene Blue
PTTF	:	Polytetrafluoro Ethylene
PZC	:	Point of Zero Charge
SEM	:	Scanning Electron Microscope

STM	:	Scanning Tunnelling Microscopy
SWW	:	Synthetic Wastewater
TEM	:	Transmission Electron Microscope
TOC	:	Total Organic Carbon
UV	:	Ultra Violet
VB	:	Valance Band
XRD	:	X-ray diffraction

Table of Contents

List of Figures

List of Tables

Abstract

Nanotechnology has great potential in advancing water and wastewater treatment to improve treatment efficiency. Several nanotechnology approaches to water purification are currently being investigated and some already are in use. Photocatalysis is a new advanced oxidation process based on the irradiation of semiconductor materials, normally TiO_2, with UV light and has been demonstrated to be one of the "green" and more effective strategies for environmental remediation. Recently, photo-induced desorption of dissolved organic compounds in aqueous media during photocatalysis provides an exciting opportunity in wastewater treatment which significantly facilitates the regeneration of the adsorbent with low energy consumption. The scope of this research is to elucidate the photodesorption of organic matter from TiO_2 under UV irradiation. In addition, this research also includes synthesis of titania-based photocatalytic adsorbent nanomaterials produced by self-assembly for water purification. For this purpose, potassium titanate was synthesised using Degussa P25 as a titanium precursor in the presence of hydrogen peroxide as an oxidising agent and potassium hydroxide in alkaline solution via alkaline hydrothermal condition. As a part of nanotechnology, the development of the photocatalytic adsorbent nanofibre is of great importance to establish adsorption and photocatalytic water treatment an attractive and cost-effective process.

Photo-induced desorption of organic compounds from TiO_2 particles in aqueous media during photocatalysis has promising applications in water treatment. Photodesorption is a relatively fast phenomenon that facilitates the regeneration of photocatalysts with low energy consumption while concentrating the waste products in an energy and water efficient process. It has been proposed that this transport phenomenon involves a

significantly reduced affinity between the photocatalyst and pollutants upon UV illumination, and leads to the rapid detachment/decomposition of adsorbed pollutants.

Initially, organic matters were allowed to adsorb on the surface of the photocatalyst (Degussa P25) until adsorption equilibrium was achieved. When adsorption equilibrium had been reached, it was observed that photodesorption was observed shortly with UV-light illumination of TiO_2 before the bulk photocatalytic oxidation takes place. The effects of specific experimental conditions (pH, photocatalyst loading, organic loading, UV light irradiation, flow rate, specific organic compounds) on this phenomenon were also examined. The pH of the solution was found to influence both the adsorption and desorption percentages, thus revealing the role of particle charge on this phenomenon. Additionally, a 1 g/L loading of photocatalyst, 150 ml/min flow rate, 24 W light intensity showed an optimum photodesorption rate using a single strength synthetic wastewater at pH 7.

Photodesorption was observed only for sodium lauryl sulphate (50%), sodium lignin sulphonate (43.47%), beef extract (20.35%) and tannic acid (10.5%) indicating that photodesorption is specific to some organic compounds but not to all. Using liquid chromatography-organic carbon detection, untreated beef extract and sodium lignin sulphonate contained significant amounts of humic substances (~1,000 g/mol), which decreased in concentration after dark phase adsorption. A significant increase in low molecular weight (<350 g/mol) concentrations was observed after photodesorption. UV-treated sodium lauryl sulphate photodesorbed to give both higher molecular weight (HMW) and lower molecular weight (LMW) organics. Thus, the HMW fractions of organic compounds decomposed into smaller compounds after UV irradiation, which

subsequently desorbed from the TiO_2 surface. However, untreated tannic acid contained a larger proportion of LMW acids, which showed a high adsorption affinity to TiO_2 during adsorption and poorly desorbed upon irradiation.

Apart from an investigation on photodesorption, this research presents a synthesis of potassium titanate nanostructures by hydrothermal treatment of TiO_2 (P25) in KOH and H_2O_2. As-produced powders were characterised by scanning electron microscopy, energy-dispersive X-ray spectroscopy, transmission electron microscopy, X-ray diffraction, and nitrogen adsorption-desorption methods. Longitudinally-oriented-wire-like structures up to several micrometres in length and diameters ranging from 10 to 30 nm were obtained. BET surface area analysis indicates macroporous sized titanate with had 5-6 times larger specific surface area (235.81-330.10 m^2/g) than the precursor P25. TEM images reflected belt-like structures of an isolated fibre with the presence of lattice fringes, which indicated a crystalline structure aligned with orientation of their basal nanobelts. The XRD spectra of potassium titanate were attributed to the transfer of a portion of anatase into mixed species of potassium titanate ($K_2Ti_8O_{17}$, $K_2Ti_6O_{13}$, K_2TiO_3 and $K_3Ti_8O_{17}$). They were recovered by calcining the specimens suggesting the possible existence of crystallisation sites under hydrothermal treatment in aqueous solution of H_2O_2 and KOH. Larger size fibrous nanowires resulting from the hydrothermal treatment demonstrated high affinity in adsorbing crystal violet (CV), which was mainly due to their high surface area. The photocatalytic bleaching of CV solution revealed that the wires are photoactive under UV light irradiation. Macroporous nanowires are considered to be effective adsorbents of CV, capable of its photocatalytic degradation, and they can be easily separated from the solution by settling.

Solar photocatalytic degradation of organic water pollutants can be used to destroy toxic organic pollutants in water. Hence, potassium titanate nanofibres synthesized by an aqueous peroxide route at high pH were examined as photocatalysts for the photodegradation of methylene blue (MB) using a solar simulator. The results show that potassium polytitanate nanofibres were effective adsorbents of MB and also facilitated its photocatalytic degradation. Sulphate ion evolution during photocatalysis confirms some mineralisation occurred and hence photo-oxidative degradation of MB. The optimum operational conditions for the photocatalytic degradation of MB were found at 0.05 g/L of photocatalyst, 10 mg/L MB and pH 7. The stability of a photocatalyst specimen was also studied for 3 degradation cycles using adsorption/photocatalysis model.

Potassium polytitanate nanofibres prepared via the hydrothermal method were investigated for their possible application in removing toxic metals from aqueous solution. Particular attention was paid to employing the titanate as novel effective adsorbents for the removal of Pb(II). Batch adsorption experiments demonstrated that the adsorption was influenced by various conditions such as solution pH, adsorbent dosage and initial Pb(II) concentration. The results showed that the adsorption rate was faster in the first 5 min and equilibrium was achieved after 180 min. The maximum amount of adsorption was detected at pH 5. Potassium titanate showed much higher adsorption capacity compared to P25. The kinetic studies indicated that the adsorption of Pb(II) onto titanate best fit the pseudo-second-order kinetic model. FTIR spectra revealed that the hydroxyl groups in titanate were responsible for Pb(II) adsorption. It was concluded that ion exchange and oxygen bonding may be the principal mechanisms

for the adsorption of Pb(II). The adsorption-desorption results demonstrated that the titanate could be readily regenerated after adsorption. Therefore the titanate exhibited great potential for removing of Pb(II) from wastewater.

List of publications included in the Thesis

Chapter 4

El Saliby, I., **Shahid, M.**, McDonagh, A., Shon, H.K. & Kim, J.-H. 2012, 'Photodesorption of organic matter from titanium dioxide particles in aqueous media', *Journal of Industrial and Engineering Chemistry*, vol. 18, no. 5, pp. 1774-80.

Shahid, M., Saliby, I.E., McDonagh, A., Kim, J.-H. & Shon, H.K. 2014, 'Photodesorption of specific organic compounds from titanium dioxide particles in aqueous media', *Desalination and Water Treatment*, vol. 52, no. 4-6, pp. 867-72.

Chapter 5

Shahid, M., El Saliby, I., McDonagh, A., Tijing, L.D., Kim, J.-H. & Shon, H.K. 2014, 'Synthesis and characterisation of potassium polytitanate for photocatalytic degradation of crystal violet', *Journal of Environmental Science* vol. 26, no. 11, pp. 2348-54*)*.

Chapter 6

Shahid, M., El Saliby, I., McDonagh, A., Tijing, L.D., Kim, J.-H. & Shon, H.K. 2014, ' **‘**Adsorption and photocatalytic degradation of methylene blue using potassium polytitanate and solar simulator’', **(*Submitted to Journal of Nanoscience and Nanotechnology).***

Chapter 7

Shahid, M., El Saliby, I., McDonagh, A., Tijing, L.D., Kim, J.-H. & Shon, H.K. 2014, ‘Adsorption behavior of Pb(II) onto Potassium Polytitanate Nanofibre', ***(Abstract submitted to International Conference on Nano Science and Nano Technology 2014).***

Other publications during the PhD candidature*

Kim, J.B., Lee, K.W., Park, S.M., Shon, H.K., **Shahid, M.**, Saliby, I.E., Lee, W.E., Kim, G.-J. & Kim, J.-H. 2013, 'Preparation of Iron-Doped Titania from Flocculated Sludge with Iron-Titanium Composite Coagulant', *Journal of Nanoscience and Nanotechnology*, vol. 13, no. 6, pp. 4106-9.

Shahid, M., McDonagh, A., Kim, J.H. & Shon, H.K. 2014, 'Magnetised titanium dioxide (TiO_2) for water purification: preparation, characterisation and application', *Desalination and Water Treatment*, pp. 1-24.

Park, S.M., Chekli, L., Kim, J.B., **Shahid, M.**, Shon, H.K., Kim, P.S., Lee, W.-S., Lee, W.E. & Kim, J.-H. 2014, 'NOx removal of mortar mixed with titania produced from Ti-salt flocculated sludge', *Journal of Industrial and Engineering Chemistry*, vol. 20, no. 5, pp. 3851-6.

Shahid, M., El Saliby, I., McDonagh, A., Tijing, L.D., Kim, J.-H. & Shon, H.K. 2014, ' Synthesis and Characterisation of Silica-modified Titania for Photocatalytic Decolouration of Crystal Violet', **(Accepted for publication in *Journal of Nanoscience and Nanotechnology*).**

*(not related to the Thesis)

Conference papers and presentations

El Saliby, I., **Shahid, M.**, McDonagh, A., Shon, H.K. & Kim, J.-H., 'Photodesorption of organic matter from titanium dioxide particles in aqueous media', Presented at the 4th International Conference on the "Challenges in Environmental Science and Engineering" (CESE-2011), 25-30 September 2011, Tainan City, Taiwan

Shahid, M., El Saliby, I., McDonagh, A., Kim, J.-H. & Shon, 'Synthesis and Characterisation of Silica-modified Titania for Photocatalytic Decolouration of Crystal Violet', Presented at the 5th International Conference on the "Challenges in Environmental Science and Engineering" (CESE-2012), 9-13 September 2012, Melbourne, Australia

Shahid, M., Saliby, I.E., McDonagh, A., Kim, J.-H. & Shon, H.K., 'Photodesorption of specific organic compounds from titanium dioxide particles in aqueous media', Presented at the 5th International Conference on the "Challenges in Environmental Science and Engineering" (CESE-2012), 9—13 September 2012, Melbourne, Australia

Shahid, M., El Saliby, I., McDonagh, A., Kim, J.-H. & Shon, H.K., 'Synthesis and Characterisation of Silica-modified Titania for Photocatalytic Decolouration of Crystal Violet', Presented at the 11th International conference on Nano Science and Nano Technology (ICNST 2013), 7-8 November 2013, Chosun University, Gwangju, Korea

Shahid, M., McDonagh, A., Kim, J.H. & Shon, H.K. 2014, 'Magnetised titanium dioxide (TiO2) for water purification: preparation, characterisation and application', Presented at the 6th International Conference on the "Challenges in Environmental Science and Engineering" (CESE-2013), 29 October-2 November 2013, Daegu, Korea

U T S

University of Technology Sydney
FACULTY OF ENGINEERING

Chapter 1: Introduction

1.1 Nanotechnology for water purification

Nanotechnology is a collective term, referring to a wide range of tools, techniques and applications that involve specific manipulation of particles in terms of qualities and structures at nanoscale level (1–100 nm). Particles of this size have some unique physicochemical and surface properties compared to the volume quantities of the materials; also they often exhibit novel uses. Due to their unique activity involving recalcitrant contaminants many nanomaterials are being actively researched and developed. Hence, it is expected that research on nanoscale level will contribute to solutions for several major global problems. These includes, for example, ensuring a safe drinking water supply for a growing world population, improving agricultural practices and output, enhancing medical science and the energy sector.

Nanotechnology has great potential in advancing water and wastewater treatment to improve treatment efficiency. It is also important to augment water supplies through safe use of unconventional water sources (Qu et al., 2013). Advances in nanoscale science and engineering suggest that many current problems involving water quality could be resolved or greatly enhanced using nanosorbents, nanocatalysts, bioactive nanoparticles, nanostructured catalytic membranes and nanoparticle enriched filtration resulting from the development of nanotechnology. Innovations in the development of novel technologies to desalinate water are among the most exciting and promising. Apart from this, nanotechnology-derived products that reduce the concentrations of toxic compounds to sub-ppb levels can assist in attaining satisfactory water quality standards and health advisories (Savage et al., 2005).

Several nanotechnology approaches to water purification are currently being investigated and some already are in use. Water treatment devices that incorporate nanoscale materials are already available, such as carbon nanotubes and alumina fibres for nanofiltration. It also utilizes the existence of nanoscopic pores in zeolite filtration membranes, as well as nanocatalysts and magnetic nanoparticles. Nanosensors, such as those based on titanium oxide nanowires or palladium nanoparticles are used for analytical detection of contaminants in water samples.

The researchers point out that several fundamental aspects of nanotechnology have raised concerns among the general public and activist groups. They concede that the risks associated with nanomaterials may not be the same as those associated with the bulk versions of the same materials. This is because the much greater surface area to volume ratio of nanoparticles can make them more reactive than bulk materials and lead to so far unrecognized and untested interactions with biological surfaces. Water purification based on nanotechnology has not yet led to any human health or environmental problems but the team echoes the concerns of others that further research into the biological interactions of nanoparticles should be carried out.

1.2 Photocatalysis over Titanium dioxide

Photocatalysis is a new advanced oxidation process based on the irradiation of semiconductor materials, normally TiO_2, with UV light having a wavelength smaller than 390 nm (Lasa et al., 2005). Photocatalytic technology has been demonstrated to be one of the “green” and more effective strategies for environmental remediation. This sort of technology is on the verge of creating a new market. Both the technological and economic importance of photocatalysis has increased considerably over the past decade.

Improvements in performance have been strongly correlated to advances in nanotechnology. For example the introduction of nanoparticulate photocatalysts has greatly enhanced the catalytic efficiency of specific materials. However, owing to low photocatalytic efficiency, the environmental applications of various photocatalytic technologies are still very limited. Thus, more investigations are required from the viewpoint of practical use and consequently, extensive research continues to further optimize this technology and to widen the spectrum of potential applications.

Since the discovery of photocatalytic water splitting on titanium dioxide electrodes by Fujishima and Honda (1972), interest in applying TiO_2 semiconductor as a photocatalyst has grown significantly. Most research emphasizes semiconductor photocatalysis for water/air purification (Fujishima et al., 2000; Herrmann 1999; Hoffmann et al., 1995; Lee et al., 2013), but very few of them are related to photocatalytic hydrogen production (Ashokkumar 1998). Both photocatalytic water/air purification and photocatalytic hydrogen production require essential photon generation of hole/electron pairs. However, their utilization of holes/electrons as well as system processing is different. In photocatalytic water/air purification, valence band holes are the key elements that induce decomposition of contaminants.

When the absorbed UV photons have energy that is greater than the energy gap of the semiconductor, hole/electron pairs are formed, which can either recombine or migrate to the semiconductor surface and then react with chemical species adsorbed on the surface (Zaviska et al., 2009). The photogenerated holes are strong oxidants, and the photogenerated electrons are reducing enough to yield superoxide from dioxygen. The photogenerated holes are able to either directly oxidise the absorbed pollutants or

oxidise the hydroxyl groups located at the TiO_2 surface to form OH radicals, whose redox potential is only slightly decreased (Fujishima et al., 2000). Consequently, the degradation of pollutants contained in contaminated waters can take place either: firstly, directly at the semiconductor surface or secondly, indirectly through interactions with the OH radicals. Indirect oxidation by the radicals is currently the most favoured degradation pathway.

TiO_2 has proved itself to be the most efficient semiconductor available for photocatalysis. Due to its physical and chemical stability, cheaper cost and resistance to corrosion, TiO_2 is the most commonly used photocatalyst for environmental applications. TiO_2 is very easy to produce, active from the photocatalysis standpoint, and it has an energy gap comparable to that of solar photons (Pignatello 1992; Zaviska et al., 2009). Moreover, the photogenerated holes are strong oxidants, and the photogenerated electrons for the remediation of ground water and wastewater have increased. This is particularly due to their potential to degrade a wide range of organic and inorganic compounds.

1.3 Photodesorption of organic matter

A process in which atomic/molecular species residing on the surface of a solid leave the surface and enter the surrounding media is known as desorption. This process is opposite of the sorption which occurs in a system at sorption equilibrium either in gas or liquid phase (Henderson 2013; Shen et al., 2011) In photon stimulated desorption, species residing on a surface are made to desorb by incident electrons or photons. Photodesorption of organic and inorganic compounds from semiconductors, carbon nanotubes and TiO_2 surfaces is well established at gaseous state as reported in literatures

(Chen et al., 2001; Kornblit et al., 1984; Lichtman et al., 1976; Shapira et al., 1976). Recently, photo-induced desorption of dissolved organic compounds in aqueous media during photocatalysis has been reported (Ambrus et al., 2008; Bjorklund et al., 2001; El Saliby et al., 2012; Erdei et al., 2008; Shahid, Saliby, et al., 2014; Shon, Vigneswaran, Ngo & Kim 2005). The phenomenon is observed after the UV illumination of the water suspension for a short period of time. This process provides an exciting opportunity in wastewater treatment which significantly facilitates the regeneration of the adsorbent with low energy consumption.

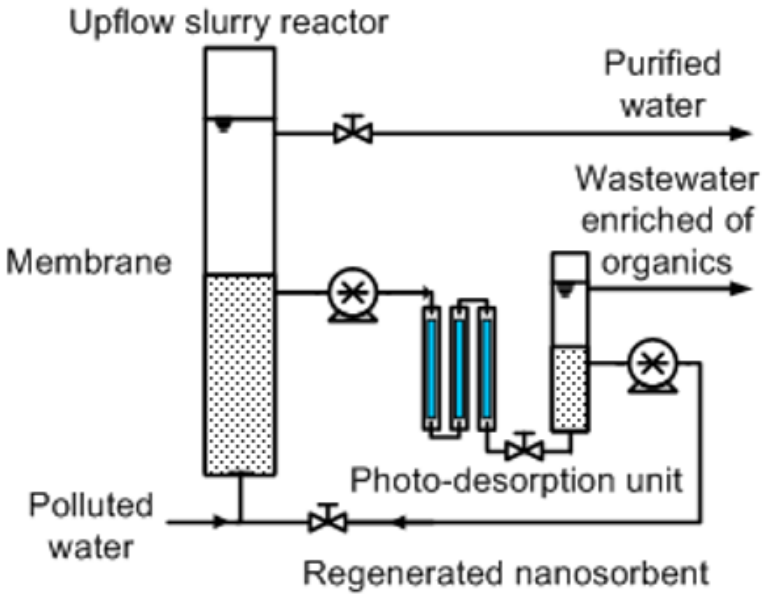

Figure 1-1. Photodesorption phenomena for water and waste water purification

Dissolved organic matter provides precursors for the formation of disinfection-by-products, fouls membranes, causes aesthetic and corrosion problems. While its separation from water is highly desirable, its destruction is a questionable aim, as it is often unnecessary and costly. Humic materials are ubiquitous, harmless and sometimes benign in the aquatic environment. Thus, instead of their unnecessary and expensive destruction, a rational treatment aim might be their physical separation and removal after photodesorption. The proposed mechanisms for adsorption of organics and

heterogeneous photocatalysis over TiO_2 under UV illumination were used to explain photo-induced desorption of the organic matter. Process scheme is shown in Figure 1-1:

1.4 Higher-order assemblies of Titania nano structure

Nanoscale fabrication is now one of the most active research areas of material science. A diverse range of properties are accessible through the numerous types of nanostructures that can be produced from synthetic efforts. Assimilating these nanoparticles in nanoscale will require the development of appropriate methods to assemble these materials. This level of control also provides an advanced understanding of the phenomenon of aggregation, which has long been a subject of research on small-sized nanomaterial fabrication. In this scenario, several researchers have successfully assemble nanoparticles on interesting template morphologies (Peng et al., 2003; Xiong et al., 2006). Therefore, the arrangement of nanostructures in desired shapes and forms can also be tailored by the following simple procedures, such as the morphology transcription of templates (Kuchibhatla et al., 2007; Ou & Lo 2007).

Titania nanotubes, nanorods, nanowires and nanobelts have all been synthesized along with various titanates and nanotube composites (Kuchibhatla et al., 2007; Li et al., 2012; Ou & Lo 2007). Template-based, hydrothermal, sol–gel and anodic oxidation were used for synthesizing the nanotubular structures of titania and various conditions for tailoring structural and morphological features were established. The thickness of these arrangements can be controlled by contact time, solution pH, and the concentration of the nanostructure solution. However, the mechanism of structural growth and the reasons for enhanced performance are still the subject of debate. Despite the controversy about the chemical structure and mechanism for the formation of titania

nanostructure, they are becoming prominent owing to their unique features. These include large specific surface area, photocatalytic potential and ion-exchangeable ability.

1.5 Research objective and scope

The scope of this research is to elucidate the photodesorption of organic matter from TiO_2 under UV irradiation. In addition, this research also includes synthesis of titania-based photocatalytic adsorbent nanomaterials produced by self-assembly for water purification. For this purpose, potassium titanate was synthesised using Degussa P25 as a titanium precursor in the presence of hydrogen peroxide as an oxidising agent and potassium hydroxide in alkaline solution via alkaline hydrothermal condition. As a part of nanotechnology, the development of the photocatalytic adsorbent nanofibre is of great importance to establish adsorption and photocatalytic water treatment an attractive and cost-effective process.

The use of a peroxide method for preparing photocatalysts using conventional titania precursors, such as titanium metal and its organic complexes, and $TiCl_4$ etc (Ichinose 1996; Yada et al., 2006) has been presented in the literature. However, the use of titanium dioxide (Degussa P25) as a precursor has hardly been investigated, and relevant research papers were limited to the study. The use of KOH to produce nanofibre is well documented but there is much less known about utilizing low temperature hydrothermal methods.

The main objective of the study is to:

- Explore and utilise photodesorption phenomena using TiO_2

- Synthesise potassium titanate nanoparticles produced by hydrothermal treatment
- Characterise self-assembling potassium titanate using SEM/EDX, TEM, XRD and BET surface area
- Assess the potential applications of synthesised potassium titanate in water remediation

1.6 Thesis Structure

This dissertation reviews the effectiveness of synthesis, characterisation and use of potassium polytitanate nanofibre to reduce the concentration of toxic compounds (such as crystal violet, methylene blue and lead) to sub-ppb levels. As per the research goal, the thesis chapters are organised and summarised as follows:

- Chapter 1 introduces the concept of the subject and establishes research objectives.
- Chapter 2 compiles the comprehensive literature review of the subject matter.
- Chapter 3 outlines the synthesis procedures, characterisation technique and experimental setup.
- Chapter 4 discusses photodesorption of dissolved organic matter by titanium dioxide in aqueous media
- Chapter 5 reports on the synthesis and characterisation of potassium polytitanate.
- Chapter 6 investigates the solar assisted photocatalysis of methylene blue using potassium polytitanate.
- Chapter 7 explores the adsorption behaviour of Lead on potassium titanate.
- Chapter 8 summarises the major findings of this study and recommendation for future research.

University of Technology Sydney
FACULTY OF ENGINEERING

Chapter 2: Literature review

2.1 Nanotechnology for water treatment

Nanotechnology refers to a wide variety of tools, techniques and applications that simply involve particles ranging from a few to hundreds of nanometres in diameter. Particles of this size have unique physicochemical and surface properties that lend themselves to novel uses. Because of their unique activity toward recalcitrant contaminants, advocates of nanotechnology suggest that this area of research could contribute to solutions for some of the major problems we face globally. These include, for example, ensuring a supply of safe drinking water for a growing population, as well as addressing issues in medicine, energy, and agriculture (Hillie et al., 2007; Mamalis 2007; Pendergast et al., 2011).

Nanotechnology is truly revolutionary technology and it describes a range of technologies performed on a nano meter scale with widespread applications. Nanotechnology encompasses the production and application of physical, chemical, and biological systems at scales ranging from individual atoms or molecules to around 100 nanometres, as well as the integration of the resulting nanostructures into larger systems. Nanotechnology, which is the engineering and art of manipulating matter at nano scale offers the potential of novel materials for treatment of surface water, ground water and wastewater contaminated by toxic metals ions, organic and inorganic solutes and microorganisms (Mamalis 2007; Theron et al., 2008).

The principal approach nanotechnologies can help alleviate water problems is by solving the technical challenges that removing water contaminants including bacteria, viruses, toxic metals, pesticides and salts present. Numerous researchers claim that nanotechnologies offer more affordable, effective, efficient and durable ways of

achieving specific nanoparticles for water treatment. These will allow manufacturers to prepare less toxic particles using classical methods (Savage et al., 2005; Theron et al., 2008).

2.1.1 Current potential applications of nanotechnology for water and wastewater treatment

Progress in nanotechnology has led to the development of novel materials and methods that significantly expand the performance of conventional water treatment processes. Recently, researchers have reported the application of nanotechnology for wastewater treatment using various nanomaterials such as metal nanoparticles, metal oxides, carbon compounds, zeolite, filtration membranes, etc. (Bora et al., 2014; Kanchi 2014; Qu et al., 2013). Some promising water treatment techniques/tools introduced by nanotechnology are described as below:

2.1.1.1 Adsorption

Adsorption is commonly employed as a polishing step to remove organic and inorganic contaminants in water and wastewater treatment. The efficiency of conventional adsorbents is usually limited by three issues: the surface area or active sites, the lack of selectivity and adsorption kinetics. Nano-adsorbents offer a significant advantage because of their unique characteristics at small size with their extremely high specific surface area to volume ratio and associated sorption sites (Mamalis 2007). In addition to having high specific surface areas, nanoparticles also have unique adsorption properties due to different distributions of reactive surface, disordered surface regions, short intraparticle diffusion distance, tunable pore size and surface chemistry (Qu et al., 2013). When a nanoparticle is dispersed in an aqueous solution, surface ionization and

the adsorption of cations or anions result in the generation of the surface charge and an electric potential will be developed between the particle surface (Suttiponparnit et al., 2011) .

Khajeh, et al., (2013) outline the potential of nanomaterial as nano-adsorbents and investigate their role in the past two decades as adsorbents in pre-concentration and cleaning up processes in aqueous media. These materials can be functionalized using different chemical groups to enhance their affinity to a given compound. They can also be employed as high selectivity/capacity recyclable ligands for toxic elements and organic and inorganic solutes/anions in aqueous media.

The common oxides used as adsorbents are mostly oxides of iron (Fe), manganese (Mn), silicon (Si), titanium (Ti) and tungsten (W). The sorption is mainly controlled by complexion between dissolved metals and the oxygen in metal oxides (Koeppenkastrop et al., 1993). As adsorbent materials, metal oxides have the advantages of being low-cost materials and can be functionalized easily to tune their adsorption capacity and selectivity. Their nanoscale complements have higher adsorption capacity and faster kinetics due to the higher specific surface area, shorter intraparticle diffusion distance and larger number of surface reaction sites (Yean et al., 2005). Metal-based nanomaterials have been explored for their ability to remove a variety of heavy metals such as arsenic, lead, mercury, copper, cadmium, chromium, nickel, and have shown great potential to outcompete activated carbon (Sharma et al., 2009). Several metal oxide nanomaterials including nanosized magnetite and TiO_2 have shown arsenic adsorption performance superior to activated carbon (Deliyanni et al., 2003; Mayo et

al., 2007). Nanosorbents based on Fe-oxides have been recently explored removing of several organic pollutants in water (Zhang, Niu, et al., 2010; Zhong et al., 2006).

Carbon nanomaterials have been extensively used for the adsorption of various organic and inorganic pollutants in water. Of these nanomaterials, activated carbon is the most popular carbon material due to its high adsorption capacity, high thermal stability, excellent resistance against attrition losses, and low cost. Granular activated carbon was used to remove various organic contaminants as well as odorous pollutants from water (Çeçen et al., 2011; Chaudhary et al., 2003). However, a major drawback of activated carbon is its low adsorption affinity for low molecular weight polar organic compounds. Carbon nanotubes (CNTs) have been more efficient than activated carbon for adsorbing various organic chemicals (Pan et al., 2008). Its high adsorption capacity mainly stems from the large specific surface area and the diverse contaminant-CNT interactions. In the aqueous phase, CNTs form loose aggregates due to the hydrophobicity of their graphitic surface, reducing the effective surface area. On the other hand, CNT aggregates contain interstitial spaces and grooves, which are high adsorption energy sites for organic molecules (Pan et al., 2008). Although activated carbon possesses comparable measured specific surface area as CNT bundles, it contains a significant number of micropores inaccessible to bulky organic molecules such as many antibiotics and pharmaceuticals (Ji et al., 2009). Consequently, CNTs have much higher adsorption capacity for some bulky organic molecules because of their larger pores in bundles and more accessible sorption sites.

It has been observed that some organic pollutants cannot be completely removed from the water body due to the very low concentration of these pollutants, typically in the

range of picogram or nanograms per litre of water (Zhang et al., 2003). To efficiently remove of such pollutants, biosorbents have found promising, which are typically derived from biological or agricultural materials. Compared to conventional absorbents, biosorbents have many advantages, like low cost, high efficiency, low agricultural and biological sludge, no additional nutrient requirements, and they are regenerative as well.

Mamalis (2007) reported that nanoparticles are able to efficiently remove metallic species such as Cr(VI), Cu(II), Co(II), Cd(II), As(V), As(III) and Hg(II) pollutant species from aqueous solutions. Applications of nano-adsorbents for removing arsenic have been commercialized, and their performance and cost have been compared to other commercial adsorbents in pilot tests (Aragon et al., 2007). ArsenX^{np} is a commercial hybrid ion exchange medium comprising iron oxide nanoparticles and polymers. ADSORBSIA^{TM} is a nanocrystalline titanium dioxide medium in the form of beads from 0.25 to 1.2 mm in diameter. Both nano-adsorbents were highly efficient in removing arsenic and ArsenX^{np} required little backwash (Aragon et al., 2007; Sylvester et al., 2007). ArsenX^{np} and ADSORBSIA^{TM} have been employed in small to medium scale drinking water treatment systems and proved to be cost-competitive.

Zeolites have high specific surface area and high ion exchange capacity, making them an attractive adsorbent for water treatment. Most zeolites occur naturally and can also be produced commercially. Hexadecyltrimethylammonium (HDTMA)-modified zeolite was developed by Dong et al., (2010) and used for the adsorption of phenol derivatives from water. HDTMA molecules form a bilayer micelle at the surface of the zeolite and increase the adsorption capacity of the nanosorbent. Degradation of pyridine and quinoline in wastewater using zeolite was studied by Bai et al., (2010).

2.1.1.2 Membranes and membrane processes

Membranes provide a physical barrier for removing undesired constituents and allow the passage of certain constituents based on their size. Membrane filtration processes such as microfiltration, ultrafiltration, nanofiltration and reverse osmosis have played a significant roles in reducing pollutants and producing high quality pure water (Strathmann 2001). According to Qu et al., (2013), the major challenge of membrane technology is the inherent trade-off between membrane selectivity and permeability, and the high energy consumption required for the wide application of pressure driven membrane processes. In addition, membrane fouling adds to the energy consumption and the complexity of the process design and operation which reduces the lifetime of membranes and membrane modules.

Nanotechnology is being applied in the production of water purification membranes used in advanced treatment. The performance of membrane systems is largely decided by the membrane material. Incorporation of functional nanomaterials into membranes offers a great opportunity to improve the membrane permeability, fouling resistance, mechanical and thermal stability, as well as to render new functions for contaminant degradation and self-cleaning. Theron et al., (2008) reported the following water filtration membranes are produced from nanomaterials: i) nanostructured membranes made from carbon nanotubes, nanoparticles and dendrimeres; and ii) nanoreactive membranes made from metal nanoparticles and other nanomaterials.

In the last two decades, the development of polymeric and ceramic membranes has positively impacted on the use of membrane. The surface modification of the hydrophilic layer on nanofibrous ultrafiltration membranes was achieved with high flux

for oil-in-water emulsion separation serving as an alternative to traditional polymer filtration membranes (Ma et al., 2010; Wang et al., 2005; Wang, Zhang, et al., 2010; Zhu et al., 2014)

Recently, Pendergast et al., (2011) discussed the nanotechnology-enabled water treatment membranes that encompass many different objectives and performance enhancements. Chemically stable ceramic membranes have been modified for high selectivity nanofiltration and potentially reverse osmosis membranes with zeolite thin film coatings. Self-cleaning and catalytic membranes have been formed with antimicrobial and photocatalytic nanoparticle coatings. Mixed matrix membranes offer enhanced separation performance, fouling resistance, and mechanical stability for filtration applications. Thin film nanocomposites seek to produce compaction resistant membranes with silica, self-cleaning photocatalytic membranes with titania nanoparticles, or highly permeable and selective membranes with molecular sieve zeolites. Biologically inspired membranes aquaporins, aligned CNTs, and block copolymers seek to simultaneously improve selectivity and permeability. Each of these innovative materials promises unique performance enhancements and each has unique hurdles to overcome before it is commercially viable.

The past few years have seen nanofibre being employed as promising membrane materials for filtration, water and wastewater treatment, and water purification applications. Electrospinning of nanofibers has gained much interest and attention from researchers in their application for membrane distillation and so far this process has produced promising results for membrane distillation application (Tijing et al., 2014).

2.1.1.3 Photocatalysis

Photocatalysis is a promising technique for water purification that uses a light active nanostructured catalyst medium to degrade various pollutants present in the water. Photocatalysis is a surface phenomenon which involves five basic steps (Ibhadon et al., 2013; Pirkanniemi et al., 2002): (i) diffusion of reactants to the surface of the catalyst; (ii) adsorption of the reactants on the surface of the catalyst; (iii) reaction at the surface of the catalyst; (iv) desorption of the products from the surface of the catalyst; and (v) diffusion of the products from the surface of the catalyst.

In photocatalysis, semiconductors function by absorbing a photon of energy greater than their own bandgap energy, and creating an electron–hole (e–h) pair via excitation of electrons from the conductive to the valence band (Hoffmann et al., 1995; Keane et al., 2014). The photo-generated e–h pair then produces highly reactive oxidizing and/or reducing radicals, such as super oxides (O_2^-) and hydroxyl radicals ($OH^\bullet$) in water. These radicals then degrade organic/inorganic pollutant molecules present in the contaminated water through some secondary reactions. Degradation of the water contaminants can also occur through direct transfer of the photo-generated electrons or holes from the catalyst surface to the contaminant molecules.

Heterogeneous photocatalysis opens up new opportunities for water purification since it allows complete mineralization of the organic pollutants into environmentally neutral compounds, such as CO_2 and H_2O, with reactions occurring at room temperature at relatively low costs (Chong et al., 2010; Mukherjee et al., 1999; Romão et al., 2014).

Some examples of typically used nanostructured photocatalysts are titanium dioxide (TiO_2), zinc oxide (ZnO), ferric oxide (Fe_2O_3), zinc sulfide (ZnS) and cadmium sulfide (CdS), cerium oxides (CeO_2), copper oxides (CuO), iron oxides (FeO), manganese oxides (MnO_2) and vanadium oxides (VO) (Bora et al., 2014; Chaturvedi et al., 2013; Colmenares et al., 2009; Sobczyński et al., 2001). Of these AOPs, heterogeneous photocatalysis employing semiconductor catalysts (TiO2, ZnO, Fe_2O_3, CdS, GaP and ZnS) has demonstrated its efficiency in degrading a wide range of ambiguous refractory organics into readily biodegradable compounds, and eventually mineralized them to innocuous carbon dioxide and water (Chaturvedi et al., 2013). Of the semiconductor catalysts TiO_2 has received the greatest interest regarding its application in photocatalysis technology. TiO_2 is the most active photocatalyst under the photon energy of 300 nm < l < 390 nm and remains stable after repeated catalytic cycles, whereas Cds or GaP are degraded to produce toxic products (Malato et al., 2009).

2.1.2 Significance of Nanotechnology in Wastewater Treatment

Nanotechnology research and development is a promising novel technology, for the treatment of wastewaters which is vital to human beings. These technologies are economical, reliable, rapid and durable and they treat wastewaters by eliminating specific types of pollutants from water (Savage et al., 2005). Nanotechnology-based multifunctional and highly efficient processes are providing affordable solutions to water treatments that do not rely on large infrastructures or centralized systems (Amin et al., 2014). Nanotechnology applications for sustainable water supplies include water filtration, water treatment, desalination, and using such techniques as sensors, nanoparticles, and catalysts.

Advances in nanotechnology developed novel materials and methods. Several issues relating to water quality could be determined and the significant usage of novel nanomaterials and related stuff for positive implication for water purification. Treatment of industrial wastewater with newly synthesized nanomaterials is another potentially useful application. Nanomaterials have a number of unique physicochemical properties that make them particularly attractive as separation media for water purification. This includes high surface area, photosensitivity, catalytic and antimicrobial activity, electrochemical, optical, and magnetic properties, and tunable pore size and surface chemistry, provide useful features for many applications (Qu et al., 2012). Nanomaterials can be functionalized with various chemical groups to increase their affinity to a given compound (Suttiponparnit et al., 2011). Nanomaterials serve as high capacity/ selectivity and recyclable ligands for toxic metal ions, radionuclides, organic and inorganic solutes/ anions in aqueous solutions (Savage et al., 2005). Apart from this, nanomaterials also provide unprecedented opportunities to develop more efficient water-purification catalysts and redox active media due to: firstly their large surface areas; and secondly, their size and shape-dependent optical, electronic and catalytic properties.

Nanotechnology is being applied for developing smart membranes with improved membrane performance, fouling resistant surface, mechanical and thermal stability, as well as to render new functions for contaminant degradation and self-cleaning (Theron et al., 2008). Nanotechnology is applied to enhance conventional ceramic and polymeric materials for water purification. According to Pendergast et al., (2011), the most promising concepts include zeolitic; and catalytic nanoparticle coated ceramic membranes, hybrid inorganic–organic nanocomposite membranes, and bio-inspired

membranes such as hybrid protein–polymer biomimetic membranes, aligned nanotube membranes, and isoporous block copolymer membranes.

The development of visible light-activated TiO_2 nanoparticles has a significant impact on water supply. Controlling the release of these nanoparticles into surface waters exposed to sunlight could significantly reduce organic carbon load through oxidative photochemical degradation (Riss et al., 2007; Savage et al., 2005). Most remediation technologies available today, while effective, are typically expensive and time consuming, particularly pump-and-treat methods. The capability to remove toxic compounds from surface and sub-surface and other environments is very difficult to access in situ, and doing so rapidly, efficiently and as cost-effectively as possible is the ultimate goal (Kanchi 2014). Hence, nanotechnology-based waste water treatment effectively eliminates contaminants and helps in the recycling process to get purified water, which leads to reduced labour, time and expenditure in industry and solves the various environmental issues.

2.1.3 Techniques and Instruments used to analysis nanomaterials

Current advances that have emerged in nanoscience and nanotechnology have led to improvements in investigating and manipulating small objects. Such developments were mostly driven the improvements in the resolution, reliability and availability of electron microscopy, including scanning (SEM) and transmittance (TEM) modes. The recent invention of scanning tunnelling (STM) and atomic force (AFM) microscopy has also provided additional tools for probing and manipulating atomic scale objects. SEM, AFM and STM instruments detect the surface features of nanostructured objects. However, the method which can only differentiate between the tubular or rod shape of

the nanostructure is TEM imaging with the projection of the object. Furthermore, in order to avoid misinterpretation associated with TEM imaging it is necessary to detect the nanotubes oriented parallel to the electron beam casting the projection in the shape of a circle. Although electron microscopy imaging allows direct detection of the shape and dimensions of the objects with greater accuracy, the disadvantage is that it covers only the limited area of the sample. Consequently, there are always doubts as to how representative the imaged object of the sample actually is.

One of method which measures macroscopic parameters and associates them with microscopic parameters is gas adsorption into the porous samples. The most popular and developed method is nitrogen adsorption, which has been widely used in the investigation of catalysts for the characterisation of porous materials. In typical experiments, the adsorption of gaseous nitrogen on the surface of material is studied at a temperature of -196°C, in the range of relative pressure from 0 to 1. Using an adsorption model, it is possible to determine the specific surface area (BET) and the pore size distribution (BJH). These data can be then associated with the morphology and size of the nanostructure. The advantage of this method is the simplicity, cost and reproducibility. The disadvantage is that it requires a model which can associate pore size distribution with the dimensions of the nanostructure. This approach is usually applicable only to nanostructures from the same family such as nanotubes, nanoparticles, etc.

The degree of atomic order in nanostructures can be studied using electron or X-ray diffraction methods. There are some difficulties with the interpretation of diffraction data, due to the relatively small size or polycrytallinity of nanostructures resulting in a

widening of the reflexes. Furthermore, some nanostructures such as as-prepared TiO_2 anodized nanotubes may be amorphous. The electronic structure and the nature of the surface atoms has been actively studied using conventional spectroscopy methods.

The methods of computational chemistry are also widely used in nanoscience. With reference to titanate nanotubes, however, their use is limited due to the massive number of atoms in its nanostructure, resulting in the huge set of atomic orbitals. For example, a typical 100 nm long titanate nanotube contains more than ten thousand titanium atoms, making direct calculations impossible using current computing facilities. However, future developments in computing technology and the implementation of various models' approximations will permit further simulation and stimulate progress in the discovery of new nanomaterials.

2.1.4 Nanotechnology and the challenges

The water industry is required to produce drinking water of high quality. Hence, there is a clear need for the development of cost-effective and stable materials and methods to address the challenges of providing fresh water in adequate amounts. Nanotechnology is already being used to remove contaminants from drinking water and increase the availability of fresh water, but there is still a long way to go. Nanotechnology needs to be stable, economical, and more effective compared with the already existing techniques. For improvements to occur, traditional treatment technologies have to be modernized, that is, updated or modified or replaced by developing materials and methods which are efficient, cost-effective, and reliable. This is particularly important to achieve a considerable potable water savings through reuse of wastewater in addition to tackling the day-by-day worsening quality of drinking water.

Apart from water treatment applications, expanding the array of nanomaterials' usage in diagnostic and therapeutic agents, stain-resistant clothing, solar cells, sun blocks, and cosmetics will lead to great exposure of workers, consumers, and the environment to them. This raises fundamental question concerning the potential harms of such application to human and the ecosystem (Samet 2014; Schulte et al., 2014). Usually, the human body can be exposed to nanoparticles through different routes such as skin absorption, ingestion and inhalation (Reed et al., 2014). The toxicity of nanoparticles is much more pronounced because they have higher surface area and can react more easily than microparticles. Some studies have reported that carbon nanotubes can damage the lungs if inhaled, while other studies discussed the damage caused to the liver and brain by fullerenes (Kunhikrishnan et al., 2014; Manke et al., 2014). A few years ago, Savolainen et al. (2010) reported that the health concerns generated by nanomaterials on individuals have focused on their impact on lungs, circulation, brains and genotoxic and possible carcinogenic effects.

2.2 Heterogeneous Photocatalysis

Heterogeneous photocatalysis can be described as the acceleration of photoreaction in the presence of a catalyst. In heterogeneous photocatalysis, activation of the catalyst occurs through the absorption of photons of light and has emerged as a promising technology that could be instrumental in eliminating pollutants from air and water streams. Photocatalyst activity depends on the ability of semiconductor materials to create electron−hole charge carrier pairs when exposed to light. Photocatalytically active materials are typical semiconductors and the most common are metal oxides or

sulfides such as TiO_2, ZnO, ZrO_2, CeO_2, SnO_2, CdS, ZnS, Fe_2O_3 and WO_3 (Chong et al., 2010; Herrmann 2005; Vinu et al., 2012).

Of all the semiconductor catalysts, TiO_2 has received the greatest interest for its application in heterogeneous photocatalysis technology. TiO_2 is the most active photocatalyst under the photon energy of 300 nm < λ < 390 nm and remains stable following repeated catalytic cycles. Conversely, Cds or GaP are degraded and this produce toxic products (Chong et al., 2010; Malato et al., 2009). Furthermore, the multi-faceted functional properties of TiO_2 catalyst, which include its chemical and thermal stability or resistance to chemical breakdown and strong mechanical properties, have promoted its widespread application in photocatalytic water treatment.

The process of semiconductor photocatalysis basically involves the following stages. Light energy of a certain wavelength is made to fall on to a semiconductor. If the energy of the incident light is equivalent to the band gap energy of the semiconductor, electrons will be excited from the valence band to the conduction band of the semiconductor and holes will be left in the valence band (Fox et al., 1993; Herrmann 1999). These electrons and holes could undergo subsequent oxidation and reduction reactions with any species, which might be adsorbed on the surface of the semiconductor to produce the necessary products (Lasa et al., 2005). The semiconductor catalyst has demonstrated its efficiency in degrading a wide range of ambiguous refractory organics into readily biodegradable compounds, and eventually mineralized them to innocuous carbon dioxide and water.

2.2.1 History and overview

In the contexts of history, heterogeneous photocatalysis began in the early 1970s when Fujishima et al., Fujishima et al., (1972 discovered the photochemical splitting of water into hydrogen and oxygen in the presence of TiO_2. As pointed in several studies (Frank et al., 1977; Fujishima et al., 2000; Mills et al., 1997; Oturan et al., 2014; Pelaez et al., 2012), their fundamental work led to the development of a new advanced oxidation process, that was based on semiconductor photocatalysis, for numerous environmental and energy applications.

Since then, extensive research has been carried out to produce hydrogen from water in oxidation reduction reactions using a variety of semiconductor catalyst materials. The field of heterogeneous photocatalysis has expanded rapidly within the last four decades, having undergone various developments especially in relation to energy and the environment. The two most significant applications of photocatalysis have been in solar water splitting and the purification of air and water containing low concentrations of pollutants. Furthermore, in order for this technology to be successful and to have many applications, significant advances are still required. This is particularly true removing organic and inorganic species from air and water streams and for the inactivation of water-contaminating microorganisms.

Until now, several photocatalytic materials have been investigated for their photocatalytic properties. According to Rajeshwar et al., (2001) an ideal photocatalyst should possess the following properties:

- Stability and sustained photocatalytic activity
- Good overlap of absorption cross-section with solar spectrum

- High conversion efficiency and quantum yield
- Compatibility with a variety of substrates and reaction environments
- Low cost

TiO_2 is the most widely used semiconductor photocatalyst in water treatment due to its low cost, chemical stability and abundance. Current research focuses on increasing photocatalytic reaction kinetics and the range of photo activity provide either high performance UV-activated photocatalytic reactors or energy-efficient solar/visible light-activated photocatalytic reactors.

2.2.2 Fundamentals of Photocatalysis

The fundamental principles of heterogeneous photocatalysis have been extensively reported (Chong et al., 2010; Herrmann 1999; Hoffmann et al., 1995; Linsebigler et al., 1995). Heterogeneous photocatalysis involve several processes whereby illumination of a semiconductor particulate (such as TiO_2) with UV/visible light suitable to its bandgap energy ultimately generates conduction band electrons (e^-) and valence band holes (h^+). After illumination, the following photocatalytic reactions can occur on the surface of TiO_2 as mechanistic steps which govern the photocatalysis process (Herrmann 1999; Hoffmann et al., 1995).

A photo-excited TiO_2 generated an electron and a positive electron-hole.

$$TiO_2 + h\nu \rightarrow e^- + h^+ \quad \text{..... 2.1}$$

Electron transfers from the valance band to conduction band, adsorb the OH^- ion from water, to the positive electron-hole.

$$OH^- + h^+ \rightarrow {}^{\bullet}OH \quad \text{..... 2.2}$$

The third step is of great importance, mostly because of the high concentrations of OH^-, given water dissociation into ions.

$$H_2O \rightarrow OH^- + H^+ \text{ …….. 2.3}$$

Molecular oxygen acts as an acceptor species in the electron-transfer reaction.

$$O_2 + e^- \rightarrow {}^{\bullet}O_2^- \text{ ……..….. 2.4}$$

Super-oxide anions, (2.4), can subsequently be involved in the following reactions.

$$^{\bullet}O_2^- + H^+ \rightarrow {}^{\bullet}HO_2\text{……. 2.5}$$

$$2{}^{\bullet}HO_2 \rightarrow O_2 + H_2O_2\text{…… …..... 2.6}$$

$$H_2O_2 + {}^{\bullet}O_2^- \rightarrow OH^- + {}^{\bullet}OH + O_2\text{……...… 2.7}$$

Photo-conversion of hydrogen peroxide gives more $^{\bullet}$OH free radical groups.

$$H_2O_2 + h\nu \rightarrow 2{}^{\bullet}OH\text{……...…. 2.8}$$

Finally, $^{\bullet}$OH radicals oxidize organic adsorbed pollutants onto the surface of the titanium dioxide particles.

$$^{\bullet}OH + \text{organic pollutant} \rightarrow \text{Intermediate……..…… 2.9}$$

Chatterjee et al. (2005) outline the simplified mechanism for the photo activation of a semiconductor. Initially, an electron-hole pair is generated in the semiconductor particles when radiation of energy greater than or equal to the band gap is shone on the surface. Electrons are excited from the valence band (VB) to the conduction band (CB) of the semiconductor, thus creating an electronic vacancy at the valence band edge. The valence band hole is strongly oxidizing, whereas the conduction band electron is strongly reducing. A hole can migrate to the surface and oxidize an electron donor; in turn, while at the surface, the semiconductor can donate electrons to reduce an electron acceptor. Consequently, following irradiation, the semiconductor particle can act as either an electron donor or an electron acceptor for molecules in the surrounding medium, depending on the charge transfer to the adsorbed species (Linsebigler et al., 1995).

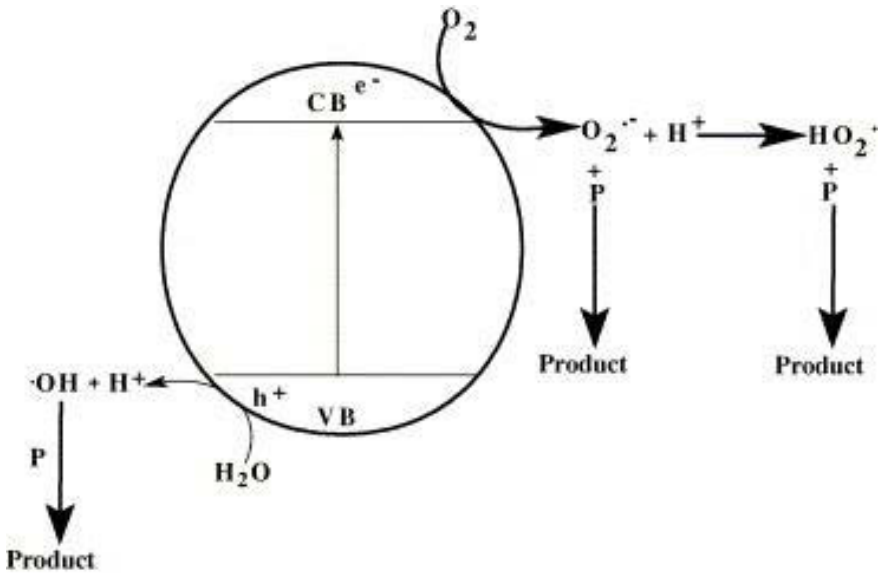

Figure 2-1 Principle of photo activation of TiO_2 semiconductor.

2.2.3 Factor influencing Photocatalytic degradation

There are several factors that directly influence the overall photocatalytic process efficiency. The most significant factors include photocatalyst loading, composition and characteristics of the catalyst, contaminant composition and concentration, light intensity, pH of the solution, oxygen supply, and the temperature of reaction. Other engineering parameters such as the detention time and reactor hydraulics are case-specific.

2.2.3.1 Adsorption

There is some evidence to indicate that the degradation of substrate occurred on the surface of the photocatalyst (Hoffmann et al., 1995; Pelizzetti et al., 1993; Turchi et al., 1989). It is therefore logical to expect that the rate of degradation of the substrate will be a function of the adsorbed substrate concentration. Thus, the extent of adsorption of the substrate may be an important factor. Several investigators have concluded that there is a clear relationship between substrate adorability and photocatalytic degradation (Noguchi et al., 1998; Subramanian et al., 2000; Tanaka et al., 2000).

Noguchi et al., (1998) investigated the photocatalytic degradation of formaldehyde and concluded that it was much higher than acetaldehyde. This was attributed to differences in their adsorption capabilities. In the case of photocatalytic degradation of azo dyes, Tanaka et al., (2000) discovered that adsorption of the dye on TiO_2 was an important factor in determining the degradation rate. Dagan et al., (1993) revealed that the adsorption of salicylic acid was indicated by a bright yellow colour on the TiO_2 surface which after illumination changed gradually to dark brown. This indicated that adsorption and the reaction are occurring at the surface, followed by decolourisation on the surface. It is therefore reasonable to conclude that degradation of the substance depends on its adsorption on the photocatalytic surface.

2.2.3.2 Pollutant concentration

Often, wastewater contains a mixture of pollutants, organic solvents as well as dissolved organic matter and humic substances if mixed with other waste streams. In general, the dark adsorption of organics onto the TiO_2 surface precedes photo oxidation process that occurs during UV irradiation. However, at higher contaminant loading, pollutants may compete for the active sites on the TiO_2 surface or deactivate the photocatalyst and, subsequently, decrease the degradation rate of the target contaminants (Konstantinou et al., 2004). Alternatively, they may act as light screens, thus reducing the photon receiving efficiency (Arana et al., 2004; Saquib et al., 2003).

2.2.3.3 Photocatalyst loading

Concentration of TiO_2 in the photocatalytic water treatment system determines photocatalytic reaction rate where the amount of TiO_2 is directly proportional to the

photocatalytic reaction rate (Gaya et al., 2008). The increase of TiO_2 loading increases the rate of the photocatalytic reaction because of the increase in the surface area of the photocatalyst available for adsorption and degradation (Mozia 2010). A linear dependency holds until certain extent when the reaction rate starts to degrade and becomes independent on TiO_2 concentration. The excess TiO_2 particles above a saturation level leads to a high turbidity state where the light photon absorption decreases because of a light screening effect. This attributes to reduce the surface area of TiO_2 being exposed to light illumination and the photocatalytic efficiency. It is therefore essential to find an optimum catalyst loading for particular a photo reactor so that any reduction in photocatalytic activity can be avoided (Bamba et al., 2008; Gaya et al., 2008).

2.2.3.4 Effect of pH

In general, the pH has a varied effect on the photocatalytic reaction rate and it is expected the increase or decrease in pH should affect the rate of degradation. The effect of pH on the reaction rate can be interpreted in terms of electrostatic interactions between charged TiO_2 particles and pollutants. It affects the adsorption processes, and it is believed that the photocatalytic reactions are surface reactions. The principal amphoteric surface functionality is the titanol fraction (>TIOH),and consequently any variation in pH also affects the surface speciation due to the amphoteric nature of the titanium dioxide particles (Jackson et al., 2007); consequently affecting the adsorption and photocatalytic reactions of pollutants. The point of zero charge ($pH_{(PZC)}$) of metal oxide is defined as the pH at which the concentrations of protonated and deprotonated groups are equal. The $pH_{(PZC)}$ of TiO_2 is 3.5 - 6.7, depending on the origin of the sample. As an outcome of this amphoteric behaviour, the TiO_2 surface is predominantly

negatively charged at pH > $pH_{(PZC)}$, and positively charged at pH < pH at point of zero charge (PZC). For example, methylene blue prefers to be absorbed on TiO_2 and readily degraded photocatalytically in alkaline solutions because its molecule and the surface of TiO_2 possess opposite charges; however, only little degradations were obtained in the acidic solutions (Hasnat et al., 2005). Evidently, the pH of the solution has an influence on the dispersion stability and also on the photodegradation rates (van Dyk et al., 1998).

2.2.3.5 Light intensity and radiation time

UV light provides photon required for the electron transfer from valance band to the conduction band of the photocatalyst. The UV light irradiation has the dramatic effect as the energy provider on the photo-degradation of the reactants. The activity of the photocatalyst strongly depends on the light irradiation per unit area or the photon flux on the catalyst's surface. The energy of the photon is related to wavelength and overall energy input to a photocatalyst process is depends on the light intensity. Therefore, the effect of both intensity and wavelength is important.

Ollis et al., (1991) reviewed studies reported for the effect of light intensity on the kinetics of the photocatalysis process. They stated that: (i) at low light intensities (0 to 20 mW/cm^2), the rate would increase linearly with increasing light intensity (first order); (ii) at intermediate light intensities beyond a certain value (approximately 25 mW/cm^2) (Herrmann 1999), the rate would depend on the square root of the light intensity (half order); and (iii) at high light intensities the rate is independent of light intensity. This is likely because at low light intensity reactions involving electron–hole formation are predominant and electron–hole recombination is negligible. However, at increased light intensity electron–hole pair separation competes with recombination,

thereby having less effect on the reaction rate. In the studies reviewed (Neppolian et al., 2002; Sakthivel et al., 2003; So et al., 2002), the enhanced rate of decolourization as the light intensity increased was also observed.

It is evident that the percentage of decolourization and photodegradation increases with increase in irradiation time. The reaction rate decreases with irradiation time since it follows apparent first-order kinetics and additionally a competition for degradation may occur between the reactant and the intermediate products. The slow kinetics of dye degradation after certain time limit is due to: (a) the difficulty in converting the N-atoms of dye into oxidized nitrogen compounds (Bandara et al., 1997); (b) the slow reaction of short chain aliphatics with $^{\bullet}OH$ radicals (Walling 1975); and (c) the photocatalyst's short life-time of photocatalyst due to active sites being deactivated by the deposition of strong by-products (carbon, etc.).

2.2.3.6 Dissolved oxygen

Dissolved oxygen plays an important role in the TiO_2 photocatalytic reaction pathway of organic pollutants (Saquib et al., 2008). Oxygen mainly has two important roles in the photocatalytic degradation process. Firstly, oxygen scavenges electrons at the irradiated TiO_2 surface to form super oxides radical anion which prevent the recombination of an electron–hole pair (Chong et al., 2009; Subramanian et al., 2004). Secondly, dissolved oxygen has a key role in the formation of reactive species and the stabilisation of intermediates. It was also reported to induce the cleavage mechanism for aromatic rings in organic pollutants (Chong et al., 2010). The dissolved oxygen concentration is determined by the balance between consumption and generation of oxygen in the photodecolorization process and absorption of oxygen through free-

surface. The absence of dissolved oxygen can alter the reaction pathway for photocatalytic reaction significantly and hinder photo-mineralization (Wang et al., 2000). However, increased photocatalytic activity may also occur in the absence of oxygen, which is attributed to the adsorption of UV photons by dissolved oxygen molecules at $\lambda < 254$ nm. The DO molecules acted as an inner filter and reduced the effective photonic flux on the photocatalyst surface (Shirayama et al., 2001).

2.2.3.7 Temperature

The photocatalytic reaction can proceed at ambient water temperature and do not require increasing the temperature because the photonic activation energy is often very small in the temperature ranging from 20 to 80°C for activation of photocatalytic reaction (Herrmann 2005; Malato et al., 2009). The photocatalytic activity at a temperature below 0°C hinders desorption of the final product from the catalyst surface. The desorption of the final product becomes the rate limiting step and signals an increase in the apparent activation energy. On the other hand, when temperature increases above 80°C, the exothermic adsorption of pollutant is disfavour and becomes the rate limiting step. As a result, the activity decreases (Chong et al., 2010; Herrmann 1999; Mozia 2010). However, with reference to the temperature range of 20–60°C in increase of the photodecomposition rate with increasing the reaction temperature has been observed (Malato et al., 2009; Thiruvenkatachari et al., 2008).

2.2.4 Photo reactor design for water treatment

The photocatalytic reactor design is complicated in that it involves major engineering factors such as geometry of the photo reactor for light illumination of total surface area of catalyst while mixing with pollutant. Besides this, a high degree of interactions

among the transport processes, reaction kinetics, and light absorption leads to a strong coupling of physicochemical phenomena and are major concerns for the development of photocatalytic reactors (Ray 1999).

Several problems have to be solved for the effective design of photocatalytic reactor. These include: (i) the efficient exposure of the catalyst to light irradiation must be achieved since the catalyst shows no activity without photons of appropriate energy; (ii) the photocatalytic reaction rate is usually slow compared to conventional chemical reaction rates, due to the small concentration levels of the pollutants; and (iii) large amounts of active and stable catalyst must be provided inside the reactor to provide a large processing capacity (Mukherjee et al., 1999). However, the development of a viable and practical reactor system for treating water with heterogeneous photocatalysis on industrial scale has not yet been successfully achieved.

There are several methods to classify the photocatalytic reactors for water treatment. Based on the type of light, reactors can be divided into two categories: reactors using solar irradiation and those using artificial UV lamps. The design of TiO_2-based photocatalytic reactors has mainly focused on using either slurry or immobilized configurations. In slurry reactors, the catalyst particles are freely dispersed in the aqueous phase and consequently, the photocatalyst is fully integrated in the liquid mobile phase. The immobilized catalyst reactor design features a catalyst anchored to a fixed support, dispersed on the stationary phase. Many studies proved that slurry-type reactors are much more efficient than immobilised-catalyst type reactor (Beydoun et al., 2000; Beydoun et al., 2001; de Lassa et al., 2005; Geissen et al., 2001; Shahid, McDonagh, et al., 2014). Comparisons between photocatalytic slurry-type reactors and

immobilised-type reactors are described in Table 2-1. In water and wastewater purification applications, photocatalytic reaction with TiO_2 can either be carried out in a slurry system or immobilised system. Despite of its great properties it seems that TiO_2 may cause difficulties during the separation phase from water.

Table 2-1. Comparison of photocatalytic slurry-type and immobilised-type reactors
Note: Adopted from (de Lassa et al., 2005)

	Slurry-Type Reactors	**Immobilised-Type Reactors**
Advantages	• Fairly uniform catalyst distribution • High photocatalytic surface area to reactor volume ratio • Limited mass transfer • Minimum catalyst fouling effects due to the possible continuous removal and catalyst replacement • Well mixed particle suspension • Low pressure drop through the reactor	• Continuous operation • Improved removal of organic material from water phase while using a support with adsorption properties • No need for an additional catalyst separation operation
Disadvantages	• Requires post – process filtration • Important light scattering and adsorption in the particle suspended medium • Difficult to recover the fine photocatalyst particles from treated effluent	• Low light utilisation efficiencies due to light scattering by immobilised photocatalyst • Restricted processing capacities due to possible mass transfer limitations • Possible catalyst deactivation and catalyst wash out

Although the slurry-type reactor was effective, it requires a post-process separation stage, additional chemicals, and it is difficult to recover fine photocatalyst particles from the treated effluent, which limits the potential use of TiO_2 on a commercial scale

(de Lassa et al., 2005; Watson et al., 2005). One approach to overcome this separation problem lies in by developing a stable magnetic photocatalyst. This allows for easy remaining recovery by the use of external magnetic field and thus, it increases the reusability of the photocatalyst.

2.2.5 Kinetics of photocatalysis

Photocatalytic degradation of organic pollutants needs the participation of organic and oxygen molecules, simultaneously. Oxygen is generally abundant, and therefore it can be considered that its concentration is constant during photocatalysis. When a given photocatalyst and reaction conditions satisfy thermodynamic requirements for photocatalysis, the photocatalytic reaction may proceed and rates of the chemical reactions can be predicted by kinetics. The kinetics of photocatalytic mineralisation in heterogeneous photocatalysis is often described using the Langmuir-Hinshelwood (L-H) model. The kinetics of a photocatalytic reaction is discussed in the following section. In the L-H model the *r* rate of reaction is proportional to the θ fraction of surface covered by the substrate (pollutant):

$$r = -\frac{dC}{dt} = k\theta \qquad \text{Eq. 2.1}$$

Adsorption of organic substances on the semiconductor surface is necessary for photocatalysis. The adsorption–desorption equilibrium is considered to follow a Langmuir isotherm. From Langmuir's equation

$$\theta = \frac{K.C}{1+K.C} \qquad \text{Eq. 2.2}$$

with *k* reaction rate, *K* constant of adsorption equilibrium, and *C* substrate concentration at *t* time.

Therefore,

$$r = k.\theta = k\frac{K.C}{1+K.C} \qquad \text{Eq. 2.3}$$

Integrating Eq. 2.3 between zero and *t* times gives

$$ln\left(\frac{C_0}{C_t}\right) + K.(C_0 - C_t) = k.K.t \text{.....,.....Eq. 2.4}$$

with C_0 initial and C_t substrate concentration at zero and *t* irradiation times, respectively.

Solving Eq. 2.4 for *k* requires the knowledge of *K*. The θ surface coverage fraction can also be expressed from the number of adsorbed molecules at a given final (equilibrium) concentration:

$$\theta = \frac{n_{ads}}{n_0} = \frac{K.C}{1+K.C} \text{.....Eq. 2.5}$$

$$\frac{1}{n_{ads}} = \frac{1}{n_0} + \frac{1}{n_0 K}.\frac{1}{C} \text{.....Eq. 2.6}$$

with n_{ads} covered and n_0 total number of available adsorption sites. Noting that Eq. 2.6 is linear, both *K* and n_0 can be determined from plotting $1/n_{ads}$ versus $1/C$.

Since organic concentration is generally very low for standard photocatalytic conditions, *KC* in Eq. 2.3 is much lower than 1. It also can be seen from Eq. 2.3 that for relatively high substrate concentrations (and/or *K* values) (KC>> 1) the reaction will be of zero order, while for relatively low substrate concentration and/or *K* values (KC<<1) will be of first order. Typically, in most applications of photocatalysis, the denominator in Eq. 2.3 approaches 1 (one), and thus:

$$r = k.\theta = k.K.C = k_a.C \text{.....Eq. 2.7}$$

with k_a apparent (pseudo) rate constant. The integral form of Eq. 2.16 is:

$$C_t = C_0 e^{-k_a t} \text{.....Eq. 2.8}$$

The linearized form of Eq. 2.8

$$ln\left(\frac{C_0}{C_t}\right) = k_a t \text{.....Eq. 2.18}$$

is often used to obtain the k_a apparent reaction rate.

A plot of $ln\ (C_o/C_t)$ versus t represents a straight line, the slope of which upon linear regression equals the apparent first-order rate constant k_a. It has been agreed, with minor doubts that the expression for the rate of photo-mineralization of organic substrates with irradiated TiO_2 follows the L–H law for the four possible situations; (a) the reaction takes place between two adsorbed substances, (b) the reaction occurs between a radical in solution and an adsorbed substrate molecule, (c) the reaction takes place between a radical linked to the surface and a substrate molecule in solution, and (d) the reaction occurs with both of species being in solution (Konstantinou et al., 2004). In all cases, the expression for the rate equation is similar to that derived from the L–H model, which has been useful in modelling the process, although it is not possible to discover whether the process takes place on the surface in the solution or at the interface (Bianco Prevot et al., 2001).

However, data linearization also transforms the random (Gaussian) distribution of the error term, which is contrary to the fundamental assumption of random errors used in the derivation of linear regression. Therefore, data linearization techniques are suitable for only preliminary examinations. The correct values of the reaction rates can be obtained from Eq. 2.17 using nonlinear regression/fitting techniques that are provided by many modern statistical software packages.

It is also emphasised that both the k reaction rate constant were used in the L-H model and the k_a apparent reaction rate constants used in the first order model are lumped (bulk) parameters. These parameters take into account a number of factors, such as hydraulic conditions and photonic conditions. It follows that the obtained rate values, that are valid only for the given experimental conditions, cannot be used for the up-

scaling of equipment, nor to compare catalyst performances reported elsewhere. Their main use is to quantify and compare: firstly, the relative performance of a given catalyst, and secondly, the effect of various experimental factors.

2.3 Synthesis methods for higher order assemblies titania

Photo-oxidation of organic contaminants occurs due to the electron-hole pairs of the TiO_2 semiconductor after being excited by UV light with energy equal to or greater than the band gap energy of semiconductor. However, the transportation of photo-excited electrons is limited due to low electron diffusion coefficients and the scattering effect of free electrons (Roy et al., 2010). The electron-trapped sites could occur at defects, surface states and grain boundaries between nanoparticles (Yan et al., 2011). Consequently, charge collection efficiency declined due to the increment of charge recombination at the trapping sites (Park et al., 2006). In addition, the substantial drawback of TiO_2 as a photocatalyst is its wide band gap which is only effective under UV irradiation and not under solar light that contain about 4% of UV rays (Kim et al., 2005; Wang, Yu, et al., 2007). Other significant drawbacks of TiO_2 nanoparticles are often related to the separation and recycling of the particulate catalysts from the reaction media (Costa et al., 2009). Filtration of ultra-fine nanoparticles is a tedious and time-consuming separation process.

Several attempts have been made to overcome these limitations. Recent studies have focused on nano structuring of titania such as nano-tubes, nanorods and nanowires and is a proven method to optimize and fine tune the photochemical process (Liu et al., 2012). Titanates exhibit unique properties of high aspect ratio of TiO_2 nanotubes including large surface area, distinct crystal structures, high cation exchangeability, high

catalytic activity, easier separation and recyclability (Izawa et al., 1982; Lee et al., 2000; Mohamed et al., 2011; Um et al., 2001) and photocatalysis (Dmitry et al., 2008; Ishihara et al., 2002; Zhuang et al., 2007). These advantages make nanostructuring attractive for industrial scale applications. The higher ordered assemblies of TiO_2 nanotube arrays are expected to improve the charge collection efficiency due to the fast electron transportation along the 1D channel with minimum charge recombination site. Ohsaki et al., (2005) utilised TiO_2 nanotubes and were able to suppress the possibility of charge recombination.

Apart from this, the electron diffusion coefficients of TiO_2 nanotubes exhibit longer diffusion lengths and longer electron life time with excellent electron transport. Moreover, TiO_2 nanotubes can deliver a strong light scattering effect and enhance light harvesting properties (Yan et al., 2011). The larger surface area is available to enhance the adsorption and chemical reaction of organic pollutant. For this reason, researchers are interested in synthesising ordered arrays of nanotubes especially in the application of photo electrochemical water splitting and dye sensitized solar cells (Roy et al., 2011; Roy et al., 2010). However, dispersed non-ordered nanotubes demonstrated great potential as heterogeneous catalysts that could accelerate the photocatalytic degradation of organic pollutants in liquid medium (Neville et al., 2013).

There are three popular approaches to the synthesis of TiO_2 and titanate nanotubes, namely, chemical (template) synthesis, electrochemical approaches (e.g., anodizing of Ti), and the alkaline hydrothermal method. Each fabrication method has unique advantages and functional features and comparisons of these three approaches are compiled in Table 2-2.

Table 2-2: Comparison of typical synthesis of titanate

Fabrication methods	**Characteristics**
Template-assisted method	• Ordered arrays • Advantages: The dimension of nanotubes can be controlled by the size and type of applied templates; Uniform size of nanotubes can be created • Disadvantages: Nanotubes morphology may be destroyed during post-removal of the templates; Dissolution of template may result in contamination of nanotubes
Electrochemical anodization method	Oriented arrays • Advantages: The dimension of nanotubes can be controlled by varying the voltage, electrolyte, pH and anodizing time; Ordered alignment of nanotubes with high aspect ratio can be formed • Disadvantages: The requirement of fabrication apparatus Length distribution and separation of nanotubes over a large surface area is not well-developed
Hydrothermal treatment	• Random alignment or can be aligned • Advantages: Easy route to obtain nanotubes in relatively large amount • Disadvantages: Difficult in achieving uniform size of nanotubes

Source: (Liu et al., 2014; Ou & Lo 2007; Pang et al., 2014)

2.3.1 Chemical template synthesis

This method utilizes the morphological properties of known and characterized materials (i.e. templates) in order to construct materials with a similar morphology by methods including reactive deposition or dissolution. Adjusting the morphology of the template material, it is possible to prepare numerous new materials with a regular and controlled morphology on the nano and micro scale. Generally, TiO_2 nanotubes derived from the

templates are obtained after removing templates by selective chemical etching (Qiu et al., 2012) or thermal decomposition (Kim et al., 2012). It is prerequisite that the template material needs be destroyed after synthesis which leads to an increase in the cost of materials. Moreover, it is also essential to maintain a high level of surface cleanliness to ensure good adhesion between the substrate and the surface coating.

The synthesis of TiO_2 nanotubes by chemical templating usually involves controlled sol-gel hydrolysis of solutions of titanium-containing compounds in the presence of templating agents, followed by polymerization of TiO_2 in the self-assembled template molecules or deposition of TiO_2 onto the surface of the template aggregates. The next stages are selective removal of the templating agent and calcination of the sample. This sol-gel template processing making use of porous alumina, polymer fibres or super molecular compound as a template, and their diameters was normally larger than 50 nm (Ji et al., 2007; Jung et al., 2002; Jung et al., 2005). The walls of the TiO_2 nanotubes, prepared by deposition in porous alumina membrane, consisted of anatase nanoparticles and contained mesopores arising from the spaces between the anatase particles (Imai et al., 1999; Yuan & Su 2004). Hoyer's research team (1996), firstly reported the formation of the pore diameter of 70-100 nm TiO_2 nanotubes via sol-gel transcription process.

Porous alumina, produced by the anodization of aluminium foil, has been widely used as a template for the preparation of TiO_2 nanotubes. The internal surface of cylindrical pores of anodic alumina is used for the deposition of TiO_2 thin films from various precursors (Inoue et al., 2003; Liu et al., 2002). After selective removal of alumina, the external diameter of the TiO_2 hollow fibres corresponds to the diameter of the pores in

the alumina. Recently, Kara-man et al., (2013) illustrated that TiO_2 nanotubes thin films could be deposited over electrospun polymethyl methacrylate fibres using the hot filament chemical vapour deposition method. Post-heat treatment of the deposited materials leads to the decomposition of polymericinner layer and formation of randomly distributed anatase TiO_2 nanotubes. Several types of soft template had been reported in the literature such as core-shell-corona cylindrical polymer brushes, self-assembled block copolymers and biological superstructures (Müllner et al., 2012).

2.3.2 Electrochemical anodization synthesis

Highly ordered and vertically oriented TiO_2 nanotubes can be fabricated by potentiostatic anodization of Ti metal under suitable electrolyte and processing conditions. TiO_2 nanotubes are obtained after the process which initially involves the formation of a barrier layer and followed by rather well-defined nanoporous structure (Grimes 2007; Lai et al., 2011; Macak et al., 2007; Macak et al., 2006). The Ti metal was used as substrate for TiO_2 nanotubes to grow. The amorphous TiO_2 nanotubes can be obtained at the end of the anodization process. This amorphous phase of nanotubes needs to be crystallized using the high temperature annealing process (Lai et al., 2012; Mahajan et al., 2008; Mor et al., 2005).

Electrochemical anodization is an electrolytic process that creates a protective or decorative oxide layer over a metallic surface (Lai & Sreekantan 2014). Synthesis of TiO_2 nanotubes using electrochemical anodization method is preferred due to the simplicity in preparation and handling and being more controllable than the other methods (Fujishima et al., 1972). Generally, vertically oriented nanotubes offer large specific surface areas, which have tube-like structures with circular nanotubular opening

that serve as a scaffold to anchor light-harvesting assemblies (Grimes 2007; Sun et al., 2010). The diameter of the opening ranges from 20 nm to 350 nm and the length of the tube can vary from 0.2 μm to 1000 μm depending on the processing parameter. The bottom parts of the nanotubes which are in the form of domes are called barrier layers, typically in shapes of hexagons or pentagons (Mohapatra et al., 2007; Mor et al., 2006; Paulose et al., 2007).

In the anodizing cell, Ti is used as an anode and it is connected to positive terminal of power source, whereas platinum is used as a cathode that is connected to a negative terminal of a power source (Macak et al., 2008; Macak et al., 2006). There are a few other candidates for the cathode, which consists of carbon, lead, nickel, or stainless steel. The cathode has to be an inert electrode and nonreactive in the electrolyte bath (Allam et al., 2008; Mor et al., 2006). Generally, the geometrical feature of the nanotubes is controlled by a variety of parameters such as anodization potential, electrolyte composition, and properties such as conductivity and viscosity, as well as anodization time and temperature. From the theoretical perspective, an anodic oxide layer growth involves field assisted oxidation of anodic Ti film. The high electric field across the anodic oxide layer will induce the Ti–O bond polarization. Then, Ti–O polarization will lead to pit formation. These random pits will then etch into the nanotubular structure in the presence of fluoride ions via chemical dissolution reaction.

2.3.3 Hydrothermal method

Hydrothermal synthesis can be defined as a heterogeneous reaction in the presence of aqueous solvents under high pressure and temperature to produce the crystalline structure (Lai, Juan, et al., 2014; Nakahira et al., 2010; Yada et al., 2008; Yoshimura et

al., 2008). The crystal growth occurs in a steel pressure vessel known as an autoclave where a nutrient is supplied along with water. A temperature gradient must to be maintained in the growth chamber so that the hotter end dissolves the nutrients whereas the cooler end causes the seeds to grow further. The growth rate of the seeds will increase with increasing concentration of solvent, crystallization temperature, and temperature gradient (Huang et al., 2003; Nian et al., 2006; Yuan & Su 2004).

Initially, Kasuga et al. (1998) reported a hydrothermal method for the synthesis of TiO_2 nanotubes by treatment of amorphous TiO_2 with a concentrated solution of NaOH in a polytetrafluoroethylene-lined batch reactor at elevated temperatures. In a typical process, several grams of TiO_2 raw material were converted into nanotubes at temperatures ranging from 110 to 150°C, followed by washing with water and HCl. Since then, the hydrothermal method has attracted more attention from the scientific community due to the simple, cost-effective and environmental friendly method for large scale production of nanotubes. These synthesis conditions could be adjusted to fabricate alternative low dimensional of TiO_2 nano-structures (Bavykin et al., 2006). These nanostructures included TiO_2 nanotubes, nanofibres, nanowires, nanoribbons and nanorods by controlling various parameters during hydrothermal synthetic conditions.

However, the main disadvantage of hydrothermal fabrication is the inability to form nanostructured tubes which are well aligned and ordered. Furthermore, hydrothermal treatment requires long reaction duration and the addition of highly concentrated NaOH which has difficulty in obtaining uniform size of TiO_2 nanotubes (Lei et al., 2010). Although this synthesis method had been carried out extensively over the past decade,

the crystalline structure, composition, thermal stability and formation mechanisms are still not fully understood and proved to be controversial.

2.3.4 Mechanism of Titanate formation via alkali hydrothermal treatment

The fabrication of titania nanotubes by hydrothermal synthesis is done by reacting titania nanopowders with an alkaline aqueous solution (NaOH or KOH) as a mineralizer. The hydrothermal method of titania nanotube production has been comprehensively investigated in the past decade, while the formation mechanisms, compositions, crystalline structures, thermal stabilities and post-treatment functions still remain areas of debate (Bavykin et al., 2004; Guo et al., 2008; Morgan et al., 2011). This technique is usually carried out in an autoclave (a steel pressure vessel) under controlled temperature and/or pressure. The operating temperature is held above the water boiling point to self-generate saturated vapour pressure (Chen & Mao 2007; Wang, Shi, et al., 2007). This hydrothermal process is hence performed at high pH values and pH plays an important role in controlling the shape and crystal structure of the 1D nanostructured titanate intermediate compound (Einarsrud et al., 2014; Pang et al., 2014; Santara et al., 2013). TiO_2 nanoparticles will transform to nanotubes when the reactive Na^+ and OH^- species react with TiO_2 and form Ti–O–Na and Ti–OH bonds. At this stage, the particles will be transformed into lamellar structure and finally roll up to form tubular structure to reduce the high energy (Mohamed et al., 2011; Viriya-Empikul et al., 2008). Furthermore, taking Na-titanate as an example, it can be turned into H-titanate through acid exchange with acids such as HNO_3, HCl or acetic acid (Dmitry et al., 2008; El Saliby et al., 2013). These metastable 1D H-titanate structures are ideal precursors for further conversion into anatase nanorods by heat treatment at about

500°C. The simplified chemical reactions of the as-prepared materials are illustrated in 2.10 to 2.12.

$$5TiO_2 + 2NaOH \rightarrow Na_2Ti_5O_{11}.H2O \quad \text{.....Eq. 2.10}$$

$$Na_2Ti_5O_{11}.H2O + 2HCl \rightarrow H_2Ti_5O_{11}.H_2O + 2NaCl \quad \text{.....Eq. 2.11}$$

$$H_2Ti_5O_{11}.H2O \rightarrow 5TiO_2 + 2H_2O \quad \text{.....Eq. 2.12}$$

Thus the final TiO_2 anatase nanostructures are obtained by a three-step reaction process: (i) the reaction of TiO_2 precursor with alkaline NaOH solution under hydrothermal conditions to form an intermediate rod shaped titanate compound; (ii) the ion exchange of the intermediate titanate compound to replace Na^+ with H^+ and finally; and (iii) final calcination to form the target rod-shaped compound.

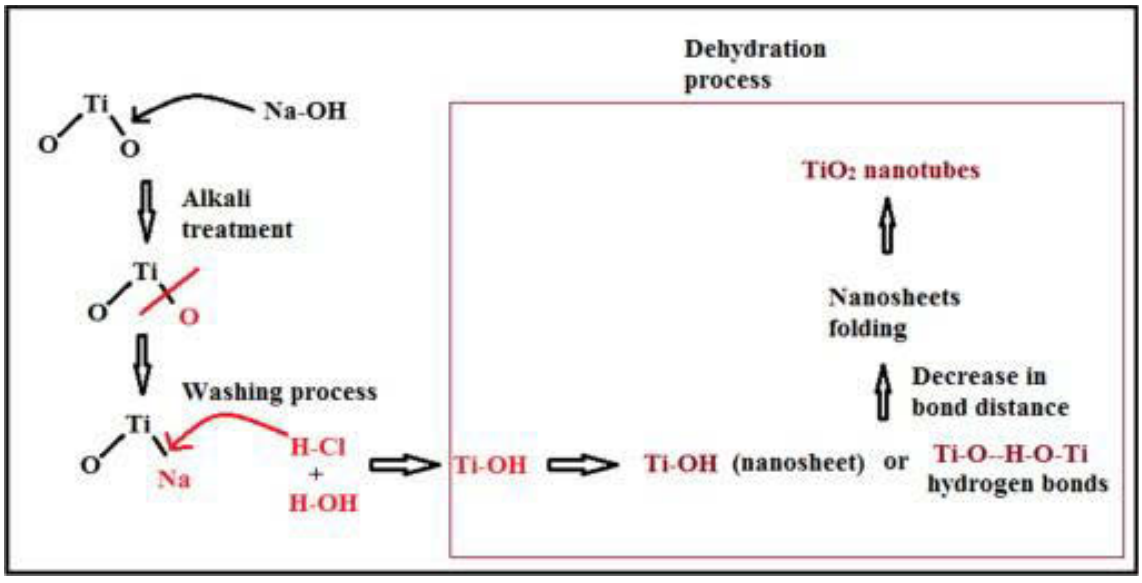

Figure 2-2: Formation mechanism of TiO_2 nanotubes using hydrothermal method (Chen & Mao 2007; Wong et al., 2011).

K-titanate can also be transformed into 1D TiO_2 nanostructures through a second hydrothermal synthesis. Currently our understanding of the formation mechanism of the 1D TiO_2 nanostructures is incomplete, but it is most probable that the titanates are formed by a dissolution-reprecipitation mechanism leading to highly anisotropic

structures. For example there is mechanism where nanosheets are exfoliated from the crystalline TiO_2 precursors and combined into the titanates (Einarsrud et al., 2014; Santara et al., 2013). Figure 2-2 shows the schematic model for the formation of TiO_2 nanotubes.

2.3.5 Influencing factors of hydrothermal method on titania

The structure of titanate nanotubes is easily affected by the phases and particle sizes of the starting materials (Morgan et al., 2011), concentrations and types of the alkaline solution (Sikhwivhilu et al., 2009), synthesizing conditions (reaction time and synthesis temperature)(Viriya-empikul et al., 2009) and post-hydrothermal treatments (acid washing and calcination temperature) (Turki et al., 2013). Apart from this, assisted method of hydrothermal synthesis such as the conventional (Kitano et al., 2013), ultra sonication (Viriya-empikul et al., 2009; Zhu et al., 2001) and microwave-hydrothermal (Huang et al., 2013; Ou et al., 2008) have influenced titanate fabrication.

2.3.5.1 Titanium source

The hydrothermal synthesis of titania nanotubes can start with different titania powders such as rutile or anatase TiO_2, Degussa TiO_2 (P25) nanoparticles, layered titanate $Na_2Ti_3O_7$, Ti metal, $TiOSO_4$, molecular Ti^{IV} alkoxide, doped anatase TiO_2, or SiO_2-TiO_2 mixture (Wang et al., 2008). It has been observed that the structural properties of the nanostructured TiO_2 products are markedly dependent on different starting TiO_2 materials. However, the effects of different phases and particle sizes of the starting materials for titanate nanotubes are still being debated (Pang et al., 2014). Basically, nanotubes with outer diameters between 10 and 20 nm can be obtained using the hydrothermal method when starting with titania powder having a relatively large

particle size, such as rutile TiO_2, Degussa TiO_2 (P25), and SiO_2-TiO_2 mixture (Wang et al., 2008). Several researchers summarizes their results for the formation morphology of titanate nanotubes using different types of starting materials, alkaline solution and hydrothermal treatments (Liu et al., 2014; Ou & Lo 2007; Pang et al., 2014; Wang et al., 2008).

Morgan et al., (2011) observed that the dissolution process of anatase precursor corresponded to zero-order kinetics, where the dissolution was independent of precursor concentrations. They also observed that anatase with small crystalline and rutile phase with big crystalline size could produce nanotubes with lengths up to several hundred nanometres, but the former starting material could produce nanotubes with a smaller average external diameter. Although Yuan et al., (2004) reported that amorphous TiO_2 could only produce nanofibres and not nanotubes, Ylhäinen et al., (2012) claimed to obtained nanotube products from amorphous precursors. Hence, it seems that there were other parameters playing a role apart from the crystalline form of TiO_2.

Yuan and Su (2004) reported that the effect of particle size of the starting material toward the yield of the produced nanotubes was quite small in comparison to the hydrothermal temperature and concentration of alkaline solution. On the other hand, Dawson et al., (2010) concluded that the length of titanate nanotubes was influenced by both phase and particle size of the starting material. Pure anatase phase with a particle size of 300 nm could produce nanotubes up to 1 m in length, micrometre sized of TiO_2 with mixed phases produced tubes with lengths between 200 and 500 nm, while P25 mixed phases with particle size of 30 nm produced lengths of less than100 nm.

2.3.5.2 Type and concentration of alkaline

Types of alkaline type and their concentrations play an important role in the hydrothermal process. Hydrothermal treatment of TiO_2 in the presence of a concentrated solution of KOH always transforms titania into titanate nanofibre over a wide range of temperatures (Jiasheng et al., 2012; Sun et al., 2002; Yuan, Zhang, et al., 2004; Zaremba et al., 2010). Furthermore, Bavykin et al., (2010) discovered that titanate nanotubes could be prepared using 10 M KOH and low temperature of 56°C after 12 days. The concentration of dissolved Ti^{4+} in 10 M KOH solution also positively depends on temperature but is several times higher than in NaOH solutions. The most favourable titanate nanotubes were prepared via hydrothermal treatment of TiO_2 powders in a 10 M NaOH solution (Morgado Jr et al., 2007; Papa et al., 2009). In contrast, only small proportion of nanotubes were formed when NaOH concentration was less than 5 M or higher than 18 M (Sikhwivhilu et al., 2009).

The concentration of dissolved Ti^{4+} in solution can determine the rate of crystallization of titanate nanosheets, which in turn controls the morphology of the final nanostructures (Bavykin et al., 2006). Bavykin et al., (2004) found that an increment in the molar ratio of TiO_2 to NaOH generally resulted in higher average pore diameter and a reduction in the specific surface area. Meanwhile, the pore volume of nanotubes was independent of the molar ratio of TiO_2 to NaOH. Furthermore, Huang et al., (2011) demonstrated that nanosheets, nanotubes and nanowires were three kinetic products derived from the reaction of TiO_2 with NaOH when increasing alkaline condition from 5 to 12 M. They observed that the nanowires had wider diameters and were longer in length when compared to the nanotube' morphology. However, Sikhwivhilu et al., (2009) reported that a small portion of shorter nanotubes was produced when the concentration of

NaOH solution increased to 18 M. Thus, the concentration of NaOH could influence the yield of tubular morphology.

Furthermore, Bavykin et al., (2010) discovered that titanate nanotubes could be prepared using 10 M potassium hydroxide (KOH) and low temperature of 56°C after 12 days. Thus, titanate nano-tubes could also be produced using a NaOH/KOH binary aqueous mixture at 100°C (Bavykin et al., 2010). A few years ago, Sikhwivhilu et al., (2009) found that potassium titanate nanotubes could also be produced by hydrothermal treatment in 10 M KOH at 120 and 150°C for 24 h. They reported that KOH was more reactive with TiO_2 and yielded different shapes of nanostructured materials compared to NaOH. Ammonium hydroxide solution demonstrated no influence on the microstructure of TiO_2. Meanwhile, similar spherical morphology was observed in 10 M lithium hydroxide (LiOH) at the temperatures of 120 and 150°C (Sikhwivhilu et al., 2009), whereas a flower-like structure on the TiO_2 surface could be obtained when treated in 10 M LiOH solution at a temperature of 80°C (Hasegawa et al., 2012).

2.3.5.3 Temperature and duration

Generally, the amount, length and crystallinity of titanate nanotubes increase when the hydrothermal temperature also increases (100-200°C) (Sreekantan et al., 2010). In this context, the largest specific surface area along with the larger inner diameter of titanate emerged at synthesis temperature of 130-150°C (Horváth et al., 2007; Seo et al., 2001; Viriya-empikul et al., 2009). Elevated temperatures from 180 to 250°C mainly produce nanoribbons or nanowires like morphologies if KOH were used as the alkaline solution (Ou & Lo 2007). Subsequent rises in temperature resulted in a sharp reduction in pore volume of produced samples and wider size distribution in the diameter of fibres

morphology. However, the average outer diameters of the nanotubes produced at 110, 130 and 150°C for 24 h were similar and observed to be about 10 nm (Sreekantan et al., 2010). A reasonable explanation was proposed that temperatures less than 130°C led to less cleavage of Ti–O–Ti bonds, which was the initial stage in synthesizing titanate (Ou & Lo 2007). Treatment at a temperature >130°C would destroy the lamellar TiO_2, an intermediate in the titanate formation process. Poudel et al., (2005) first related the filling fraction and pressure of the autoclave to the characterizations of TNTs. Either case of filling fraction or acid washing governs the performance of crystallization, where the optimum filling fraction (86% to the vessel volume) and 0.1N HCl were reported to be capable of good crystalline formation.

On the other hand, the production of nanotubes increases with prolonged duration of hydrothermal treatment, but this prolonged duration may lead to the transformation from nanotube to nanofibre (Ma, Fukuda, et al., 2005). At higher temperatures, the time required for the formation of titanate should be reduced in order to get nanotubular structure. According to Dong et al., (2011), many thin sheets and some nanotubes coexist at 130°C if the hydrothermal reaction time is extended to 12 h. At 24 h, many nanotubes and quite a few thin sheets are observed. After 36 h of hydrothermal reaction, almost all the products are nanotubes. At a temperature of 150°C, 15 h are enough for the complete conversion of commercial titania nanoparticles into nanotubes (Sreekantan et al., 2010). This indicates that reaction temperature and duration is a key factor in determining the overall morphology of the product.

2.3.5.4 Washing procedure

Acid washing might affect the nanotubes formation (Kasuga et al., 1999), crystalline structure or even chemical composition of the final nanotubes product (Preda et al., 2013) during the hydrothermal treatment. Kasuga et al., (1999) conclude that acid washing was a crucial step in the titanate formation process and its purpose was to remove electrostatic repulsion of residual charge, in which Ti O Na was converted into TiOH. Then, the dehydration of Ti-OH bonds could result in the formation of nanotubes from nanosheets. Alternatively, several other researchers suggested that acid washing was applied for the ion-exchange process because they found that titanate nanotubes were formed during hydrothermal reaction (Du et al., 2001; Lan et al., 2005; Morgado Jr et al., 2006; Morgan et al., 2011; Seo et al., 2008). According to Morgado Jr et al., (2006) acid washed titanate nanotubes possess stronger hydroxyl bonds after replacement of sodium ion by proton, which results in decrement of interlayer spacing and increment in specific surface area. Researchers often reported an optimum concentration of hydrochloric acid (HCl) during acid washing in order to effectively prepare the sodium-free nanotubular structure. An optimum concentration of HCl (0.2N) during the washing process was suggested because the rapid removal of electrostatic charges caused by high acid concentration is detrimental to the formation of titanate nanotube (Tsai et al., 2004). Any further increase in the concentration of HCl will destroy nanotubular structures (Turki et al., 2013).

2.3.5.5 Calcination

Various morphologies of titanate fabricated using hydrothermal treatment are the result of the post-treatment. The calcination process that takes place during post-treatment is believed to affect the phase structures and microstructure of titanate nanotube products

(Wang et al., 2008; Wong et al., 2011). It is believed that calcination process can induce the transformation of titanate to anatase phase, modify microstructure based on the amount of sodium present in nanotubes, improve crystallinity and reduce the material's surface defects (Chen & Mao 2007). From the point of view of practical usage, it is essential to study the structural stability of the titanate nanotubes and their corresponding microstructure changes at various calcination temperatures. Lan et al. (2005) found that short, solid nanotubes were obtained at a calcination temperature of 500°C. The radius of the titanate nanotubes was 8 to 22 nm and the calcined product was consistent with the structure of a pure anatase phase. Weng et al., (2006) stated that the crystallinity of the titanate nanotubes increased with the calcination temperature. The TiO_2 powders assumed a thin wall nanotubular structure when treated at 400°C while its microstructure was comparable to samples that were not subjected to the calcination process. At 600°C, the nanotubes amalgamated and agglomeration of nanoparticles was observed when the calcination temperature rose to 800°C.

2.3.5.6 Assisted hydrothermal synthesis

Recently, Pang et al., (2014) summarises the details of several assisted hydrothermal techniques on the conventional (Kitano et al., 2013), ultra sonication (Viriya-empikul et al., 2009; Zhu et al., 2001) and microwave-hydrothermal (Huang et al., 2013; Ou, Lo, et al., 2007) methods for synthesizing titanate nanotubes (Table 2-3).

Table 2-3: Assisted hydrothermal method for preparation of titanate nanotubes.

Auxiliary methods	**Conditions hydrothermal reaction**	**Dimensions of nanotubes**
Conventional hydrothermal	• 5 g TiO2 powder in 10 M sodium hydroxide (NaOH) • 150 ◦C for 20 h • Acid washing with 0.1 M nitric acid (HNO_3)	Average (D_o) = 9 nm Average (D_i) = 6 nm ; Interlayer spacing= 0.7 nm (2-4 walls); L = 0.3–3.0 m; Specific surface area = 423 m2/g (Kitano et al., 2013)
Ultrasonication-assisted hydrothermal	• 150 mg TiO2 powder in 30 mL of 10 M NaOH • Mixture was sonicated at 280 W for 60 min • 110 ◦C for 4 h • Acid washing with 0.1 M HNO_3	Average Do = 5 nm Wall thickness = 1.3 nm L = 200–300 nm (Zhu et al., 2001)
	• 0.5 g TiO2 powder in 50 ml 10 M NaOH • Mixture was sonicated at 7.6, 38.1 W for 8 min • 150 ◦C for 3 days • Acid washing with 0.1 M hydrochloric acid (HCl)	D_i = 4–6 nm; Interlayer spacing = 0.8 nm (2-6 walls); Average hydrodynamic size of 53, 490 & 1760 nm at sonication power of 0, 7.6 & 38.1 W; Specific surface area = 179, 258 & 248 m^2/g at sonication power of 0, 7.6 & 38.1 W (Viriya-empikul et al., 2009)
Microwave-assisted hydrothermal	• 0.5 g TiO2 rutile in 25 ml of 10 M NaOH • Microwave power for 45 min at 200 ◦C • Acid washing with 0.1 M HNO3	D_i = 3–5 nm D_o = 8–10 nm L = 100–500 nm Interlayer spacing = 1 nm (3–4 walls) Specific surface area = 214 m^2/g (Huang et al., 2013)
	• 0.6 g P25 TiO2 in 70 ml 10 M NaOH • Microwave power of 70, 400, and 700 W at 130°C for 3 h Acid washing with 0.5 M HCl	Average D_o = 9.9 nm Average D_i = 5.1 nm; Interlayer spacing = 0.82, 0.86 & 0.90 nm at microwave power of 70, 400 & 700 W (4–5 walls) Specific surface area = 323, 367 & 320 m^2/g at microwave power of 70, 400 & 700 W (Ou, Lo, et al., 2007)

Source: (Pang et al., 2014)

In the synthesis a larger range of nanomaterials including titanate nanotubes, ultrasound technology has been widely employed (Guo et al., 2008; Ma et al., 2006; Tan et al., 2012; Viriya-empikul et al., 2009; Zhu et al., 2001). During the hydrothermal synthesis of titanate nanotubes, the sonication-assisted technique not only disperse TiO_2 precursor uniformly in the alkali solution (Guo et al., 2008; Tan et al., 2012), but also controls the morphology of the titanate nanotubes. Sonicating the mixing solution facilitates the formation of thin and small titanate sheets even prior to the hydrothermal treatment (Zhu et al., 2001) and the length, BET surface area and morphology of TiO_2 nanotubes can be enhanced by applying a combination of sonication pre-treatment and varying there action temperature (90–180◦C) (Viriya-empikul et al., 2009).

Hydrothermal reaction via microwave irradiation has gained interest in the past decade as it saves time, energy, and is environmental friendly method. Ou et al., (2007) successfully synthesised titanate nanotube having the composition of $Na_xH_2{-}xTi_3O_7$ with BET surface area of 256 m^2/g under 400 W irradiation at 130°C for only 1.5 h and suggested that Na Ti O bonds are favourably generated under a higher microwave irradiation power. The multiwall structured titanate nanotubes with central hollow, open-ended tubes with diameters of 8–12 nm, and lengths of 200–1000 nm can be synthesized by irradiating the mixture of (anatase or rutile) TiO_2 precursor and 8–12 M NaOH solution in the microwave reactor (195 W) for only 90 min (Wu et al., 2005). The positive effect of microwave irradiation on their morphology could enhance the photocatalytic efficiency of titanate nanotubes as reported by Huang et al., (2013) for photocatalytic activity for NO decomposition and methylene blue degradation. Peng et al., (2010) also reported nitrogen-doped titanate nanotubes synthesized by the

microwave hydrothermal method indicated a marked ability photodegrade methyl orange under visible-light illumination.

2.4 Model water pollutant

Over the last two decades, photocatalysis with TiO_2 nanoparticles has been shown to be useful for the degradation of wastewater pollutants. This process has several advantages including complete mineralization of organic pollutants like aliphatics, aromatics, polymers, dyes, surfactants, pesticides and herbicides to CO_2, water and mineral acids, no waste solids to dispose of and mild temperature and pressure conditions. However, the model pollutants utilised as per this research study's specific are summarised in the sub-sections below:

2.4.1 Synthetic wastewater

Synthetic wastewater (SWW) is a complex blend of several organic and inorganic compounds. The organic constituents are; beef extract (a mixture of peptides and amino acids, nucleotide fractions, organic acids, minerals and some vitamins (Asif Durrani 2011), peptone (an enzymatic digest of animal protein consisting of short polymers of amino acids linked by peptide bonds (Payne et al., 1994); humic acid (a complex mixture of acids containing carboxyl and phenolated groups that behave as a dibasic or occasionally a tribasic acid (Stevenson 1982)); tannic acid (a polyphenolic compound containing hydroxyl groups that cross link to other compounds; sodium lauryl sulphate (an anionic orthosulfonate consisting of a 12-carbon chain attached to a sulfate group (Tupker RA 1997)); and gum arabic powder (a mixture of polysaccharides and glycoproteins (Anderson et al., 1966; Street 1983)). This SWW represents effluent organic matter generally found in the biologically treated sewage effluent which

eventually consists of mixed particulates and soluble substance. This is combined with natural organic matter from drinking water and soluble microbial product derived from biological treatment (Shon, Vigneswaran, Ngo & Ben Aim 2005).

2.4.2 Crystal violet

Crystal violet (CV) is also known as basic violet 3, gentian violet, and methyl violet 10B. Its IUPAC name is N-[4-[bis[4-dimethylamino)-phenyl]-methylene]-2,5-cyclohexadien-1-ylidine]-N-methylmethanaminium chloride (molecular formula $C_{25}H_{30}N_3Cl$ and molecular weight 407.98) and belongs to the class of triarylmethane dyes. The absorption maximum ranges from 589 to 594 nm (Mittal et al., 2010). Chemically, crystal violet is also known as hexamethyl pararosaniline chloride. The chemical structure of the dye is shown in Figure 2-3.

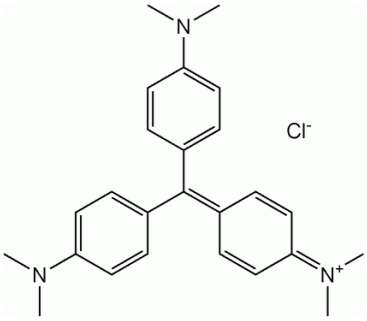

Figure 2-3: Chemical structure of CV

Among the many available dyes, CV is a well-known dye that is used in a variety of ways: as a biological stain; dermatological agent; veterinary medicine; additive to poultry feed to inhibit propagation of mold, intestinal parasites, and fungus; etc. It is also extensively used in textile dying, paint and paper printing (Mittal et al., 2010). However, crystal violet is also a mutagen and mitotic poison (Au et al., 1978; Mohanty et al., 2006).

Aromatic dyes such as crystal violet CV exhibit two main mechanisms of photodegradation. One path involves the consecutive departure of terminal methyl groups (N-demethylation) while the aromatic structure of the molecule is preserved. During this process, a complete transformation of CV into fuchsine basic occurs with an absorption maximum displacement from 590 to 540 nm (Chen et al., 2006; Chen, Mai, et al., 2007). The other path involves the rupture of the conjugated structure, producing the instant bleaching of aromatic dyes. Then, CV arises as a suitable probe that follows the competition between the N-demethylation over the disruption of the conjugated structure (Couselo et al., 2008).

2.4.3 Methylene blue

Methylene blue (MB) is a cationic dye with a molecular formula of $C_{16}H_{18}N_3SCl$ and a molar mass of 319.85 g/mol. Figure 2-4 illustrates the chemical structure of MB. Basically, MB is used in industrial processes such as textile dyeing, chemical manufacturing and in medicine. MB is characterised by high molecular weight, high chemical stability and high water solubility. Textile dyeing processes use large amount of water and therefore they leads to the discharge of significant amounts of coloured wastewater containing toxic wastes. This includes suspended solid, unreacted dye stuffs and auxiliary chemicals (Zhang et al., 2002). From an environmental point of view, the removal of synthetic dyes is of great concern, since some dyes and their degradation products may be carcinogens and toxic. Consequently, their treatment cannot depend on bio-degradation alone (Kannan et al., 2001; Pagga et al., 1986).

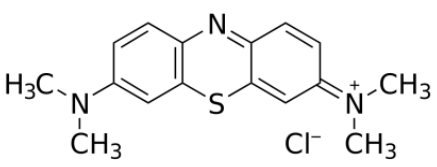

Figure 2-4: Chemical structure of MB.

The photocatalytic degradation of MB over an illuminated suspension or deposited thin films of TiO_2 was achieved under both UV and solar light (Houas et al., 2001; Zhang et al., 2002). Houas et al., (2001) explained the details reading the pathway of MB mineralisation using the evolution of resulting ions (sulphate, nitrate and ammonium) and CO_2 gas via following reaction:

$$C_{16}H_{18}N_3SCl + 25.5O_2 \rightarrow 16CO_2 + 6H_2O + 3HNO_3 + H_2SO_4 + HCl$$

The aromatic metabolites were detected by Gas chromatography/Mass spectrometry (GC/MS) and liquid chromatography/Mass spectrometry (LC/MS) and are presented in Figure 2-5.

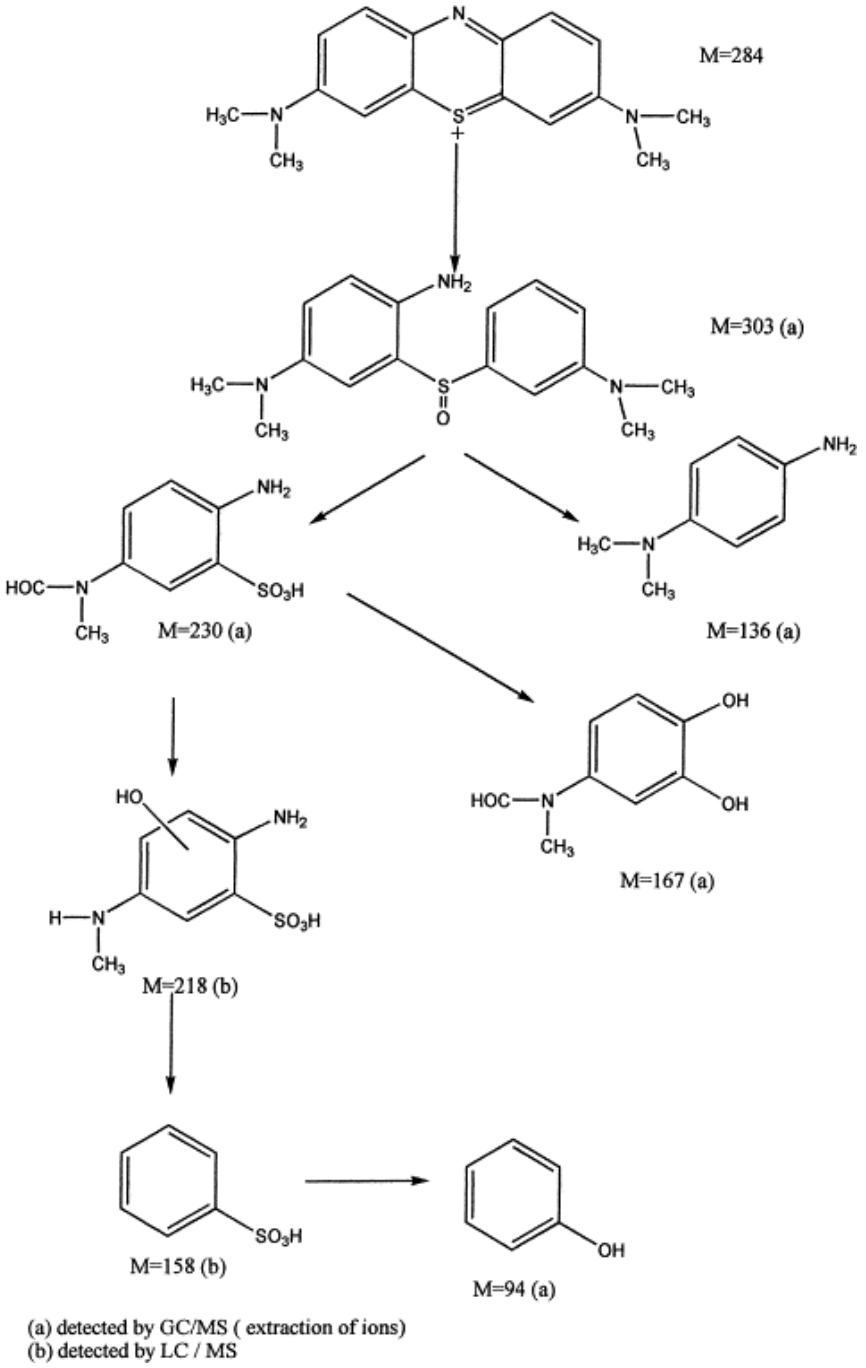

Figure 2-5: Pathway of MB decomposition (Houas et al., 2001)

The mineralisation of MB was plotted in two patterns, one for sulphur and another for nitrogen containing groups. For sulphur, the degradation of MB was initiated by the cleavage of the bonds of the C─S+═C functional group by the attack of an $OH^{\bullet}$ radical to form a sulfoxide (R─S(═O)─R'). A second attack resulted in the formation of a sulfone, a third attack gave sulfonic acid and the final or fourth attack was found to be

enough for the total mineralisation and the formation of SO_4^{2-} anion. In the case of nitrogen, two pathways were described through the progressive attacks of $OH^{\bullet}$ producing phenolic compounds and alcohols/aldehydes before the formation of ammonium and nitrate ions.

2.4.4 Lead

Worldwide, toxic metal pollution in waters is a serious environmental issue due to their toxicity and carcinogenicity. Some toxic metals are dangerous even at trace amounts. Lead (Pb) was selected as a model toxic metal because of its high toxicity and carcinogenicity and because it is listed as a priority heavy-metal pollutant by most national environmental protection agencies.

Various technologies including chemical precipitation (Fu et al., 2012), membrane (Wei et al., 2013) adsorption (Zhang et al., 2013) and electrodialysis (Mahmoud et al., 2012) are well developed for trapping toxic metals from water. With the reference to the available methods, adsorption is one of the most attractive options (Zhang et al., 2013). One dimensional (1D) materials with large surface areas and abundant active sites have been exploited as ideal adsorbents for environmental remediation.

Titanate nanotubes which are usually synthesized via hydrothermal reaction of TiO_2 in alkaline condition possess special physicochemical properties, like uniform microstructure, small tube diameter, large specific surface area (Bavykin et al., 2006; Chen & Peng 2007). Furthermore, titanate nanomaterials with abundant hydroxyl groups on the surface and low point of zero charge can effectively adsorb cations via ion-exchange, and so are good adsorbents for heavy metals (Chen et al., 2010; Xiong et

al., 2011). Consequently, such titanates are increasingly being used as adsorbents to remove various pollutants from waste waters, such as heavy metal cations.

U T S

University of Technology Sydney
FACULTY OF ENGINEERING

Chapter 3: Materials and Methodology

3.1 Materials

3.1.1 Chemicals

All the chemicals used in this research work are listed in Table 3-1 with their respective details.

Table 3-1. List of chemicals

Chemical name	**Supplier**	**Purity (%)**
Hydrogen peroxide	Australian Scientific Pty Ltd.	50
Potassium hydroxide	ChemSupply	85
Sodium hydroxide	ChemSupply	97
Hydrochloric acid	ScharlauChemie S.A	37
Lead nitrate	ChemSupply	99.9
Methylene Blue	ChemSupply	86
Crystal violet	ChemSupply	86
Beef Extract	Bacto Laboratories	(*)
Peptone	Bacto Laboratories	(*)
Humic acid	Sigma Aldrich	(*)
Tannic acid	Sigma Aldrich	99.9
Sodium lignin sulfonate	Sigma Aldrich	(*)
Sodium lauryl sulphate	Sigma Aldrich	99.9
Arabic gum powder	Sigma Aldrich	(*)
Arabic acid (polysaccharide)	Sigma Aldrich	(*)
$(NH_4)_2SO_4$	Unilab	98.5
K_2HPO_4	Unilab	99
NH_4HCO_3	Unilab	98
$MgSO_4 \cdot 7H_2O$	Sigma Aldrich	99.5

*Not specified by the manufacturer.

3.1.2 Synthetic Wastewater

The chemicals used in the preparation of synthetic wastewater (SWW) are listed in Table 3-2. Tap water was used for making up SWW; it has a pH of 6.8 to 7.2, an average DOC of 0.5 mg/L and an average electrical conductivity of 166.4 μS/cm.

Table 3-2. **S**ynthetic wastewater constituents

Compounds	**Concentration (mg/L)**	**Fraction by organic matter**	**Supplier and purity**
Beef extract	1.8	0.065	Bacto Laboratories (*)
Peptone	2.7	0.138	Bacto Laboratories (*)
Humic acid	4.2	0.082	Sigma Aldrich (*)
Tannic acid	4.2	0.237	Sigma Aldrich (99.9%)
Sodium lignin sulfonate	2.4	0.067	Sigma Aldrich (*)
Sodium lauryl sulphate	0.94	0.042	Sigma Aldrich (99%)
Arabic gum powder	4.7	0.213	Sigma Aldrich (*)
Arabic acid	5.0	0.156	Sigma Aldrich (*)
$(NH_4)_2SO_4$	7.1	0	Unilab (98.5%)
K_2HPO_4	7.0	0	Unilab (99%)
NH_4HCO_3	19.8	0	Unilab (98%)
$MgSO_4 \cdot 7H_2O$	0.71	0	Sigma Aldrich (99.5%)

3.1.3 Degussa P25

Titanium dioxide Degussa P25 is a mixed phase nanopowder with anatase, rutile and amorphous structures. It has a surface area of about 50 m^2/g, an isoelectric point around pH 6 and an apparent density of 130 kg/m^3 and mean particle size of about 30 nm (Figure 3-1 and Figure 3-2).

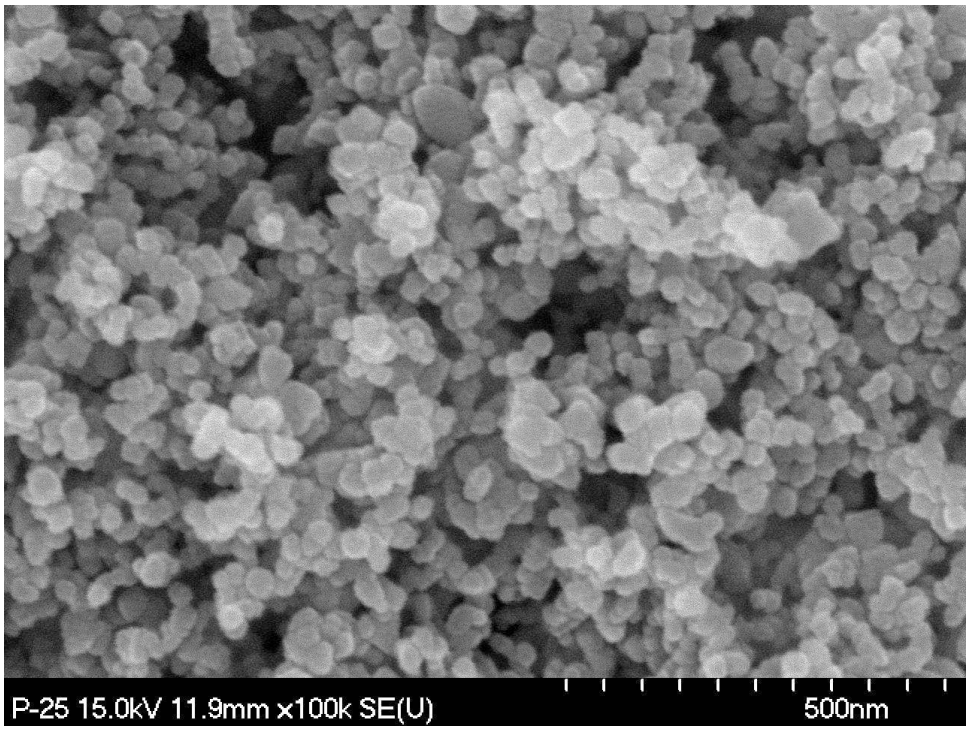

Figure 3-1. SEM image to Degussa P25 titanium dioxide nanopowder

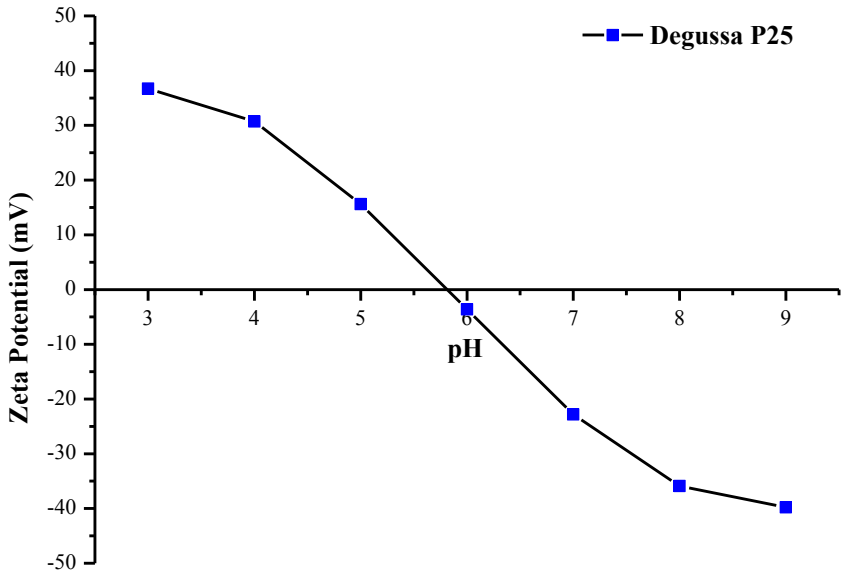

Figure 3-2. Zeta potential of 100 mg/L Degussa P25 suspension in MQ water.

3.1.4 Crystal Violet

Crystal violet (CV) is also known as basic violet 3, gentian violet, and methyl violet 10B. Its IUPAC name is N-[4-[bis[4-dimethylamino)-phenyl]-methylene]-2,5-cyclohexadien-1-ylidine]-N-methylmethanaminium chloride (molecular formula $C_{25}H_{30}N_3Cl$ and molecular weight 407.98) and belongs to the class of triarylmethane dyes. The absorption maximum ranges from 589 to 594 nm (Mittal et al., 2010). Chemically, crystal violet is also known as hexamethyl pararosaniline chloride. The chemical structure of the dye is shown in Figure 2-3.

3.1.5 Methylene Blue

Methylene blue (MB) is a cationic dye with a molecular formula of $C_{16}H_{18}N_3SCl$ and a molar mass of 319.85 g/mol. Figure 2-4 illustrates the chemical structure of MB. Basically, MB is used in industrial processes such as textile dyeing, chemical manufacturing and in medicine. MB is characterised by high molecular weight, high chemical stability and high water solubility

3.1.6 Lead Nitrate

Lead(II) nitrate is an inorganic compound with the chemical formula $Pb(NO_3)_2$. It commonly occurs as a colourless crystal or white powder and, unlike most other lead(II) salts, is soluble in water.

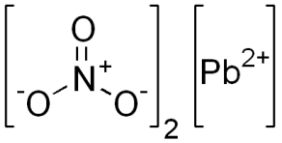

Chemical structure of lead nitreate

3.2 Synthesis

A modified peroxotitanate method was adopted, which involved mixing of 2 g of Degussa P25 titanium dioxide nanopowder with 1% (designated as method A), 3% (designated as method B) and 5% (designated as method C) of H_2O_2 (50%w/w) in 10 M of KOH. The mixtures were homogenised using a magnetic stirrer and placed separately into Teflon-coated Pyrex containers, which were sealed and heated at 100°C in an oven for 24 h. After the hydrothermal treatment, the autoclave was naturally cooled to room temperature. The solid specimens were recovered by centrifugation (Centurion Sci., 2040) at 3000 rpm for 5 min, washed with 1M HCl solution and Milli-Q water until pH 7, and then dried in an oven at 100°C for 12 h. The obtained powder samples, designated as A, B, and C from their respective synthesis methods, were also calcined in a furnace (Labec, CE-MLS) at 600°C for 4 h. These samples are designated as AC, BC and CC, respectively.

3.3 Characterisation and Methods

3.3.1 Scanning Electron Microscope / Energy Dispersive X-ray

Morphology and elemental composition analyses were carried out using a scanning electron microscope (SEM, Hitachi S-4700) equipped with an energy dispersive X-ray detector (EDX-250 supplied by Horiba) operating at 15 kV. The powder samples of potassium polytitanate characterised were dried in an oven at 100°C for 3 h to remove moisture before imaging. The powder specimens were spread on a carbon tape and excess powders were removed by blowing air so as to get uniform particles dispersion. Following this the specimens were positioned in the vacuum chamber of the SEM and images were taken using computer imaging softwares. The elemental compositions of specimens were also examined using an Energy Dispersive X-ray spectroscopy (EDS)

detector. The procedure consisted of pointing the cursor shown on the screen to randomly selected points on the powder and analysing the composition using different software. The elemental composition was generated in terms of percentage.

3.3.2 Transmission Electron Microscope

A Philips CM200 (Netherlands) transmission electron microscope (TEM) operating at 200 kV was employed to obtain micrographs of the potassium polytitanate specimens. First of all, powder samples were dispersed in isopropanol and ultrasonicated for 10 minutes to avoid nano powders aggregations. Two drops of the specimen suspension were placed on a carbon-coated copper grid followed by the evaporation of alcohol at ambient temperature. Afterwards samples were then imaged using TEM and images were obtained at different magnifications.

3.3.3 Specific surface area and pore size measurements

Brunauer, Emmet and Teller (BET) surface area analyses were performed on an automated surface area analyser (Micromeritics Gemini 2360, USA) by means of nitrogen adsorption–desorption. The BET surface area was determined by a multipoint BET method using the adsorption data in the relative pressure (P/P_0) range of 0.05–0.18. Samples' mean pore diameter and total pore volume were determined from the desorption isotherm via the Barret–Joyner–Halender (BJH) model. These samples were purged in N_2 flow for 5 H to remove impurities before measuring their surface area by N_2 adsorption at 77 K with the instrument.

3.3.4 X-ray Diffractometer

X-ray diffraction (XRD) patterns were generated on a MDI Jade 5.0 (MaterialsData Inc., USA) X-ray diffractometer with Cu Kα radiation source. The data were measured

within the range of scattering angle 2θ of 5–90°. The powders of the specimens were used without further treatment.

3.3.5 Malvern Zetasizer

The Zetasizer (ZEN3600, Malvern Instrument, UK) operating with a He-Ne laser at a wavelength of 633 nm was used to measure the zeta potential of potassium titanate nano fibres.

3.4 Photocatalytic reactors

3.4.1 Photo reactor 1

A recirculating photoreactor setup was employed to study the photodesorption of dissolved organic compounds from TiO_2 surface (Figure 3-3). The setup is divided into two different compartments: i) the photoreactor stainless steel columns (C1, C2 and C3) and ii) the adsorption tank (T1). The volume of each column was 70 mL and enclosed 8 watts UVC lamp (Sankyo Denki, G8T5, Japan), while the adsorption tank has a 1 L volume. The suspension of TiO_2 and SWW in the adsorption tank was continuously stirred at 400 rpm using a magnetic stirrer (IKA, C-MAG, MS7). Influent (Q1) was pumped to the first column by an adjustable flow FMI lab pump (Fluid metering, INC, USA, Model QD) through the connections tubes (Masterflex, precision pump tube, 06508-17).

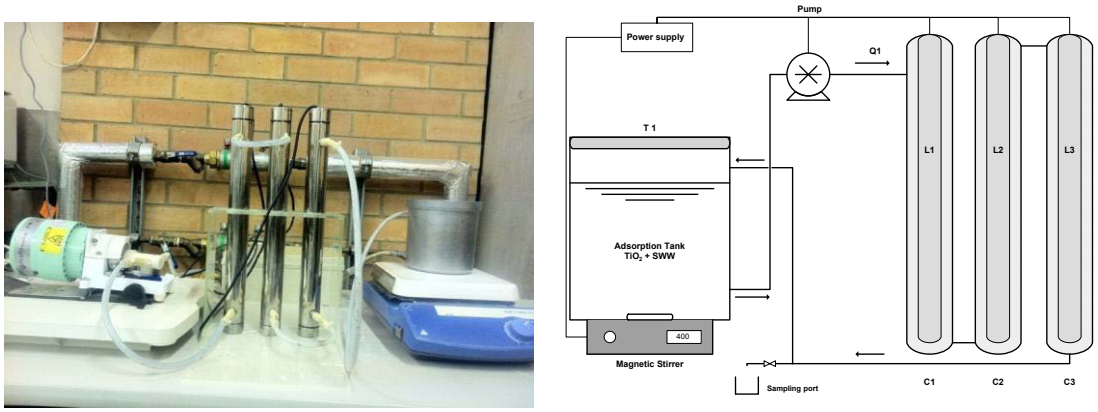

Figure 3-3. Recirculating photoreactor unit (T1: adsorption tank; Q1: influent flow rate; C1, C2 and C3 are the photoreactor columns, L1, L2 and L3 are UVC lamps of 8 watts each) (Left photo and right schematic diagram)

3.4.2 Photo reactor 2

The cylindrical photo reactor of 40 cm × 10 cm dimension had three UVC lamps (Perkin Elmer, 15 W each), a temperature controlling device and an air sparger (0.6 L/min). The lamps enclosed in quartz sleeves were submerged in slurry. The slurry was continuously stirred at 400 rpm using a magnetic stirrer and air sparger. The photocatalytic activity of potassium titanates was assessed by the batch experiments. After the addition of 0.05 g/L photocatalyst, the slurry was mixed with a magnetic stirrer at 400 rpm for 30 min for dark adsorption. Photocatalysis was carried out for 120 min at a stable temperature of 26°C. Slurry samples were then collected at designated intervals and analysed for crystal violet decomposition.

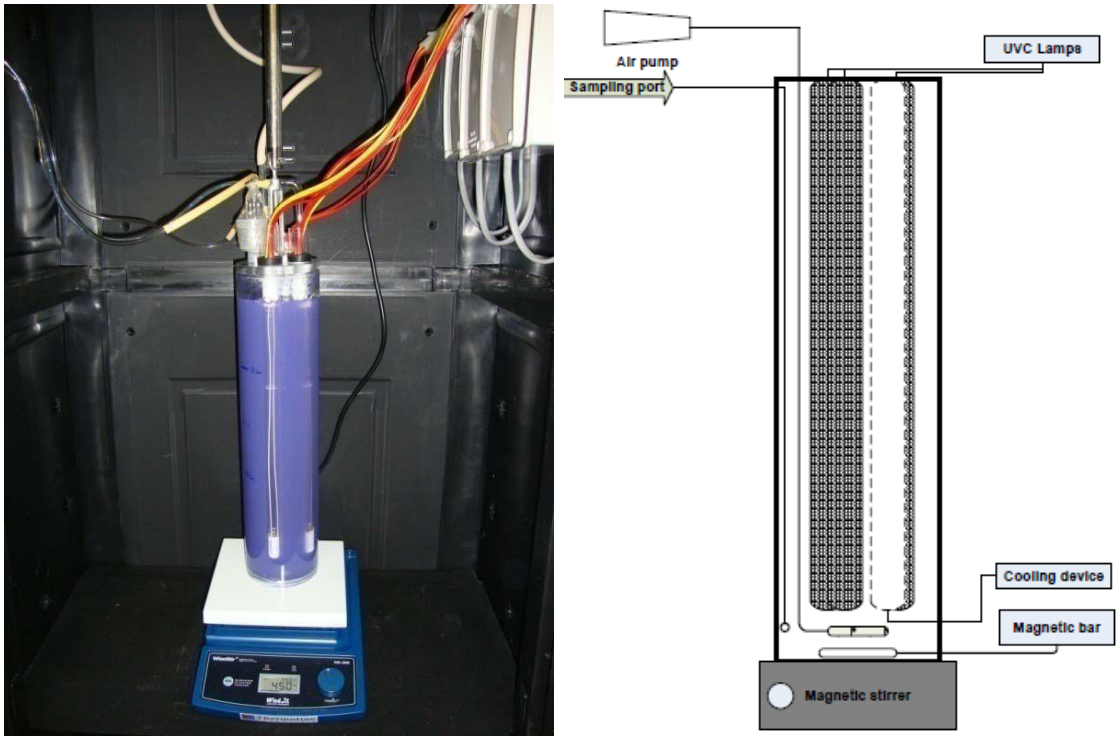

Figure 3-4. Photo (left) and a schematic diagram (right) of batch reactor.

3.4.3 Photo reactor 3

The Luzchem Research SolSim Xenon photoreactor featured an enclosed exposure chamber, an exhaust system and thermostatic control to ensure the chamber temperature remained close to ambient temperature. The Luzchem's SolSim delivers solar simulated radiation based on a powerful 300 W Xenon lamp installed at the top the photoreactor chamber along with a custom filter assembly. The filter system ensured emission that closely matches the AM1.5 spectrum. The solar simulation filters are placed on a stand 3" above the chamber floor, with samples beneath in a 250 ml beaker. Air sparging was adjusted at 0.6 L/min to provide adequate dissolved oxygen to the reaction.

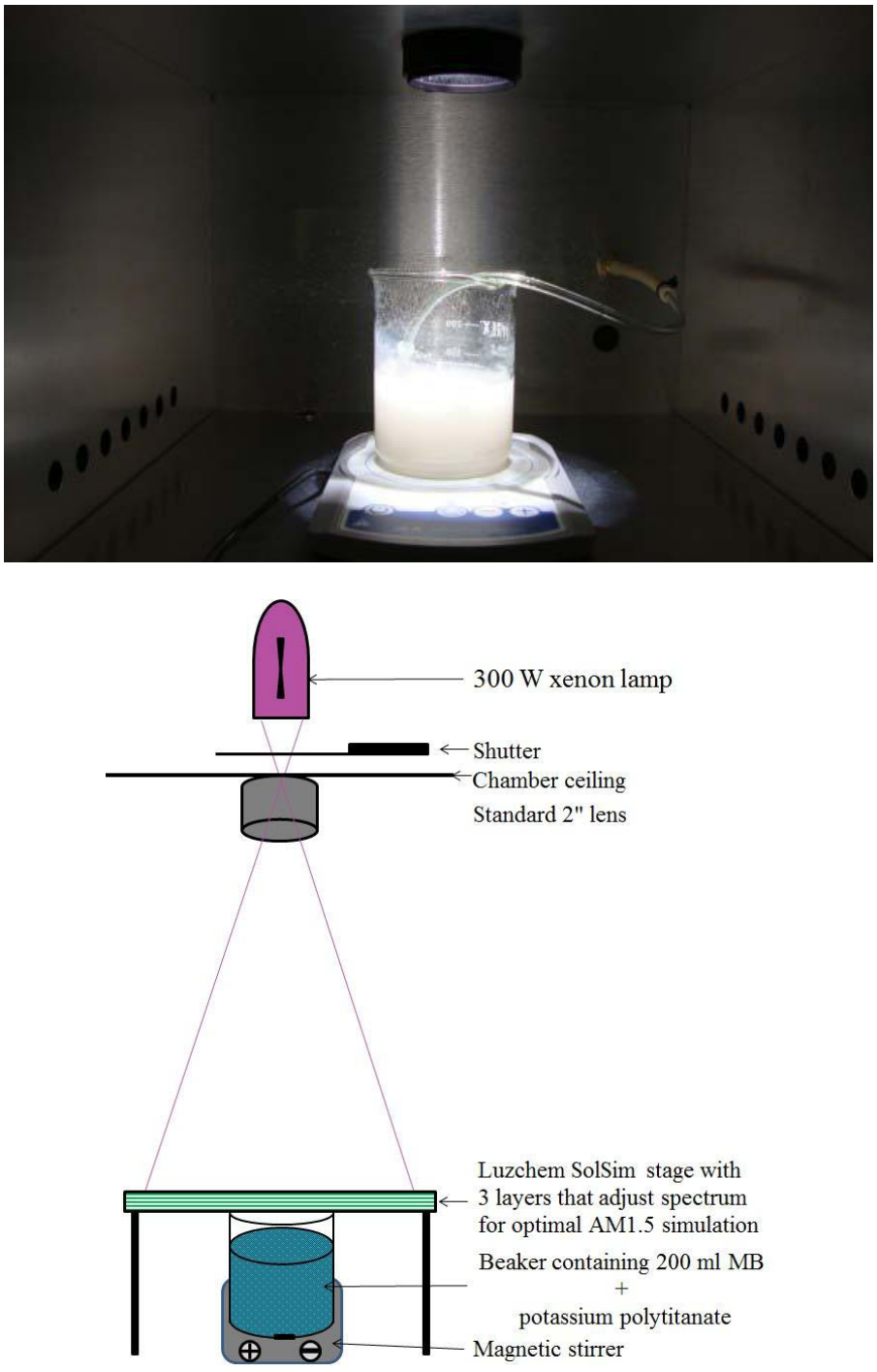

Figure 3-5. Photo and a schematic diagram of solar simulator.

3.5 Auxiliary Laboratory instruments

pH Meter: pH of sample solution was monitored by using a TPS 90FL pH meter (TSP Pty Ltd, Brisbane, Australia). The pH meter was calibrated by using buffer solutions (pH = 6.88, TPS 121380 and pH = 4, TPS 121382).

Hydrothermal autoclave: Hydrothermal autoclave is a closed stainless steel vessel with an internal cylindrical container and lid made of Teflon. Hydrothermal autoclave reactor with Teflon-coated Pyrex containers that can hold 550 mL volume was used to synthesis potassium titanate. The instrument was charged with reagents, and closed. Under external heating the contents were subjected to higher temperatures and pressures than inside an unsealed container. The autoclaves were specifically designed for use in hydrothermal synthesis at very high pressures and temperatures. They were particularly suited to very high pressures (up to 6000 bar). Due to their cone/cone sealing, they can safely withstand this at temperatures of up to 900°C.

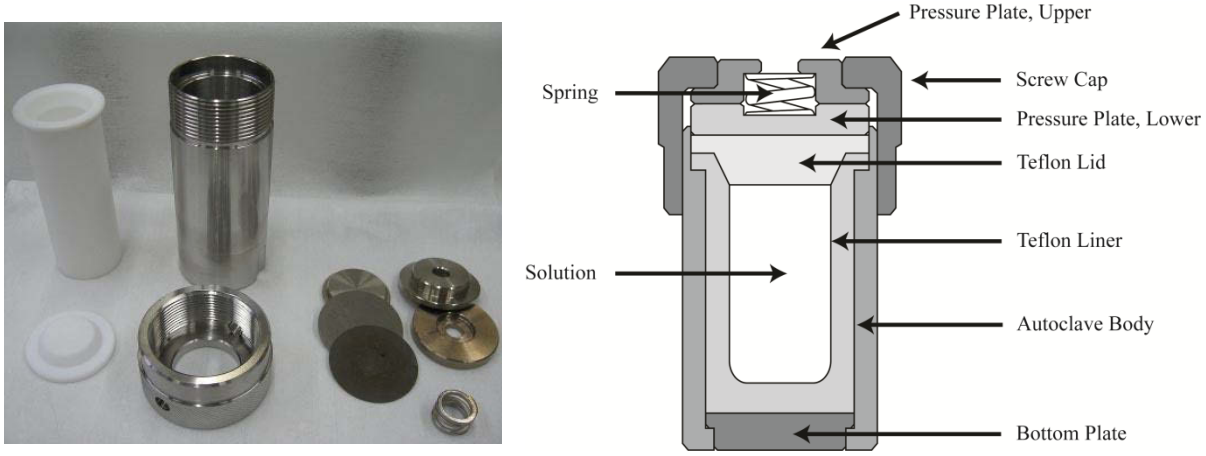

Figure 3-6. Photo (left) and a schematic diagram (right) of hydrothermal autoclave.

Centrifuge: Potassium titanate was retained by using centrifuge (Centurion Sci., 2040). 50 ml conical centrifuge tube (Axygen, SCT-50ML-R-S) with solution was used to separate the photocatalyst and this was achieved at 3000 rpm for 5 min.

Oven and furnace: Photocatalyst drying and calcination was carried out in an oven (labmaster oven, temperature range RT-200 ^{o}C) and a muffle furnace (Labec, CE-MLS), respectively at designated temperature and duration.

Orbital shaker: 100 ml of slurry solution in a 250 ml conical flask (Erlenmeyer) was used to execute the dark phase adsorption in orbital shaking incubator (Thermoline, TU400) at designated rpm and temperature.

Turbidity meter: Separation of the photocatalyst was monitored by turbidity meter (Hach HI 934). The turbidity of the sample was measured and plotted against time to evaluate the settling of the photocatalyst.

3.6 Analytical equipment and procedures

3.6.1 UV-vis Spectrophotometer

A Shimadzu UV-1700 spectrophotometer was used in this study to measure crystal violet and methylene blue degradation. The data was generated using computer software provided by Shimadzu Scientific Instruments Pty Ltd. The spectrophotometer was calibrated using Milli-Q water. Then, samples were placed in standard square 1 cm quartz cuvette, which was inserted in the spectrophotometer's cuvette holder. Spectral data was saved for processing following a scan in the 200 - 700 nm range.

Figure 3-7. Shimadzu UV-1700 spectrophotometer.

3.6.2 Dissolved Organic Carbon Measurement

A multi N/C 3100 analyser (Analytic Jena AG, Germany) was used to measure total carbon content in samples (Figure 3-8). Samples were filtered through 0.45 μm syringe filters. Therefore, the obtained results signify dissolved organic carbon (DOC). For sample analysis, at least 10 mL of aqueous samples were loaded into the auto-sampler (APG-64). The injection volume was adjusted to 500 μL by running the TOC measurement method.

Figure 3-8. A multi N/C 3100 analyser

3.6.3 LC-OCD

LC-OCD stands for Liquid Chromatography - Organic Carbon Detection. Organic matter used was identified and classified using LC-OCD detector and software (Model 8, DOC-Labor, Germany). The LC-OCD chromatogram categorises the organic fractions found in sample solution i.e. biopolymers, humics, building blocks and low molecular weight acids and neutrals.

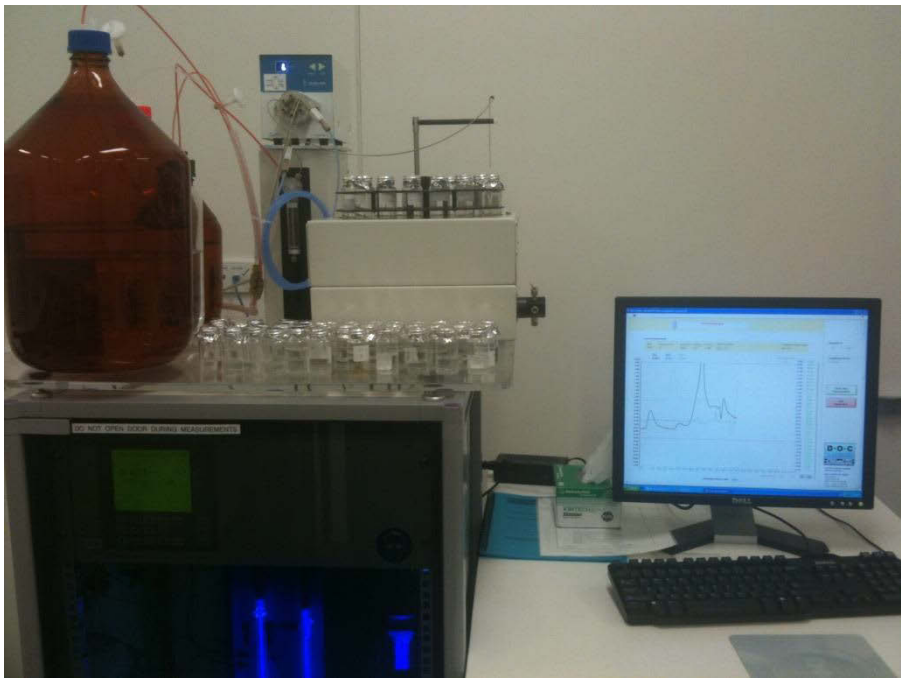

Figure 3-9. LC-OCD analyser

3.6.4 Ion Chromatography

The mineralisation of MB was measured by sulphate determination using a Metrohm ion chromatograph (790 IC) equipped with a Metrosep A Supp 5-150 (150 x 4.0 mm, 5 µm) column. The eluent consisted of 1 mmol/L of sodium hydrogen carbonate and 3.2 mmol/L of sodium carbonate dissolved in MilliQ water. The total injection volume was 5 mL (1 mL used for data generation while 4 mL was used for rinsing) and the run time lasted 22 min. The evolution of sulphate was assessed from the peak area that was converted into sulphate concentration using the standard curve.

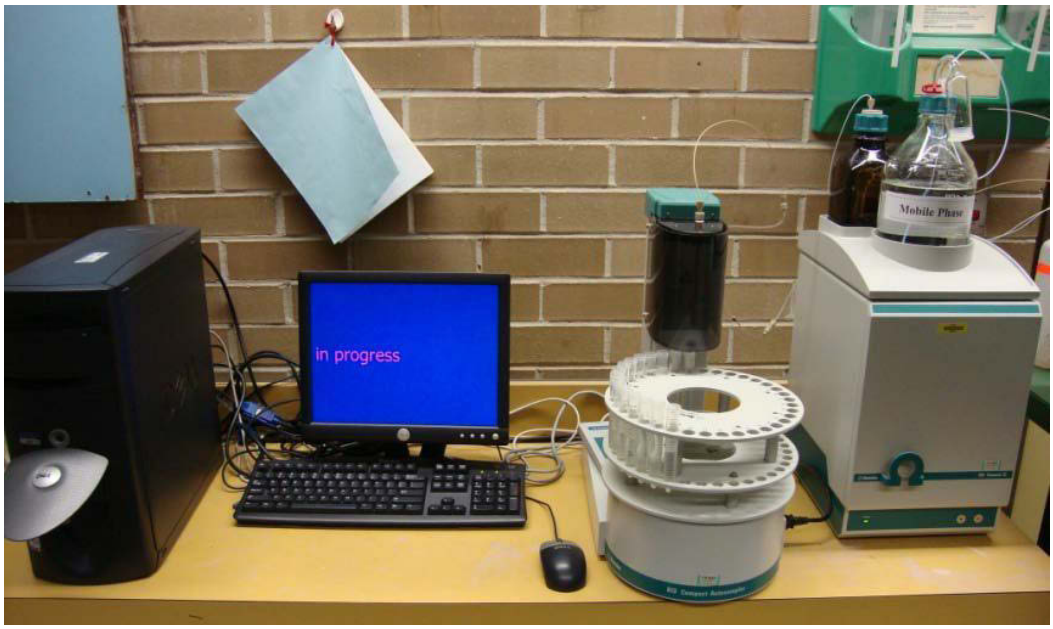

Figure 3-10 Metrohm ion chromatograph.

3.6.5 Metal analyser

Adsorption behaviour of Pb(II) was analysed using an Agilent Microwave Plasma Atomic Emission Spectrometer (4200 MP-AES, Agilent Technologies) sustained with nitrogen gas as source of emission. The total injection volume was 5 mL and the run time was 3 min. The concentration of Pb(II) was assessed from the peak area that was converted to Pb(II) concentration using the standard calibration curve.

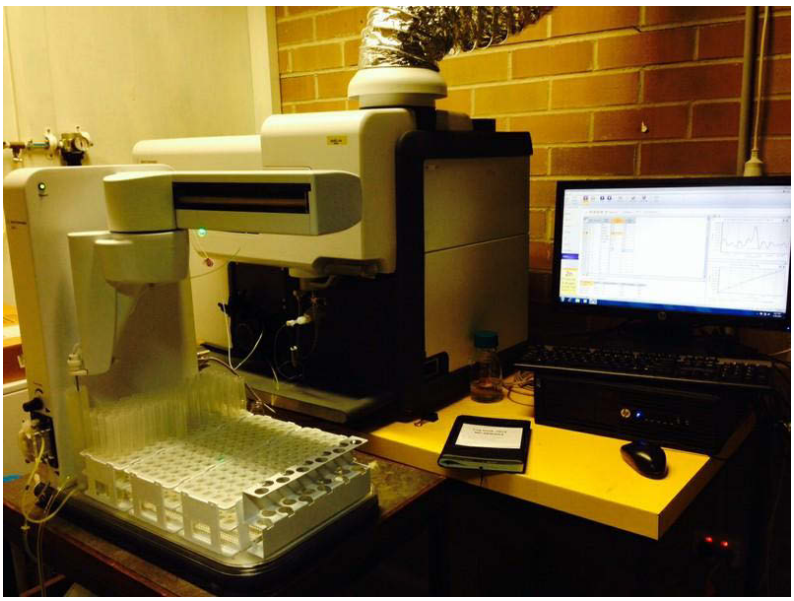

Figure 3-11. MP-AES analyser.

3.7 Data processing

All data were processed using OriginPro Acadamic version 8.5.0 SR0 b130 (OriginLab Corporation).

U T S

University of Technology Sydney
FACULTY OF ENGINEERING

Chapter 4: Photodesorption of Organic Matter from Titanium Dioxide Particles in Aqueous Media

4.1 Introduction

Photocatalytic reactions facilitate the degradation of organic pollutants. Titanium dioxide (TiO_2) is an effective photocatalyst that can be used to decompose natural and recalcitrant pollutants from air and water. The process first involves adsorption of the organic matter onto the TiO_2 surface, mostly through electrostatic interactions and ligand exchange mechanisms (Vermeer et al., 1998; Yang et al., 2009). Yang et al., (2009) reported that electrostatic interactions between negatively charged humic acids and positively charged nano-oxides surfaces are responsible for the adsorption. The highest humic acid adsorption was observed by nano-TiO_2 and γ-Al_2O_3. For nano-TiO_2, the adsorption was greatly affected by pH variations, which alter the surface charges and can either increase or decrease adsorption. On the other hand, Kim et al., (2009) concluded that the interaction between natural organic matter and TiO_2 is governed by acid-base and van der Waals forces, while the role of electrostatic forces is relatively insignificant.

More recently, photo-induced desorption of dissolved organic compounds in aqueous media during photocatalysis has been reported (Ambrus et al., 2008; Bjorklund et al., 2001; Erdei et al., 2008; Shon, Vigneswaran, Ngo & Kim 2005). The phenomenon is observed after the UV illumination of the water suspension for a short period of time and provides an exciting opportunity in wastewater treatment as it can significantly reduce process times and facilitate the regeneration of the adsorbent with low energy consumption.

Photodesorption itself is well established with examples of gaseous organic and inorganic compounds photodesorbing from semiconductors, carbon nanotubes and TiO_2

surfaces (Chen et al., 2001; Kornblit et al., 1984; Lichtman et al., 1976; Shapira et al., 1976) and recently by employing ultra-high vacuum surface science (Henderson et al., 2011). In the aqueous system, this transport phenomenon may involve a significantly reduced affinity between the photocatalyst and pollutants upon illumination, and leads to the detachment/degradation of adsorbed pollutants. The photodesorption effect strongly depends on the photonic flux, and the nature and concentration of organics and photocatalyst (Shon, Vigneswaran, Ngo & Kim 2005). Under dark conditions the adsorption of dissolved organic matter (DOM), typically humic and fulvic acids, on TiO_2 can achieve up to 80% removal in a contact time of only 15 to 30 minutes. Similarly, photodesorption of pollutants requires relatively short light illumination, a mere fraction of the treatment times employed in photocatalysis. This implies that photodesorption has significantly lower energy and reactor volume requirements than heterogeneous photocatalysis. Thus, the spent photoreactive adsorbent can be separated, rejuvenated and recycled for repeated use in a relatively small volume of water. Using suitably tailored materials, effective DOM removal can be achieved to match the performance of currently employed DOM removal processes, such as enhanced coagulation and flocculation. With low quality water sources, these methods might be used in conjunction, to dramatically reduce coagulant demand and sludge emission.

In this study, the effect of pH, TiO_2 loading, organic loading, UV light irradiation, flow rate and individual organic constituents of SWW on the photodesorption of DOM has been studied in a recirculating photocatalytic reactor. Organic compounds from synthetic wastewater were allowed to adsorb onto the surface of the photocatalyst (Degussa P25) until adsorption equilibrium was reached. After UV light illumination,

the photo-induced desorption was measured by dissolved organic carbon (DOC) analysis.

4.2 Experimental

4.2.1 Materials

TiO_2 Degussa P25 is a mixed phase nanopowder with anatase, rutile and amorphous structures. It has a surface area of ~ 50 m^2/g, an isoelectric point at pH 6 - 6.5 and an apparent density of 130 kg/m^3. Sodium hydroxide (97% w/w) was obtained from ChemSupply Pty Ltd and hydrochloric acid (37% v/v) from Scharlau Chemie S.A. The chemicals used in the preparation of SWW are listed in Table 3-2. Tap water was used for making SWW; it has a pH of 6.8 to 7.2, an average DOC of 0.5 mg/L and an average electrical conductivity of 166.4 µS/cm.

4.2.2 Photoreactor setup

A recirculating photoreactor setup was used in these experiments to study the photodesorption of DOC from TiO_2 surface (Figure 3-3). The setup is divided into two different compartments: i) the photoreactor stainless steel columns (C1, C2 and C3) and ii) the adsorption tank (T1). The volume of each column is 70 mL and encloses an 8 watt UVC lamp (Sankyo Denki, G8T5, Japan), while the adsorption tank has a 1 L volume. The suspension of TiO_2 and SWW in the adsorption tank was continuously stirred at 400 rpm using a magnetic stirrer (IKA, C-MAG, MS7). Influent (Q1) was pumped to the first column by an adjustable flow FMI lab pump (Fluid metering, INC, USA, Model QD) through the connections tubes (Masterflex, precision pump tube, 06508-17).

4.2.3 Photodesorption of dissolved organic carbon

The organic composition of SWW used is relatively similar to the effluent organic matter generally found in biologically treated sewage effluent (Seo et al., 1997). The photodesorption of DOC was studied under different operating conditions (pH, TiO_2 loading, organic concentration, UV light irradiation, flow rate and individual organic constituents of SWW). The pH of the slurry was adjusted using 0.1 N HCl and 0.1 N NaOH. Experiments were carried out using a 1 L volume of SWW with an initial DOC of 5.5-7 mg/L and a pH of 7.28. After the addition of the desired amount of TiO_2, the slurry was mixed with a magnetic stirrer at 400 rpm for 30 min (dark adsorption). The dark adsorption took place in T1 and allowed the adsorption of organics onto TiO_2 nanoparticles. Afterwards, the slurry was pumped to the photoreactor columns and UVC lamps were switched on. Photodesorption shortly started after illuminating the suspension flowing through in the columns. Slurry samples were collected at fixed time intervals, filtered through 0.45 μm regenerated cellulose filters (Whatman, UNIFLO) and analysed using a Multi N/C 3100 (Analytik Jena) DOC analyser. Organic matter was identified and classified using LC-OCD detector and software (Model 8, DOC-Labor, Germany). The adsorption and desorption percentages were calculated as follows:

$$Adsorption(\%) = \frac{[C_0 - C_{ads}]100}{C_0} \quad \text{.....Eq 4.1}$$

Where C_0 is the DOC concentration in mg/L at t = 0, C_{ads} is the DOC at t = 30 min.

$$Photodesorption\ (\%) = \frac{[C_{des} - C_{ads}]100}{[C_0 - C_{ads}]} \quad \text{.....Eq 4.2}$$

Where C_{des} is the DOC concentration in mg/L at t = 33 min (maximum photodesorption).

4.3 Results and Discussion

4.3.1 Flow rate

The photodesorption of DOM from TiO_2 particles was studied under different flow rates, Q1 = 15, 90, 150 and 280 mL/min at 1 g/L TiO_2 loading (Figure 4-1). Q1 variations directly affected the detachment of the adsorbed organics from TiO_2 surfaces under a short period of UV-light irradiation. After allowing 30 min for the adsorption process, the DOC of SWW was reduced by 64.1, 69.4, 67.5 and 53.4%, at the flow rates of 15, 90, 150 and 280 ml/min, respectively. The variation in DOC removal under similar experimental conditions is attributed to the differences in the initial DOC of SWW, and also to the characteristics of tap water used. Flow rate did not affect initial DOM adsorption as the adsorption was carried out in T1 before the pump was turned on. Photodesorption was recorded in the first five minutes after L1, L2 and L3 lamps and the pump were turned on. At Q1 = 15 mL/min, no photodesorption was detected. The detachment of organics appeared at relatively higher flow rates, Q1 > 90 mL/min. The highest photodesorption was recorded at 150 mL/min flow rate (optimum flow rate), further increase in Q1 induced a decrease in photodesorption (Figure 4-1b). At low flow rates (15 <Q1 < 90 mL/min), the residence time of slurry in the columns (C1, C2 and C3) permitted the initiation of photocatalysis (generation of $OH^{\bullet}$, photo oxidation of attached organics, degradation of DOM in solution by oxidising species) making DOM photodesorption from TiO_2 surface of low significance. Moreover, the constant adsorption of desorbed/cleaved organics might have also contributed to the reduction of photodesorption at low flow rates. On the other hand, the increase of Q1 above 150 mL/min resulted in short residence times and consequently less photodesorption efficiency under the experimental setup used in this study. Thus, all subsequent experiments were carried out at Q1 = 150 mL/min.

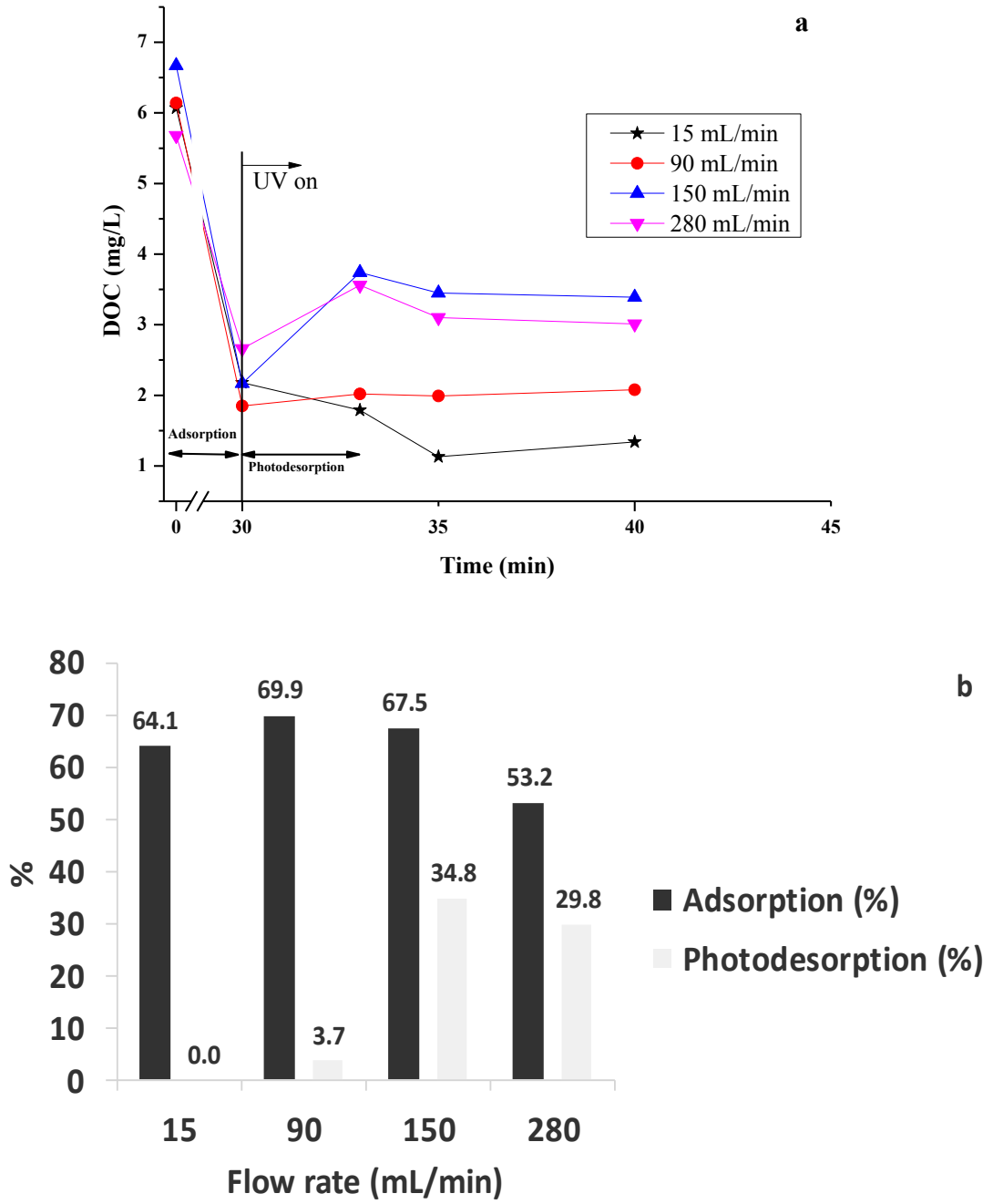

Figure 4-1. (a) Effect of recirculating flow rate on photodesorption of DOM and (b) the percentage of adsorption and photodesorption in relation to flow rate (0 min < adsorption < 30 min, 30 min < photodesorption < 33 min. Experimental conditions: TiO_2 = 1 g/L, T = 22°C, intensity = 24 W, pH = 7, no air sparging).

4.3.2 UV irradiation

UV light irradiation triggers the photodesorption of DOM from TiO_2 surfaces. It may be expected, therefore, that modifying the exposure to UV light would affect the rate of DOM detachment. Experiments were performed to determine the effect of UV light exposure upon photodesorption. The detachment of DOM was studied by monitoring the concentration of DOC in suspensions of SWW and TiO_2. Results using L1 (8 W), L1+L2 (16 W) and L1+L2+L3 (24 W) are presented in
Figure 4-2.

The maximum photodesorption was recorded for the maximum UV light exposure (24 W, 3 lamps) used in the experimental setup. Decreasing the UV light exposure attenuated the desorption rate of DOM. After 3 min of UV light irradiation, a total of 34.8%, 31.6% and 28.2% of DOM were desorbed for intensities equal to 24, 16 and 8 W, respectively. Shon et al., (2005) observed the same phenomenon using a batch reactor system but for a prolonged period of time (up to 2 h) after UV light irradiation. They reported that the rate constant of the reverse reaction (photodesorption) using three lamps (24 W) was 27.6 times higher than that of one lamp. In our reactor setup, the reverse reaction was observed for a short period of time (up to max 10 min) and no such big differences in photodesorption were recorded for the increase in light exposure. This can be due to several factors such as, the differences between batch and recirculating reactors, the residence time in the columns, and the sampling method. In our study, the maximum light exposure (24 W) was considered optimum and was used in the next experiments.

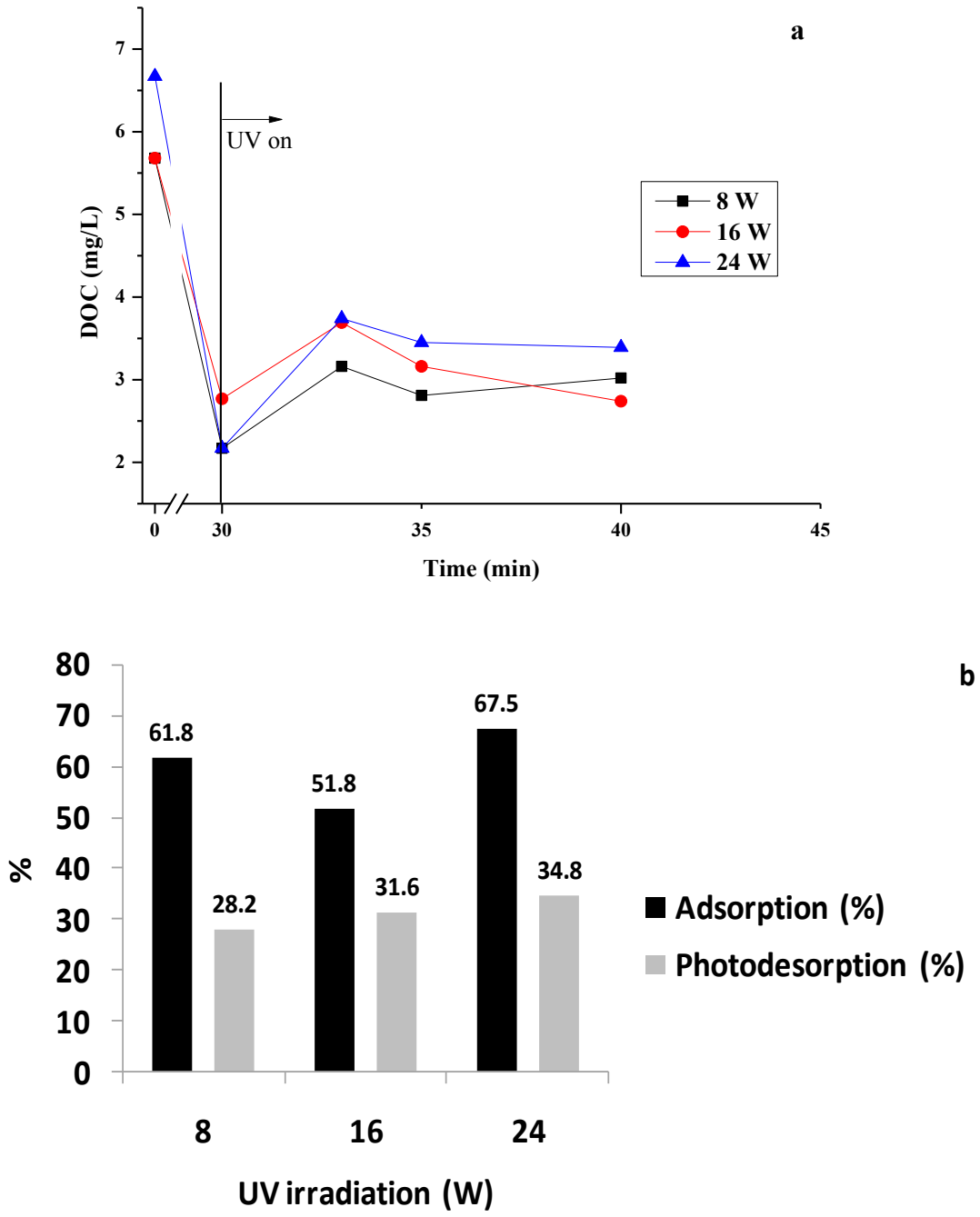

Figure 4-2. (a) Effect of light intensity on the photodesorption of DOM and (b) the percentage of adsorption and photodesorption under different light intensities (0 min < adsorption < 30 min, 30 min < photodesorption < 33 min. Experimental conditions: TiO_2 = 1 g/L, T = 22°C, Q1 = 150 mL/min, pH = 7, no air sparging).

4.3.3 Effect of TiO_2 loading

Figure 4-3 shows the effect of the TiO_2 loading on the photodesorption of DOM using four loadings (0.1, 0.5, 1 and 2 g/L). The adsorption of organics increased linearly with TiO_2loading. On the other hand, the photodesorption of organics was low below 1 g/L of TiO_2 loading, increased to maximum at 1 g/L and then decreased again. At loadings less than 1 g/L, the photodesorption was observed but the percentage of desorption was relatively low being 11.4% and 20.7% for 0.1 and 0.5 g/L of TiO_2 concentration, respectively (Figure 4-3b). This can be due to the low DOM - TiO_2 surface adsorption and the high adsorption of DOM with in the TiO_2 aggregated structures. This fact resulted in hindering the exposure of adsorbed organic molecules onto TiO_2 to UV light and consequently reducing their photodesorption. On the other hand, increasing TiO_2 concentration caused more UV light scattering and less photodesorption efficiency (Cassano et al., 2000; Herrmann 2005; Malato et al., 2009). Hence, the next experiments were carried out at 1 g/L TiO_2 loading.

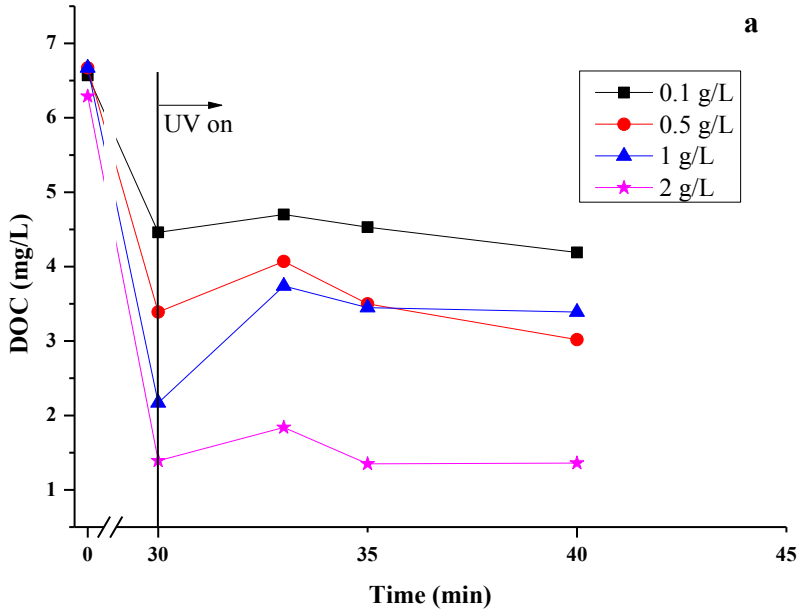

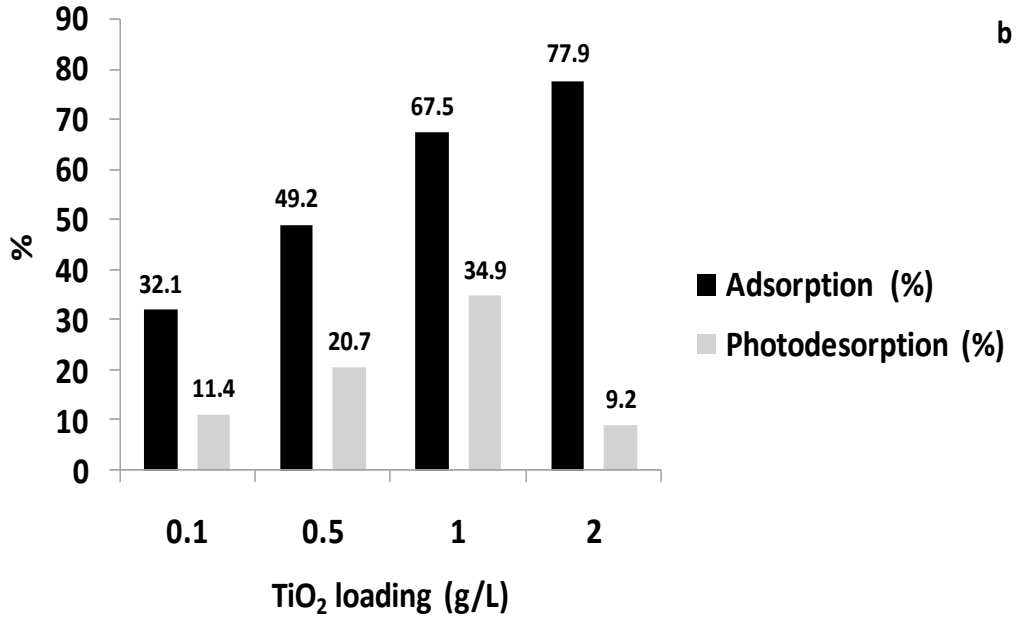

Figure 4-3. (a) Effect of TiO_2 loading on photodesorption of DOM and (b) the percentage of adsorption and photodesorption over different TiO_2 loading (0 min < adsorption < 30 min, 30 min < photodesorption < 33 min. Experimental conditions: T = 22°C, Q1 = 150 ml/min, intensity = 24 W, pH = 7, no air sparging).

4.3.4 Organic concentration

Increasing the organic concentration of SWW diminished the amount of DOM that photodesorbed from TiO_2. Doubling (12 mg/L) and tripling (20.8 mg/L) the concentration of compounds in SWW reduced the photodesorption to 4.35 and 0%, respectively (Figure 4-4). The adsorption percentage of DOM decreased with organic loading increase, while the actual amount of adsorbed DOC increased. At a stable TiO_2 loading, the increase in organic loading usually leads to increase in adsorption until it reaches a point at which it becomes steady (Yang et al., 2009). This steady state is due to the surface saturation of TiO_2. In the same way, the photocatalytic reaction is highly influenced by the concentration of contaminants in solution. Malato et al., (2009) reported that at high organic concentrations the photocatalytic reactions show similar

rates due to photocatalyst surface saturation. As photodesorption is a photo-induced phenomenon, the irradiation of the photocatalyst surface is essential to get desired results. The reduction of photodesorption with organic loading increase could be mainly due to the shading effect, which was exercised by the mass of aggregated organics on TiO_2 surface. This prohibited UV light penetration and detrimentally reduced the efficiency of the photodesorption.

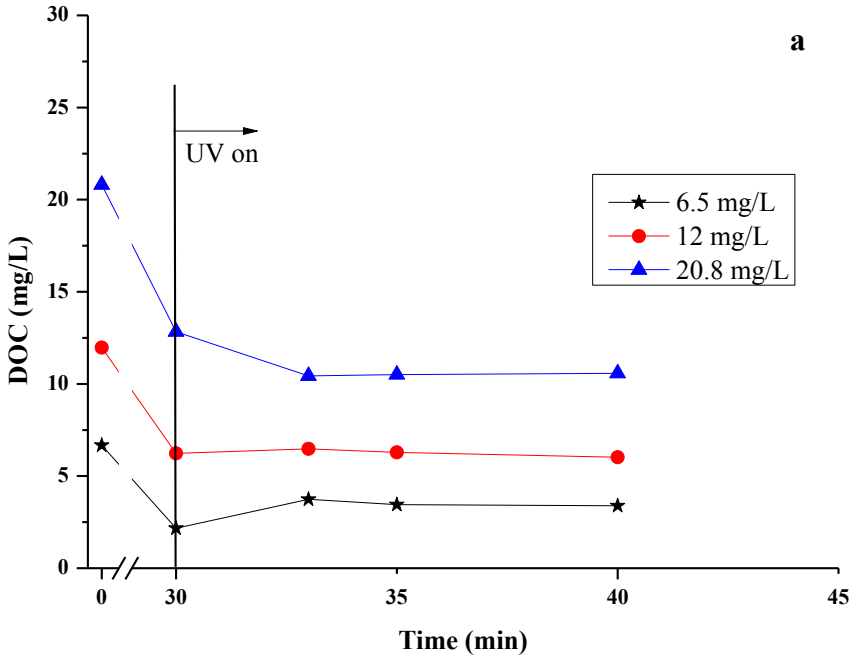

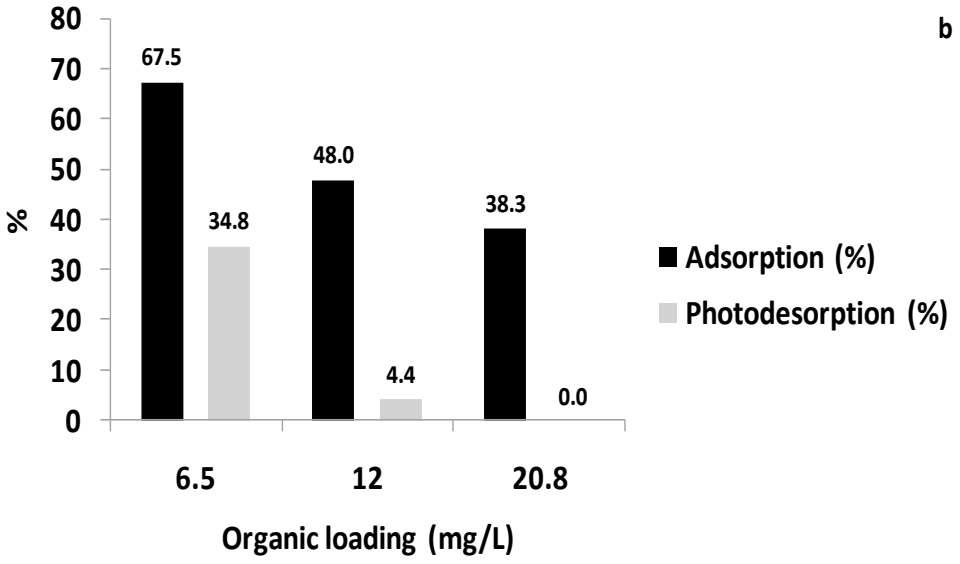

Figure 4-4**.** (a) Effect of organic loading on photodesorption of DOM and (b) the percentage of adsorption and photodesorption for different organic loadings (0 min < adsorption < 30 min, 30 min < photodesorption < 33 min. Experimental conditions: TiO_2 = 1 g/L, T = 22°C, Q1 = 150 ml/min, intensity = 24 W, pH = 7, no air sparging).

4.3.5 pH of the solution

The photodesorption of DOM under different solution pH conditions was examined to assess the applicability of this technique to water treatment procedures. The pH of wastewater usually varies depending on several factors. The pH affects the aggregation properties and solubility of organic matter. For instance, humic acids are more soluble at higher pH, whereas the aggregation of humics is dominant at low pH. The effect of solution pH on the photodesorption of DOM is shown in

Figure 4-5. As expected, the initial DOC of the SWW increased with pH increase indicating the dissolution of particulate organics. The commencement of DOM adsorption onto TiO_2 is influenced by electrostatic attractions and ligand exchange

(Vermeer et al., 1998; Yang et al., 2009). Van der Waals forces and acid-base interactions can also play a temporary role in this process, but it is of lower significance. Our results show that the adsorption of DOM increased from 66.7 to 74.3% with pH decrease from 10 to 4, respectively. We assign this to the alteration of TiO_2 surface charges increasing the attraction between the more-positively charged TiO_2 surface and the negatively charged DOM. The adsorption of DOM was lowered by pH increase even if the amount of DOM was increased (DOC increased by approx. 2 mg/L between pH 7 and 10). Repulsive forces are presumably responsible for the decrease in adsorption due to the similar surface charges between TiO_2 and DOM.

The photodesorption percentage of DOM increased with pH increase. At pH 4, 26.1% of DOC was desorbed from the surface of P25, while 41.3% was desorbed at pH 10. This can be explained by the weak attraction at high pH leading to an easier detachment of DOM after UV light irradiation. Upon UV irradiation, the surface charge of TiO_2 is disturbed and unstable mainly because the UV photon excitation induces a charge migration in the photocatalyst. The migration of charge from the centre to the TiO_2 surface, where both oxidation and reduction reactions take place, changes the chemical forms of several attached hydroxyl, peroxo and carboxyl species or groups. Surface charge alteration will result in the photodesorption or decomposition of weakly attached DOM for a short period of time before the generation of $OH^{\bullet}$ becomes dominant and the photo oxidation process prevails.

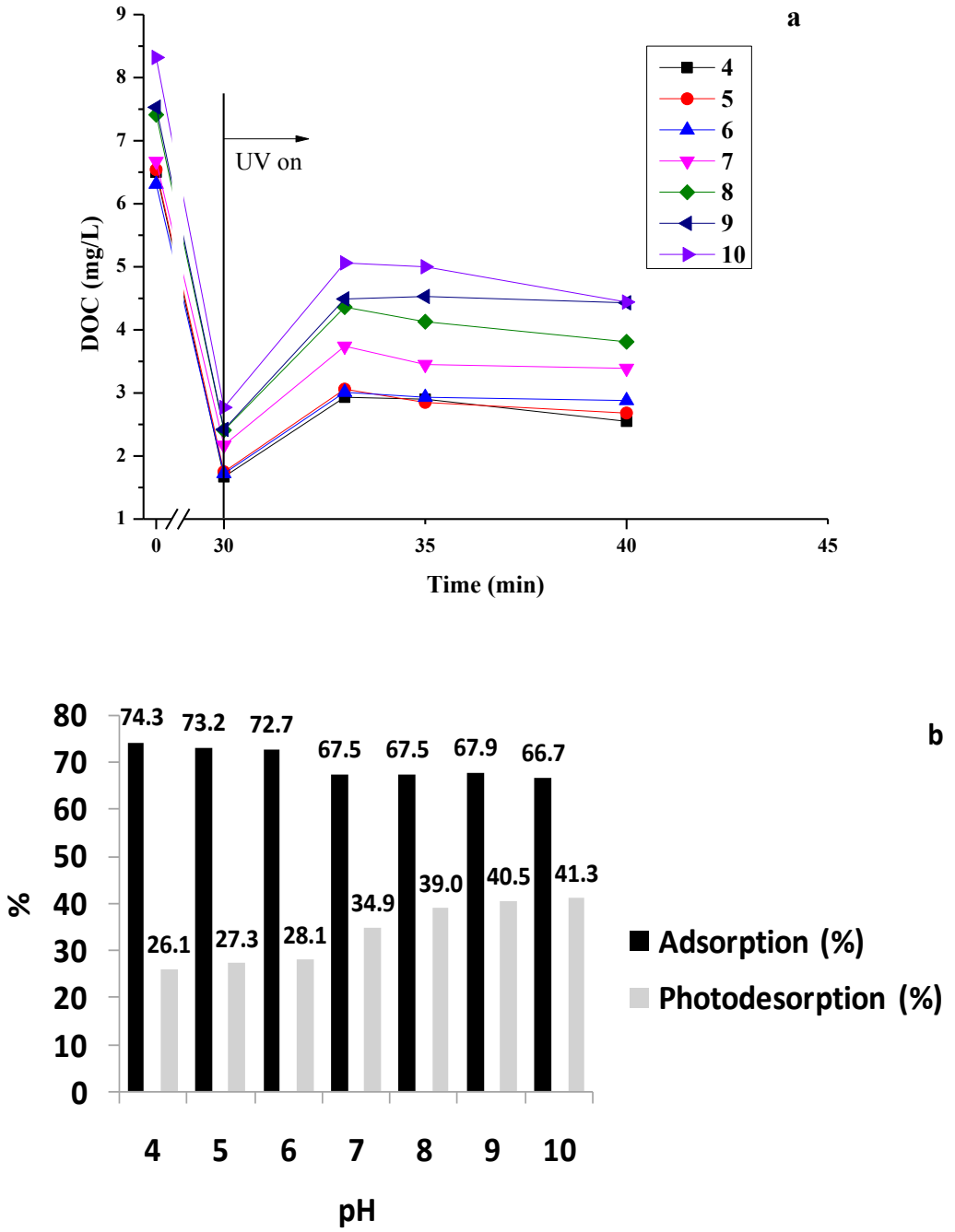

Figure 4-5. (a) Effect of SWW pH on photodesorption of DOM and (b) the percentage of adsorption and photodesorption for different solution pH (0 min < adsorption < 30 min, 30 min < photodesorption < 33 min. Experimental conditions: TiO_2 = 1 g/L, T = 22°C, Q1 = 150 ml/min, intensity = 24 W, no air sparging).

4.3.6 Photodesorption of Specific Organic Compounds

The photodesorption effect strongly depends on the nature of organic compounds and their constituents. SWW is a complex blend of several organic and inorganic compounds. The organic constituents are; beef extract (a mixture of peptides and amino acids, nucleotide fractions, organic acids, minerals and some vitamins (Asif Durrani 2011), peptone (an enzymatic digest of animal protein consisting of short polymers of amino acids linked by peptide bonds (Payne et al., 1994)), humic acid (a complex mixture of acids containing carboxyl and phenolated groups that behaves as a dibasic or occasionally a tribasic acid (Stevenson 1982)), tannic acid (a polyphenolic compound containing hydroxyl groups that cross link to other compounds), sodium lauryl sulphate (an anionic orthosulfonate consisting of a 12-carbon chain attached to a sulfate group (Tupker RA 1997), and gum arabic powder (a mixture of polysaccharides and glycoproteins (Anderson et al., 1966; Street 1983)).

Beef extract, peptone, humic acid, tannic acid, sodium lignin sulphonate, sodium lauryl sulphate and arabic acid were studied individually by adjusting the DOC to 7 mg/L at pH 7 and with a catalyst loading of 1g/L (TiO_2). As shown in
Figure 4-6a, after allowing 30 minutes for dark phase adsorption, the DOC of tannic acid and beef extract was reduced by 97.25% and 42.79%, respectively, whereas the other organic compounds had adsorption ranging from 8 to 22%.

After adsorption in the dark, the influent was pumped to a photoreactor and illuminated with UVC light.

Figure 4-6a illustrates the detachment of sodium lauryl sulphate, sodium lignin sulphonate, beef extract and tannic acid from TiO_2 surfaces after UV light irradiation, indicated by an increase in DOC immediately after irradiation.

In particular (see

Figure 4-6b), photodesorption of sodium lauryl sulphate was 50% of the adsorbed fraction (14.73%), sodium lignin sulphonate (43.47% of adsorbed fraction), beef extract (16.49% of adsorbed fraction) and tannic acid (3.35% of adsorbed fraction). Photodesorption did not occur with peptone, humic acid, arabic gum powder and arabic acid.

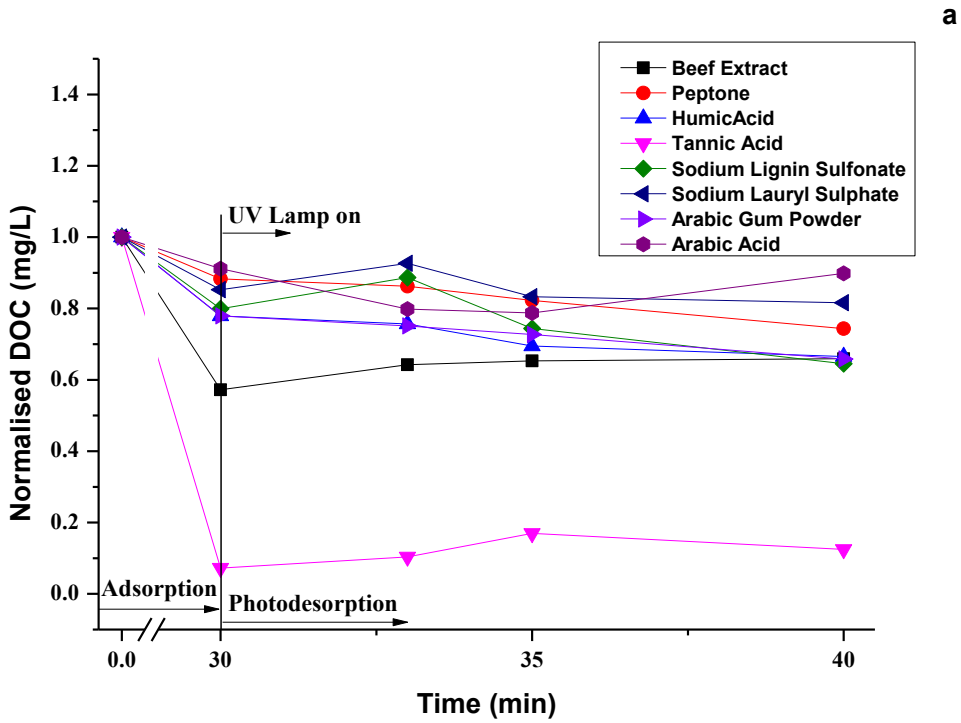

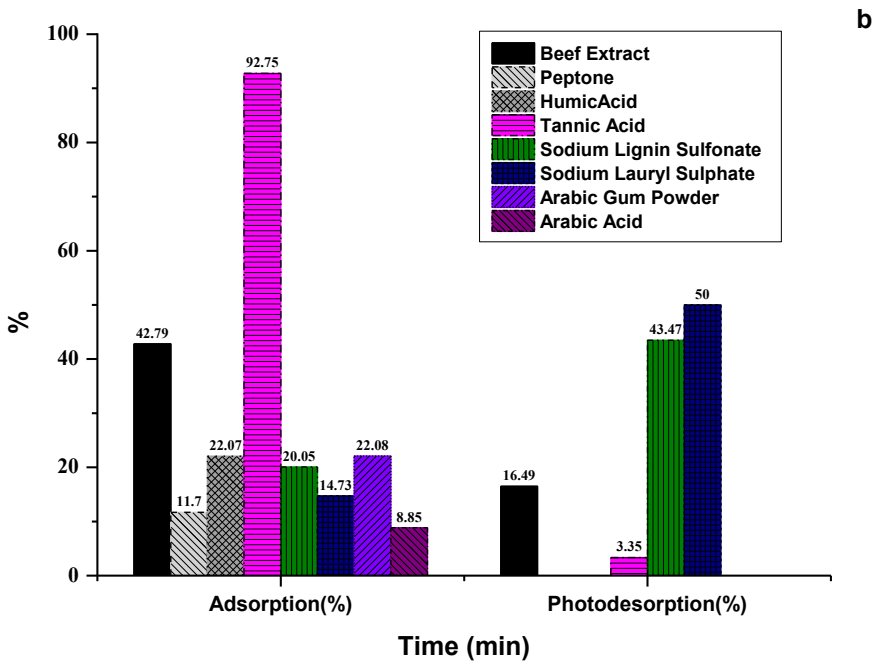

Figure 4-6**.** (a) Effect of individual organic constituents of SWW on photodesorption of DOM and (b) the percentage of adsorption and photodesorption for different organic constituents (0 min < adsorption < 30 min, 30 min < photodesorption < 33 min. Experimental conditions: TiO_2 = 1 g/L, T = 22°C, Q1 = 150 ml/min, intensity = 24 W, no air sparging).

4.3.7 LC-OCD analysis

The SWW used in this study is a complex organic mixture of polysaccharides (beef extract, Arabic gum powder, Arabic acid), phenolic and carboxylic compounds (humic acid, tannic acid and sodium lignin sulphonate), protein and amino acids (beef extract, peptone) and organ sulphates (sodium lauryl sulphate).The LC-OCD fingerprint and fraction assignation has been discussed in detail by Huber et al., (2011). To further probe the nature of the organic species before and after desorption, LC-OCD experiments were conducted at optimum conditions.

The LC-OCD chromatogram shown in Figure 4-7 reveals the organic fractions found water samples i.e. biopolymers, humics, building blocks and low molecular weight acids and neutrals. As shown in Figure 4-7a, the untreated SWW contains a large portion of high molecular weight (HMW) compounds in addition to low molecular weight (LMW) organic fractions. After adsorption, the majority of HMW compounds have been adsorbed onto the surface of the TiO_2. However, after photodesorption only LMW organics were recovered in the solution.

a

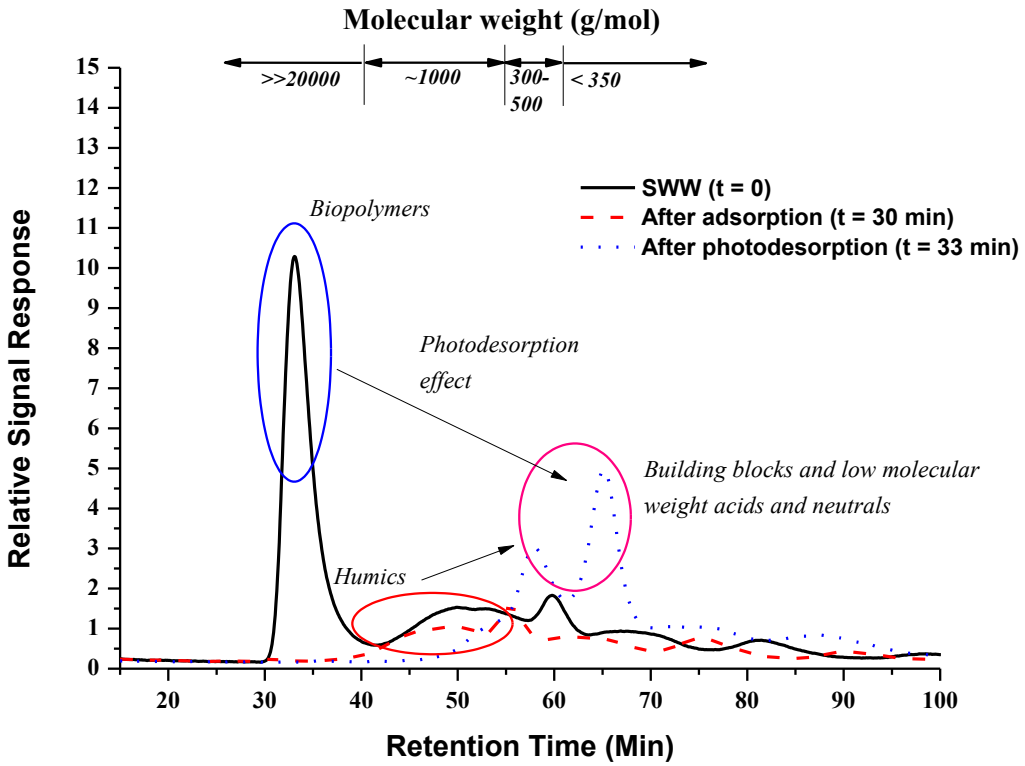

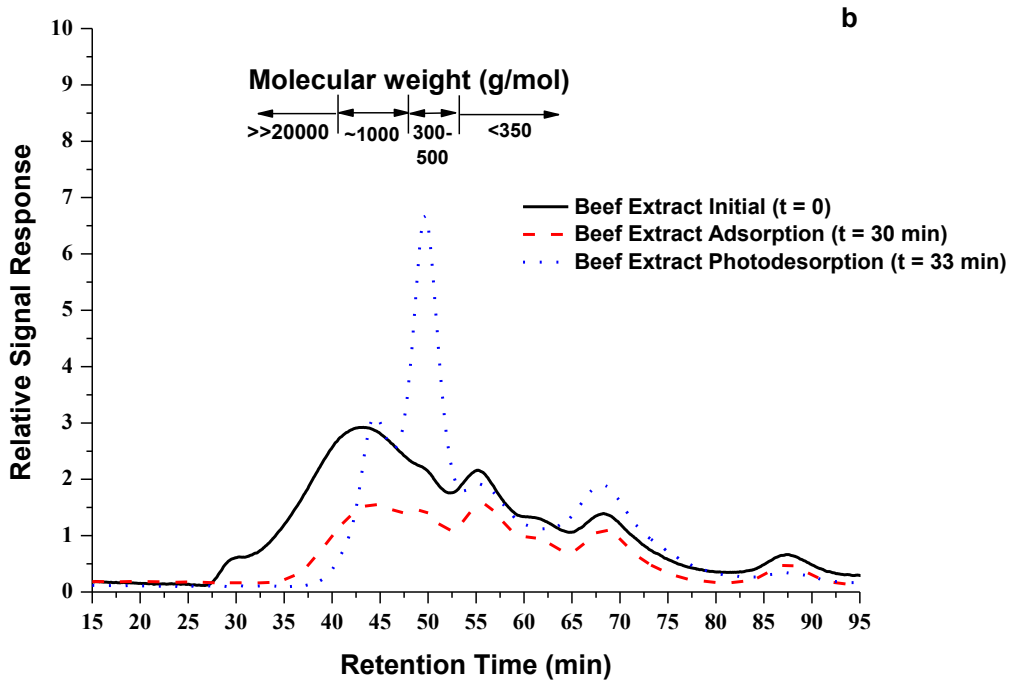
b
Molecular weight (g/mol)
>>20000
~1000
300-500
<350
Beef Extract Initial (t = 0)
Beef Extract Adsorption (t = 30 min)
Beef Extract Photodesorption (t = 33 min)
Relative Signal Response
Retention Time (min)

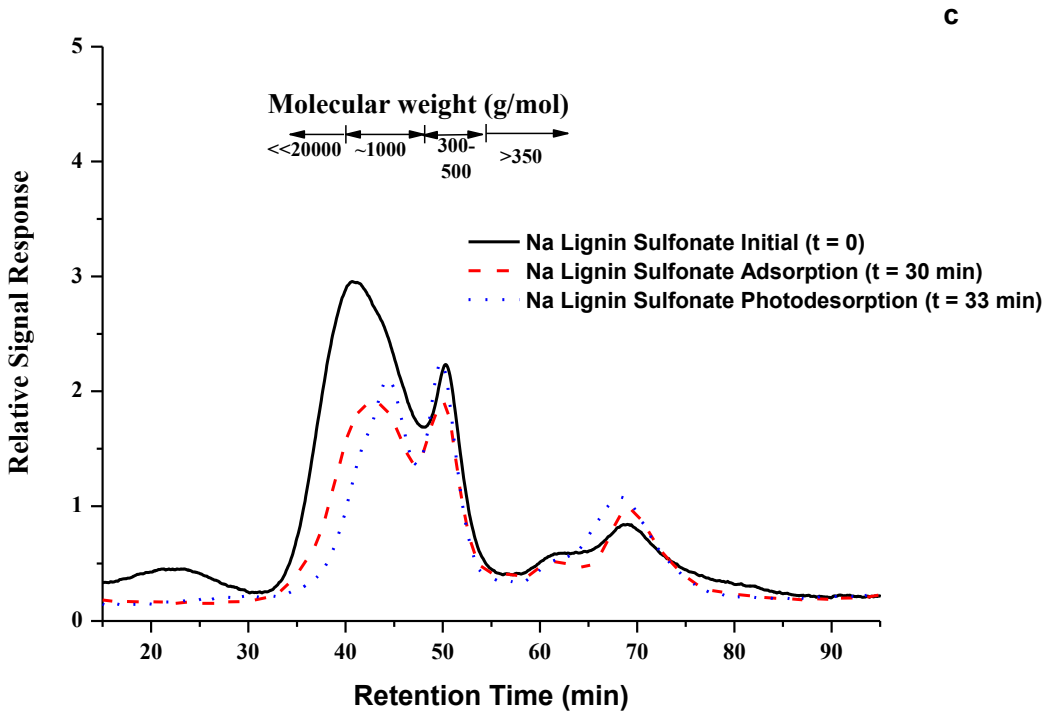
c
Molecular weight (g/mol)
<<20000
~1000
300-500
>350
Na Lignin Sulfonate Initial (t = 0)
Na Lignin Sulfonate Adsorption (t = 30 min)
Na Lignin Sulfonate Photodesorption (t = 33 min)
Relative Signal Response
Retention Time (min)

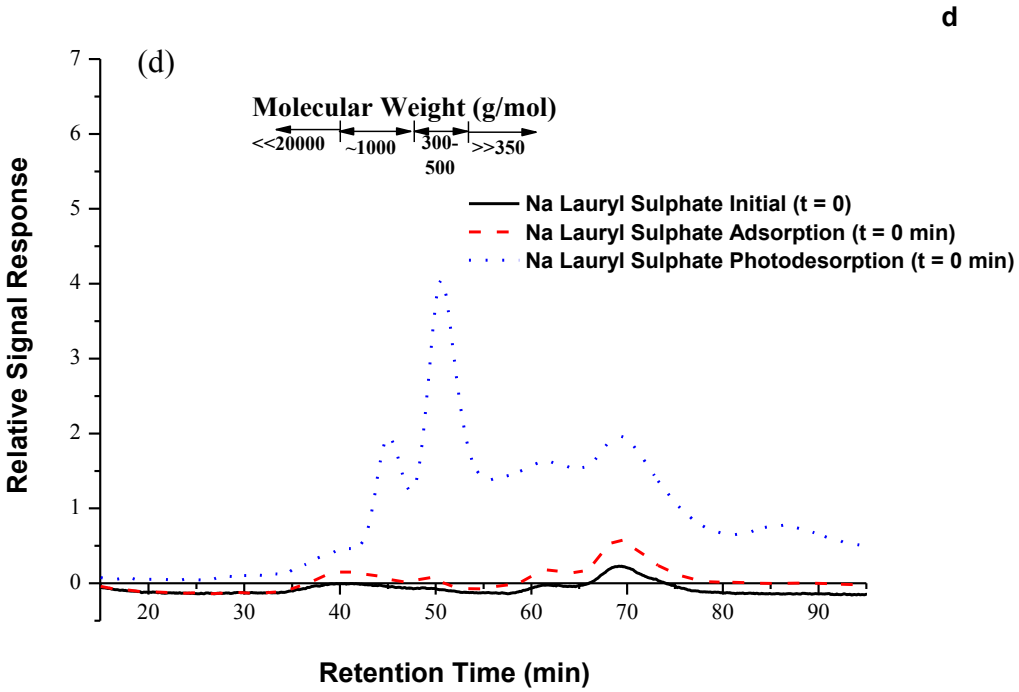

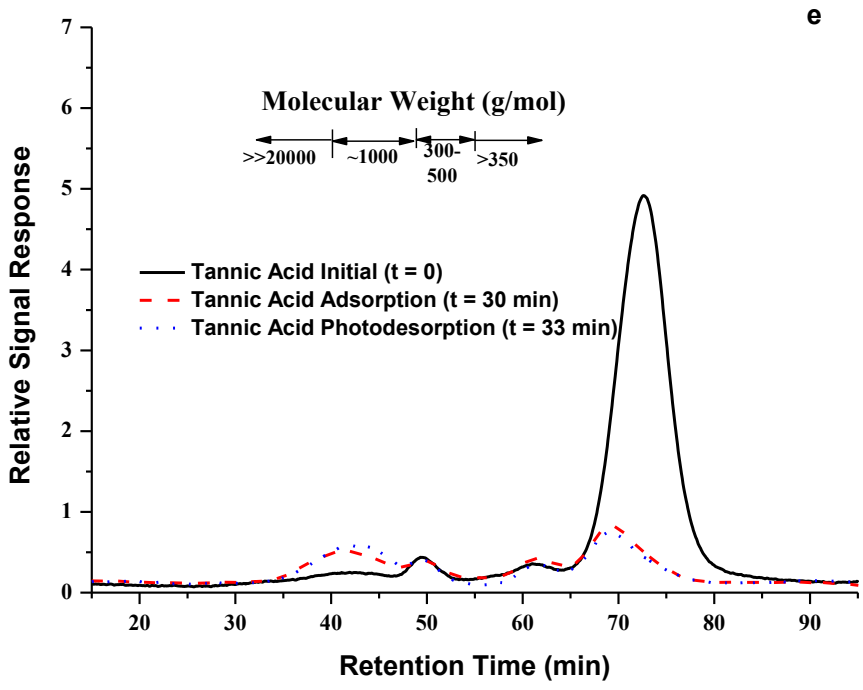

Figure 4-7. LC-OCD chromatograms of DOM before treatment (black line), after adsorption (red line) and after photodesorption (blue line) for (a) SWW, (b) Beef extract. (c) Sodium lignin sulphonate. (d) Sodium lauryl sulphate. (e) Tannic acid.

LC-OCD chromatograms of water containing beef extract, tannic acid, sodium lauryl sulphate and sodium lignin sulphonate are shown in

Figure 4-7 (b to e). The untreated beef extract and sodium lignin sulphonate solution (Figure 4-7 b and c) contain significant amounts of humic substances (~1000 g/mole). After the dark adsorption phase, the amounts of high molecular weight (HMW i.e., ~1000 g/mole) species remained in solution decreases. After photodesorption, the beef extract shows a significant increase in low molecular weight (LMW i.e., <350 g/mole). Therefore, the process of adsorption/desorption converted a reasonable proportion of HMW organics into LMW organic material. This process also occurred to a lesser extent in the sodium lignin sulphonate sample.

In contrast, the LC-OCD chromatogram of UV treated sodium lauryl sulphate (Figure 4-7d) reveals the photodesorption of larger fraction of both HMW and LMW organic. Upon UV irradiation, fractions of hydrophobic constituents of sodium lauryl sulphate degrade into hydrophilic species (Ikeguchi et al., 1998) by oxidation of carbon-containing groups into carbonyl groups (Panich et al., 2008), which photodesorb (Table 4-1). However, the LC-OCD chromatograms of untreated tannic acid (

Figure 4-7e contained a larger proportion of LMW acids, which showed a high adsorption affinity to TiO_2 during dark phase adsorption and were found to poorly desorb upon irradiation. The photodesorption of HMW organic compounds such as beef extract, sodium lignin sulphonate and sodium lauryl sulphonate was observed to be higher than the LMW tannic acid. Thus, the HMW fractions of organic compounds decomposed into smaller compounds after UV irradiation, which was subsequently desorbed from TiO_2 surface.

Table 4-1. LC-OCD fractionation results of organic compounds, after adsorption and photodesorption								
Sample	Total DOC	Total DOC		Approximate molecular weight distribution (g/mol)				
		HOC	CDOC	CDOC				
				>>20000	~1000	300-500	<350	<350
	Dissolved	Hydrophobic	Hydrophilic	Biopolymer	Humic Substance	Building Blocks	LMW Neutrals	LMW Acids
SWW Initial	100%	15.8%	84.2%	40%	35.4%	0.8%	7.9%	0%
SWW Adsorption	100%	40.5%	59.5%	2.6%	8.3%	15.8%	30.5%	2.3%
SWW Photodesorption	100%	13.9%	86.1%	1.1%	2.6%	15.5%	63.0%	3.9%
Beef Extract Initial	100%	16.6%	83.4%	1.50%	34.4%	10.5%	36.8%	0.2%
Beef Extract Adsorption	100%	24.1%	75.9%	--	25.6%	7.5%	42.1%	0.7%
Beef Extract Photodesorption	100%	25.0%	75.0%	1.40%	17.9%	9.8%	35.6%	10.4%
Na Lignin Sulphonate Initial	100%	35.8%	64.2%	--	49.7%	--	8.2%	6.8%
Na Lignin Sulphonate Adsorption	100%	52.6%	47.4%	0.3%	25.3%	4.7%	12.1%	4.9%
Na Lignin Sulphonate Photodesorption	100%	33.4%	66.6%	5.7%	25.9%	2.0%	25.4%	7.3%
Na Lauryl Sulphate Initial	100%	97.4%	2.6%	--	0.7%	0.2%	1.7%	--
Na Lauryl Sulphate Adsorption	100%	95.7%	4.3%	--	1.0%	0.3%	2.9%	0.1%
Na Lauryl Sulphate Photodesorption	100%	63.4%	36.6%	1.1%	5.7%	6.7%	23.0%	0.1%
Tannic Acid Initial	100%	51.2%	48.8%	0.1%	1.9%	1.0%	45.0%	0.8%
Tannic Acid Adsorption	100%	51.7%	48.3%	--	16.1%	1.9%	28.6%	1.7%
Tannic Acid Photodesorption	100%	67.40%	32.60%	1.30%	12.50%	0.70%	16.50%	1.50%

The data reveal that the HMW organic compounds were degraded into LMW fractions upon UV irradiation in the presence of TiO_2. An alternative interpretation that only LMW compounds desorb from TiO_2 (and the HMW compounds remain bound) is implausible because the percentage of LMW in SWW is lower than that recorded after photodesorption. Similar findings were reported by Shon et al., (2005) after conducting a high performance size exclusion chromatography (HP-SEC) analysis on desorbed fractions. The desorption of LMW organics was enhanced by the build-up of negative charge on TiO_2 surface upon irradiation. The accumulation of negative charge on $TiO_2$was characterised by photoelectrophoretic and electrochemical measurements (Dunn et al., 1981). It was found that the surface charge of TiO_2 after irradiation was more negative than its surface charge before irradiation. This special characteristic was also used to control the electroosmotic flow in TiO_2 coated micro channels using UV light (Moorthy et al., 2001).

Figure 4-8 shows a graphical representation of the process proposed below:

1. HMW and LMW compounds adsorb under dark conditions onto the TiO_2 surface by electrostatic forces, van der Waals and ligand exchange.
2. After UV light irradiation, the surface charge of TiO_2 is modified (Dunn et al., 1981; Moorthy et al., 2001) affecting the electrostatic attraction of organics.
3. Some of the LMW organic compounds desorb from the TiO_2 while HMW are decomposed into smaller fractions, which subsequently desorb from the surface. The remainder of the LMW and HMW organic compounds remain adsorbed.
4. LMW organics and the decomposed HMW are dispersed in suspension and contribute to the increase of DOC.

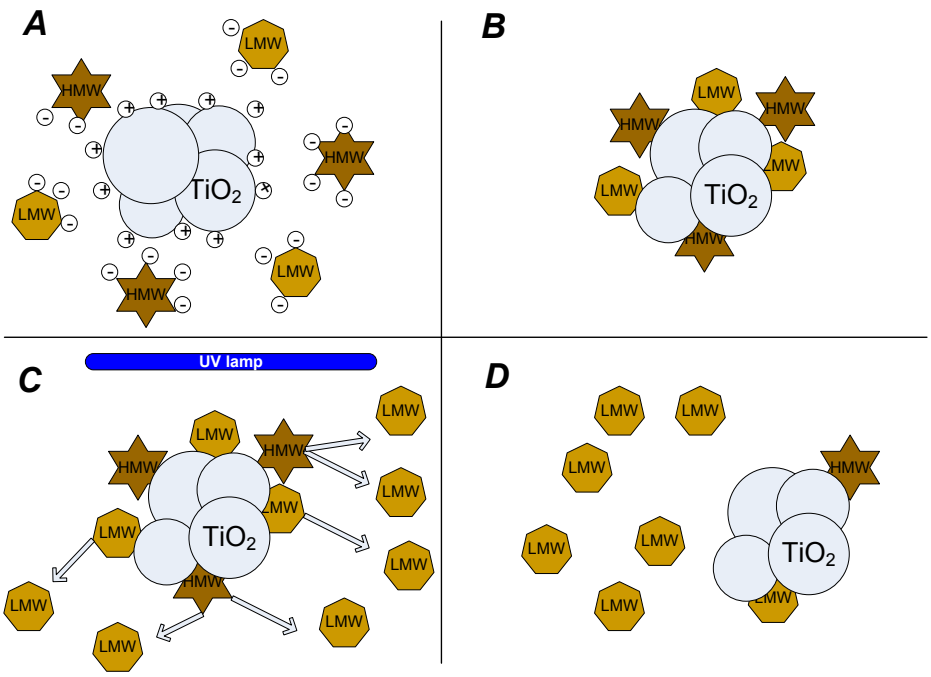

Figure 4-8. Photodesorption of DOM (HMW and LMW organics) from TiO_2 surface in SWW, (A) before adsorption, (B) after adsorption, (C) during photodesorption, (D) after photodesorption.

4.4 Conclusions

The photodesorption of DOM from TiO_2 was investigated using a recirculated reactor system. Process optimisation was carried out by changing the flow rate, TiO_2 loading, light intensity, organic loading and pH. Photodesorption of DOM increased with flow rate with an optimum photodesorption recorded at Q1 = 150 mL/min. The use of three lamps showed the highest desorption. Increasing TiO_2 concentration above 1 g/L had a detrimental effect on the photodesorption while lower TiO_2 loadings were not sufficient to get optimum photodesorption. Optimal organic loading concentration was found equal to 6.5 mg/L, while higher photodesorption was recorded at high pH indicating a significant role of electrostatic interactions in the photodesorption of organics. In addition, photodesorption of specific organic compounds with DOC of 7 mg/L was

investigated, which reveals that sodium lauryl sulphate, sodium lignin sulphonate and beef extract were the major contributing organic compounds for photodesorption in terms of adsorption of DOC and efficiency of photodesorption. LC-OCD fractionation indicated that the desorbed compounds are in majority LMW acids and neutrals. The decomposition of polysaccharides, humic substances and polypeptides found in SWW is believed to occur during photodesorption.

U T S

University of Technology Sydney
FACULTY OF ENGINEERING

Chapter 5: Synthesis and Characterisation of Potassium Polytitanate for Photocatalytic Degradation of Crystal Violet

5.1 Introduction

Nanostructured titanates produced by hydrothermal treatment of titanium dioxide (TiO_2) with strong alkaline solutions have generated much interest due to their unique combination of physico-chemical (Bavykin et al., 2006; Chen & Mao 2007; Morgan et al., 2008) and structural (Chen & Peng 2007; Yang et al., 2003) properties. Titanates, typically potassium titanate, exhibit attractive physico-chemical properties owing to their distinct crystal structures, which show great potential for cation exchange, catalysis (Izawa et al., 1982; Lee et al., 2000; Um et al., 2001) and photocatalysis (Dmitry et al., 2008; Ishihara et al., 2002; Zhuang et al., 2007).

Numerous potassium titanates, each with unique crystal structures containing layered and tunnel structures, have been synthesised (Berry et al., 1960; Masaki et al., 2000). Potassium titanates can be fabricated in the form of whiskers and fibres and have been applied as photocatalysts for water cleavage (Inoue et al., 1991; Janes et al., 2004). Masaki and Uchida (2000) adopted a hydrothermal oxidation of titanium metal powder in concentrated potassium hydroxide solutions above 150°C to obtain potassium titanates ($K_2Ti_2O_5$, $K_4Ti_3O_8$ and $KTiO_2(OH)$) as a single phase and fibrous amorphous product. It was then transformed into $K_2Ti_4O_9$, $K_2Ti_6O_{13}$ or $K_2Ti_2O_5$ by calcination. Hydrothermal reaction of TiO_2 nanoparticles and KOH solution resulted in titanate ($K_2Ti_6O_{13}$) nanowires with diameters of ~10 nm and lengths ranging from 500 nm to 2 μm (Du et al., 2003). Fine nanowires of $K_2Ti_8O_{17}$ with diameters of 5–10 nm and a surface area>300 m^2/g have been synthesised by a hydrothermal treatment of titania particles with KOH solution (Yuan, Zhang, et al., 2004). Due to their large surface areas, titanate nanowires can potentially be applied to environmental purification with enhanced photocatalytic activity (Du et al., 2003; Fujishima et al., 1972).

Over the past decades, several reports have been published on the synthesis and characterisation of potassium titanate nanostructures by high temperature hydrothermal treatment of powdered TiO_2 in a strong aqueous alkaline solution. Potentially, nanostructured titanates can be utilised in applications including catalysis, photocatalysis, lithium batteries and solar cells. However, rapid preparation route combining the use of low temperature, atmospheric pressure and a simple apparatus in the preparation of higher-order assemblies of titanate has not been well investigated. Therefore, in this work, attempts have been made to achieve a faster rate of nanofibre formation by carrying out reflux synthesis in a mixture of aqueous KOH and H_2O_2 at relatively low temperature. We report here on the synthesis of potassium titanate nanostructures utilising a redox strategy combined with a hydrothermal reaction involving TiO_2 powder, a basic KOH solution and an oxidising H_2O_2 solution. The adoption of the environmentally friendly H_2O_2-assisted hydrothermal route has been employed to synthesise other inorganic materials under hydrothermal conditions (Li et al., 2006; Piquemal et al., 2013). The nanostructures were characterised and tested for their adsorption and photocatalytic activity using crystal violet (CV) as a model pollutant.

5.2 Experimental

5.2.1 Materials

Titanium dioxide (Degussa P25) was used for the synthesis of potassium titanate. P25 is a mixed phase nanopowder with 70% anatase and 30% rutile with a surface area 50 m^2/g and a mean primary particle size of about 30 nm. Hydrogen peroxide (50% w/w) was obtained from Australian Scientific Pty Ltd., hydrochloric acid (37%, v/v) from

ScharlauChemie S.A., and potassium hydroxide (85%, w/w) and crystal violet (86%, w/w) from ChemSupply. Milli-Q water was used to prepare solutions and to wash powder samples.

5.2.2 Synthesis of potassium titanate

A modified peroxotitanate method was adopted, which involved mixing 2 g of P25 powder with 1% (designated as method A), 3% (designated as method B) and 5% (designated as method C) of H_2O_2 (50%w/w) in 10 M of KOH. For example, to prepare the samples through method A, 2 g P25 powder was added to a solution containing 1 mL H_2O_2 and 99 mL KOH. The mixtures were homogenised using a magnetic stirrer and placed separately into Teflon-coated containers, which were sealed and heated at 100°C in an oven for 24 h. After the hydrothermal treatment, the autoclave was naturally cooled to room temperature. The solid specimens were recovered by centrifugation (Centurion Sci., 2040) at 3000 rpm for 5 min, washed with 1 M HCl solution and Milli-Q water until pH 7, and then dried in an oven at 100°C for 12 h. The obtained powder samples, designated as A, B, and C from their respective synthesis methods, were also calcined in a furnace (Labec, CE-MLS) at 600°C for 4 h. Subsequently, these samples were designated as AC, BC and CC, respectively.

5.2.3 Characterisation

Morphology and elemental composition analyses were carried out using a scanning electron microscope (SEM, Hitachi S-4700) equipped with an energy dispersive X-ray detector (EDX-250 supplied by Horiba) operating at 15 kV. A Philips CM200 (Netherlands) transmission electron microscope (TEM) operating at 200 kV was employed to obtain micrographs of the specimens. X-ray diffraction (XRD) patterns

were generated on a MDI Jade 5.0 (MaterialsData Inc., USA) X-ray diffractometer with Cu Kα radiation source. The data were measured within the range of scattering angle 2θ of 5–90°. Powders of specimens were used without further treatment. Brunauer, Emmet and Teller (BET) surface area analyses were performed on an automated surface area analyser (Micromeritics Gemini 2360, USA) by means of nitrogen adsorption–desorption. The BET surface area was determined by a multipoint BET method using the adsorption data in the relative pressure (P/P_0) range of 0.05–0.18. The mean pore diameter and the total pore volume of samples were determined from the desorption isotherm via Barret–Joyner–Halender (BJH) model.

5.2.4 Adsorption and photocatalysis

CV powder was dissolved in pure water to prepare a stock solution of 10 mg/L concentration and the pH of the solution was adjusted to 7 using 0.1N NaOH. Dye adsorption experiments were conducted in an orbital shaking incubator (TU-400, Thermoline Sci.) operating at 150 rpm and 25°C for 30 min to reach adsorption equilibrium. Samples were collected and filtered through 0.45 μm (PTTF) syringe filters before analyses.

The photocatalytic activity of potassium titanates was assessed by batch experiments using photo reactor 2, a 2 L volume of stock CV solution. After the addition of 0.05 g/L photocatalyst, the slurry was mixed with a magnetic stirrer at 400 rpm for 30 min for dark adsorption. The cylindrical reactor (40 cm × 10 cm) vessel had three (15 W each) immersed UVC lamps (Perkin Elmer), a temperature controlling device and an air sparger (0.6 L/min) to provide dissolved oxygen. Photocatalysis was carried out for 120 min at a stable temperature of 26°C. Slurry samples were collected at 15 min intervals

and analysed for CV decomposition at λ = 590 nm using a Shimadzu UV-Vis1700 spectrophotometer. Dissolved organic carbon (DOC) concentrations were monitored using a Multi N/C 3100 (Analytik Jena) DOC analyser.

5.2.5 Separation by settling

After the photocatalysis procedure, the separation of catalyst particles was studied by monitoring the turbidity of the supernatant as a function of time at room temperature. Samples were collected at specific time intervals (0, 15, 30, 60, 90 and 120 min) at a depth of 5 cm and examined for changes in turbidity. The turbidity was measured using a turbidity and chlorine meter (HI 93414, Hanna instruments, USA), which was calibrated using standard turbidity solutions.

5.3 Results and Discussion

5.3.1 Characterisation of potassium titanate

5.3.1.1 SEM/EDX and TEM

SEM images of the potassium titanate specimen revealed longitudinally-oriented wire-like structures with a length up to several micrometres and diameters ranging from 10 to 30 nm (Figure 5-1). This hierarchical 3D nanowire network structure growth was formed by joining or welding P25 nanoparticles in KOH solution (Hu et al., 2013). Under hydrothermal conditions, titania reacted with the KOH solution and as a result potassium titanate nanocrystallines were created. These nanocrystallines began to grow on the substrate through the dissolution-recrystallisation process that formed nanowire-like structure (Hu et al., 2011).

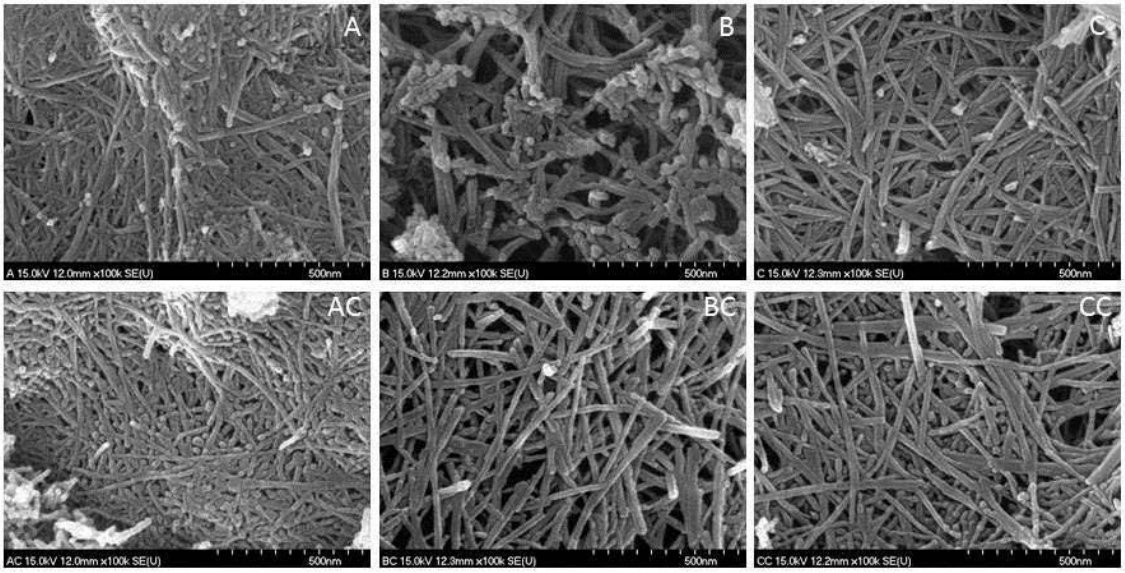

Figure 5-1. SEM images of the potassium titanate powders: as-prepared (A, B, and C) and calcined samples (AC, BC and CC).

TEM images showed belt-like structures of an isolated fibre, which was clearly visible in the transmitted electron image (Figure 5-2). The presence of lattice fringes indicated that the potassium titanate nanowires have a crystalline structure aligned with the orientation of their basal nanobelts. Parallel fringes in the walls correspond to a distance of about 1 nm, which can also be detected as abroad reflection by X-ray and electron diffraction (Patzke et al., 2002).

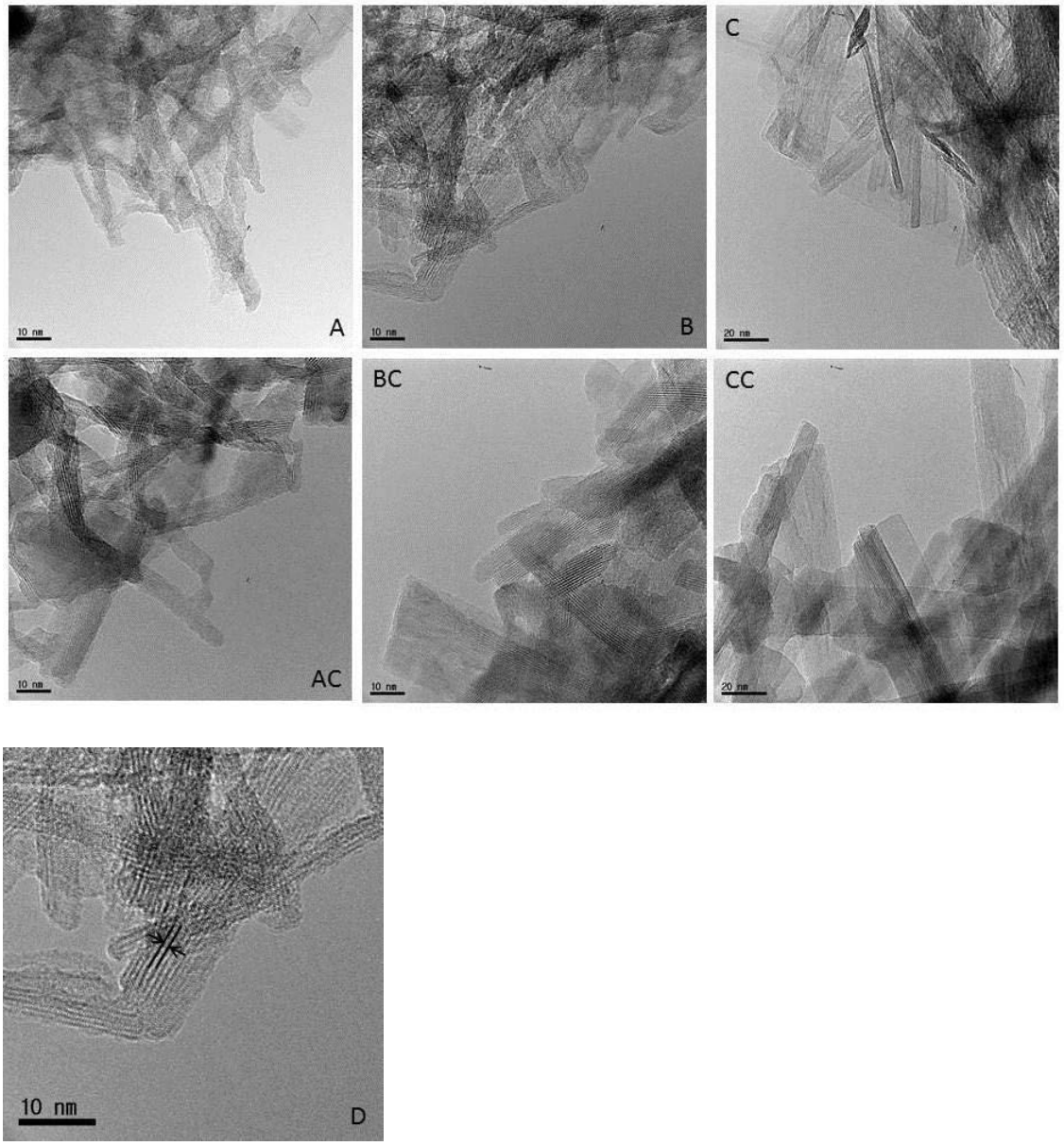

Figure 5-2. TEM images of potassium titanate powders: as-prepared (A, B, and C), and calcined samples (AC, BC and CC). The presence of crystalline lattice fringes oriented parallel to the belt orientation with a distance of about 1 nm (D).

5.3.1.2 Textural Property

Surface area, pore size and pore volume were determined using BET analysis. The data obtained from N_2 adsorption-desorption isotherms (see Appendix C) revealed typical IUPAC type (III) adsorption characteristics, with a significant hysteresis loop. The data

shown in Table 5-1 indicate that the obtained potassium titanates are macroporous (pore diameter >50 nm) materials. The surface area of P25 powder was 50 m^2/g but after hydrothermal growth, the surface area of specimens A, B and C increased to 330.1, 263.7 and 235.8 m^2/g, respectively. The increase in surface area of A, B and C can be attributed to the morphological change from nanoparticles to nanostructures (Di Wu et al., 2006; El Saliby et al., 2011; Sikhwivhilu et al., 2012; Yuan & Su 2004). However, after calcination at 600˚C, the BET surface area of specimens AC, BC and CC decreased significantly to 116.3, 105.1 and 84.9 m^2/g, respectively which is attributed to a change from nanotubes to nanorods at this temperature (Xiao et al., 2010; Yuan & Su 2004). The total pore volume of potassium titanate indicated an expected decline, whereas the mean pore diameter increased after calcination. The total pore volume decrease is due to the collapse of small pores during the calcination process (El Saliby et al., 2011; Zhou et al., 2009).

Table 5-1. Textural parameters of nanomaterials synthesis in this study

Sample	BET surface area (m^2/g)	Total pore volume (cm^3/g)	Mean pore diameter (Å)
P25	57.14	0.4277	80.72
A	330.10	1.271	96.11
AC	116.30	0.6063	150.70
B	263.68	1.1644	95.16
BC	105.09	1.482	129.52
C	235.81	1.103	104.26
CC	84.92	0.8928	208.96

5.3.1.3 X-ray Diffraction/EDX

The XRD peaks of P25 and potassium titanate powders were recorded for 2θ diffraction angles from 5^o to 90^o (Figure 5-3). The precursor (Evonik P25) is a mixed phase

catalyst showing anatase and rutile peaks. Five primary peaks of anatase phase at 25.42^{o}, 37.12^{o}, 48.05^{o}, 54.37^{o} and 63.19^{o} were recorded, while small diffraction peaks at 27.5^{o} and 55.4^{o} indicated the rutile phase. The XRD spectra of samples A, B and C were attributed to the transfer of a portion of anatase into mixed species of potassium titanate, and were recovered by calcining the specimens (i.e. AC, BC and CC) at 600^{o}C for 4 h. Calcination at high temperature resulted in the stronger diffraction peak, which indicates the formation of titania anatase (Xiao et al., 2010). Mixed species ($K_2Ti_8O_{17}$, $K_2Ti_6O_{13}$, K_2TiO_3 and $K_3Ti_8O_{17}$) of potassium titanate were identified (DIFFRAC^{Plus}Basic Evaluation Package, SEARCH/MATCH 10.1, Release 2004) as possible crystallisation sites under hydrothermal treatment in aqueous solution of H_2O_2 and KOH. This was consistent with TEM images (Figure 5-2), which revealed that some fraction of anatase was transformed into potassium titanate nanowires after 24 h (Riss et al., 2007). EDX spectra of the of P25 and potassium titanate were recorded and plotted in Appendix B. The EDX analysis confirmed the empirical composition of 45.97 wt% Ti which was observed to be in accordance with the theoretical compositions with the standard deviation of ±3% (Table 5-2).

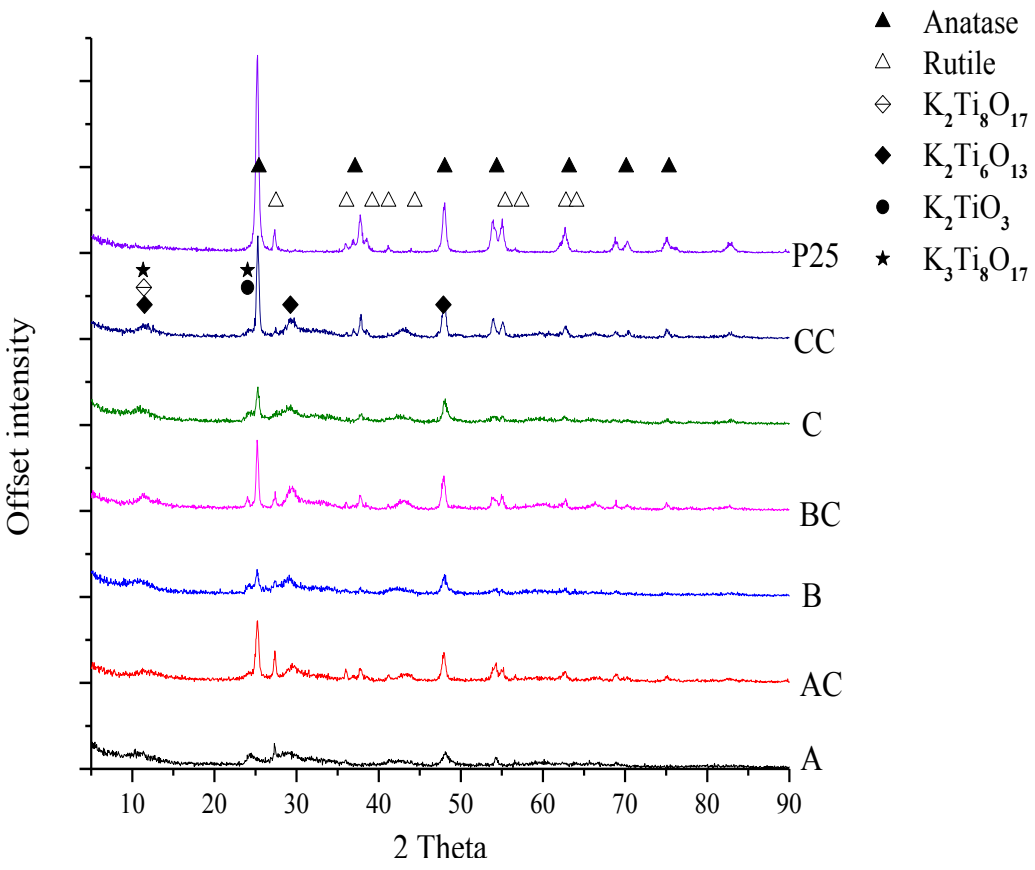

Figure 5-3. Powder XRD patterns of Degussa P25 and of the as-prepared (A, B and C) and calcined samples (AC, BC and CC).

Table 5-2. Elemental composition of the as-prepared (A, B and C) and calcined samples (AC, BC and CC).

	Elements	P25	A	AC	B	BC	C	CC
Weight %	O	52.37	41.65	43.20	45.82	41.06	43.51	44.11
	K	-	10.85	9.48	11.69	11.15	10.63	11.00
	Ti	47.63	47.50	47.32	42.49	47.79	45.86	44.89
Atomic %	O	69.27	58.59	64.20	62.50	61.43	62.32	64.96
	K		12.31	9.04	12.22	10.35	10.96	9.78
	Ti	30.73	29.09	26.76	25.28	28.22	26.71	25.26

5.3.2 Adsorption of crystal violet on potassium titanate

The adsorption of CV on the surface of the catalysts was studied and the results are shown in

Figure 5-4. Dispersed powders were coloured purplish-blue after mixing them with CV stock solution, indicating that the removal of CV is due to the adsorption of CV molecules on the potassium nanowires. After 30 min, complete decolourisation was reached for A and B, which completely adsorbed CV at 0.05 g/L catalyst loading. Catalyst A showed superior colour adsorption capacity and DOC removal. Adsorption followed the trend A>B>C>AC>BC>CC. Catalyst A had the greatest surface area (330.1 m^2/g) and largest pore volume (1.27 cm^3/g). Calcination had little negative effect on the adsorption capacity of the fibrous nanowires at low powder loading (0.05 g/L, 0.1 g/L and 0.2 g/L) but no effect on high loading (0.5 g/L). This can be explained by the decrease in surface area, pore volume and the increase of mean pore diameter. The effect of surface area of the catalysts on CV adsorption revealed that as-prepared potassium nanowire-assemblies are more effective adsorbent of CV than calcined nanowires. This was due to the biggest surface area showing the highest CV adsorption, while calcined specimens exhibited the lowest overall adsorption.

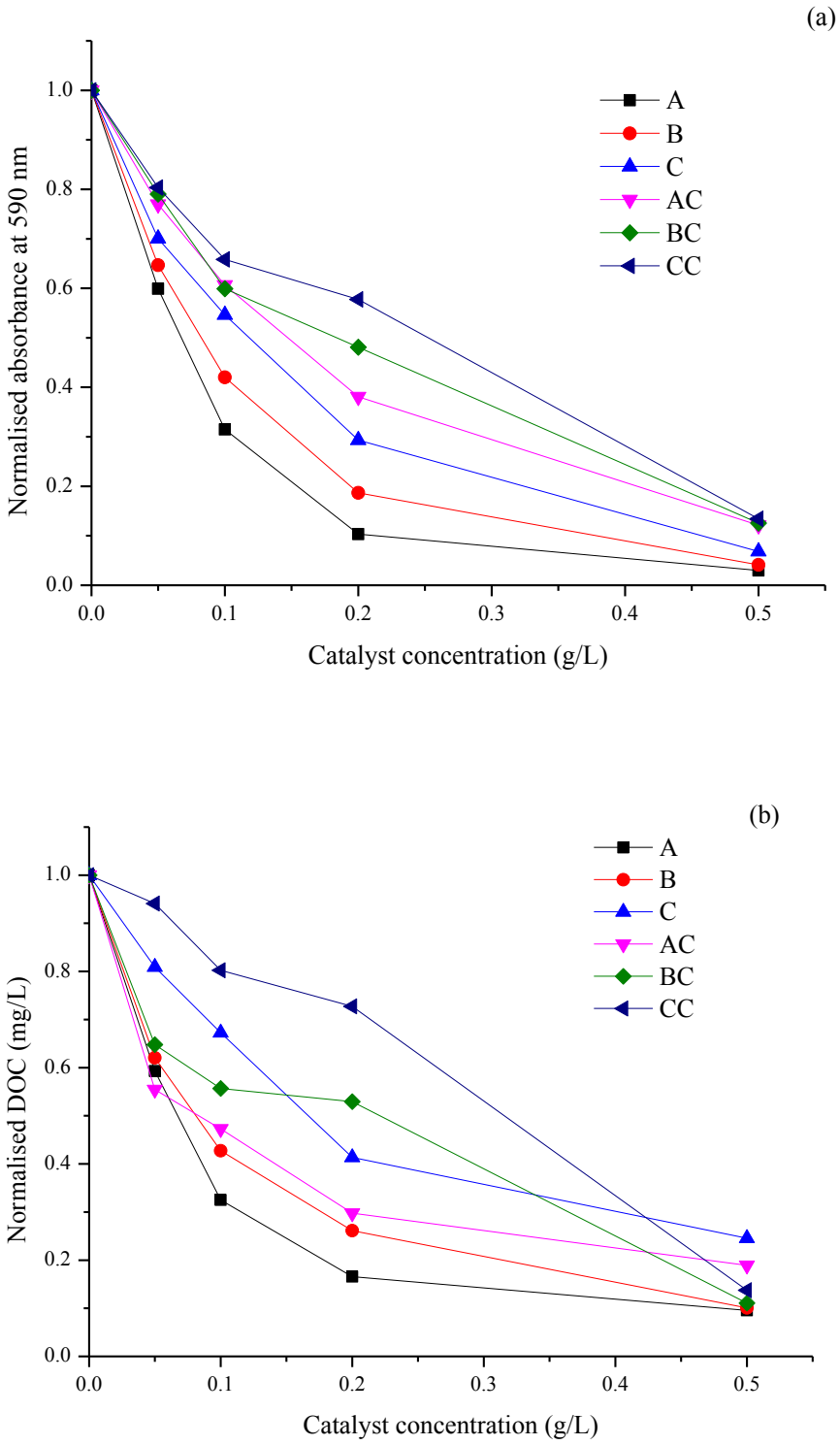

Figure 5-4. (a) Decolouration of 10 mg/L CV solution by adsorption on as-prepared samples (A, B and C) and calcined samples (AC, BC and CC); (b) DOC removal of 10 mg/L CV solution by adsorption on as-prepared samples (A, B and C) and calcined samples (AC, BC and CC).

5.3.3 Photocatalytic decolouration of crystal violet

The photocatalytic activity of synthesised potassium titanate was assessed by batch experiments using a 2 L volume of 10 mg/L CV solution with 0.05 g/L catalyst loading. Degussa P25 was used as a reference photocatalyst. CV was adsorbed onto the catalysts surface for 30 min in the dark before UV lamps were switched on. The decolourisation of the slurry was complete after 2 h of illumination and CV removal was assessed by the decrease in the absorbance at 590 nm and the decrease in DOC. Figure 5-5 shows the photocatalytic degradation of CV under UV light over time. Heterogeneous photocatalysis over titania follows a well-defined mechanism, which is initiated by the adsorption of efficient photons by titania, and is maintained through a series of reactions that involve the production of positives holes (h^+) and hydroxyl radicals ($OH^\bullet$) (Senthilkumaar et al., 2005). The photo oxidation of organic compounds is thus reached via successive attacks by $OH^\bullet$. In the present study, the photo oxidation of the slurry was completed after 150 min illumination, and was around 90% for A, and 85% for B followed by AC>C>BC>CC. The results showed that catalyst A was comparatively the best photocatalyst in terms of CV decolourisation and DOC removal as relative absorbance was reduced by 65% and the DOC was reduced by 50% at equilibrium. After 30 min of UV illumination, the removal of CV using macroporous nanowires decreased in the order A>B>C>AC>P25>BC>CC. The photocatalytic decolourisation of CV was not coupled with DOC.

However, the decrease in colour only indicated the photo-bleaching of dye but not their complete mineralisation of CV in the photocatalytic reaction. The photodegradation pathways of CV occurred in several steps (El Saliby et al., 2014): firstly, the generation of many N-demethylated intermediates and following this, pararosaniline was formed

as a final dye. Martins et al., (2006) investigated the photodegradation of pararosaniline and examined the formed by-products generated by the degradation process. They reported that formic acid is the main organic compound present in the solution in addition to carboxylic acid, aldehydes and ketones. These by-products contributed to residual DOC which was revealed by the persistence of organic by-products in the solution. The calcination of powders had a negative effect on the increase of the photoactivity of the catalysts, which can be described via the changes in morphology. Macroporous nanowires had lower BET surface area and pore volume after calcination, which reduced their photocatalytic activity.

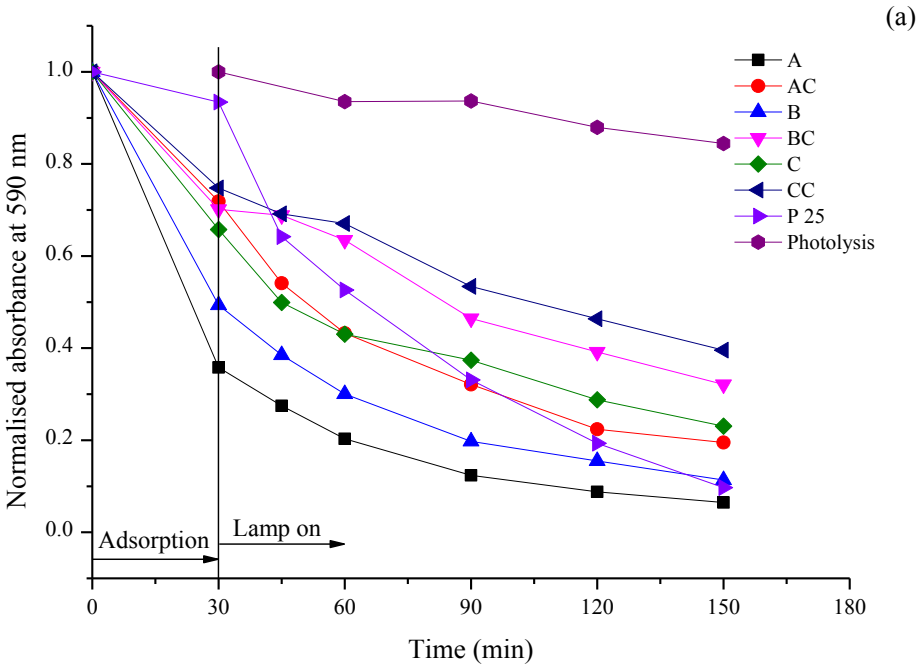

(b)

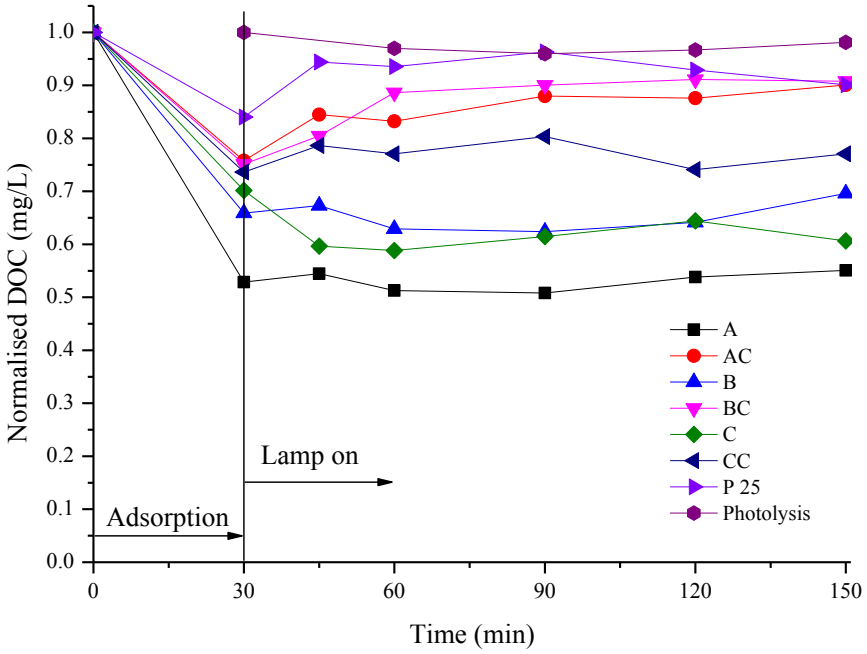

Figure 5-5.(a) Decolourisation and (b) photodegradation of CV monitored by DOC analysis on Degussa P25, as-prepared potassium titanate (A,B and C) and respective calcined samples (AC, BC and CC).([CV] = 10mg/L, pH 7, photocatalyst loading = 0.05 g/L).

5.3.4 Supernatant turbidity

For photocatalytic water treatment processes, separation of catalysts is a real burden after photocatalysis. For this reason, prepared photocatalysts were investigated for their ability to separate. A turbidity meter was used to monitor the decrease in solution turbidity over time which indicates an increase in the sedimentation rate of suspended particles. In Figure 5-6, normalised turbidity was plotted to compare all the photocatalysts' separation ability. After 2 h of static conditions, the decrease in solution turbidity was recorded as 75% for CC and 60% for C, while it was approximately 40% for A, AC, B and BC. On the other hand, the turbidity of the P25 suspension was

obtained relatively high with only a 30% decrease in turbidity after 2 h at static conditions.

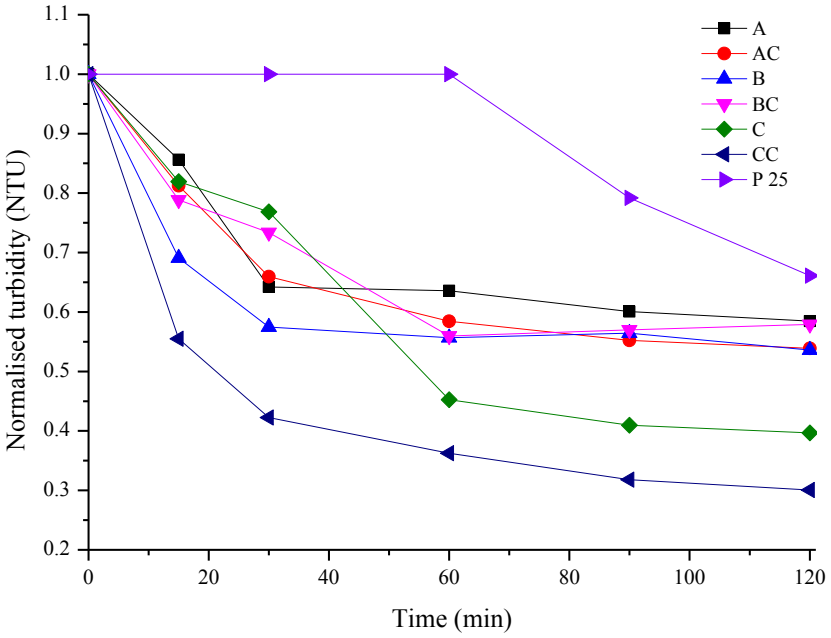

Figure 5-6. Normalised decrease in the supernatant turbidity using prepared samples (A, B and C) and calcined samples (AC, BC and CC) with 0.05 mg/L photocatalyst loading.

5.4 Conclusions

Potassium titanate nanostructures were synthesised using a hydrothermal method. Longitudinally-oriented wire-like structures with a length up to several micrometres in length and diameters ranging from 10 to 20 nanometres were produced by the treatment of TiO_2 (P25) with KOH and H_2O_2. Potassium titanate 'A' showed superior photocatalyst activity following the trend A>B>C>AC>BC>CC. Larger pore size fibrous nanowires resulting from this treatment showed high affinity in adsorbing CV, which was mainly due to the high surface area. The binding of K^+ and peroxo groups had a detrimental effect on the adsorption of the cationic dye because of surface

saturation, which decreased the adsorption sites. The decolourisation revealed their photocatalytic activity under UV light irradiation. It can be concluded that macroporous nanowires are effective adsorbents of CV and are capable of photocatalytic degradation. Finally, they can be easily separated from the solution by settling.

UTS

University of Technology Sydney
FACULTY OF ENGINEERING

Chapter 6: Adsorption and photocatalytic degradation of methylene blue using potassium polytitanate and solar simulator

6.1 Introduction

Dyeing industries consume large volumes of water and dye for dyeing process. Consequently a substantial quantity of dye is lost during this process (Prieto et al., 2005) and remains a major problem for the dying industry. Strong colour of residual dyes, high concentrations of salts, detergents and soaps, oil and grease, sulphide and sodas are the major constituents of dye wastewater (Rodriguez et al., 2002). Such industrial effluents pose serious threats to the environment due to their toxicity and often their non-biodegradability. Conventional treatment techniques such as adsorption on activated carbon (Ahmad et al., 2010; Khaled et al., 2009), coagulation/flocculation (Khouni et al., 2011; Riera-Torres et al., 2010) and reverse osmosis (Chen et al., 1998; Suksaroj et al., 2005) are ineffective for decolouring the effluents. This is because these techniques generate adsorbents or sludge as hazardous wastes (Torrades et al., 2004), which require further treatments. Therefore, efficient technologies with low energy consumption have motivated intensive research.

Alternative to conventional methods are advanced oxidation processes (AOPs) based on the generation of very reactive species such as hydroxyl radicals that oxidize a broad range of organic pollutants quickly and non-selectively (Vilar et al., 2011). One of AOPs, the photocatalytic oxidation which uses a semiconductor such as TiO_2 as a photocatalyst is a promising technology for removing toxic organic and inorganic contaminants from water. However, the development of a practical photocatalytic system is focused more on the cost effectiveness of the process. Recent advances in the field of semiconductors have attracted much attention in the synthesis of one-dimensional titanate nanostructures such as nanowires, nanospheres and nanofibres. Specifically, titanate nanofibres and nanowires are interesting because these

nanomaterials are different from those of the bulk materials. They have relatively large specific surface area, which may enhance their photocatalytic activity, leading to a greater potential for applications in water purification (Du et al., 2003). It is widely known that nanotubes are formed under alkaline reaction at high temperatures (Diebold 2003; Liu et al., 2006; Ma, Sasaki, et al., 2005; Masaki et al., 2002), which can promote unidirectional crystal growth, leading to the formation of nanowires (Sikuvhihulu et al., 2008) or nanowhiskers (Sikhwivhilu et al., 2012).

In this study, potassium polytitanate nanofibres synthesised by a relatively low temperature hydrothermal conditions were utilized for photocatalytic mineralization of MB using a solar simulator. Solar photocatalytic mineralization of organic water pollutants has a strong potential in the destruction of toxic organics in water as this has been widely demonstrated (Fernández-Ibáñez et al., 2003; Kaneco et al., 2004; Khanna et al., 2014; Malato et al., 2009; Robert et al., 2002; Vilar et al., 2011). The use of renewable solar energy as a UV photon source for the photocatalytic degradation of organic contaminants could be highly economical compared to the processes employing artificial UV irradiation, which require substantial electrical power input. Abundant solar energy could be utilized efficiently in the photocatalytic processes for degrading organic pollutants. For this reason, solar photocatalytic activity of potassium polytitanate catalyst was investigated using a batch reactor system exposed to artificial solar irradiation. The effects of MB concentration, catalyst loading, pH of the solution and light intensity on solar light-induced photocatalysis are investigated here to evaluate their significant potential applications.

6.2 Experimental

6.2.1 Materials

Potassium polytitanate nanofibres were synthesised by using titanium dioxide (Degussa P25) as a precursor in the presence of 1% (designated as A), 3% (designated as B) and 5% (designated as C) H_2O_2 (50% w/w, Australian Scientific Pty Ltd.) and KOH (10 N, 85% w/w, ChemSupply) by hydrothermal treatment at 100°C for 24 h as a modified peroxotitanate method (Shahid, El Saliby, et al., 2014). The samples were then calcined at 600℃ for 4 h and designated as AC, BC and CC, respectively. Hydrochloric acid (37%, V/V) was obtained from ScharlauChemie S.A. whereas sodium hydroxide (97%, w/w), potassium hydroxide (85%, w/w) and MB (86%, w/w) were purchased from ChemSupply Pty Ltd. Milli Q water was used to prepare the solutions and wash the powder samples.

6.2.2 Photoreactor

The Luzchem Research SolSim Xenon photoreactor (Figure 3-5) was used in the present study. It features an enclosed exposure chamber, an exhaust system and thermostatic control to maintain the chamber temperature close to ambient temperature. The Luzchem's SolSim delivers solar simulated radiation based on a powerful 300 W Xenon lamp installed at the top of the photoreactor chamber along with a custom filter assembly. The filter system ensured emission to closely match the AM1.5 spectrum. The solar simulation filters are placed on a stand 3 in above the chamber floor, with samples placed beneath them in a 250 ml beaker. Air sparging was adjusted at 0.6 L/min to provide adequate dissolved oxygen to the reaction.

6.2.3 Adsorption and photocatalysis

MB powder was dissolved in pure water to prepare a stock solution of 10 mg/L concentration and the pH of the solution was adjusted to 7 using 0.1 N NaOH. Dye adsorption experiments were carried out in an orbital shaking incubator (TU-400, Thermoline Sci.) operating at 150 rpm and 25°C for 30 min to reach adsorption equilibrium. Samples were collected and filtered through 0.45 μm (PTFE) syringe filters before being subjected to analysis.

The photocatalytic activity of potassium polytitanate was assessed using 200 mL of MB solution. The titanate loading and MB concentration were selected based on the results obtained in the adsorption experiments. The effect of solution pH (4, 7 and 9) and solar light intensity (5000, 15000 and 28000 lx; measured by a digital power meter AR 823) on the removal of MB was studied. MB molecules were adsorbed on potassium polytitanates in the dark after mixing at 450 rpm for 30 min. The solution was then placed in the solar simulator and photocatalysis was carried out for 180 min at a stable temperature of 26°C. MB degradation was monitored by collecting samples (filtered by 0.45 μm PTFE syringe filters) at fixed time intervals and analysed for colour removal at λ = 664 nm using a Shimadzu UV–Vis 1700 spectrophotometer. Samples were also examined for removal of dissolved organic carbon (DOC) using a Multi N/C 3100, Analytik Jena instrument. Mineralisation of MB was assessed by sulphate determination in collected samples using a Metrohm ion chromatograph (790 IC) equipped with a Metrosep A Supp 5-150 (150 mm × 4.0 mm, 5 μm) column. The kinetics of the photocatalytic discolouration of MB at different operating condition were analysed by nonlinear data fitting (OriginPro v8 software, OriginLab) to the equation:

$$C_t = C_0 e^{-k_a t} \quad \text{.....(6.1)}$$

where, C_t (mg/L) is the concentration of MB time t, C_0 (mg/L) is the initial concentration of MB, t is time, and k_a is the apparent pseudo first order constant.

6.2.4 Regeneration of catalyst

The photocatalytic stability of photocatalysts was studied by running the photodegradation experiments for 3 times under similar experimental conditions (MB blue = 10 mg/L, catalyst loading = 0.05 g/L, UV-Vis absorbance at λ= 664 nm). The cycled degradation was monitored by collecting samples at t = 0 (after 30 min adsorption), 90, 150 and 210 min of photoreaction and analysed for the decrease of absorbance at λ = 664 nm. After each degradation cycle, the supernatant was poured out from the reactor vessel and the photocatalyst was recovered by centrifugation at 3000 rpm for 5 min. The recovered powder was washed with 0.1 N HCl, pure ethanol and MQ water to remove any residual by products resulting from the photodegradation of MB. After each wash, the powder was separated by centrifugation and finally dried at 100 $^{\circ}$C for the next degradation cycle.

6.3 Results and Discussion

6.3.1 Adsorption and photocatalytic decolourisation of MB and DOC removal

Figure 6-1a shows the kinetics of the photocatalytic degradation of MB (10 mg/L) under solar simulator. Before the slurry was illuminated, MB was adsorbed onto the catalyst surface for 30 min in dark conditions and the adsorption capacity was obtained to be 71% for A, 33% for AC, 64% for B, 17 % for BC, 56% for C and 14% for CC. It is evident that the adsorption played a significant role in the degradation process. The

decolourisation of specific catalysts and slurry solutions was completed after 180 min illumination and was around 94% for A, 61% for AC, 90% for B, 44% for BC, 81% for C and 30% for CC. The baseline photolysis experiments showed that solar light illumination alone (i.e. in the absence of catalyst) for 180 min reduced the adsorption peak by 2% at $\lambda = 664$ nm. Relatively higher decolourisation potential of A was due to its high adsorption capacity, which adsorbed 71% of MB at equilibrium. A significant decrease in DOC (

Figure 6-1b) was observed during adsorption but not throughout the illumination phase, thus indicating there was an insignificant correlation between absorbance data and DOC measurements. Despite the removal of most of the colour from the solution by the catalyst, a large portion of organic carbon still remained in the solution. This indicated that while MB was degraded to the point where the colour was lost, it was not completely oxidized to carbon dioxide. This had been previously reported by other studies carried out on the degradation of MB (Beydoun et al., 2001). Such studies have indicated the formation of reaction intermediates and pointed to the difficulty of completely oxidizing organic dyes. A longer residence time, however, should lead to a greater extent of mineralization of the organic. The removal efficiency of MB using macroporous potassium titanate catalysts decreased in the order A > B > C > AC > BC > CC. Calcination of the powders did not increase the photoactivity of the catalysts, which can be attributed to the changes in textural parameters. Potassium titanate catalysts had lower BET surface area and pore volume after calcination (Shahid, El Saliby, et al., 2014), which negatively affected their photocatalytic activity. Degussa P25 was used as a reference photocatalyst and showed 95% decolourisation of MB solution and 85% DOC removal after 1 h of UV-irradiation at 50 mg/L load.

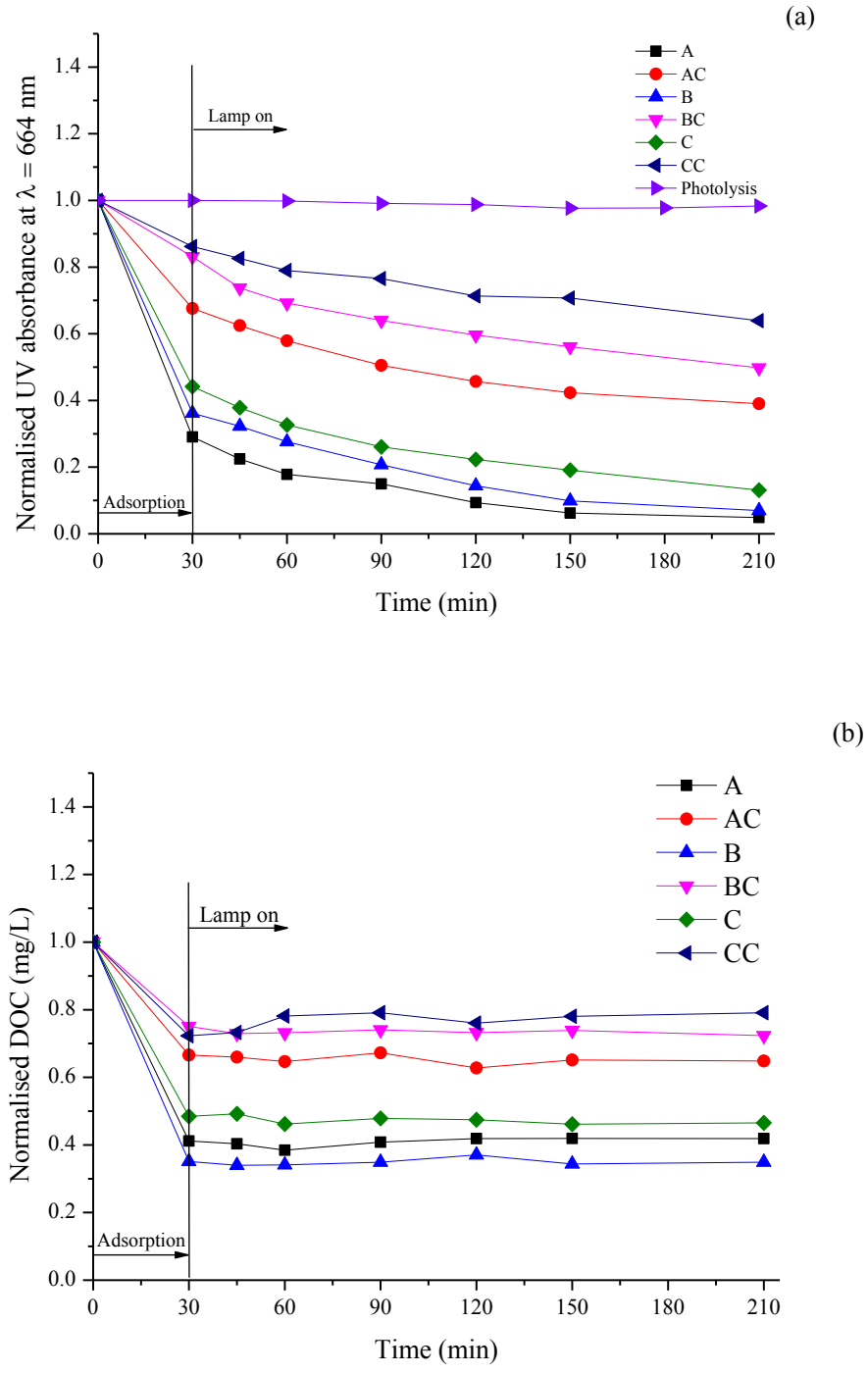

Figure 6-1. Kinetics of the (a) decolouration (UV-Vis absorbance at λ= 664 nm), and (b) photocatalytic degradation of MB on potassium titanate A, B, C, AC, BC and CC. (MB = 10 mg/L, pH = 7, catalyst loading = 0.05 g/L)

6.3.2 Mineralization of MB

The degradation of MB leads to the conversion of organic carbon into harmless gaseous CO_2 and that of nitrogen and sulphur into inorganic ions, such as nitrate and ammonium, and sulphate ions, respectively (Houas et al., 2001). The first step of MB degradation can be described by the cleavage of the bonds of the C–S^+=C functional group in MB. This will result in the formation of sulphate ions probably via the formation of a sulfoxide as an intermediate compound (El Saliby et al., 2011; Houas et al., 2001). The formation of inorganic sulphate ions is described in Figure 6-2 for an irradiation period of 3 hrs.

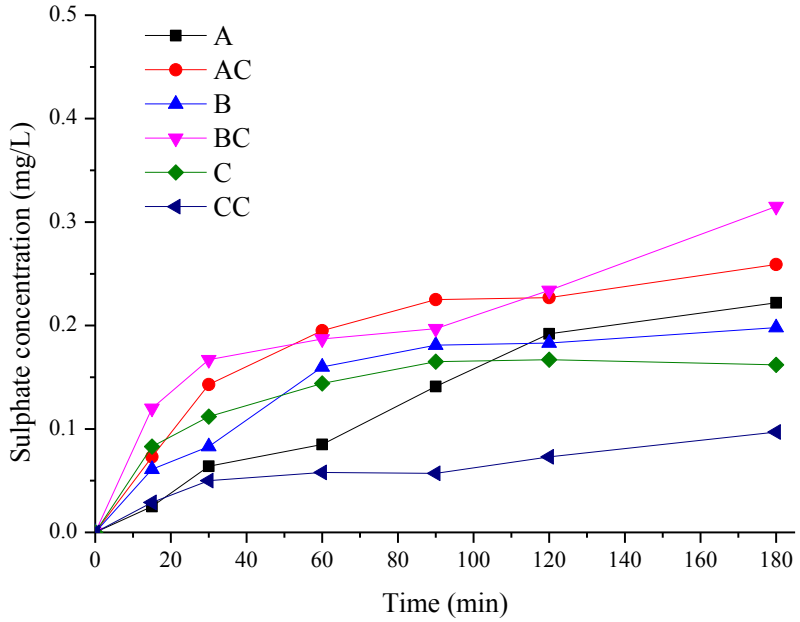

Figure 6-2. Evolution of sulphate ions during the photocatalytic degradation of MB over potassium polytitanate A, B, C, AC, BC and CC. (MB concentration = 10 mg/L, pH = 7, catalyst loading = 0.05 g/L)

In the photocatalytic degradation of MB over titania, two oxidative agents can be considered: i) photo-produced holes h^+ and ii) the strongly active $OH^\bullet$ radicals. In MB

degradation, h^+ is not involved in the initial step (cleavage of the bonds of the C-S+=C) of degradation since MB is a cationic dye (not an electron donor). Therefore, $OH^\bullet$ radicals are essential for the initiation of the MB degradation, which proceeds through a set of chemical reactions (Eq. 1). The end of the mineralisation is attained when the sulphur reaches its final maximum oxidation degree (+6) and SO_4^{2-} is produced after a 4th attack from $OH^\bullet$ radicals on the final by-product: $R\text{-}C_6H_4\text{-}SO_3H$ (Houas et al., 2001).

$$R\text{-}C_6H_4\text{-}SO_3H + OH^\bullet \rightarrow R\text{-}C_6H_4 + SO_4^{2-} + 2H^+ \qquad (1)$$

Thus, the increase in sulphate concentration in the solution indicates the mineralisation of MB.

6.3.3 Effect of operating conditions

6.3.3.1 Effect of MB concentration

Figure 6-3 shows the dark phase adsorption and photodecomposition of the initial concentrations of MB (5, 10 and 20 mg/L) using potassium polytitanate A. It is evident that the initial MB concentration played a significant role in the adsorption process, where 91%, 71% and 33% of MB were adsorbed at MB concentrations equal to 5, 10 and 20 mg/L, respectively. The discolouration of the solution was almost complete after 180 min of light irradiation. Catalyst A adsorbs almost all the dye at a relatively low initial concentration. In general, the dark adsorption of dye onto the catalyst surface follows the photo-oxidation process that occurs during UV irradiation. However, at high pollutant loadings, the surface saturation becomes a 'shading' barrier to the absorption of photons by catalyst leading to performance degradation by photocatalyst deactivation (Arana et al., 2004; Saquib et al., 2003).

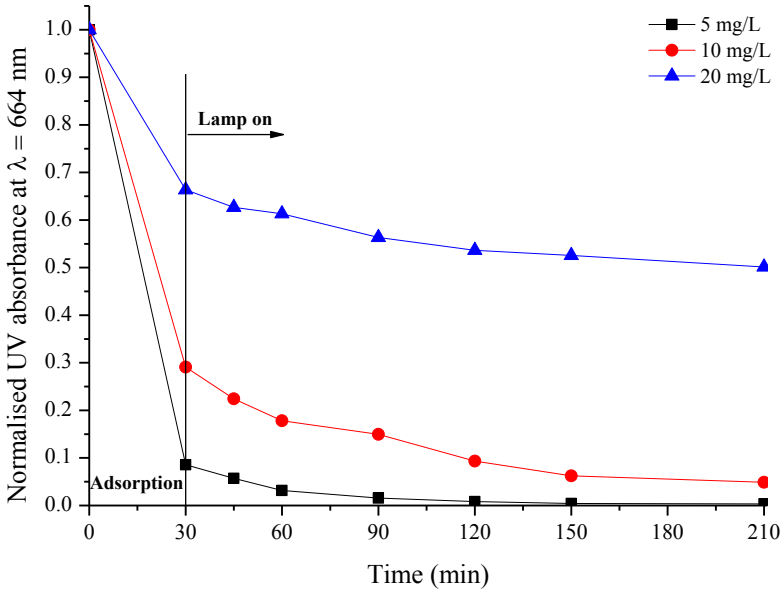

Figure 6-3. Effect of initial concentration of MB on the photodegradation efficiency (5, 10, and 20 mg/L). (pH = 7, catalyst loading = 0.05 g/L, UV-Vis absorbance at λ = 664 nm)

6.3.3.2 Effect of catalyst loading

The effect of catalyst A loading on the removal of initial 10 mg/L MB was studied at pH 7 using photocatalyst loadings of 0.01, 0.02, 0.05 and 0.1 g/L. The result on the effect of catalyst loading shown in Figure 6-4 illustrate an increase in adsorption with catalyst loading, which manifests as a major role player in the MB removal process. At 0.1 g/L catalyst loading, the adsorption of MB dominated (96%) which results in light screening (shading effect) and consequently reduced its photocatalytic activity (Chong et al., 2010). Furthermore, increased particle collision and agglomeration at high loadings also resulted in loss of the active surface area (Kaneco et al., 2004). At a catalyst loading of less than 0.1 g/L, the photocatalytic activity was absorbed efficiently but the MB decolourising efficiency was relatively low being 42%, 68% and 96%

compared to 99.9% at a loading of 0.1 g/L. Photocatalytic activity is dependent on the surface absorption of photons. With the increase of catalyst loading, the rate of the photocatalytic reaction increases due to the increase in the surface area of the photocatalysts available for adsorption and degradation (Mozia 2010).

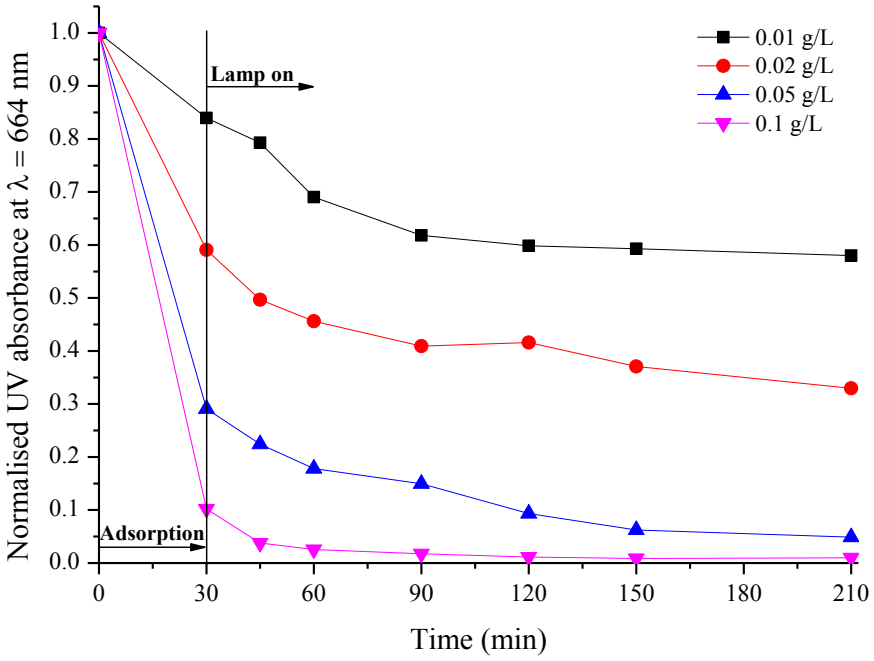

Figure 6-4. Effect of photocatalyst loading (0.01, 0.02, 0.05 and 0.1 g/L) on the removal of MB. (MB concentration = 10 mg/L, pH = 7, catalyst loading=0.05 g/L, UV-Vis absorbance at λ= 664 nm)

6.3.3.3 Effect of pH

Variation in pH of slurry solution directly affects the adsorption of MB molecules onto the catalyst because of the alteration in electrostatic interactions. The photocatalytic degradation of MB was studied using slurry (0.05 g/L of catalyst A and 10 mg/L of MB) at pH 4, 7 and 9 assuming that the initial concentration of MB is constant (Shimizu et al., 2007). The effect of pH on the decolouration of MB solution is shown

in Figure 6-5 after 30 min adsorption and 180 min of light irradiation. MB is a cationic dye which produces an intense molecular cation (C^+) and reduced ions (CH^+) (Kavitha et al., 2007). At high pH, OH^- on the surface of potassium titanate catalyst will favour the adsorption of cationic dye molecules on negatively charged surfaces (Fetterolf et al., 2003) of titanate. The zeta potential measurements of catalyst revealed that the point of zero charge is around pH 3.7 and the surface charge of the nanofibre was negative over a wide pH range (3.7 to 14). At pH 7 and 9, the electrostatic binding forces between the titanate and MB molecules dominated the adsorption process, leading to a higher overall adsorption (25% after 30 min) and photodegradation hereafter.

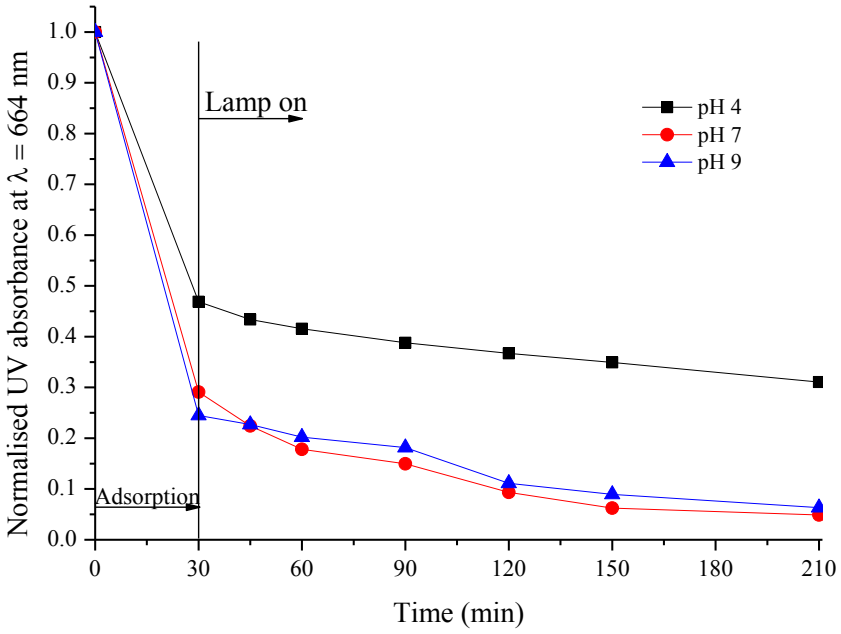

Figure 6-5. Effect of pH (4, 7 and 9) on the photodegradation of MB. (MB concentration = 10 mg/L, catalyst loading = 0.05 g/L, UV-Vis absorbance at λ = 664 nm)

6.3.3.4 Effect of light intensity

The effect of light intensity on the photodegradation of MB was studied and the results are indicated in Figure 6-6. The light intensity of the system can affect the electron/hole formation, and their separation and recombination rate. However, this can also be affected by the emitted wavelength of the lamp and the type of photocatalyst. In the reactor used in the present experiments, the increase of light intensity from 5000 lx to 28000 lx did not significantly alter the degradation rate of MB after 180 min of light irradiation. The excitation of catalyst surface by a radiant photonic flux ($\lambda < 400$ nm) occurs at very low light intensity. Fujishima et al., (2000) indicated that few photons of energy (as low as 1 $\mu W/cm^2$) are sufficient for the initiation of the photocatalytic reaction. However, the increase of light intensity is essential to ensure that the photocatalyst surface is being appropriately irradiated.

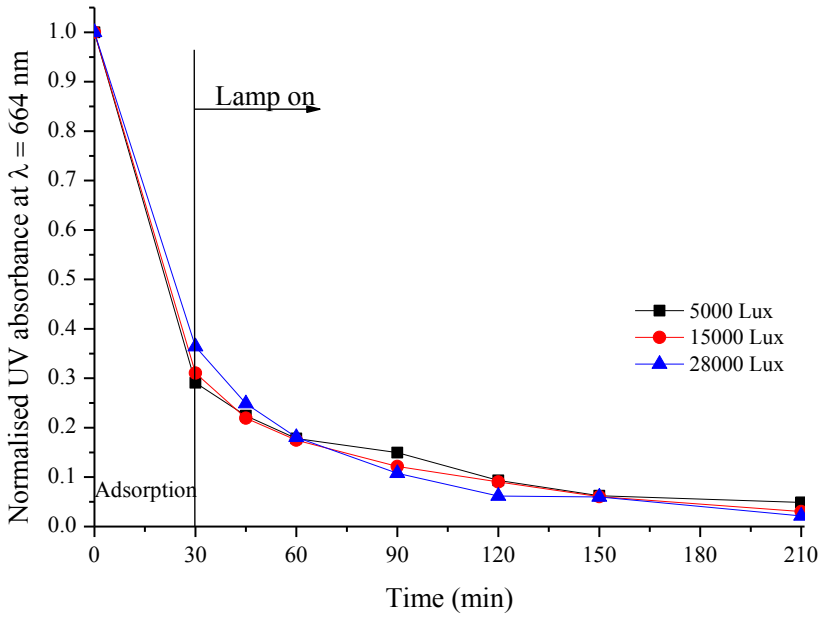

Figure 6-6. Effect of light intensity (5000, 15000 and 28000 Lux) on the photodegradation of MB. (MB concentration = 10 mg/L, catalyst loading = 0.05 g/L, UV-Vis absorbance at $\lambda = 664$ nm)

The photo discolouration of MB over titanate followed the pseudo-first order reaction kinetics. Similar finding was reported by (Houas et al., 2001) for the photodegradation of MB over Degussa P25. The pseudo-first order apparent constants are shown in Table 6-1. These were calculated by using the decrease in MB concentration (k_a) at different operating conditions such as MB concentration, catalyst loading, pH and light intensity. The apparent rate constant increased with the increase in catalyst loading and light intensity whereas k_a decrease with the increase in MB concentration.

Table 6-1. Apparent pseudo-first order kinetics for the photocatalytic degradation of MB over K-titanate 'A' under various operating conditions.

Parameter				Operating conditions									
	MB concentration			Catalyst loading				pH			Light intensity		
	5 mg/L	10 mg/L	20 mg/L	0.01 g/L	0.02 g/L	0.05 g/L	0.1 g/L	4	7	9	5000 lx	15000 lx	28000 lx
k_a (min^{-1})	0.021	0.011	0.001	0.002	0.003	0.011	0.014	0.002	0.011	0.007	0.011	0.013	0.016
R^2	0.897	0.947	0.856	0.574	0.711	0.947	0.929	0.939	0.947	0.971	0.947	0.979	0.956

k_a constant were calculated from the MB concentration degradation curve.

6.3.3.5 Regeneration of catalyst

The regeneration of catalyst A was monitored over three consecutive photodegradation cycles of MB solution (10 mg/L) at 0.05 g/L catalyst load (Figure 6-7). The photocatalyst was recovered after each cycle by sedimentation, washing and separation by centrifugation and drying at 100°C before using in the next cycle. Compared to the first cycle, the regenerated catalyst A shows a reduction in adsorption performance by 29% (second cycle) and 38% (third cycle). As shown in Figure 6-7, the MB degradation performance also decreased by 38% (second cycle) and 44% (third cycle) compared to the first cycle.

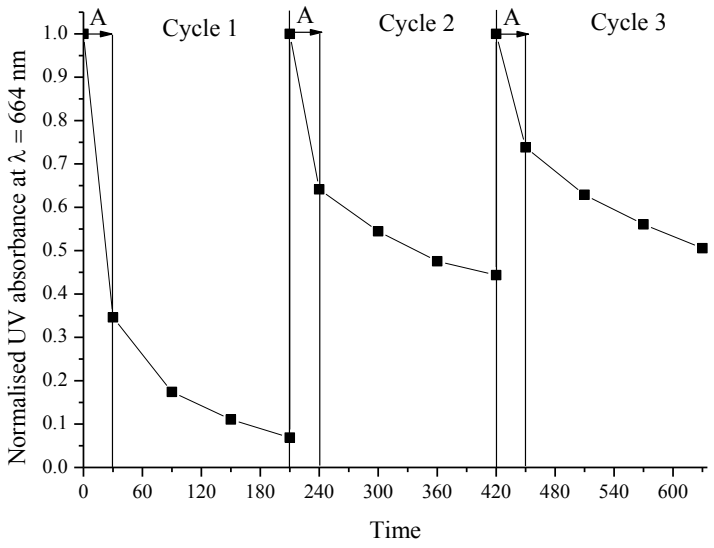

Figure 6-7. Photocatalytic life cycle of potassium polytitanate 'A' (MB concentration =10 mg/L, catalyst loading = 0.05 g/L, UV-Vis absorbance at λ = 664 nm)

6.4 Conclusion

The adsorption and photocatalytic degradation of MB onto potassium polytitanate was studied under solar light. These potassium polytitanate nanofibres are considered as effective adsorbents of MB and are also capable of its photocatalytic degradation. The

significant decrease of DOC was observed during adsorption but not throughout illumination showing insignificant correlation between absorbance data and DOC measurements. The mineralisation of MB was studied for sulphate evolution, which confirms the photo-oxidative degradation of the pollutant, and therefore the photocatalytic activity of potassium polytitanate. The photocatalyst A was found to be efficient in photocatalytic degradation of MB and was used to investigate the effects of MB loading, catalyst loading, pH and light intensity. The optimum operational conditions for the photocatalytic degradation of MB were found at 0.05 g/L of photocatalyst, 10 mg/L MB and pH 7. Moreover, stability of photocatalytic A was studied for 3 degradation cycles using adsorption/photocatalysis model.

University of Technology Sydney
FACULTY OF ENGINEERING

Chapter 7: Adsorption behaviour of Pb(II) onto potassium Polytitanate nanofibre

7.1 Introduction

Lead is a highly toxic metal that increasingly accumulates in the living environment from both natural and anthropogenic sources. Worldwide, lead is used in the production of automobile and industrial lead–acid batteries. Other anthropogenic sources of lead include the combustion of coal, incineration of refuse of lead containing pesticides, processing and manufacturing of lead products. The extraction of lead and smelting processes generate large volumes of lead-containing wastewater. Furthermore the presence of lead in water bodies is of critical concern since these pollutants invariably persist in the environment. Elevated levels of lead may have adverse impacts on the ecosystem (Fang 2004; Velez et al., 1998) and pose serious public human health risks (Matlock et al., 2002; Yang et al., 2004) due to toxicity, bioaccumulation, and non-biodegradation (Semerjian 2010; Sousa et al., 2010; Wong et al., 2003). Exposure to lead can cause severe damage to the kidneys, nervous system, reproductive system, liver and brain (Matlock et al., 2002). Consequently aqueous lead pollution poses significant dangers to the environment.

To remove heavy metal ions from aqueous system, many conventional methods, including ion-exchange (Misra et al., 2011), oxidation, chemical precipitation and coagulation (Chen et al., 2009; El Samrani et al., 2008), membrane separation (Min et al., 2012) and adsorption (Senthil Kumar et al., 2012; Wang, Yang, et al., 2010) have been investigated. Of those methods, adsorption is a promising one, mainly because it is easy to implement (Senthil Kumar et al., 2012; Wong et al., 2003). An ideal adsorbent should have a high surface area with uniformly accessible pores and physical and chemical stability (Kim et al., 2004). Recently, nanomaterials have been investigated in the search for highly effective adsorbents that remove toxic metal due to

their unique chemical and physical properties (Zhang & Fang 2010). Titanate nanostructures with small diameters prepared by using the alkaline hydrothermal method have attracted a great deal of attention since the innovative work of Kasuga et al. (1999). This material can be fabricated by employing the hydrothermal treatment of TiO_2 in concentrated alkaline conditions at moderate temperatures (90-180^oC) with resulting in high quality and efficient yield (Bavykin et al., 2006). This method, therefore, can potentially be used in for large-scale industrial production (Sun et al., 2003). Due to their cation exchange ability (Bavykin et al., 2006; Bavykin et al., 2005; Sun et al., 2003) and large surface area (Kim et al., 2008), titanates have the potential to be used as effective adsorbents for toxic metal removal from wastewater.

In this study, potassium polytitanate nanofibres synthesised under relatively low temperature hydrothermal conditions were utilized as adsorbents to remove lead ions from aqueous media. The effects of lead ion concentration, adsorbent loading and pH of the solution were examined. The adsorption kinetics and mechanism were also analysed.

7.2 Experimental

7.2.1 Materials

Hydrochloric acid (37%, V/V) was obtained from ScharlauChemie S.A. whereas sodium hydroxide (97%, w/w), potassium hydroxide (85%, w/w) and lead nitrate (99.9%, w/w) were obtained from ChemSupply Pty Ltd. Milli Q water was used to prepare the solutions. Potassium polytitanate nanofibres were synthesised by the hydrothermal treatment of 2 g of TiO_2 (Degussa P25) in 1 ml of H_2O_2 (50% w/w,

Australian Scientific Pty Ltd.) and 99 ml KOH (10 N, 85% w/w, ChemSupply) at 100°C for 24 h (Shahid, El Saliby, et al., 2014).

7.2.2 Adsorption experiment

Analytical grade lead nitrate was used to prepare a stock solution of Pb(II) (1000 mg/L) in Milli Q water and was diluted to the desired concentrations for adsorption experiments. The adsorption experiments were performed in 250 mL conical glass Erlenmeyer flasks containing 100 mL of Pb(II) solution. The pH of Pb(II) solution was adjusted after adding desired amount of titanate by using HCl (0.1 N) or NaOH (0.1 N). Homogeneity of suspensions was maintained by placing the flasks in an orbital shaking incubator (Thermoline, TU400) at a set temperature of 25°C and a shaking speed of 150 rpm for 2 h. Samples were collected at designated time intervals, filtered through 0.45 mm polytetrafluoro-ethylene (PTFE) membrane syringe filters, and analysed for Pb(II) concentration using an Agilent Microwave Plasma Atomic Emission Spectrometer (4200 MP-AES, Agilent Technologies). The amount of Pb(II) ion adsorbed q_t (mg/g), at time t (min) , was calculated by

$$q_t = \frac{(C_i - C_t)V}{m} \quad \text{Eq.7.1}$$

where C_i *and* C_t *(mg/L)* are initial and final concentrations of Pb(II) ion , respectively, V (L) is the volume of Pb(II) ion solution, and m (g) represents the mass of the titanates.

Effect of pH

The pH of the solution is known to affect the surface charge of the nanofibres, and consequently the adsorption of Pb(II) molecules. Experiments were conducted at pH values of 5, 7 and 9 while all other factors were kept constant, i.e. titanate loading 0.5 g/L, Pb(II) = 10 mg/L and T= 25°C.

Effect of adsorbent dose

In this experiment, four different powder loadings (0.01, 0.02, 0.05 and 0.1 g/L) were selected to study the adsorption of Pb(II) molecules onto titanate. The experimental conditions were: Pb(II) concentration = 10 mg/L, pH = 5 (after adding the titanate pH was adjusted) and T= 25°C.

Effect of Pb(II) concentration

After optimising the titanate loading, three Pb(II) concentrations (2, 5 and 10 mg/L) were selected to study the kinetics of adsorption. The experiment was performed under the following conditions: titanate loading 0.5 g/L, pH = 5 and T= 25°C.

Adsorption kinetic modelling

To understand the adsorption mechanism of Pb(II) ion onto titanate , the uptake rate of metal ions were analysed using a pseudo-second order kinetic model. The pseudo-second-order kinetics is described by the following equation.

$$\frac{t}{q_t} = \frac{1}{k_2 q_e^2} + \frac{1}{q_e} t \quad \text{..... Eq.7.2}$$

Where q_t and q_e are the amount of Pb(II) ion adsorbed at elapsed time t and equilibrium, respectively, k_2 (g mg^{-1} min^{-1}) is a pseudo-second order rate constant. The value of $_{k2}$ and q_e can be calculated from the slope and intercept of the plot of t/q_t versus time t. The initial adsorption rate h (mg g-1 min-1), is estimated at time t as follows

$$h = k_2 q_e^2 \quad \text{..... Eq.7.3}$$

7.2.3 Adsorption mechanism

The adsorption mechanism was examined by analysing the FTIR spectra of titanate adsorbents and Pb-loaded titanate and ion exchange results. The FTIR spectra of the pure titanate and Pb-loaded titanate samples were obtained using an IRAffinity-1 (SHIMADZU) and analysed for adsorption peaks of titanate and Pb^{+2} ion-loaded titanate. The K^{+} ion in the sample solution was determined using a Metrohm ion chromatography (790IC) equipped with a Metrosep A Supp 5-150 (150 x 4.0 mm, 5µm) column. The Zetasizer (ZEN3600, Malvern Instrument, UK) operating with a He-Ne laser at a wavelength of 633 nm was measure the zeta potential.

7.2.4 Desorption and reusability studies

In a typical experiment, 0.05 g/L of titanates were initially contacted with 10 mg/L Pb(II) solution at pH 5 for adsorption. After each adsorption cycle, the Pb-loaded titanates were separated and added to 1M HCl solution for desorption. The suspensions were retained on an orbital shaker at 150 rpm for the purpose of desorption. After the desorption, the titanate were washed with MilliQ water several times to remove the residual desorption agent by centrifugation and dried in an oven at 100°C overnight for reuse in another cycle. Three cycles of consecutive adsorption–desorption-regeneration were carried out to test the reusability of titanate for the removal of Pb(II).

7.3 Results and Discussion

7.3.1 Effect of pH

The pH of a solution is an important parameter affecting metal ion adsorption (Iftikhar et al., 2009) as it influences the surface charge of absorbents, the degree of metal ionization and the metal speciation, all of which can affect the adsorption mechanism

and the uptake capacity (Babel et al., 2004). The effect of pH on the surface charge of titanate can be characterised by the zeta potential.

The role of hydrogen ion concentration on Pb(II) adsorption on titanate was examined at different pH (3, 5, 7 and 9) (Figure 7-1). The removal of Pb(II) from solution increased significantly with an increase in pH. Lead may be present in solution in the forms of Pb^{2+}, $Pb(OH)_2^0$ and $Pb(OH)_3^-$ at different pH values (Xu et al., 2008). At pH < 6, the predominant lead species is Pb^{2+}. Therefore, the low Pb^{2+} sorption that takes place at low pH can be attributed partly to the competition between H^+ and Pb^{2+} ions on the surface sites (Weng et al., 2004; Xu et al., 2008). At pH 7 and 9, the concentration of Pb(II) remaining in solution is similar but significantly lower than at pH 3 or 5. The main species at pH 7–9 are $Pb(OH)^+$ and $Pb(OH)_2^0$ and consequently the removal of Pb is possibly accomplished by simultaneous precipitation of $Pb(OH)_2^0$ and sorption of $Pb(OH)^+$.

The effect of pH on the adsorption of Pb(II) may be explained by the net charge difference on the surface of titanate and H^+ competition for adsorption sites (Xiong et al., 2011). As shown in

Figure 7-2, the surfaces of titanate became negatively-charged which enhanced the adsorption of positively charged Pb(II) by electrostatic attraction. The maximum difference in zeta potential value was obtained at around pH 5 between positively-charged titanate and negatively-charged Pb(II). Therefore, electrostatic attraction was enhanced between Pb(II) and titanate. Meanwhile, at pH 5, the concentration of H^+ ions decreased with the increase in pH, leaving fewer H^+ ions available to compete with Pb(II) ions for adsorption sites.

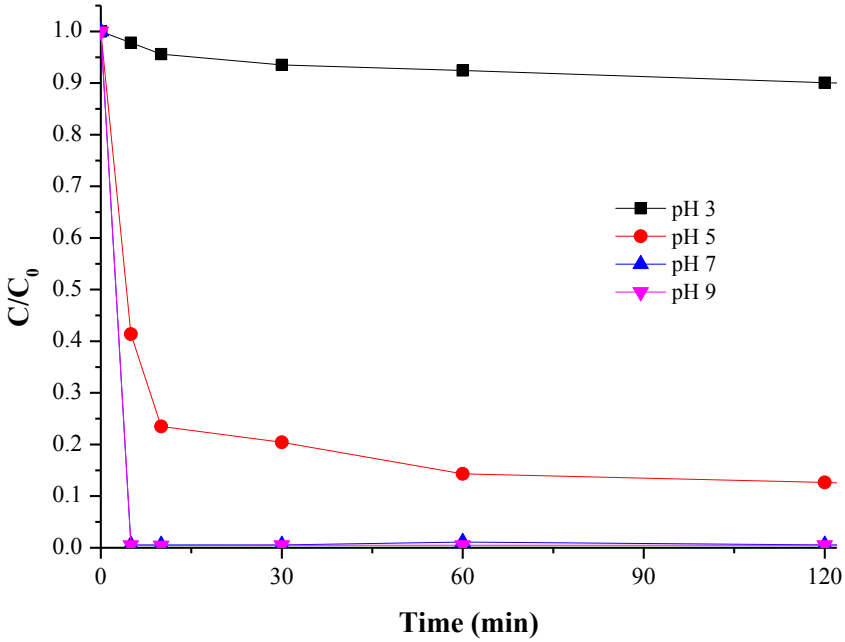

Figure 7-1. Effect of solution pH on the adsorption of Pb(II) from solution. (Experimental conditions: Pb(II) concentration = 10 mg/L, T = 25°C, shaking speed = 150 rpm, titanate dose = 0.05 g/L).

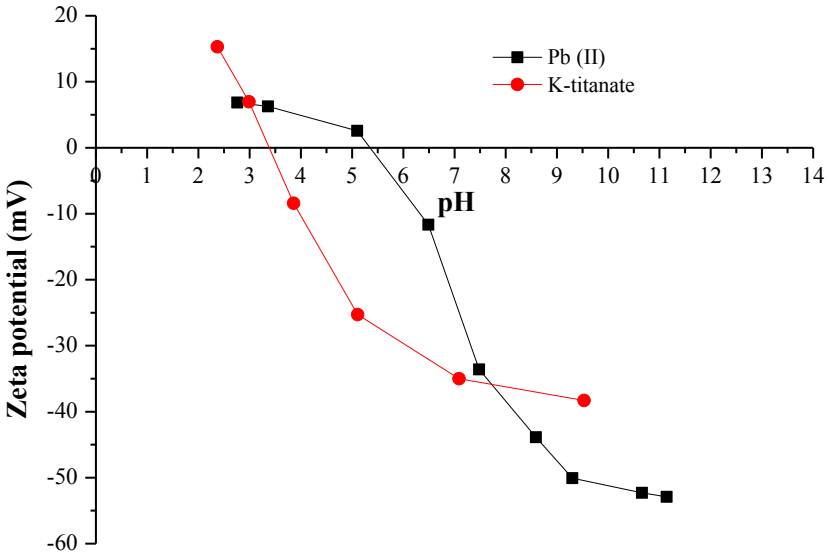

Figure 7-2. Zeta potential of 10 mg/L suspension of potassium titanate and Pb(II).

7.3.2 Effect of adsorbent dose

The effect of adsorbent concentration on Pb(II) (10 mg/L) adsorption kinetics was examined with 0.01, 0.02, 0.05 and 0.1 g/L of titanate. Figure 7-3 illustrates the fraction of Pb(II) adsorbed on titanate with time at 4 different adsorbent concentrations and at pH 5. The adsorption of Pb(II) onto titanate was completed quickly, and 30 min was enough to reach equilibrium for all the experiments. It is evident that the initial uptake of Pb(II) determines the adsorption capacity which can probably be attributed to a number of available active sites on the surface of the adsorbent (Rafatullah et al., 2009). An increase in titanate dosage from 0.01 to 0.1 g/L increased the adsorption of Pb(II) from 43.75% to a remarkably high 99.13% in 2 h. As the titanate concentration increased, the fraction of Pb(II) ion adsorption increased as anticipated since the available surface site increased with the adsorbent concentration (Jayaram et al., 2009).

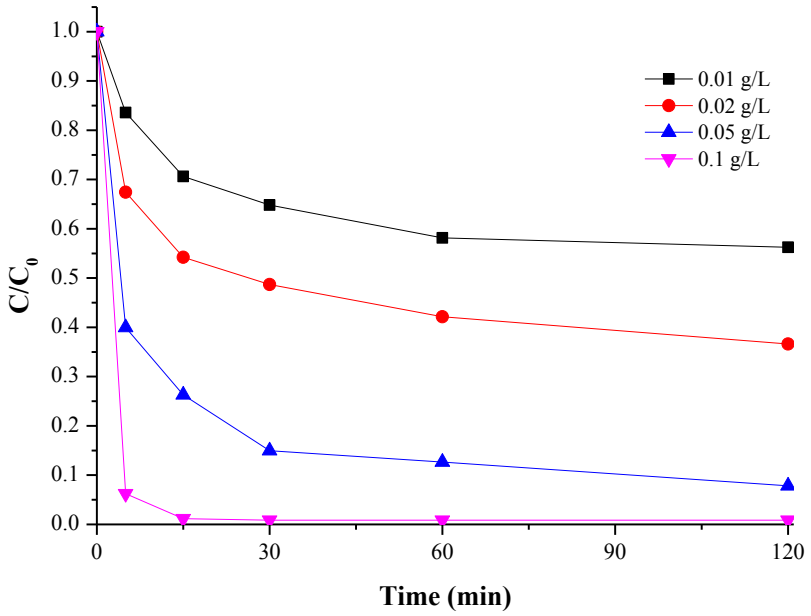

Figure 7-3. Effect of titanate dose on the adsorption of Pb(II) from solution. (Experimental conditions: Pb(II) concentration = 10 mg/L, T = 25°C, shaking speed = 150 rpm and pH = 5).

7.3.3 Effect of initial concentration of Pb(II)

Figure 7-4 shows the adsorption of Pb(II) onto titanate using initial Pb(II) concentrations of 5, 10, and 20 mg/L at pH 5 and titanate dosage of 0.05 g/L. 97%, 95% and 50% of Pb(II) were removed at Pb(II) concentrations equal to 5, 10 and 20 mg/L, respectively. The amount of Pb(II) adsorbed increased over time until the equilibrium was attained at 30 min for high Pb(II) concentrations (10 and 20 mg/L), while almost all Pb(II) was adsorbed within 5 min at 5 mg/L of Pb(II). The initial uptake (first few minutes) for Pb(II) was high because a large number of adsorption sites were available for adsorption (Rafatullah et al., 2009). Later on, the adsorption decreased as the repulsive forces between the adsorbed Pb(II) on titanate and the Pb(II) molecules in the solution increased (Fetterolf et al., 2003; Xiong et al., 2010).

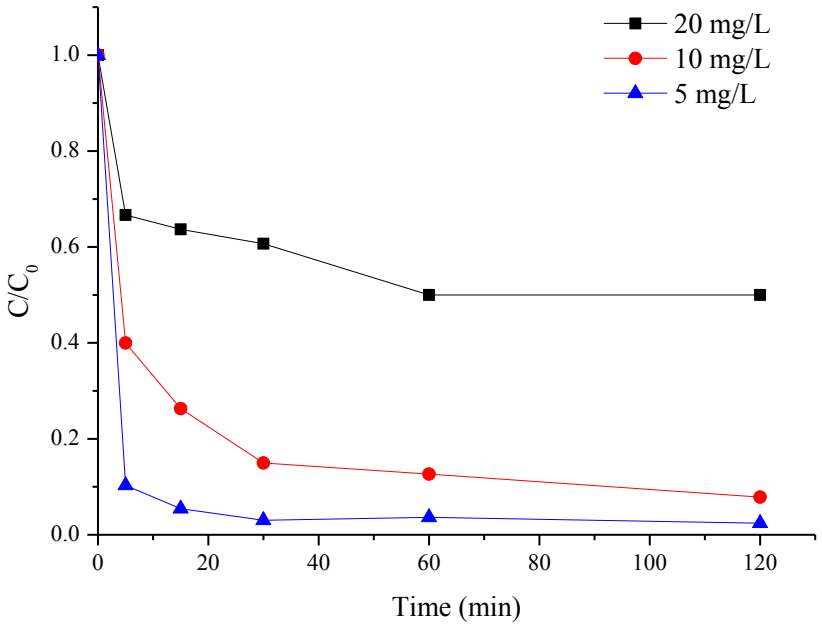

Figure 7-4. Effect of initial concentration of Pb(II) on the adsorption of Pb(II) from solution. (Experimental conditions: Titanate loading = 0.05 g/L, T = 25°C, shaking speed = 150 rpm and pH = 5).

7.3.4 Comparison of potassium titanate with P25 for Pb(II) removal

The adsorption capacity of the titanate was compared with that of P25. Adsorption experiments were conducted with 10 mg/L Pb(II) concentration and 0.05 g/L adsorbent loading at pH 5. Figure 7-5 compares Pb(II) adsorption capacity on potassium titanate and P25 which illustrated the adsorption capacity of titanate is higher than P25. The titanate has a relatively larger surface area (330 m^2/g in comparison to 50 m^2/g for P25) and a lower point of zero charge (pH_{PZC} = 3.4) than that of P25 (pH_{PZC} = 6). These two factors contribute to the enhanced adsorption capacity. Moreover, the hydroxyl groups located on the surface of titanate are functional binding groups for Pb(II) adsorption (Chen et al., 2010; Xiong et al., 2011).

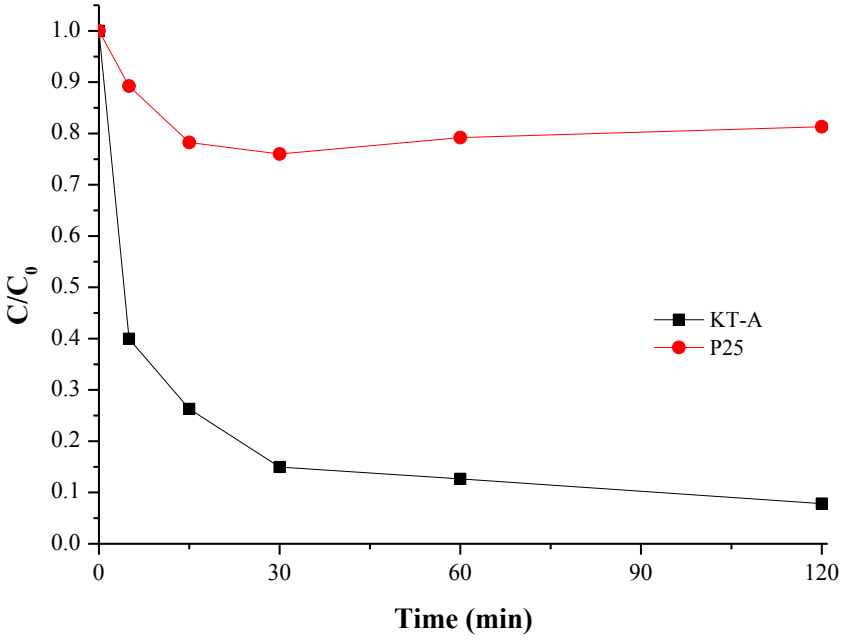

Figure 7-6. Comparison of potassium titanate with P25 on the adsorption of Pb(II) from solution. (Experimental conditions: Pb(II) concentration = 10 mg/L, titanate and P25 = 0.05 mg/L, T = 25°C, shaking speed = 150 rpm and pH = 5).

7.3.5 Adsorption kinetics

To understand the adsorption mechanism of Pb(II) onto titanate, the uptake rate of Pb(II) ions at various pH (3,5,7 and 9), titanate concentrations (0.01, 0.02, 0.05 and 0.1 g/L) and initial concentrations (5, 10 and 20 mg/L) were respectively analysed by kinetic models. The parameters of kinetic models were calculated and a pseudo-second-order model showed excellent correlation coefficients ($R^2 > 0.98$) and achieved good agreement between $q_{e.cal}$ and $q_{e.mea}$ of Pb(II) as listed in Table 7-1. This indicates that the rate-controlling step is achieved through chemisorption (Ho et al., 1998). Similar kinetics were observed in the adsorption of Pb(II) (Liu et al., 2010; Xiong et al., 2011). Moreover, with the increase in initial concentrations of Pb(II) from 5 to 20 mg/L, there was a gradual decline in the rate constants (k_2) and initial adsorption rate (h). This indicates that faster uptake of Pb(II) onto titanate will be obtained at a lower initial concentration.

Table 7-1. Kinetic parameters for the adsorption of Pb(II) onto titanate at 25°C.

Parameters	**Effect of pH**				**Effect of titanate loading**				**Effect of Pb(II) concentration**		
	pH 3	**pH 5**	**pH 7**	**pH 9**	**0.01 g/L**	**0.02 g/L**	**0.05 g/L**	**0.1 g/L**	**5 mg/L**	**10 mg/L**	**20 mg/L**
$q_{e.mea}$	1.99	18.43	Pb(II) removal by precipitation of $Pb(OH)_2^0$ and sorption of $Pb(OH)^+$ but not by adsorption		43.75	31.69	18.43	9.91	5.00	18.43	39.03
k_2	0.02	0.02			0.003	0.84	0.02	0.79	0.04	0.02	0.06
R^2	0.99	1.00			1.00	1.00	1.00	1.00	1.00	1.00	1.00
$q_{e.cal}$	2.27	18.83			46.73	33.00	18.83	9.93	5.21	18.83	39.06
$h = k_2 q_e^2$	0.10	5.89			5.68	917.11	5.89	78.12	1.07	5.89	88.35

7.3.6 Adsorption mechanism of Pb(II) onto titanate

The FTIR spectra adsorption peaks of titanate and Pb^{+2} ions loaded titanate are shown in Figure 7-7, and showed approximately similar peaks. The stretching vibration peak of OH at ~3400 cm^{-1} can be attributed to O-H stretching vibrations of adsorbed water molecules and structural OH group and the peak at ~1650 cm^{-1} can be attributed to O-H bending vibration. The band at 1637 cm^{-1} can be also seen on the spectra of Ti-O bonding and it has a stronger intensity. The lower intensity of band in the region of 1500–500 cm^{-1} is connected with neutralisation of Ti(IV) centres by electron transfer from potassium to titania (Grzechulska et al., 2002). After adsorption of Pb(II) by titanate, the band at ~3400 cm^{-1} can be apparently seen that the bands of hydroxyl groups significantly intensified as compared to that of pure titanate. This indicated that the adsorption could have mainly occurred through the interaction between Pb(II) ions and hydroxyl groups of the titanate. Similar results were reported by (Xiong et al., 2011) for the adsorption of Pb(II) onto titanate. The broad absorption band appeared in the range of 2400–1900 cm^{-1} was probably due to potassium incorporation in titanate (Grzechulska et al., 2002) and change in the intensity attribute to exchange of K^+ ions with Pb^{+2} ions. It was believed that H^+ ions from hydroxyl groups or K^+ ions could be exchanged with Pb^{+2} ions in the adsorption process, and the adsorbed Pb^{+2} ions might bond with O atoms after the adsorption (Figure 7-8). Hence it was purposed that ion exchange and oxygen bonding might be the principal mechanisms for the adsorption of Pb(II). These mechanisms were in agreement with that for Pd(II) adsorption over titanate as suggested by Kochkar et al., (2009), Chen et al., (2010) and Xiong et al., (2011) for the adsorption of Pb(II) onto titanate.

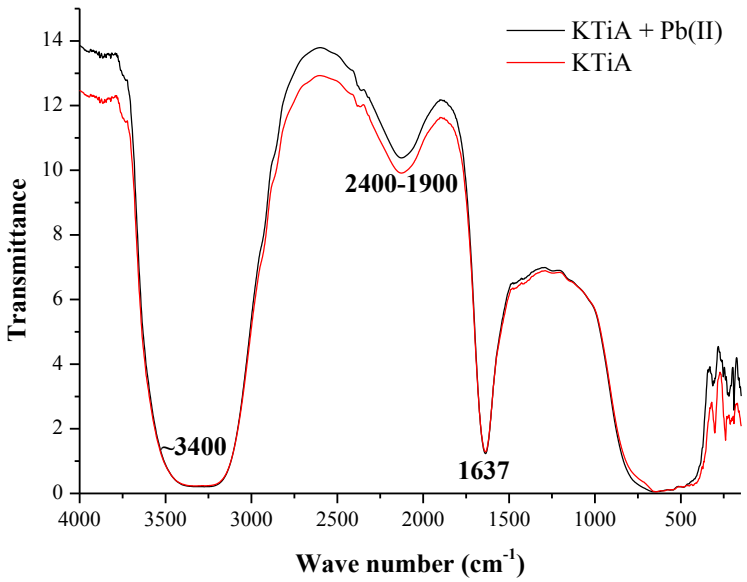

Figure 7-7. The FTIR spectra of pure titanate and Pb(II) loaded titanate.

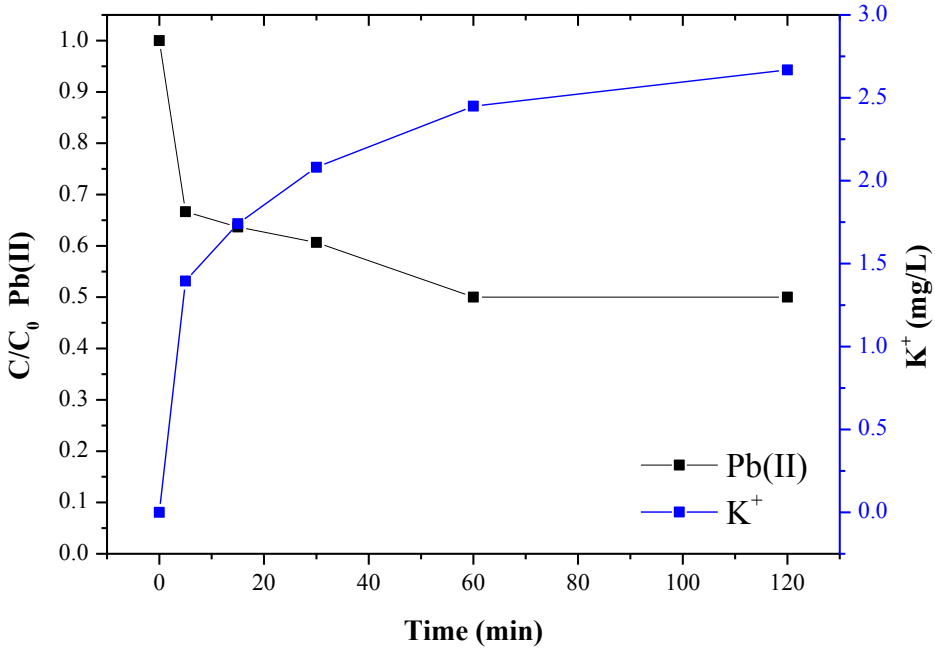

Figure 7-8. Ion exchange between K^+ and Pb^{+2} ions (Experimental conditions: Pb(II) concentration = 10 mg/L, Titanate loading = 0.05 mg/L, T = 25°C, shaking speed = 150 rpm and pH = 5).

7.3.7 Desorption and reusability studies

Repeated availability is an important factor for an advanced adsorbent. Such an adsorbent not only possess higher adsorption capability, but also shows better desorption properties, which will significantly reduce the overall cost of the adsorbent. To evaluate the regeneration performance of the titanate, regeneration experiments were conducted with 10 mg/L Pb(II) and 0.05 g/L titanate loading at pH 5 over three consecutive adsorption cycle. The adsorbent was recovered after each cycle by sedimentation, washed with 1 M HCl and MilliQ water, separated by centrifugation and dried at 100°C before being used in the next cycle. Figure 7-9 illustrates the regeneration performance of the titanate up to three different cycles. Compared to the first cycle, the regenerated catalyst A shows a reduction in adsorption performance by 34% (second cycle) and 38% (third cycle).

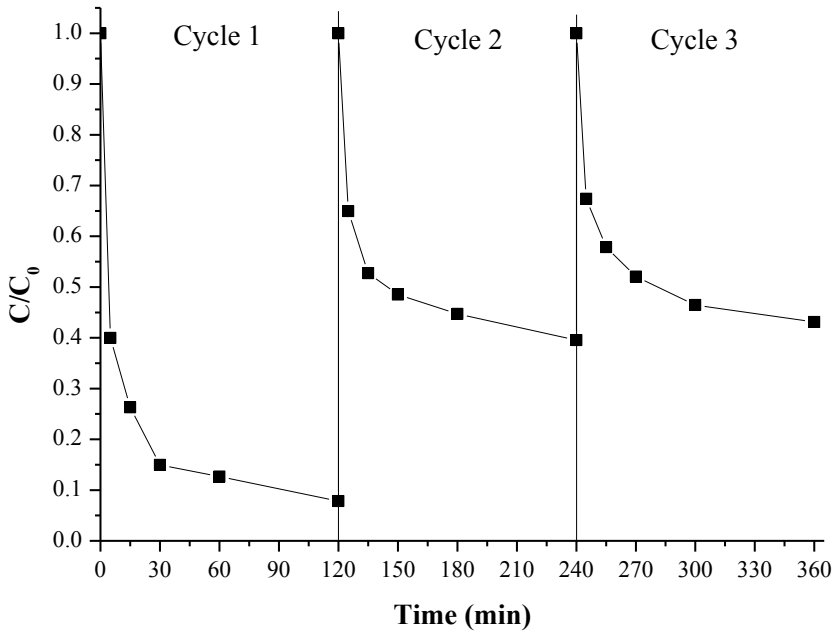

Figure 7-9. Regeneration performance of titanate. (Experimental conditions: Pb(II) concentration = 10 mg/L, Titanate loading = 0.05 g/L, T = 25°C, shaking speed = 150 rpm and pH = 5).

7.4 Conclusion

Potassium titanate nanofibres prepared by hydrothermal method were investigated for their possible application on removal of toxic metals from aqueous solution. Particular attention was paid to the utilization of the titanate as novel effective adsorbents for the removal of Pb(II). Batch adsorption experiments demonstrated that the adsorption was affected by various conditions such as solution pH, adsorbent dosage and initial Pb(II) concentration. The results showed that the adsorption rate of adsorption was faster in the first 5 min and equilibrium was achieved after 180 min. The maximum amount of adsorption was detected at pH 5. Potassium titanate showed much higher adsorption capacity compared to P25. The kinetic studies indicated that the adsorption of Pb(II) onto titanate best fit the pseudo-second-order kinetic model. FTIR spectra revealed that the hydroxyl groups in titanate were responsible for Pb(II) adsorption. It was purposed that ion exchange and oxygen bonding might be the principal mechanisms for the adsorption of Pb(II). The adsorption-desorption results showed that the titanate could be readily regenerated after adsorption. Therefore, the titanate exhibited great potential for the removal of Pb(II) from wastewater.

University of Technology Sydney
FACULTY OF ENGINEERING

Chapter 8: Conclusions and recommendations

8.1 Conclusions

In this research, photo-induced desorption of organic matter in aqueous media was investigated for the purpose of reusability of the adsorbents at low energy consumption. Apart from the photodesorption study, this research presented the synthesis of titania nanofibres, and examined their use in water purification. Titanate synthesis was achieved through the adoption of a hydrothermal treatment, to produce nano-assemblies of titanium oxide with significant properties. The physico-chemical characterisation of these titanate nanofibres have been studied for changes in morphology, surface area and chemical composition from the bulk TiO_2. Lastly, their application in water treatment applications was investigated using laboratory-scale experiments. The conclusions drawn in this research are presented in the following sections:

8.1.1 Photodesorption of Organic Matter from Titanium Dioxide Particles in Aqueous Media

Photo-induced desorption of organic compounds from TiO_2 particles in aqueous media during photocatalysis has promising applications in water treatment. Photodesorption is a relatively fast phenomenon that facilitates the regeneration of photocatalysts with low energy consumption while concentrating the waste products in an energy and water efficient process. We propose that this method of transport involves a significantly reduced affinity between the photocatalyst and pollutants upon UV illumination, and leads to the rapid detachment/decomposition of adsorbed pollutants.

In this study, the effect of certain experimental conditions (pH, photocatalyst loading, organic loading, UV light irradiation and flow rate) on this phenomenon in a recirculating photocatalysis continuous reactor was presented. Initially, organic compounds were allowed to adsorb on the surface of the photocatalyst (Degussa P25)

until adsorption equilibrium was achieved. Photodesorption phenomenon was observed shortly after UV-light illumination of TiO_2 but before the bulk photocatalytic oxidation took place.

Process optimisation was carried out by changing the flow rate, TiO_2 loading, light intensity, organic loading and pH. Photodesorption of DOM increased with flow rate with an optimum photodesorption recorded at Q1 = 150 mL/min. The use of three lamps showed the highest desorption. Increasing the TiO_2 concentration above 1 g/L had a detrimental effect on the photodesorption while lower TiO_2 loadings were not sufficient to get optimum photodesorption. Optimal organic loading concentration was found equal to 6.5 mg/L, while higher photodesorption was recorded at high pH indicating a significant role of electrostatic interactions in the photodesorption of organics. In addition, photodesorption of specific organic compounds with DOC of 7 mg/L was investigated, which revealed that sodium lauryl sulphate, sodium lignin sulphonate and beef extract were the major contributing organic compounds for photodesorption in terms of adsorption of DOC and efficiency of photodesorption. LC-OCD fractionation indicated that the desorbed compounds are in majority LMW acids and neutrals. The decomposition of polysaccharides, humic substances and polypeptides found in SWW is believed to occur during photodesorption.

8.1.2 Synthesis and Characterisation of Potassium Polytitanate for Photocatalytic Degradation of Crystal Violet

In the past decades, there have been several reports on the synthesis and characterisation of potassium titanate nanostructures by high temperature hydrothermal treatment of powdered TiO_2 in a strong aqueous alkaline solution. However, rapid

preparation route combining the use of low temperature, atmospheric pressure and simple apparatus in the preparation of higher-order assemblies of titanate has not been well investigated. Therefore, in research, attempts have been made to achieve a faster rate of nanofibre formation by carrying out reflux synthesis in a mixture of aqueous KOH and H_2O_2 at relatively low temperature. The synthesis of potassium titanate nanostructures utilising a redox strategy combined with a hydrothermal reaction involving TiO_2 powder, a basic KOH solution and an oxidising H_2O_2 solution. The adoption of the environmentally friendly H_2O_2-assisted hydrothermal route has been employed to synthesise other inorganic materials under hydrothermal conditions.

As-produced powders were characterised by scanning electron microscopy, energy-dispersive X-ray spectroscopy, transmission electron microscopy, X-ray diffraction, and nitrogen adsorption-desorption methods. Longitudinally-oriented-wire-like structures with several micrometres in length and diameters ranging from 10 to 30 nm were obtained. Larger size fibrous nanowires resulting from the hydrothermal treatment showed high affinity in adsorbing crystal violet (CV), which was mainly due to their high surface area. The photocatalytic bleaching of CV solution revealed that the wires are photoactive under UV light irradiation. Macroporous nanowires are considered to be effective adsorbents of CV, capable of its photocatalytic degradation, and they can be easily separated from the solution by settling.

The nanostructures were tested for adsorption and photocatalytic activity using CV as a model pollutant. Potassium titanate ‘A’ showed superior photocatalyst activity following the trend A>B>C>AC>BC>CC. Larger pore size fibrous nanowires resulting from this treatment showed high affinity in adsorbing CV, which was mainly due to the

high surface area. The binding of K^+ and peroxo groups had detrimental effect on the adsorption of the cationic dye because of surface saturation, which decreased the adsorption sites. The decolourisation revealed their photocatalytic activity under UV light irradiation. The macroporous nanowires are considered as effective adsorbents of CV and are also capable of photocatalytic degradation. Furthermore, they can be easily separated from the solution by settling.

8.1.3 Solar Simulator Assisted Photocatalysis of Methylene Blue using Potassium Polytitanate

The use of renewable solar energy as a UV photon source for the photocatalytic degradation of organic contaminants may be highly economical compared with processes using artificial UV irradiation, which require substantial electrical power input. In this context the solar photocatalytic activity of potassium polytitanate catalysts was investigated using a batch reactor system exposed to artificial solar irradiation. The effect of MB concentration, catalyst loading, pH of the solution and light intensity on solar light induced photocatalysis was examined. The stability of a photocatalyst specimen was also studied for 3 degradation cycles using the adsorption/photocatalysis model.

The results of adsorption and photocatalytic degradation of MB onto potassium polytitanate under simulated solar light showed that potassium polytitanate nanofibres were effective adsorbents of MB and also facilitated its photocatalytic degradation. Sulphate ion evolution during photocatalysis confirmed some mineralisation occurred and hence photo-oxidative degradation of MB. The significant decrease of DOC was observed during adsorption but not throughout illumination which might be due to

formation of intermediates aromatic rings of carboxylic acids and phenolic compounds. The mineralisation of MB was studied for sulphate evolution, which confirms the photo-oxidative degradation of the pollutant, and therefore the photocatalytic activity of potassium polytitanate. The photocatalyst 'A' was found to be efficient in photocatalytic degradation of MB and was used to investigate the effects of MB loading, catalyst loading, pH and light intensity. The optimum operational conditions for the photocatalytic degradation of MB were found at 0.05 g/L of photocatalyst, 10 mg/L MB and pH 7. Moreover, stability of photocatalytic 'A' was studied for 3 degradation cycles using adsorption/photocatalysis model.

8.1.4 Adsorption Behaviour of Pb(II) onto Potassium Polytitanate Nanofibre

Nanoparticles offer great potential to improve environmental treatment technologies due to their unique properties. Potassium polytitanate prepared by hydrothermal treatment are of special interest. These nanofibre titanate characterised by high specific surface areas and pore volumes, and they possessed good ion-exchange properties. The titanates have many functional hydroxyl groups which are readily exchanged with heavy metal ions in aqueous solutions. Until now, the studies using titanate to reduce heavy metals in aqueous solutions are very limited. The potential applications of metal ion adsorption onto titanate have not been explore in details. The purpose of this study is to investigate the feasibility of potassium polytitanate as high efficient adsorbents for the removal of Pb(II) from aqueous solutions. The effects of various operational conditions such as pH and adsorbent concentration, titanate loading were systematically studied. The adsorption kinetics and mechanism were also analysed.

Batch adsorption experiments demonstrated that the adsorption was affected by various conditions such as solution pH, adsorbent dosage and initial Pb(II) concentration. The results showed that initial uptake of Pb(II) was rapid during the first 5 min and the adsorption equilibrium was achieved after 180 min. The adsorption capacity of the titanate was detected in pH 5 and was obtained much higher as compared to P25. The kinetic studies indicated that the adsorption of Pb(II) onto titanate fits the pseudo-second-order kinetic model. FTIR spectra revealed that the hydroxyl groups in titanate were responsible for Pb(II) adsorption. We propose that ion exchange and oxygen bonding are the principal mechanisms for the adsorption of Pb(II). The adsorption-desorption results show that the titanate nanofibres can be readily regenerated after adsorption for reuse. Overall, the titanate nanofibres process exhibits great potential as a remediation method for the removal of Pb(II) from wastewater.

8.2 Recommendations

Based on the presented research findings, the following recommendations for the continuation of this research are purposed.

- Chapter 4 explored the photo-induced desorption phenomenon to facilitate the regeneration of P25 with low energy consumption. However, the development of effective and rapidly separable photoreactive nanosorbents is a significant work component since they are vital for the exploitation of this phenomenon for industrial applications.
- The results in Chapter 4 and Chapter 5 showed that potassium titanate is negatively charged over a wide pH range, and therefore very effective in removing cationic dyes from industrial effluent at lower pH values. Moreover, it

can be easily regenerated by simple exposure to solar light, and then reused in consecutive treatment cycles.

- Experiments in larger scale reactor also showed the applicability of photocatalytic degradation in commercial sizes. The process undergoes different hydrodynamics in larger scales, which may affect the effectiveness of the degradation. More studies are required to investigate the effects of scale up on photocatalytic degradation of pollutant in large scales.
- Initial investigations indicated that the potassium polytitanate produced in this study are suitable for the degradation of some PPCP (pharmaceutical and personal care products). However, further investigations are required for process optimisation and improvement.

University of Technology Sydney
FACULTY OF ENGINEERING

Appendices

Appendix A: Sketch representing synthesis of potassium polytitanate

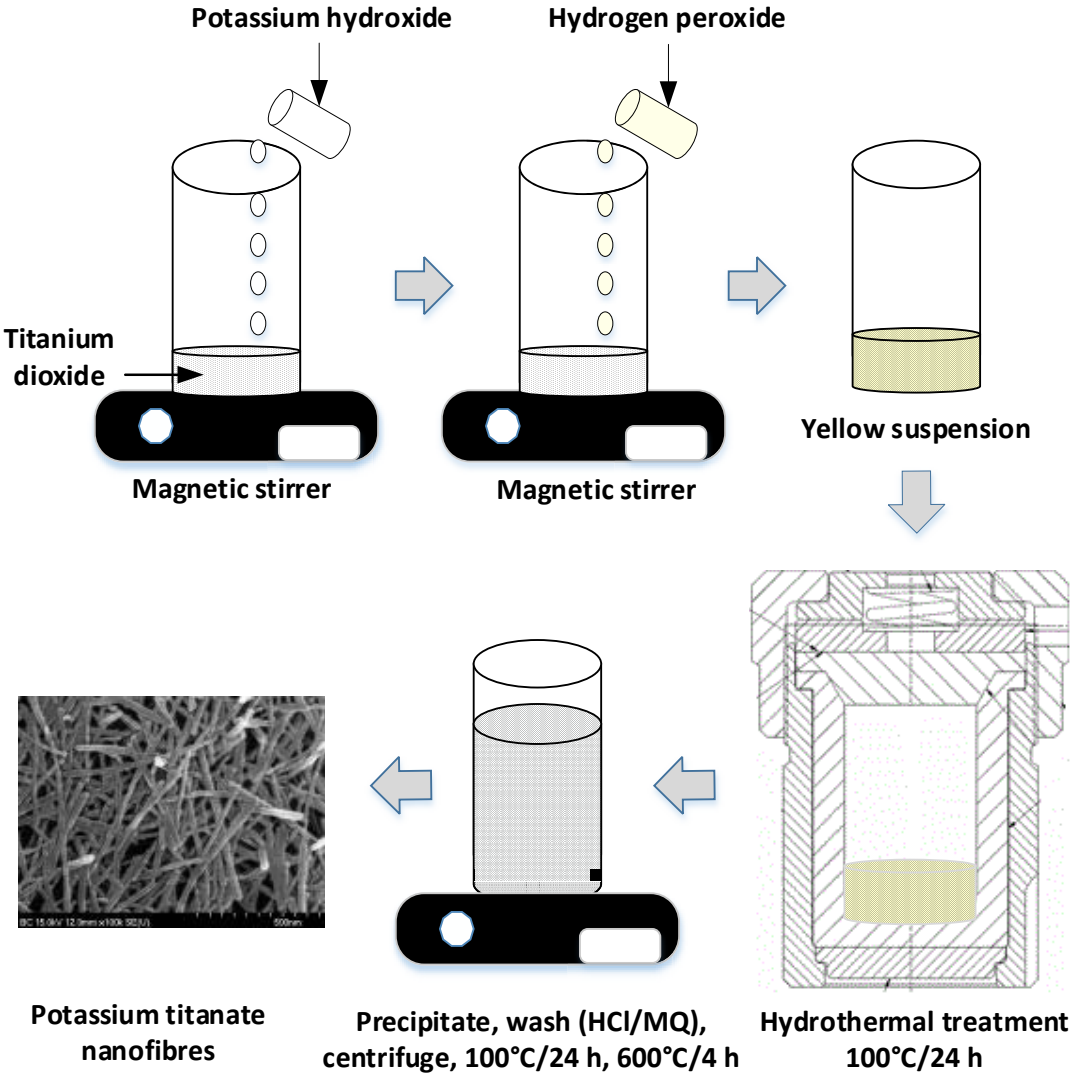

Appendix B: Energy diffraction spectra of P25 and potassium polytitanate

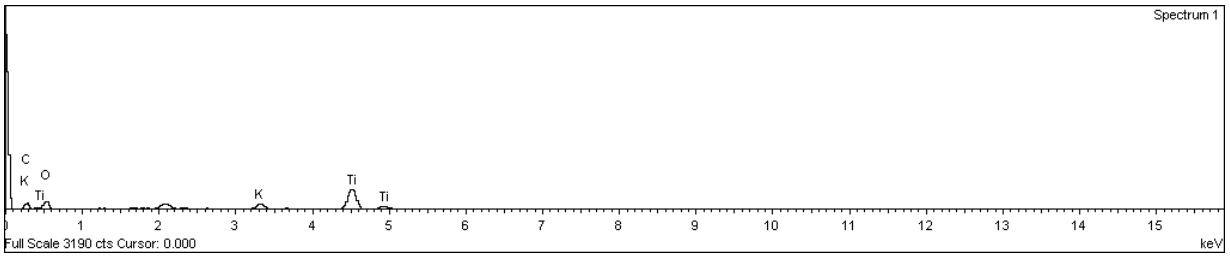

A

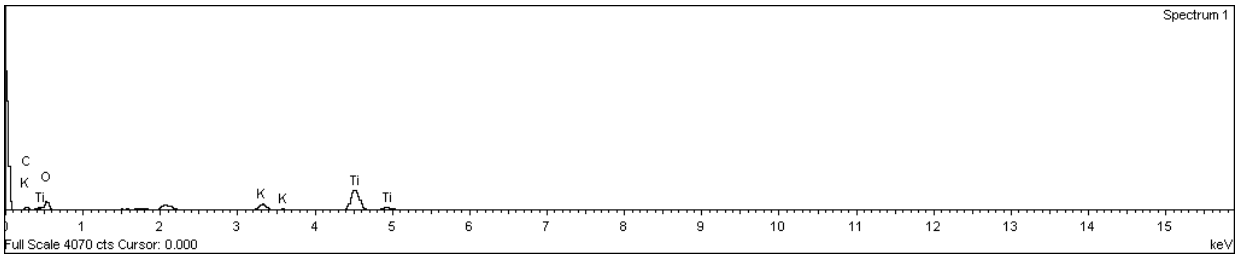

AC

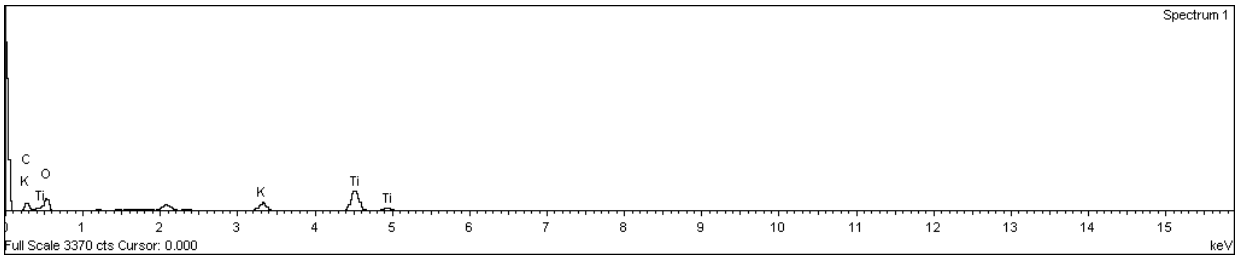

B

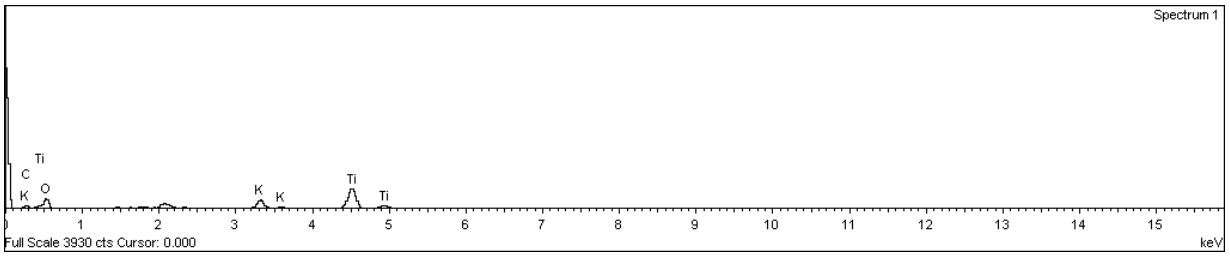

BC

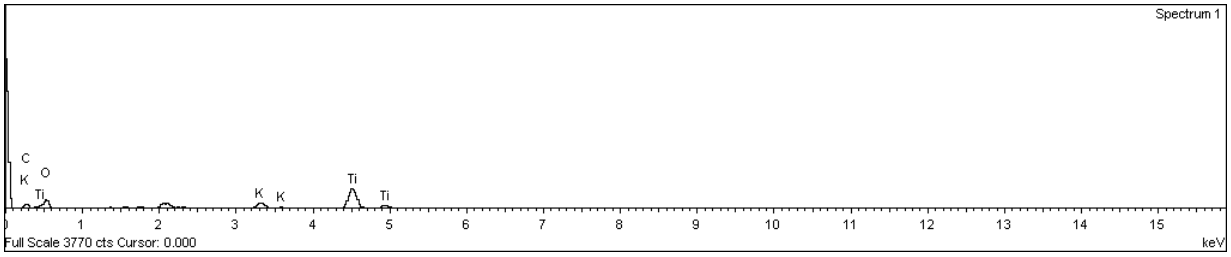

C

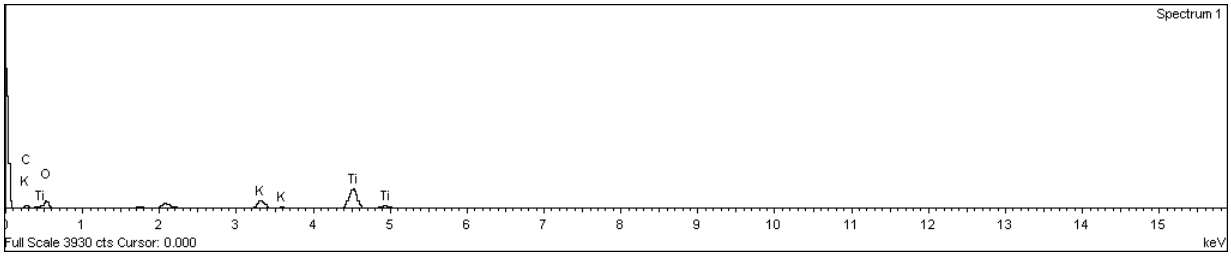
Spectrum 1
C
K
O
Ti
K
K
Ti
Ti
0
1
2
3
4
5
6
7
8
9
10
11
12
13
14
15
Full Scale 3930 cts Cursor: 0.000
keV

CC

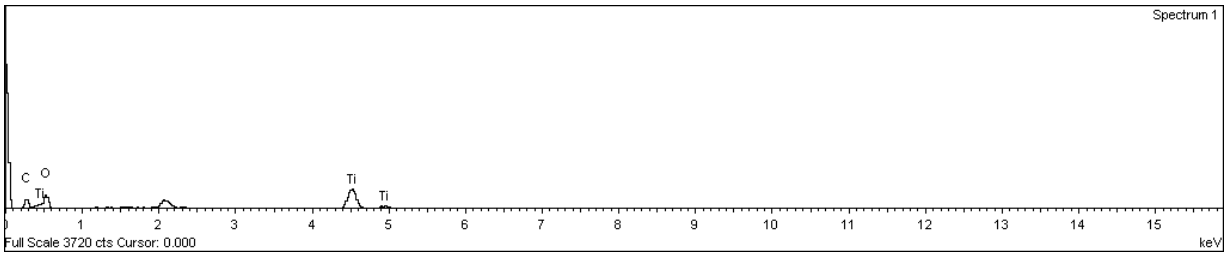
Spectrum 1
C
O
Ti
Ti
Ti
0
1
2
3
4
5
6
7
8
9
10
11
12
13
14
15
Full Scale 3720 cts Cursor: 0.000
keV

P25

Appendix C: Adsorption/desorption isotherms of P25 and potassium polytitanate

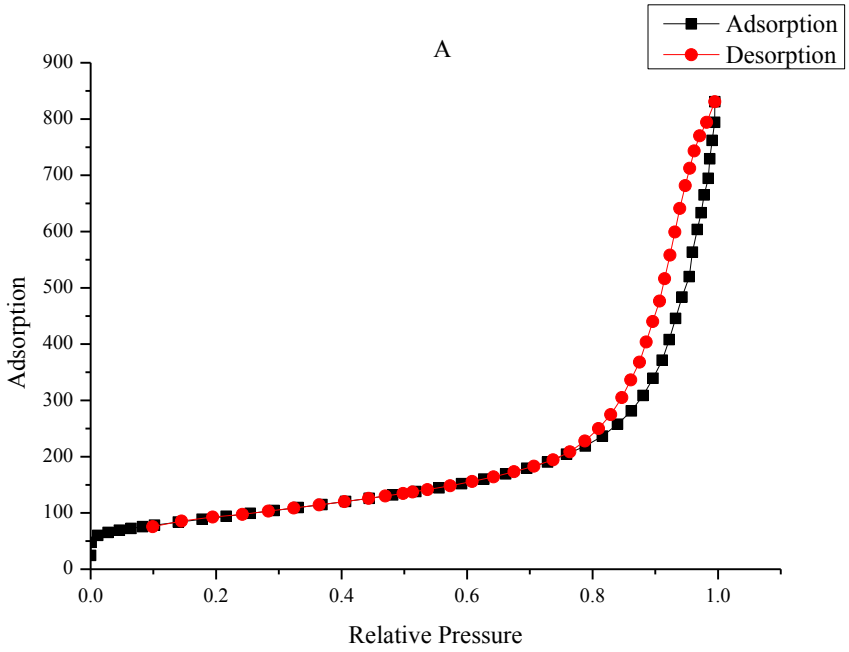

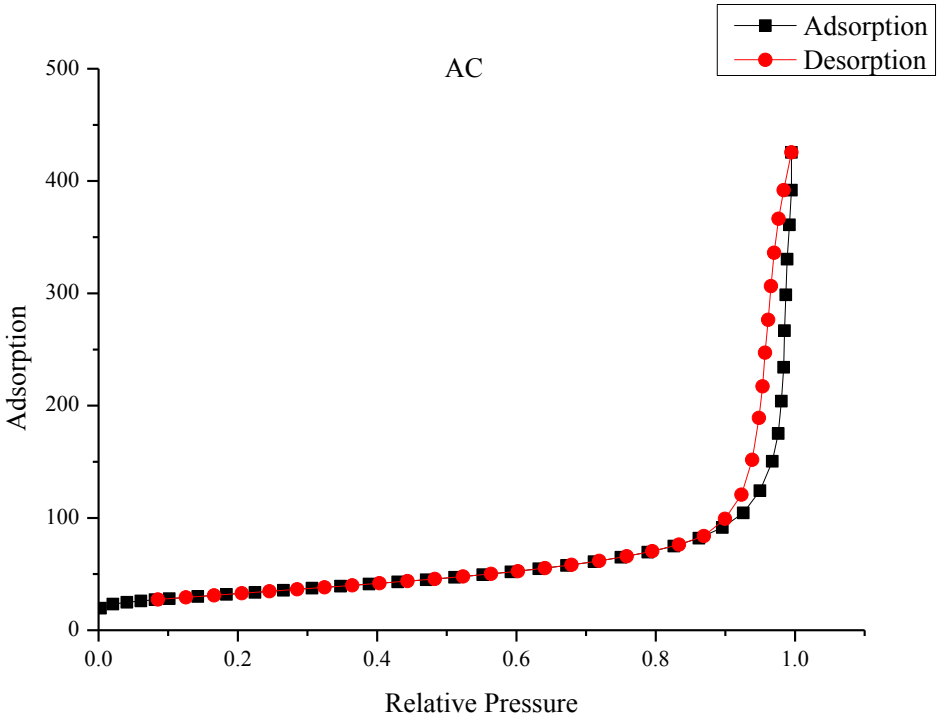

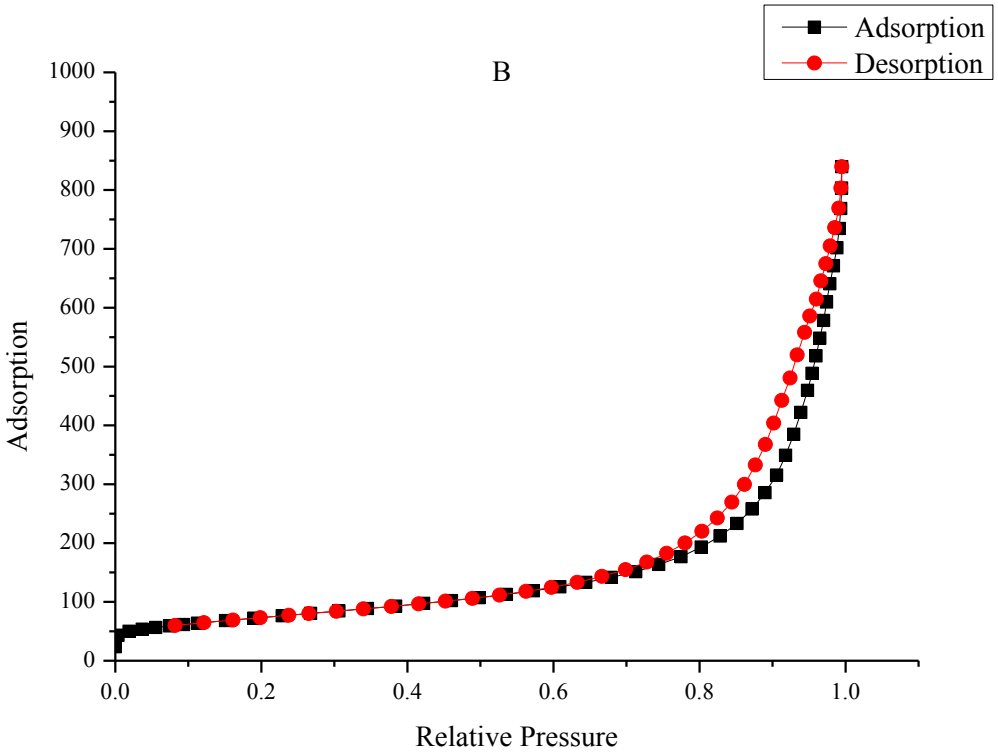
B
Adsorption
Desorption
Adsorption
Relative Pressure
0
100
200
300
400
500
600
700
800
900
1000
0.0
0.2
0.4
0.6
0.8
1.0

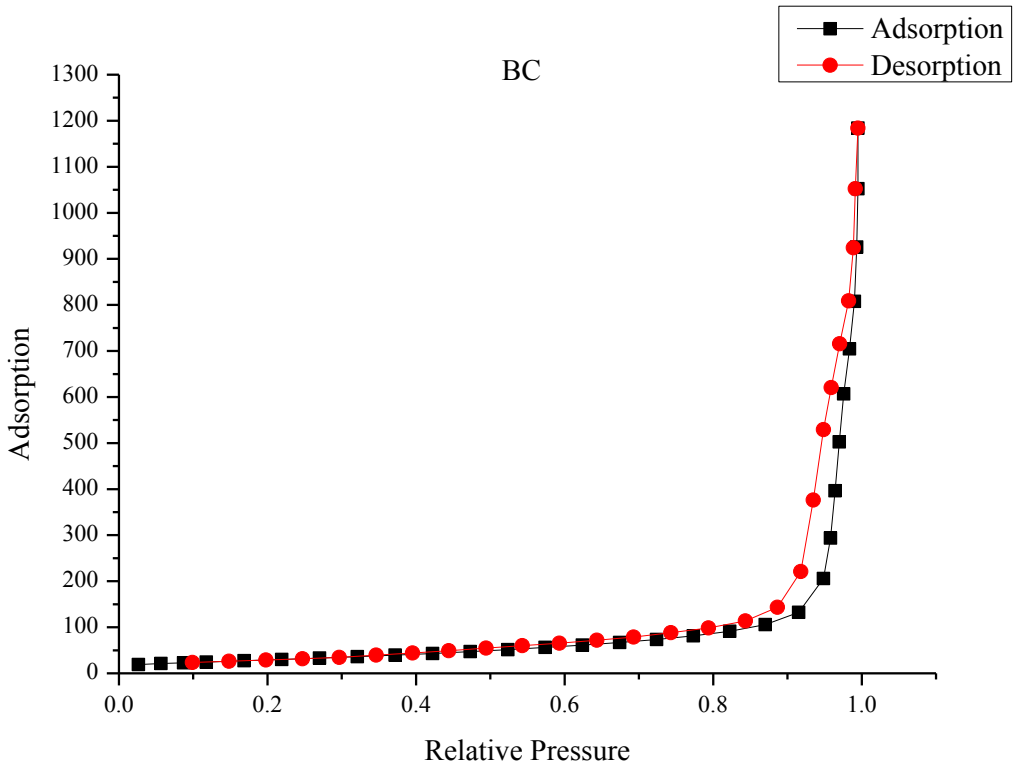
BC
Adsorption
Desorption
Adsorption
Relative Pressure
0
100
200
300
400
500
600
700
800
900
1000
1100
1200
1300
0.0
0.2
0.4
0.6
0.8
1.0

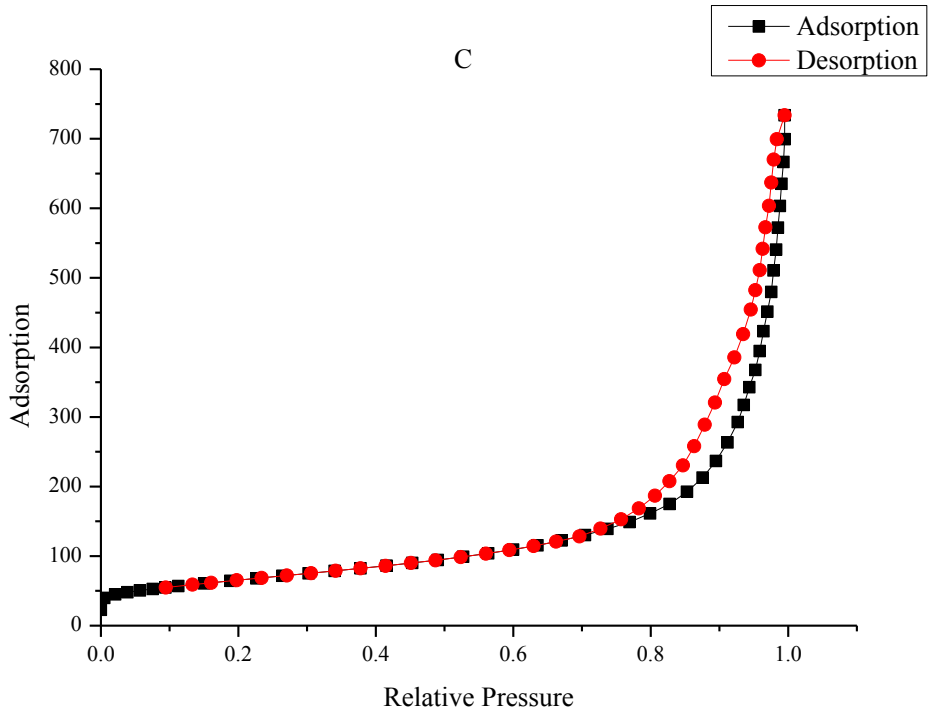
C
Adsorption
Desorption
800
700
600
500
400
300
200
100
0
Adsorption
0.0
0.2
0.4
0.6
0.8
1.0
Relative Pressure

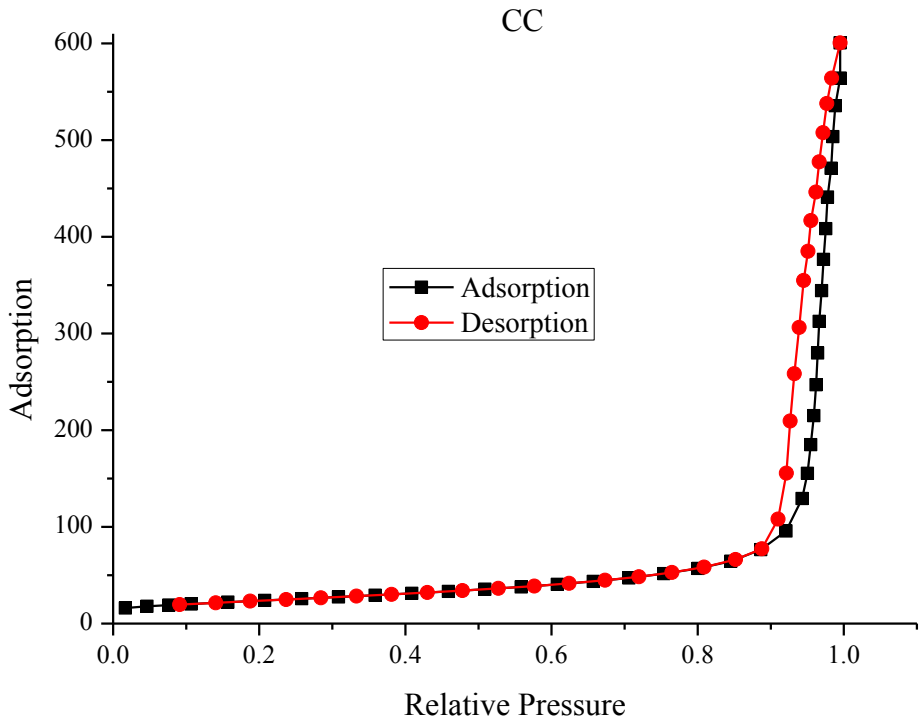
CC
600
500
400
300
200
100
0
Adsorption
Adsorption
Desorption
0.0
0.2
0.4
0.6
0.8
1.0
Relative Pressure

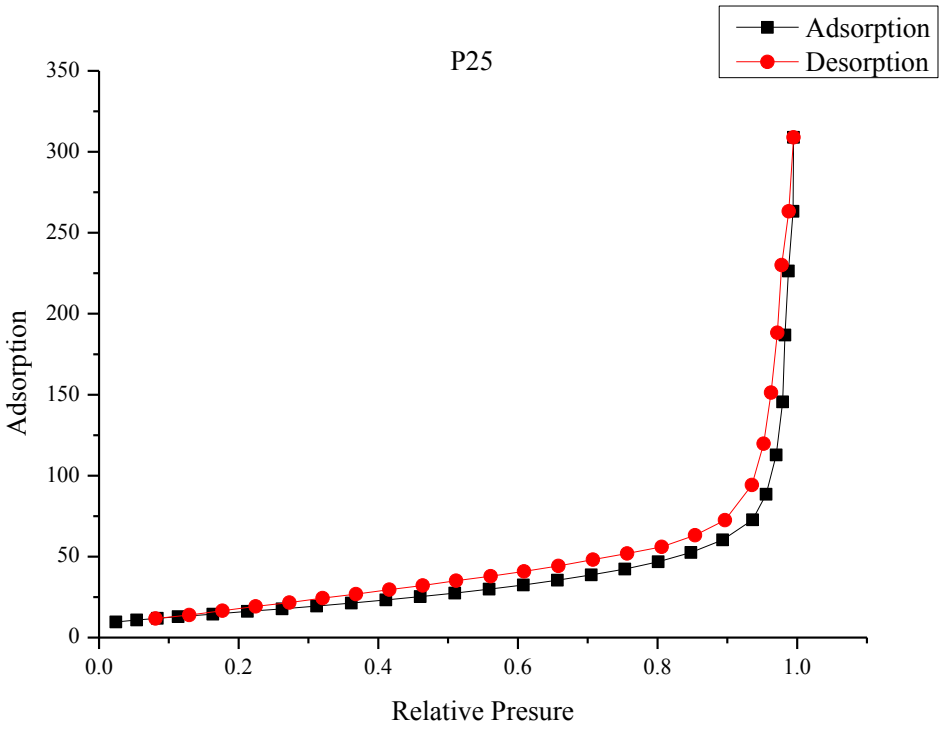
P25
Adsorption
Desorption
Adsorption
Relative Presure
0
50
100
150
200
250
300
350
0.0
0.2
0.4
0.6
0.8
1.0

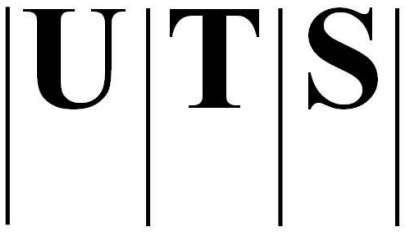

University of Technology Sydney
FACULTY OF ENGINEERING

Bibliography

Ahmad, A. & Hameed, B. 2010, 'Effect of preparation conditions of activated carbon from bamboo waste for real textile wastewater', *Journal of hazardous materials*, vol. 173, no. 1, pp. 487-93.

Allam, N.K. & Grimes, C.A. 2008, 'Effect of cathode material on the morphology and photoelectrochemical properties of vertically oriented TiO_2 nanotube arrays', *Solar Energy Materials and Solar Cells*, vol. 92, no. 11, pp. 1468-75.

Ambrus, Z., Mogyorosi, K., Szalai, A., Alapi, T., Demeter, K., Dombi, A. & Sipos, P. 2008, 'Low temperature synthesis, characterization and substrate-dependent photocatalytic activity of nanocrystalline TiO2 with tailor-made rutile to anatase ratio', *Applied Catalysis A: General*, vol. 340, no. 2, pp. 153-61.

Amin, M., Alazba, A. & Manzoor, U. 2014, 'A Review of Removal of Pollutants from Water/Wastewater Using Different Types of Nanomaterials', *Advances in Materials Science and Engineering*, vol. 2014.

Anderson, D.M.W. & Stoddart, J.F. 1966, 'Studies on uronic acid materials : Part XV. The use of molecular-sieve chromatography in studies on acacia senegal gum (gum arabic)', *Carbohydrate Research*, vol. 2, no. 2, pp. 104-14.

Aragon, M., Kottenstette, R., Dwyer, B., Aragon, A., Everett, R., Holub, W., Siegel, M. & Wright, J. 2007, *Arsenic Pilot Plant Operation and Results-Anthony, New Mexico*, Sandia National Laboratories.

Arana, J., Martınez Nieto, J., Herrera Melián, J., Dona Rodrıguez, J., Gonzalez Dıaz, O., Pérez Pena, J., Bergasa, O., Alvarez, C. & Méndez, J. 2004, 'Photocatalytic degradation of formaldehyde containing wastewater from veterinarian laboratories', *Chemosphere*, vol. 55, no. 6, pp. 893-904.

Ashokkumar, M. 1998, 'An overview on semiconductor particulate systems for photoproduction of hydrogen', *International Journal of Hydrogen Energy*, vol. 23, no. 6, pp. 427-38.

Asif Durrani, A.A., Shabbir Durrani, Jani.Basha Shaikh, A.Upadhyay & Z.H.Khan 2011, 'Non-animal Peptone for Serum Free Cultivation of Recombinant Mammalian and Animal Cells', *International Journal of Biology*, vol. 3, pp. 140-5.

Au, W., Pathak, S., Collie, C.J. & Hsu, T. 1978, 'Cytogenetic toxicity of gentian violet and crystal violet on mammalian cells in vitro', *Mutation Research/Genetic Toxicology*, vol. 58, no. 2, pp. 269-76.

Babel, S. & Kurniawan, T.A. 2004, 'Cr (VI) removal from synthetic wastewater using coconut shell charcoal and commercial activated carbon modified with oxidizing agents and/or chitosan', *Chemosphere*, vol. 54, no. 7, pp. 951-67.

Bai, Y., Sun, Q., Xing, R., Wen, D. & Tang, X. 2010, 'Removal of pyridine and quinoline by bio-zeolite composed of mixed degrading bacteria and modified zeolite', *Journal of hazardous materials*, vol. 181, no. 1, pp. 916-22.

Bamba, D., Atheba, P., Robert, D., Trokourey, A. & Dongui, B. 2008, 'Photocatalytic degradation of the diuron pesticide', *Environmental Chemistry Letters*, vol. 6, no. 3, pp. 163-7.

Bandara, J., Nadtochenko, V., Kiwi, J. & Pulgarin, C. 1997, 'Dynamics of oxidant addition as a parameter in the modelling of dye mineralization (Orange II) via advanced oxidation technologies', *Water Science and Technology*, vol. 35, no. 4, pp. 87-93.

Bavykin, D.V., Friedrich, J.M. & Walsh, F.C. 2006, 'Protonated Titanates and TiO2 Nanostructured Materials: Synthesis, Properties, and Applications', *Advanced Materials*, vol. 18, no. 21, pp. 2807-24.

Bavykin, D.V., Kulak, A.N. & Walsh, F.C. 2010, 'Metastable Nature of Titanate Nanotubes in an Alkaline Environment', *Crystal Growth & Design*, vol. 10, no. 10, pp. 4421-7.

Bavykin, D.V., Lapkin, A.A., Plucinski, P.K., Friedrich, J.M. & Walsh, F.C. 2005, 'Reversible storage of molecular hydrogen by sorption into multilayered TiO_2 nanotubes', *The Journal of Physical Chemistry B*, vol. 109, no. 41, pp. 19422-7.

Bavykin, D.V., Parmon, V.N., Lapkin, A.A. & Walsh, F.C. 2004, 'The effect of hydrothermal conditions on the mesoporous structure of TiO_2 nanotubes', *Journal of Materials Chemistry*, vol. 14, no. 22, pp. 3370-7.

Berry, K., Aftandilian, V., Gilbert, W., Meibohm, E. & Young, H. 1960, 'Potassium tetra-and hexatitanates', *Journal of Inorganic and Nuclear Chemistry*, vol. 14, no. 3, pp. 231-9.

Beydoun, D., Amal, R., Low, G.K.C. & McEvoy, S. 2000, 'Novel photocatalyst: Titania-coated magnetite. Activity and photodissolution', *Journal of Physical Chemistry B*, vol. 104, pp. 4387-96.

Beydoun, D., Amal, R., Scott, J., Low, G. & McEvoy, S. 2001, 'Studies on the Mineralization and Separation Efficiencies of a Magnetic Photocatalyst', *Chemical Engineering and Technology*, vol. 24, no. 7, pp. 745-8.

Bianco Prevot, A., Baiocchi, C., Brussino, M.C., Pramauro, E., Savarino, P., Augugliaro, V., Marci, G. & Palmisano, L. 2001, 'Photocatalytic degradation of acid blue 80 in aqueous solutions containing TiO_2 suspensions', *Environmental science & technology*, vol. 35, no. 5, pp. 971-6.

Bjorklund, R.B., Karlsson, S., Borén, H., Allard, B. & Lundström, I. 2001, 'Photodesorption of fulvic acid from iron oxide surfaces into aqueous solutions', *Applied Surface Science*, vol. 174, no. 2, pp. 167-75.

Bora, T. & Dutta, J. 2014, 'Applications of Nanotechnology in Wastewater Treatment—A Review', *Journal of nanoscience and nanotechnology*, vol. 14, no. 1, pp. 613-26.

Cassano, A.E. & Alfano, O.M. 2000, 'Reaction engineering of suspended solid heterogeneous photocatalytic reactors', *Catalysis Today*, vol. 58, no. 2, pp. 167-97.

Çeçen, F. & Aktas, Ö. 2011, *Activated carbon for water and wastewater treatment: Integration of adsorption and biological treatment*, John Wiley & Sons.

Chatterjee, D. & Dasgupta, S. 2005, 'Visible light induced photocatalytic degradation of organic pollutants', *Journal of Photochemistry and Photobiology C: Photochemistry Reviews*, vol. 6, no. 2, pp. 186-205.

Chaturvedi, S. & Dave, P.N. 2013, 'Environmental Application of Photocatalysis', *Materials Science Forum*, vol. 734, Trans Tech Publ, pp. 273-94.

Chaudhary, D., Vigneswaran, S., Jegatheesan, V., Ngo, H., Moon, H., Shim, W. & Kim, S. 2003, 'Granular activated carbon (GAC) adsorption in tertiary

wastewater treatment: experiments and models', *Water Science & Technology*, vol. 47, no. 1, pp. 113-20.

Chen, C.-C., Fan, H.-J., Jang, C.-Y., Jan, J.-L., Lin, H.-D. & Lu, C.-S. 2006, 'Photooxidative N-de-methylation of crystal violet dye in aqueous nano-TiO_2 dispersions under visible light irradiation', *Journal of Photochemistry and Photobiology A: Chemistry*, vol. 184, no. 1–2, pp. 147-54.

Chen, C.-C., Mai, F.-D., Chen, K.-T., Wu, C.-W. & Lu, C.-S. 2007, 'Photocatalyzed N-de-methylation and degradation of crystal violet in titania dispersions under UV irradiation', *Dyes and Pigments*, vol. 75, no. 2, pp. 434-42.

Chen, J., Nakajima, N., Okamoto, M., Mo, H.L., Sojka-Ledakowicz, J., Koprowski, T., Machnowski, W. & Knudsen, H.H. 1998, 'Membrane filtration of textile dyehouse wastewater for technological water reuse', *Desalination*, vol. 119, no. 1, pp. 1-9.

Chen, Q., Luo, Z., Hills, C., Xue, G. & Tyrer, M. 2009, 'Precipitation of heavy metals from wastewater using simulated flue gas: Sequent additions of fly ash, lime and carbon dioxide', *Water Research*, vol. 43, no. 10, pp. 2605-14.

Chen, Q. & Peng, L.M. 2007, 'Structure and applications of titanate and related nanostructures', *International Journal of Nanotechnology*, vol. 4, no. 1, pp. 44-65.

Chen, R.J., Franklin, N.R., Kong, J., Cao, J., Tombler, T.W., Zhang, Y. & Dai, H. 2001, 'Molecular photodesorption from single-walled carbon nanotubes', *Applied Physics Letters*, vol. 79, no. 14, pp. 2258-60.

Chen, X. & Mao, S.S. 2007, 'Titanium Dioxide Nanomaterials: Synthesis, Properties, Modifications, and Applications', *Chemical Reviews*, vol. 107, no. 7, pp. 2891-959.

Chen, Y.-C., Lo, S.-L. & Kuo, J. 2010, 'Pb (II) adsorption capacity and behavior of titanate nanotubes made by microwave hydrothermal method', *Colloids and Surfaces A: Physicochemical and Engineering Aspects*, vol. 361, no. 1, pp. 126-31.

Chong, M.N., Jin, B., Chow, C.W. & Saint, C. 2010, 'Recent developments in photocatalytic water treatment technology: a review', *Water Research*, vol. 44, no. 10, pp. 2997-3027.

Chong, M.N., Lei, S., Jin, B., Saint, C. & Chow, C.W. 2009, 'Optimisation of an annular photoreactor process for degradation of Congo Red using a newly synthesized titania impregnated kaolinite nano-photocatalyst', *Separation and Purification Technology*, vol. 67, no. 3, pp. 355-63.

Colmenares, J.C., Luque, R., Campelo, J.M., Colmenares, F., Karpiński, Z. & Romero, A.A. 2009, 'Nanostructured photocatalysts and their applications in the photocatalytic transformation of lignocellulosic biomass: an overview', *Materials*, vol. 2, no. 4, pp. 2228-58.

Costa, L.L. & Prado, A.G. 2009, 'TiO_2 nanotubes as recyclable catalyst for efficient photocatalytic degradation of indigo carmine dye', *Journal of Photochemistry and Photobiology A: Chemistry*, vol. 201, no. 1, pp. 45-9.

Couselo, N., García Einschlag, F.S., Candal, R.J. & Jobbágy, M. 2008, 'Tungsten-doped TiO_2 vs pure TiO_2 photocatalysts: effects on photobleaching kinetics and

mechanism', *The Journal of Physical Chemistry C*, vol. 112, no. 4, pp. 1094-100.

Dagan, G. & Tomkiewicz, M. 1993, 'Titanium dioxide aerogels for photocatalytic decontamination of aquatic environments', *The Journal of Physical Chemistry*, vol. 97, no. 49, pp. 12651-5.

Dawson, G., Chen, W., Zhang, T., Chen, Z. & Cheng, X. 2010, 'A study on the effect of starting material phase on the production of trititanate nanotubes', *Solid State Sciences*, vol. 12, no. 12, pp. 2170-6.

de Lassa, H., Serrano, B. & Salaices, M. 2005, 'Novel Photocatalytic Reactors for Water and Air Treatment', *Photocatalytic Reaction Engineering*, Springer US, pp. 17-47.

Deliyanni, E., Bakoyannakis, D., Zouboulis, A. & Matis, K. 2003, 'Sorption of As (V) ions by akaganeite-type nanocrystals', *Chemosphere*, vol. 50, no. 1, pp. 155-63.

Di Wu, Liu, J., Zhao, X., Li, A., Chen, Y. & Ming, N. 2006, 'Sequence of events for the formation of titanate nanotubes, nanofibers, nanowires, and nanobelts', *Chemistry of Materials*, vol. 18, no. 2, pp. 547-53.

Diebold, U. 2003, 'The surface science of titanium dioxide', *Surface Science Reports*, vol. 48, no. 5–8, pp. 53-229.

Dmitry, V.B., Barbara, A.C., Mark, E.L. & Frank, C.W. 2008, 'An aqueous, alkaline route to titanate nanotubes under atmospheric pressure conditions', *Nanotechnology*, vol. 19, no. 27, p. 275604.

Dong, P., Liu, B., Wang, Y., Guo, L., Huang, Y. & Yin, S. 2011, 'A Study on the $H_2Ti_3O_7$ Sheet-Like Products During the Formation Process of Titanate Nanotubes', *Journal of The Electrochemical Society*, vol. 158, no. 9, pp. K183-K6.

Dong, Y., Wu, D., Chen, X. & Lin, Y. 2010, 'Adsorption of bisphenol A from water by surfactant-modified zeolite', *Journal of colloid and interface science*, vol. 348, no. 2, pp. 585-90.

Du, G., Chen, Q., Che, R., Yuan, Z. & Peng, L.-M. 2001, 'Preparation and structure analysis of titanium oxide nanotubes', *Applied Physics Letters*, vol. 79, no. 22, pp. 3702-4.

Du, G., Chen, Q., Han, P., Yu, Y. & Peng, L.M. 2003, 'Potassium titanate nanowires: Structure, growth, and optical properties', *Physical Review B*, vol. 67, no. 3, p. 035323.

Dunn, W.W., Aikawa, Y. & Bard, A.J. 1981, 'Characterization of particulate titanium dioxide photocatalysts by photoelectrophoretic and electrochemical measurements', *Journal of the American Chemical Society*, vol. 103, no. 12, pp. 3456-9.

Einarsrud, M.-A. & Grande, T. 2014, '1D oxide nanostructures from chemical solutions', *Chemical Society Reviews*, vol. 43, no. 7, pp. 2187-99.

El Saliby, I., Erdei, L., Kim, J.-H. & Shon, H.K. 2013, 'Adsorption and photocatalytic degradation of methylene blue over hydrogen–titanate nanofibres produced by a peroxide method', *Water Research*, vol. 47, no. 12, pp. 4115-25.

El Saliby, I., Erdei, L., McDonagh, A., Kim, J.-B., Kim, J.-H. & Shon, H.K. 2014, 'Co-doped mesoporous titania photocatalysts prepared from a peroxo-titanium complex solution', *Materials Research Bulletin*, vol. 49, no. 0, pp. 7-13.

El Saliby, I., Erdei, L., Shon, H.K., Kim, J.B. & Kim, J.-H. 2011, 'Preparation and characterisation of mesoporous photoactive Na-titanate microspheres', *Catalysis Today*, vol. 164, no. 1, pp. 370-6.

El Saliby, I., Shahid, M., McDonagh, A., Shon, H.K. & Kim, J.-H. 2012, 'Photodesorption of organic matter from titanium dioxide particles in aqueous media', *Journal of Industrial and Engineering Chemistry*, vol. 18, no. 5, pp. 1774-80.

El Samrani, A.G., Lartiges, B.S. & Villiéras, F. 2008, 'Chemical coagulation of combined sewer overflow: Heavy metal removal and treatment optimization', *Water Research*, vol. 42, no. 4–5, pp. 951-60.

Erdei, L., Arecrachakul, N. & Vigneswaran, S. 2008, 'A combined photocatalytic slurry reactor–immersed membrane module system for advanced wastewater treatment', *Separation and Purification Technology*, vol. 62, no. 2, pp. 382-8.

Fang, F.C. 2004, 'Antimicrobial reactive oxygen and nitrogen species: concepts and controversies', *Nature Reviews Microbiology*, vol. 2, no. 10, pp. 820-32.

Fernández-Ibáñez, P., Blanco, J., Malato, S. & Nieves, F.J.d.l. 2003, 'Application of the colloidal stability of TiO_2 particles for recovery and reuse in solar photocatalysis', *Water Research*, vol. 37, no. 13, pp. 3180-8.

Fetterolf, M.L., Patel, H.V. & Jennings, J.M. 2003, 'Adsorption of methylene blue and acid blue 40 on titania from aqueous solution', *Journal of Chemical & Engineering Data*, vol. 48, no. 4, pp. 831-5.

Fox, M.A. & Dulay, M.T. 1993, 'Heterogeneous photocatalysis', *Chemical reviews*, vol. 93, no. 1, pp. 341-57.

Frank, S.N. & Bard, A.J. 1977, 'Semiconductor electrodes. 12. Photoassisted oxidations and photoelectrosynthesis at polycrystalline titanium dioxide electrodes', *Journal of the American Chemical Society*, vol. 99, no. 14, pp. 4667-75.

Fu, F., Xie, L., Tang, B., Wang, Q. & Jiang, S. 2012, 'Application of a novel strategy—Advanced Fenton-chemical precipitation to the treatment of strong stability chelated heavy metal containing wastewater', *Chemical Engineering Journal*, vol. 189, pp. 283-7.

Fujishima, A. & Honda, K. 1972, 'Electrochemical Photolysis of Water at a Semiconductor Electrode', *Nature*, vol. 238, no. 5358, pp. 37-8.

Fujishima, A., Rao, T.N. & Tryk, D.A. 2000, 'Titanium dioxide photocatalysis', *Journal of Photochemistry and Photobiology C: Photochemistry Reviews*, vol. 1, no. 1, pp. 1-21.

Gaya, U.I. & Abdullah, A.H. 2008, 'Heterogeneous photocatalytic degradation of organic contaminants over titanium dioxide: A review of fundamentals, progress and problems', *Journal of Photochemistry and Photobiology C: Photochemistry Reviews*, vol. 9, no. 1, pp. 1-12.

Geissen, S.U., Xi, W., Weidemeyer, A., Vogelpohl, A., Bousselmi, L., Ghrabi, A. & Ennabli, A. 2001, 'Comparison of suspended and fixed photocatalytic reactor systems', *Water Science & Technology*, vol. 44, no. 5, pp. 245-9.

Grimes, C.A. 2007, 'Synthesis and application of highly ordered arrays of TiO_2 nanotubes', *Journal of Materials Chemistry*, vol. 17, no. 15, pp. 1451-7.

Grzechulska, J. & Morawski, A.W. 2002, 'Photocatalytic decomposition of azo-dye acid black 1 in water over modified titanium dioxide', *Applied Catalysis B: Environmental*, vol. 36, no. 1, pp. 45-51.

Guo, Y., Lee, N.-H., Oh, H.-J., Yoon, C.-R., Park, K.-S., Lee, W.-H., Li, Y., Lee, H.-G., Lee, K.-S. & Kim, S.-J. 2008, 'Preparation of titanate nanotube thin film using hydrothermal method', *Thin Solid Films*, vol. 516, no. 23, pp. 8363-71.

Hasegawa, G., Kanamori, K., Sugawara, Y., Ikuhara, Y. & Nakanishi, K. 2012, 'Flower-like surface modification of titania materials by lithium hydroxide solution', *Journal of Colloid and Interface Science*, vol. 374, no. 1, pp. 291-6.

Hasnat, M. & Siddiquey, I. 2005, 'Comparative photocatalytic studies of degradation of a cationic and an anionic dye', *Dyes and Pigments*, vol. 66, no. 3, pp. 185-8.

Henderson, M.A. 2013, 'Photooxidation and Photodesorption in the Photochemistry of Isobutene on TiO_2 (110)', *The Journal of Physical Chemistry C*, vol. 117, no. 27, pp. 14113-24.

Henderson, M.A., Deskins, N.A., Zehr, R.T. & Dupuis, M. 2011, 'Generation of organic radicals during photocatalytic reactions on TiO_2', *Journal of Catalysis*, vol. 279, no. 1, pp. 205-12.

Herrmann, J.-M. 1999, 'Heterogeneous photocatalysis: fundamentals and applications to the removal of various types of aqueous pollutants', *Catalysis Today*, vol. 53, no. 1, pp. 115-29.

Herrmann, J.-M. 2005, 'Heterogeneous photocatalysis: state of the art and present applications In honor of Pr. RL Burwell Jr.(1912–2003), Former Head of Ipatieff Laboratories, Northwestern University, Evanston (Ill)', *Topics in Catalysis*, vol. 34, no. 1-4, pp. 49-65.

Hillie, T. & Hlophe, M. 2007, 'Nanotechnology and the challenge of clean water', *Nature Nanotechnology*, vol. 2, no. 11, pp. 663-4.

Ho, Y.-S. & McKay, G. 1998, 'Sorption of dye from aqueous solution by peat', *Chemical Engineering Journal*, vol. 70, no. 2, pp. 115-24.

Hoffmann, M.R., Martin, S.T., Choi, W. & Bahnemann, D.W. 1995, 'Environmental Applications of Semiconductor Photocatalysis', *Chemical Reviews*, vol. 95, no. 1, pp. 69-96.

Horváth, E., Kukovecz, Á., Kónya, Z. & Kiricsi, I. 2007, 'Hydrothermal Conversion of Self-Assembled Titanate Nanotubes into Nanowires in a Revolving Autoclave', *Chemistry of Materials*, vol. 19, no. 4, pp. 927-31.

Houas, A., Lachheb, H., Ksibi, M., Elaloui, E., Guillard, C. & Herrmann, J.-M. 2001, 'Photocatalytic degradation pathway of methylene blue in water', *Applied Catalysis B: Environmental*, vol. 31, no. 2, pp. 145-57.

Hoyer, P. 1996, 'Formation of a Titanium Dioxide Nanotube Array', *Langmuir*, vol. 12, no. 6, pp. 1411-3.

Hu, A., Liang, R., Zhang, X., Kurdi, S., Luong, D., Huang, H., Peng, P., Marzbanrad, E., Oakes, K. & Zhou, Y. 2013, 'Enhanced photocatalytic degradation of dyes by TiO_2 nanobelts with hierarchical structures', *Journal of Photochemistry and Photobiology A: Chemistry*.

Hu, K., Xiao, X., Cao, X., Hao, R., Zuo, X., Zhang, X. & Nan, J. 2011, 'Adsorptive separation and photocatalytic degradation of methylene blue dye on titanate nanotube powders prepared by hydrothermal process using metal Ti particles as a precursor', *Journal of Hazardous Materials*, vol. 192, no. 2, pp. 514-20.

Huang, F., Zhang, H. & Banfield, J.F. 2003, 'The role of oriented attachment crystal growth in hydrothermal coarsening of nanocrystalline ZnS', *The Journal of Physical Chemistry B*, vol. 107, no. 38, pp. 10470-5.

Huang, J., Cao, Y., Deng, Z. & Tong, H. 2011, 'Formation of titanate nanostructures under different NaOH concentration and their application in wastewater treatment', *Journal of Solid State Chemistry*, vol. 184, no. 3, pp. 712-9.

Huang, K.-C. & Chien, S.-H. 2013, 'Improved visible-light-driven photocatalytic activity of rutile/titania-nanotube composites prepared by microwave-assisted hydrothermal process', *Applied Catalysis B: Environmental*, vol. 140–141, no. 0, pp. 283-8.

Huber, S.A., Balz, A., Abert, M. & Pronk, W. 2011, 'Characterisation of aquatic humic and non-humic matter with size-exclusion chromatography – organic carbon detection – organic nitrogen detection (LC-OCD-OND)', *Water Research*, vol. 45, no. 2, pp. 879-85.

Ibhadon, A.O. & Fitzpatrick, P. 2013, 'Heterogeneous Photocatalysis: Recent Advances and Applications', *Catalysts*, vol. 3, no. 1, pp. 189-218.

Ichinose, H., Terasaki, M., and Katsuki, H., 1996, 'Synthesis of Peroxo-Modified Anatase Sol from Peroxo Titanic Acid Solution', *Journal of the Ceramic Society of Japan*, vol. 104, no. 8, pp. 715-8.

Iftikhar, A.R., Bhatti, H.N., Hanif, M.A. & Nadeem, R. 2009, 'Kinetic and thermodynamic aspects of Cu (II) and Cr (III) removal from aqueous solutions using rose waste biomass', *Journal of Hazardous Materials*, vol. 161, no. 2, pp. 941-7.

Ikeguchi, Y. & Nakamura, H. 1998, 'A Novel Method for the On-Line Room-Temperature Hydrolysis of Hydrophobic Organic Phosphates Using a Cooperative Action of Sodium Dodecyl Sulfate, Acid and UV-Irradiation', *Analytical Sciences*, vol. 14, no. 4, pp. 815-7.

Imai, H., Takei, Y., Shimizu, K., Matsuda, M. & Hirashima, H. 1999, 'Direct preparation of anatase TiO2 nanotubes in porous alumina membranes', *J. Mater. Chem.*, vol. 9, no. 12, pp. 2971-2.

Inoue, S., Chu, S.-Z., Wada, K., Li, D. & Haneda, H. 2003, 'New roots to formation of nanostructures on glass surface through anodic oxidation of sputtered aluminum', *Science and Technology of Advanced Materials*, vol. 4, no. 4, pp. 269-76.

Inoue, Y., Kubokawa, T. & Sato, K. 1991, 'Photocatalytic activity of alkali-metal titanates combined with ruthenium in the decomposition of water', *Journal of Physical Chemistry*, vol. 95, no. 10, pp. 4059-63.

Ishihara, Y., Kyono, H., Kohyama, N., Otaki, N., Serita, F. & Toya, T. 2002, 'Effects of surface characteristics of potassium titanate whisker samples on acute lung injury induced by a single intratracheal administration in rats', *Inhalation toxicology*, vol. 14, no. 5, pp. 503-19.

Izawa, H., Kikkawa, S. & Koizumi, M. 1982, 'Ion exchange and dehydration of layered [sodium and potassium] titanates, $Na_2Ti_3O_7$ and $K_2Ti_4O_9$', *The Journal of Physical Chemistry*, vol. 86, no. 25, pp. 5023-6.

Jackson, M.J. & Ahmed, W. 2007, *Surface engineered surgical tools and medical devices*, Springer.

Janes, R. & Knightley, L. 2004, 'Crystallization and phase evolution of potassium titanates from alkoxide derived precipitates', *Journal of materials science*, vol. 39, no. 7, pp. 2589-92.

Jayaram, K., Murthy, I., Lalhruaitluanga, H. & Prasad, M. 2009, 'Biosorption of lead from aqueous solution by seed powder of Strychnos potatorum L.', *Colloids and Surfaces B: Biointerfaces*, vol. 71, no. 2, pp. 248-54.

Ji, L., Chen, W., Duan, L. & Zhu, D. 2009, 'Mechanisms for strong adsorption of tetracycline to carbon nanotubes: A comparative study using activated carbon and graphite as adsorbents', *Environmental science & technology*, vol. 43, no. 7, pp. 2322-7.

Ji, Q., Iwaura, R. & Shimizu, T. 2007, 'Regulation of silica nanotube diameters: Sol-gel transcription using solvent-sensitive morphological change of peptidic lipid nanotubes as templates', *Chemistry of materials*, vol. 19, no. 6, pp. 1329-34.

Jiasheng, X., He, Z., Wenbo, L., Jie, Z., Xiaoyang, L., Xiangke, H., Dongli, X., Jianhua, Q. & Lin, L. 2012, 'Hydrothermal synthesis and characterisation of potassium/sodium titanate nanofibres at different temperatures', *Micro & Nano Letters, IET*, vol. 7, no. 7, pp. 654-7.

Jung, J.H., Kobayashi, H., van Bommel, K.J., Shinkai, S. & Shimizu, T. 2002, 'Creation of novel helical ribbon and double-layered nanotube TiO2 structures using an organogel template', *Chemistry of materials*, vol. 14, no. 4, pp. 1445-7.

Jung, J.H., Shimizu, T. & Shinkai, S. 2005, 'Self-assembling structures of steroidal derivatives in organic solvents and their sol–gel transcription into double-walled transition-metal oxide nanotubes', *Journal of Materials Chemistry*, vol. 15, no. 35-36, pp. 3979-86.

Kanchi, S. 2014, 'Nanotechnology for Water Treatment', *J Environ Anal Chem*, vol. 1, p. e102.

Kaneco, S., Rahman, M.A., Suzuki, T., Katsumata, H. & Ohta, K. 2004, 'Optimization of solar photocatalytic degradation conditions of bisphenol A in water using titanium dioxide', *Journal of Photochemistry and Photobiology A: Chemistry*, vol. 163, no. 3, pp. 419-24.

Kannan, N. & Sundaram, M.M. 2001, 'Kinetics and mechanism of removal of methylene blue by adsorption on various carbons—a comparative study', *Dyes and Pigments*, vol. 51, no. 1, pp. 25-40.

Karaman, M., Sarıipek, F., Köysüren, Ö. & Yıldız, H.B. 2013, 'Template assisted synthesis of photocatalytic titanium dioxide nanotubes by hot filament chemical vapor deposition method', *Applied Surface Science*, vol. 283, no. 0, pp. 993-8.

Kasuga, T., Hiramatsu, M., Hoson, A., Sekino, T. & Niihara, K. 1998, 'Formation of titanium oxide nanotube', *Langmuir*, vol. 14, no. 12, pp. 3160-3.

Kasuga, T., Hiramatsu, M., Hoson, A., Sekino, T. & Niihara, K. 1999, 'Titania nanotubes prepared by chemical processing', *Advanced Materials*, vol. 11, no. 15, pp. 1307-11.

Kavitha, D. & Namasivayam, C. 2007, 'Experimental and kinetic studies on methylene blue adsorption by coir pith carbon', *Bioresource Technology*, vol. 98, no. 1, pp. 14-21.

Keane, D.A., McGuigan, K.G., Ibáñez, P.F., Polo-López, M.I., Byrne, J.A., Dunlop, P.S., O'Shea, K., Dionysiou, D.D. & Pillai, S.C. 2014, 'Solar photocatalysis for water disinfection: materials and reactor design', *Catalysis Science & Technology*, vol. 4, no. 5, pp. 1211-26.

Khajeh, M., Laurent, S. & Dastafkan, K. 2013, 'Nanoadsorbents: Classification, Preparation, and Applications (with Emphasis on Aqueous Media)', *Chemical Reviews*, vol. 113, no. 10, pp. 7728-68.

Khaled, A., Nemr, A.E., El-Sikaily, A. & Abdelwahab, O. 2009, 'Removal of Direct N Blue-106 from artificial textile dye effluent using activated carbon from orange peel: Adsorption isotherm and kinetic studies', *Journal of Hazardous Materials*, vol. 165, no. 1, pp. 100-10.

Khanna, A. & Shetty, V.K. 2014, 'Solar light induced photocatalytic degradation of Reactive Blue 220 (RB-220) dye with highly efficient Ag@TiO_2 core–shell nanoparticles: A comparison with UV photocatalysis', *Solar Energy*, vol. 99, pp. 67-76.

Khouni, I., Marrot, B., Moulin, P. & Ben Amar, R. 2011, 'Decolourization of the reconstituted textile effluent by different process treatments: Enzymatic catalysis, coagulation/flocculation and nanofiltration processes', *Desalination*, vol. 268, no. 1, pp. 27-37.

Kim, J., Shan, W., Davies, S.H., Baumann, M.J., Masten, S.J. & Tarabara, V.V. 2009, 'Interactions of aqueous NOM with nanoscale TiO_2: Implications for ceramic membrane filtration-ozonation hybrid process', *Environmental science & technology*, vol. 43, no. 14, pp. 5488-94.

Kim, J.H., Zhang, X.H., Kim, J.D., Park, H.M., Lee, S.B., Yi, J.W. & Jung, S.I. 2012, 'Synthesis and characterization of anatase TiO_2 nanotubes with controllable crystal size by a simple MWCNT template method', *Journal of Solid State Chemistry*, vol. 196, pp. 435-40.

Kim, S., Hwang, S.-J. & Choi, W. 2005, 'Visible light active platinum-ion-doped TiO_2 photocatalyst', *The Journal of Physical Chemistry B*, vol. 109, no. 51, pp. 24260-7.

Kim, S., Park, H., Kwak, C., Ji, M., Lee, M., Paik, J. & Choi, B. 2008, 'Characterization of pore structure of mesoporous hydrogen titanium oxide hydrates', *Journal of Physics and Chemistry of Solids*, vol. 69, no. 5, pp. 1139-41.

Kim, Y., Kim, C., Choi, I., Rengaraj, S. & Yi, J. 2004, 'Arsenic removal using mesoporous alumina prepared via a templating method', *Environmental Science & Technology*, vol. 38, no. 3, pp. 924-31.

Kitano, M., Wada, E., Nakajima, K., Hayashi, S., Miyazaki, S., Kobayashi, H. & Hara, M. 2013, 'Protonated Titanate Nanotubes with Lewis and Brønsted Acidity:

Relationship between Nanotube Structure and Catalytic Activity', *Chemistry of Materials*, vol. 25, no. 3, pp. 385-93.

Kochkar, H., Turki, A., Bergaoui, L., Berhault, G. & Ghorbel, A. 2009, 'Study of Pd(II) adsorption over titanate nanotubes of different diameters', *Journal of Colloid and Interface Science*, vol. 331, no. 1, pp. 27-31.

Koeppenkastrop, D. & De Carlo, E.H. 1993, 'Uptake of rare earth elements from solution by metal oxides', *Environmental science & technology*, vol. 27, no. 9, pp. 1796-802.

Konstantinou, I.K. & Albanis, T.A. 2004, 'TiO2-assisted photocatalytic degradation of azo dyes in aqueous solution: kinetic and mechanistic investigations: A review', *Applied Catalysis B: Environmental*, vol. 49, no. 1, pp. 1-14.

Kornblit, L. & Ignatiev, A. 1984, 'Photodesorption threshold energies in semiconductors', *Surface Science Letters*, vol. 136, no. 2, pp. L57-L66.

Kuchibhatla, S.V.N.T., Karakoti, A.S., Bera, D. & Seal, S. 2007, 'One dimensional nanostructured materials', *Progress in Materials Science*, vol. 52, no. 5, pp. 699-913.

Kunhikrishnan, A., Shon, H.K., Bolan, N.S., El Saliby, I. & Vigneswaran, S. 2014, 'Sources, distribution, environmental fate and ecological effects of nanomaterials in wastewater streams', *Critical Reviews in Environmental Science and Technology*, no. just-accepted.

Lai, C.W., Juan, J.C., Ko, W.B. & Bee Abd Hamid, S. 2014, 'An Overview: Recent Development of Titanium Oxide Nanotubes as Photocatalyst for Dye Degradation', *International Journal of Photoenergy*, vol. 2014.

Lai, C.W. & Sreekantan, S. 2011, 'Effect of applied potential on the formation of self-organized TiO_2 nanotube arrays and its photoelectrochemical response', *Journal of Nanomaterials*, vol. 2011, p. 11.

Lai, C.W. & Sreekantan, S. 2014, 'Photoelectrochemical properties of TiO_2 nanotube arrays: effect of electrolyte pH and annealing temperature', *Journal of Experimental Nanoscience*, vol. 9, no. 3, pp. 230-9.

Lai, C.W. & Sreekantana, S. 2012, 'Higher water splitting hydrogen generation rate for single crystalline anatase phase of TiO_2 nanotube arrays', *The European Physical Journal Applied Physics*, vol. 59, no. 02, p. 20403.

Lan, Y., Gao, X., Zhu, H., Zheng, Z., Yan, T., Wu, F., Ringer, S.P. & Song, D. 2005, 'Titanate nanotubes and nanorods prepared from rutile powder', *Advanced Functional Materials*, vol. 15, no. 8, pp. 1310-8.

Lasa, H., Serrano, B. & Salaices, M. 2005, 'Novel Photocatalytic Reactors for Water and Air Treatment', in H. Lasa, B. Serrano & M. Salaices (eds), *Photocatalytic Reaction Engineering*, Springer US, pp. 17-47.

Lee, C.T., Um, M.H. & Kumazawa, H. 2000, 'Synthesis of Titanate Derivatives Using Ion-Exchange Reaction', *Journal of the American Ceramic Society*, vol. 83, no. 5, pp. 1098-102.

Lee, S.-Y. & Park, S.-J. 2013, 'TiO2 photocatalyst for water treatment applications', *Journal of Industrial and Engineering Chemistry*, vol. 19, no. 6, pp. 1761-9.

Lei, B.-X., Liao, J.-Y., Zhang, R., Wang, J., Su, C.-Y. & Kuang, D.-B. 2010, 'Ordered crystalline TiO2 nanotube arrays on transparent FTO glass for efficient dye-sensitized solar cells', *The Journal of Physical Chemistry C*, vol. 114, no. 35, pp. 15228-33.

Li, G., Pang, S., Jiang, L., Guo, Z. & Zhang, Z. 2006, 'Environmentally friendly chemical route to vanadium oxide single-crystalline nanobelts as a cathode material for lithium-ion batteries', *The Journal of Physical Chemistry B*, vol. 110, no. 19, pp. 9383-6.

Li, Y., Yang, X.-Y., Feng, Y., Yuan, Z.-Y. & Su, B.-L. 2012, 'One-dimensional metal oxide nanotubes, nanowires, nanoribbons, and nanorods: synthesis, characterizations, properties and applications', *Critical Reviews in Solid State and Materials Sciences*, vol. 37, no. 1, pp. 1-74.

Lichtman, D. & Shapira, Y. 1976, 'The role of carbon in photodesorption', *Journal of Nuclear Materials*, vol. 63, pp. 184-7.

Linsebigler, A.L., Lu, G. & Yates, J.T. 1995, 'Photocatalysis on TiO2 Surfaces: Principles, Mechanisms, and Selected Results', *Chemical Reviews*, vol. 95, no. 3, pp. 735-58.

Liu, N., Chen, X., Zhang, J. & Schwank, J.W. 2014, 'A review on TiO2-based nanotubes synthesized via hydrothermal method: Formation mechanism, structure modification, and photocatalytic applications', *Catalysis Today*, vol. 225, no. 0, pp. 34-51.

Liu, S.-Y., Gao, J., Yang, Y.-J., Yang, Y.-C. & Ye, Z.-X. 2010, 'Adsorption intrinsic kinetics and isotherms of lead ions on steel slag', *Journal of hazardous materials*, vol. 173, no. 1, pp. 558-62.

Liu, S., Gan, L., Liu, L., Zhang, W. & Zeng, H. 2002, 'Synthesis of single-crystalline TiO2 nanotubes', *Chemistry of materials*, vol. 14, no. 3, pp. 1391-7.

Liu, S., Han, L., Duan, Y., Asahina, S., Terasaki, O., Cao, Y., Liu, B., Ma, L., Zhang, J. & Che, S. 2012, 'Synthesis of chiral TiO2 nanofibre with electron transition-based optical activity', *Nature communications*, vol. 3, p. 1215.

Liu, Y., Qi, T. & Zhang, Y. 2006, 'A novel way to synthesize potassium titanates', *Materials Letters*, vol. 60, no. 2, pp. 203-5.

Ma, H., Yoon, K., Rong, L., Mao, Y., Mo, Z., Fang, D., Hollander, Z., Gaiteri, J., Hsiao, B.S. & Chu, B. 2010, 'High-flux thin-film nanofibrous composite ultrafiltration membranes containing cellulose barrier layer', *Journal of Materials Chemistry*, vol. 20, no. 22, pp. 4692-704.

Ma, R., Fukuda, K., Sasaki, T., Osada, M. & Bando, Y. 2005, 'Structural Features of Titanate Nanotubes/Nanobelts Revealed by Raman, X-ray Absorption Fine Structure and Electron Diffraction Characterizations', *The Journal of Physical Chemistry B*, vol. 109, no. 13, pp. 6210-4.

Ma, R., Sasaki, T. & Bando, Y. 2005, 'Alkali metal cation intercalation properties of titanate nanotubes', *Chemical Communications*, no. 7, pp. 948-50.

Ma, Y., Lin, Y., Xiao, X., Zhou, X. & Li, X. 2006, 'Sonication–hydrothermal combination technique for the synthesis of titanate nanotubes from

commercially available precursors', *Materials Research Bulletin*, vol. 41, no. 2, pp. 237-43.

Macak, J., Hildebrand, H., Marten-Jahns, U. & Schmuki, P. 2008, 'Mechanistic aspects and growth of large diameter self-organized TiO_2 nanotubes', *Journal of Electroanalytical Chemistry*, vol. 621, no. 2, pp. 254-66.

Macak, J., Tsuchiya, H., Ghicov, A., Yasuda, K., Hahn, R., Bauer, S. & Schmuki, P. 2007, 'TiO_2 nanotubes: Self-organized electrochemical formation, properties and applications', *Current Opinion in Solid State and Materials Science*, vol. 11, no. 1, pp. 3-18.

Macak, J.M. & Schmuki, P. 2006, 'Anodic growth of self-organized anodic TiO_2 nanotubes in viscous electrolytes', *Electrochimica Acta*, vol. 52, no. 3, pp. 1258-64.

Mahajan, V., Misra, M., Raja, K. & Mohapatra, S. 2008, 'Self-organized TiO_2 nanotubular arrays for photoelectrochemical hydrogen generation: effect of crystallization and defect structures', *Journal of Physics D: Applied Physics*, vol. 41, no. 12, p. 125307.

Mahmoud, A. & Hoadley, A.F. 2012, 'An evaluation of a hybrid ion exchange electrodialysis process in the recovery of heavy metals from simulated dilute industrial wastewater', *Water research*, vol. 46, no. 10, pp. 3364-76.

Malato, S., Fernández-Ibáñez, P., Maldonado, M.I., Blanco, J. & Gernjak, W. 2009, 'Decontamination and disinfection of water by solar photocatalysis: Recent overview and trends', *Catalysis Today*, vol. 147, no. 1, pp. 1-59.

Mamalis, A. 2007, 'Recent advances in nanotechnology', *Journal of materials processing technology*, vol. 181, no. 1, pp. 52-8.

Manke, A., Luanpitpong, L. & Rojanasakul, Y. 2014, 'Potential Occupational Risks Associated with Pulmonary Toxicity of Carbon Nanotubes', *Occup Med Health Aff*, vol. 2, p. 165.

Masaki, N., Uchida, S., Yamane, H. & Sato, T. 2000, 'Hydrothermal synthesis of potassium titanates in Ti-KOH-H_2O system', *Journal of materials science*, vol. 35, no. 13, pp. 3307-11.

Masaki, N., Uchida, S., Yamane, H. & Sato, T. 2002, 'Characterization of a New Potassium Titanate, $KTiO_2(OH)$ Synthesized via Hydrothermal Method', *Chemistry of Materials*, vol. 14, no. 1, pp. 419-24.

Matlock, M.M., Howerton, B.S. & Atwood, D.A. 2002, 'Chemical Precipitation of Lead from Lead Battery Recycling Plant Wastewater', *Industrial & Engineering Chemistry Research*, vol. 41, no. 6, pp. 1579-82.

Mayo, J., Yavuz, C., Yean, S., Cong, L., Shipley, H., Yu, W., Falkner, J., Kan, A., Tomson, M. & Colvin, V. 2007, 'The effect of nanocrystalline magnetite size on arsenic removal', *Science and Technology of Advanced Materials*, vol. 8, no. 1, pp. 71-5.

Mills, A. & Le Hunte, S. 1997, 'An overview of semiconductor photocatalysis', *Journal of Photochemistry and Photobiology A: Chemistry*, vol. 108, no. 1, pp. 1-35.

Min, M., Shen, L., Hong, G., Zhu, M., Zhang, Y., Wang, X., Chen, Y. & Hsiao, B.S. 2012, 'Micro-nano structure poly (ether sulfones)/poly (ethyleneimine)

nanofibrous affinity membranes for adsorption of anionic dyes and heavy metal ions in aqueous solution', *Chemical Engineering Journal*, vol. 197, pp. 88-100.

Misra, R., Jain, S. & Khatri, P. 2011, 'Iminodiacetic acid functionalized cation exchange resin for adsorptive removal of Cr (VI), Cd (II), Ni (II) and Pb (II) from their aqueous solutions', *Journal of Hazardous Materials*, vol. 185, no. 2, pp. 1508-12.

Mittal, A., Mittal, J., Malviya, A., Kaur, D. & Gupta, V. 2010, 'Adsorption of hazardous dye crystal violet from wastewater by waste materials', *Journal of Colloid and Interface Science*, vol. 343, no. 2, pp. 463-73.

Mohamed, A.E.R. & Rohani, S. 2011, 'Modified TiO2 nanotube arrays (TNTAs): progressive strategies towards visible light responsive photoanode, a review', *Energy Environ. Sci.*, vol. 4, no. 4, pp. 1065-86.

Mohanty, K., Naidu, J.T., Meikap, B. & Biswas, M. 2006, 'Removal of crystal violet from wastewater by activated carbons prepared from rice husk', *Industrial & engineering chemistry research*, vol. 45, no. 14, pp. 5165-71.

Mohapatra, S.K., Misra, M., Mahajan, V.K. & Raja, K.S. 2007, 'Design of a Highly Efficient Photoelectrolytic Cell for Hydrogen Generation by Water Splitting: Application of TiO_{2-x} C_x Nanotubes as a Photoanode and Pt/TiO_2 Nanotubes as a Cathode', *The Journal of Physical Chemistry C*, vol. 111, no. 24, pp. 8677-85.

Moorthy, J., Khoury, C., Moore, J.S. & Beebe, D.J. 2001, 'Active control of electroosmotic flow in microchannels using light', *Sensors and Actuators B: Chemical*, vol. 75, no. 3, pp. 223-9.

Mor, G.K., Varghese, O.K., Paulose, M. & Grimes, C.A. 2005, 'Transparent highly ordered TiO_2 nanotube arrays via anodization of titanium thin films', *Advanced Functional Materials*, vol. 15, no. 8, pp. 1291-6.

Mor, G.K., Varghese, O.K., Paulose, M., Shankar, K. & Grimes, C.A. 2006, 'A review on highly ordered, vertically oriented TiO_2 nanotube arrays: Fabrication, material properties, and solar energy applications', *Solar Energy Materials and Solar Cells*, vol. 90, no. 14, pp. 2011-75.

Morgado Jr, E., de Abreu, M.A.S., Moure, G.T., Marinkovic, B.A., Jardim, P.M. & Araujo, A.S. 2007, 'Effects of thermal treatment of nanostructured trititanates on their crystallographic and textural properties', *Materials Research Bulletin*, vol. 42, no. 9, pp. 1748-60.

Morgado Jr, E., de Abreu, M.A.S., Pravia, O.R.C., Marinkovic, B.A., Jardim, P.M., Rizzo, F.C. & Araújo, A.S. 2006, 'A study on the structure and thermal stability of titanate nanotubes as a function of sodium content', *Solid State Sciences*, vol. 8, no. 8, pp. 888-900.

Morgan, D.L., Triani, G., Blackford, M.G., Raftery, N., Frost, R.L. & Waclawik, E.R. 2011, 'Alkaline hydrothermal kinetics in titanate nanostructure formation', *Journal of Materials Science*, vol. 46, no. 2, pp. 548-57.

Morgan, D.L., Zhu, H.-Y., Frost, R.L. & Waclawik, E.R. 2008, 'Determination of a Morphological Phase Diagram of Titania/Titanate Nanostructures from Alkaline Hydrothermal Treatment of Degussa P25', *Chemistry of Materials*, vol. 20, no. 12, pp. 3800-2.

Mozia, S. 2010, 'Photocatalytic membrane reactors (PMRs) in water and wastewater treatment. A review', *Separation and Purification Technology*, vol. 73, no. 2, pp. 71-91.

Mukherjee, P.S. & Ray, A.K. 1999, 'Major challenges in the design of a large-scale photocatalytic reactor for water treatment', *Chemical Engineering and Technology*, vol. 22, no. 3, p. 253.

Müllner, M., Lunkenbein, T., Schieder, M., Gröschel, A.H., Miyajima, N., Förtsch, M., Breu, J., Caruso, F. & Müller, A.H.E. 2012, 'Template-Directed Mild Synthesis of Anatase Hybrid Nanotubes within Cylindrical Core–Shell–Corona Polymer Brushes', *Macromolecules*, vol. 45, no. 17, pp. 6981-8.

Nakahira, A., Kubo, T. & Numako, C. 2010, 'Formation mechanism of TiO_2-derived titanate nanotubes prepared by the hydrothermal process', *Inorganic chemistry*, vol. 49, no. 13, pp. 5845-52.

Neppolian, B., Choi, H., Sakthivel, S., Arabindoo, B. & Murugesan, V. 2002, 'Solar light induced and TiO_2 assisted degradation of textile dye reactive blue 4', *Chemosphere*, vol. 46, no. 8, pp. 1173-81.

Neville, E.M., MacElroy, J.M.D., Thampi, K.R. & Sullivan, J.A. 2013, 'Visible light active C-doped titanate nanotubes prepared via alkaline hydrothermal treatment of C-doped nanoparticulate TiO_2: Photo-electrochemical and photocatalytic properties', *Journal of Photochemistry and Photobiology A: Chemistry*, vol. 267, no. 0, pp. 17-24.

Nian, J.-N. & Teng, H. 2006, 'Hydrothermal synthesis of single-crystalline anatase TiO2 nanorods with nanotubes as the precursor', *The Journal of Physical Chemistry B*, vol. 110, no. 9, pp. 4193-8.

Noguchi, T., Fujishima, A., Sawunyama, P. & Hashimoto, K. 1998, 'Photocatalytic degradation of gaseous formaldehyde using TiO_2 film', *Environmental science & technology*, vol. 32, no. 23, pp. 3831-3.

Ohsaki, Y., Masaki, N., Kitamura, T., Wada, Y., Okamoto, T., Sekino, T., Niihara, K. & Yanagida, S. 2005, 'Dye-sensitized TiO_2 nanotube solar cells: fabrication and electronic characterization', *Physical Chemistry Chemical Physics*, vol. 7, no. 24, pp. 4157-63.

Ollis, D.F., Pelizzetti, E. & Serpone, N. 1991, 'Photocatalyzed destruction of water contaminants', *Environmental Science & Technology*, vol. 25, no. 9, pp. 1522-9.

Oturan, M.A. & Aaron, J.-J. 2014, 'Advanced Oxidation Processes in Water/Wastewater Treatment: Principles and Applications. A Review', *Critical Reviews in Environmental Science and Technology*, pp. null-null.

Ou, H.-H., Liao, C.-H., Liou, Y.-H., Hong, J.-H. & Lo, S.-L. 2008, 'Photocatalytic Oxidation of Aqueous Ammonia over Microwave-Induced Titanate Nanotubes', *Environmental Science & Technology*, vol. 42, no. 12, pp. 4507-12.

Ou, H.-H. & Lo, S.-L. 2007, 'Review of titania nanotubes synthesized via the hydrothermal treatment: Fabrication, modification, and application', *Separation and Purification Technology*, vol. 58, no. 1, pp. 179-91.

Ou, H.H., Lo, S.L. & Liou, Y.H. 2007, 'Microwave-induced titanate nanotubes and the corresponding behaviour after thermal treatment', *Nanotechnology*, vol. 18, no. 17, p. 175702.

Pagga, U. & Brown, D. 1986, 'The degradation of dyestuffs: Part II Behaviour of dyestuffs in aerobic biodegradation tests', *Chemosphere*, vol. 15, no. 4, pp. 479-91.

Pan, B. & Xing, B. 2008, 'Adsorption mechanisms of organic chemicals on carbon nanotubes', *Environmental Science & Technology*, vol. 42, no. 24, pp. 9005-13.

Pang, Y.L., Lim, S., Ong, H.C. & Chong, W.T. 2014, 'A critical review on the recent progress of synthesizing techniques and fabrication of TiO_2-based nanotubes photocatalysts', *Applied Catalysis A: General*, vol. 481, no. 0, pp. 127-42.

Panich, N.M., Seliverstov, A.F. & Ershov, B.G. 2008, 'Photooxidative decomposition of sodium dodecyl sulfate in aqueous solutions', *Russian Journal of Applied Chemistry*, vol. 81, no. 12, pp. 2104-7.

Papa, A.-L., Millot, N., Saviot, L., Chassagnon, R. & Heintz, O. 2009, 'Effect of Reaction Parameters on Composition and Morphology of Titanate Nanomaterials', *The Journal of Physical Chemistry C*, vol. 113, no. 29, pp. 12682-9.

Park, J.H., Kim, S. & Bard, A.J. 2006, 'Novel carbon-doped TiO_2 nanotube arrays with high aspect ratios for efficient solar water splitting', *Nano letters*, vol. 6, no. 1, pp. 24-8.

Patzke, G.R., Krumeich, F. & Nesper, R. 2002, 'Oxidic Nanotubes and Nanorods—Anisotropic Modules for a Future Nanotechnology', *Angewandte Chemie International Edition*, vol. 41, no. 14, pp. 2446-61.

Paulose, M., Prakasam, H.E., Varghese, O.K., Peng, L., Popat, K.C., Mor, G.K., Desai, T.A. & Grimes, C.A. 2007, 'TiO_2 nanotube arrays of 1000 μm length by anodization of titanium foil: phenol red diffusion', *The Journal of Physical Chemistry C*, vol. 111, no. 41, pp. 14992-7.

Payne, J.W. & Smith, M.W. 1994, 'Peptide Transport by Micro-organisms', in A.H. Rose & D.W. Tempest (eds), *Advances in Microbial Physiology*, vol. Volume 36, Academic Press, pp. 1-80.

Pelaez, M., Nolan, N.T., Pillai, S.C., Seery, M.K., Falaras, P., Kontos, A.G., Dunlop, P.S., Hamilton, J.W., Byrne, J.A. & O'Shea, K. 2012, 'A review on the visible light active titanium dioxide photocatalysts for environmental applications', *Applied Catalysis B: Environmental*, vol. 125, pp. 331-49.

Pelizzetti, E., Minero, C., Borgarello, E., Tinucci, L. & Serpone, N. 1993, 'Photocatalytic activity and selectivity of titania colloids and particles prepared by the sol-gel technique: photooxidation of phenol and atrazine', *Langmuir*, vol. 9, no. 11, pp. 2995-3001.

Pendergast, M.M. & Hoek, E.M. 2011, 'A review of water treatment membrane nanotechnologies', *Energy & Environmental Science*, vol. 4, no. 6, pp. 1946-71.

Peng, T., Hasegawa, A., Qiu, J. & Hirao, K. 2003, 'Fabrication of titania tubules with high surface area and well-developed mesostructural walls by surfactant-

mediated templating method', *Chemistry of Materials*, vol. 15, no. 10, pp. 2011-6.

Peng, Y.-P., Lo, S.-L., Ou, H.-H. & Lai, S.-W. 2010, 'Microwave-assisted hydrothermal synthesis of N-doped titanate nanotubes for visible-light-responsive photocatalysis', *Journal of Hazardous Materials*, vol. 183, no. 1–3, pp. 754-8.

Pignatello, J. 1992, 'Dark and photoassisted Fe3þ catalyzed degradation of chlorophenoxy herbicides by hydrogen peroxide.', *Environmental Science and Technology*, vol. 26, pp. 944-51.

Piquemal, J.-Y., Briot, E. & Brégeault, J.-M. 2013, 'Preparation of materials in the presence of hydrogen peroxide: from discrete or "zero-dimensional" objects to bulk materials', *Dalton Transactions*, vol. 42, no. 1, pp. 29-45.

Pirkanniemi, K. & Sillanpää, M. 2002, 'Heterogeneous water phase catalysis as an environmental application: a review', *Chemosphere*, vol. 48, no. 10, pp. 1047-60.

Poudel, B., Wang, W., Dames, C., Huang, J., Kunwar, S., Wang, D., Banerjee, D., Chen, G. & Ren, Z. 2005, 'Formation of crystallized titania nanotubes and their transformation into nanowires', *Nanotechnology*, vol. 16, no. 9, p. 1935.

Preda, S., Teodorescu, V.S., Musuc, A.M., Andronescu, C. & Zaharescu, M. 2013, 'Influence of the TiO_2 precursors on the thermal and structural stability of titanate-based nanotubes', *Journal of Materials Research*, vol. 28, no. 03, pp. 294-303.

Prieto, O., Fermoso, J., Nuñez, Y., Del Valle, J. & Irusta, R. 2005, 'Decolouration of textile dyes in wastewaters by photocatalysis with TiO_2', *Solar Energy*, vol. 79, no. 4, pp. 376-83.

Qiu, J., Li, X., Gao, X., Gan, X., Weng, B., Li, L., Yuan, Z., Shi, Z. & Hwang, Y.-H. 2012, 'Branched double-shelled TiO_2 nanotube networks on transparent conducting oxide substrates for dye sensitized solar cells', *Journal of Materials Chemistry*, vol. 22, no. 44, pp. 23411-7.

Qu, X., Alvarez, P.J. & Li, Q. 2013, 'Applications of nanotechnology in water and wastewater treatment', *water research*, vol. 47, no. 12, pp. 3931-46.

Qu, X., Brame, J., Li, Q. & Alvarez, P.J. 2012, 'Nanotechnology for a safe and sustainable water supply: enabling integrated water treatment and reuse', *Accounts of chemical research*, vol. 46, no. 3, pp. 834-43.

Rafatullah, M., Sulaiman, O., Hashim, R. & Ahmad, A. 2009, 'Adsorption of copper (II), chromium (III), nickel (II) and lead (II) ions from aqueous solutions by meranti sawdust', *Journal of Hazardous Materials*, vol. 170, no. 2, pp. 969-77.

Rajeshwar, K., Chenthamarakshan, C., Goeringer, S. & Djukic, M. 2001, 'Titania-based heterogeneous photocatalysis. Materials, mechanistic issues, and implications for environmental remediation', *Pure and Applied Chemistry*, vol. 73, no. 12, pp. 1849-60.

Ray, A.K. 1999, 'Design, modelling and experimentation of a new large-scale photocatalytic reactor for water treatment', *Chemical Engineering Science*, vol. 54, no. 15, pp. 3113-25.

Reed, R.B., Faust, J., Yang, Y., Doudrick, K., Capco, D., Hristovski, K.D. & Westerhoff, P. 2014, 'Characterization of nanomaterials in metal colloid-containing dietary supplement drinks and assessment of their potential interactions after ingestion', *ACS Sustainable Chemistry & Engineering*.

Riera-Torres, M., Gutiérrez-Bouzán, C. & Crespi, M. 2010, 'Combination of coagulation–flocculation and nanofiltration techniques for dye removal and water reuse in textile effluents', *Desalination*, vol. 252, no. 1–3, pp. 53-9.

Riss, A., Berger, T., Grothe, H., Bernardi, J., Diwald, O. & Knözinger, E. 2007, 'Chemical Control of Photoexcited States in Titanate Nanostructures', *Nano Letters*, vol. 7, no. 2, pp. 433-8.

Robert, D. & Malato, S. 2002, 'Solar photocatalysis: a clean process for water detoxification', *Science of The Total Environment*, vol. 291, no. 1–3, pp. 85-97.

Rodriguez, M., Sarria, V., Esplugas, S. & Pulgarin, C. 2002, 'Photo-Fenton treatment of a biorecalcitrant wastewater generated in textile activities: biodegradability of the photo-treated solution', *Journal of Photochemistry and Photobiology A: chemistry*, vol. 151, no. 1, pp. 129-35.

Romão, J., Barata, D., Habibovic, P., Mul, G. & Baltrusaitis, J. 2014, 'High Throughput Analysis of Photocatalytic Water Purification', *Analytical Chemistry*.

Roy, P., Berger, S. & Schmuki, P. 2011, 'TiO2 Nanotubes: Synthesis and Applications', *Angewandte Chemie International Edition*, vol. 50, no. 13, pp. 2904-39.

Roy, P., Kim, D., Lee, K., Spiecker, E. & Schmuki, P. 2010, 'TiO2 nanotubes and their application in dye-sensitized solar cells', *Nanoscale*, vol. 2, no. 1, pp. 45-59.

Sakthivel, S., Neppolian, B., Shankar, M., Arabindoo, B., Palanichamy, M. & Murugesan, V. 2003, 'Solar photocatalytic degradation of azo dye: comparison of photocatalytic efficiency of ZnO and TiO_2', *Solar Energy Materials and Solar Cells*, vol. 77, no. 1, pp. 65-82.

Samet, J.M. 2014, 'Engineered Nanomaterials and Human and Environmental Health: Research Strategies to Address Potential Risks', *Current Environmental Health Reports*, pp. 1-10.

Santara, B. & Giri, P.K. 2013, 'Impact of reaction temperature, stirring and cosolvent on the solvothermal synthesis of anatase TiO_2 and TiO_2/titanate hybrid nanostructures: Elucidating the growth mechanism', *Materials Chemistry and Physics*, vol. 137, no. 3, pp. 928-36.

Saquib, M., Abu Tariq, M., Haque, M.M. & Muneer, M. 2008, 'Photocatalytic degradation of disperse blue 1 using UV/TiO_2/H_2O_2 process', *Journal of Environmental Management*, vol. 88, no. 2, pp. 300-6.

Saquib, M. & Muneer, M. 2003, 'TiO_2-mediated photocatalytic degradation of a triphenylmethane dye (gentian violet), in aqueous suspensions', *Dyes and Pigments*, vol. 56, no. 1, pp. 37-49.

Savage, N. & Diallo, M.S. 2005, 'Nanomaterials and water purification: Opportunities and challenges', *Journal of Nanoparticle Research*, vol. 7, no. 4, pp. 331-42.

Savolainen, K., Pylkkänen, L., Norppa, H., Falck, G., Lindberg, H., Tuomi, T., Vippola, M., Alenius, H., Hämeri, K., Koivisto, J., Brouwer, D., Mark, D., Bard, D., Berges, M., Jankowska, E., Posniak, M., Farmer, P., Singh, R., Krombach, F., Bihari, P., Kasper, G. & Seipenbusch, M. 2010,

'Nanotechnologies, engineered nanomaterials and occupational health and safety – A review', *Safety Science*, vol. 48, no. 8, pp. 957-63.

Schulte, P., Geraci, C., Murashov, V., Kuempel, E., Zumwalde, R., Castranova, V., Hoover, M., Hodson, L. & Martinez, K. 2014, 'Occupational safety and health criteria for responsible development of nanotechnology', *Journal of Nanoparticle Research*, vol. 16, no. 1, pp. 1-17.

Semerjian, L. 2010, 'Equilibrium and kinetics of cadmium adsorption from aqueous solutions using untreated Pinus halepensis sawdust', *Journal of Hazardous Materials*, vol. 173, no. 1, pp. 236-42.

Senthil Kumar, P., Ramalingam, S., Abhinaya, R.V., Kirupha, S.D., Murugesan, A. & Sivanesan, S. 2012, 'Adsorption of metal ions onto the chemically modified agricultural waste', *CLEAN–Soil, Air, Water*, vol. 40, no. 2, pp. 188-97.

Senthilkumaar, S. & Porkodi, K. 2005, 'Heterogeneous photocatalytic decomposition of Crystal Violet in UV-illuminated sol–gel derived nanocrystalline TiO_2 suspensions', *Journal of Colloid and Interface Science*, vol. 288, no. 1, pp. 184-9.

Seo, D.-S., Lee, J.-K. & Kim, H. 2001, 'Preparation of nanotube-shaped TiO_2 powder', *Journal of Crystal Growth*, vol. 229, no. 1, pp. 428-32.

Seo, G., Ohgaki, S. & Suzuki, Y. 1997, 'Sorption characteristics of biological powdered activated carbon in BPAC-MF (biological powdered activated carbon-microfiltration) system for refractory organic removal', *Water science and technology*, vol. 35, no. 7, pp. 163-70.

Seo, H.-K., Kim, G.-S., Ansari, S.G., Kim, Y.-S., Shin, H.-S., Shim, K.-H. & Suh, E.-K. 2008, 'A study on the structure/phase transformation of titanate nanotubes synthesized at various hydrothermal temperatures', *Solar Energy Materials and Solar Cells*, vol. 92, no. 11, pp. 1533-9.

Shahid, M., El Saliby, I., McDonagh, A., Tijing, L.D., Kim, J.-H. & Shon, H.K. 2014, 'Synthesis and characterisation of potassium polytitanate for photocatalytic degradation of crystal violet', *Journal of Environmental Sciences*, vol. 26, no. 11, pp. 2348-54.

Shahid, M., McDonagh, A., Kim, J.H. & Shon, H.K. 2014, 'Magnetised titanium dioxide (TiO_2) for water purification: preparation, characterisation and application', *Desalination and Water Treatment*, pp. 1-24.

Shahid, M., Saliby, I.E., McDonagh, A., Kim, J.-H. & Shon, H.K. 2014, 'Photodesorption of specific organic compounds from titanium dioxide particles in aqueous media', *Desalination and Water Treatment*, vol. 52, no. 4-6, pp. 867-72.

Shapira, Y., Cox, S. & Lichtman, D. 1976, 'Chemisorption, photodesorption and conductivity measurements on ZnO surfaces', *Surface Science*, vol. 54, no. 1, pp. 43-59.

Sharma, Y., Srivastava, V., Singh, V., Kaul, S. & Weng, C. 2009, 'Nano-adsorbents for the removal of metallic pollutants from water and wastewater', *Environmental technology*, vol. 30, no. 6, pp. 583-609.

Shen, M. & Henderson, M.A. 2011, 'Impact of Solvent on Photocatalytic Mechanisms: Reactions of Photodesorption Products with Ice Overlayers on the TiO2 (110) Surface', *The Journal of Physical Chemistry C*, vol. 115, no. 13, pp. 5886-93.

Shimizu, N., Ogino, C., Dadjour, M.F. & Murata, T. 2007, 'Sonocatalytic degradation of methylene blue with TiO2 pellets in water', *Ultrasonics Sonochemistry*, vol. 14, no. 2, pp. 184-90.

Shirayama, H., Tohezo, Y. & Taguchi, S. 2001, 'Photodegradation of chlorinated hydrocarbons in the presence and absence of dissolved oxygen in water', *Water research*, vol. 35, no. 8, pp. 1941-50.

Shon, H.K., Vigneswaran, S., Ngo, H.H. & Ben Aim, R. 2005, 'Is semi-flocculation effective as pretreatment to ultrafiltration in wastewater treatment?', *Water Research*, vol. 39, no. 1, pp. 147-53.

Shon, H.K., Vigneswaran, S., Ngo, H.H. & Kim, J.H. 2005, 'Chemical coupling of photocatalysis with flocculation and adsorption in the removal of organic matter', *Water Research*, vol. 39, no. 12, pp. 2549-58.

Sikhwivhilu, L.M., Mpelane, S., Mwakikunga, B.W. & Sinha Ray, S. 2012, 'Photoluminescence and hydrogen gas-sensing properties of titanium dioxide nanostructures synthesized by hydrothermal treatments', *ACS Applied Materials and Interfaces*, vol. 4, no. 3, pp. 1656-65.

Sikhwivhilu, L.M., Ray, S.S. & Coville, N.J. 2009, 'Influence of bases on hydrothermal synthesis of titanate nanostructures', *Applied Physics A*, vol. 94, no. 4, pp. 963-73.

Sikuvhihulu, L.C., Coville, N.J., Ntho, T. & Scurrell, M.S. 2008, 'Potassium titanate: An alternative support for gold catalyzed carbon monoxide oxidation?', *Catalysis Letters*, vol. 123, no. 3-4, pp. 193-7.

So, C., Cheng, M.Y., Yu, J. & Wong, P. 2002, 'Degradation of azo dye Procion Red MX-5B by photocatalytic oxidation', *Chemosphere*, vol. 46, no. 6, pp. 905-12.

Sobczyński, A. & Dobosz, A. 2001, 'Water purification by photocatalysis on semiconductors', *Polish journal of environmental studies*, vol. 10, no. 4, pp. 195-205.

Sousa, F.W., Oliveira, A.G., Ribeiro, J.P., Rosa, M.F., Keukeleire, D. & Nascimento, R.F. 2010, 'Green coconut shells applied as adsorbent for removal of toxic metal ions using fixed-bed column technology', *J Environ Manage*, vol. 91, no. 8, pp. 1634-40.

Sreekantan, S. & Wei, L.C. 2010, 'Study on the formation and photocatalytic activity of titanate nanotubes synthesized via hydrothermal method', *Journal of Alloys and Compounds*, vol. 490, no. 1–2, pp. 436-42.

Stevenson, F.J. 1982, 'Humus Chemistry — Genesis, Composition, Reactions', *JohnWiley & Sons, NewYork* p. 443.

Strathmann, H. 2001, 'Membrane separation processes: current relevance and future opportunities', *AIChE Journal*, vol. 47, no. 5, pp. 1077-87.

Street, C.A.A., D. M. W. 1983, 'Refinement of Structures Previously Proposed for Gum Arabic and other Acacia Gum Exudates', *Talanta*, vol. 30, pp. 878-93.

Subramanian, V., Pangarkar, V. & Beenackers, A.M. 2000, 'Photocatalytic degradation of para-hydroxybenzoic acid: Relationship between substrate adsorption and photocatalytic degradation', *Clean Products and Processes*, vol. 2, no. 3, pp. 149-56.

Subramanian, V., Wolf, E.E. & Kamat, P.V. 2004, 'Catalysis with TiO2/Gold Nanocomposites. Effect of Metal Particle Size on the Fermi Level Equilibration', *Journal of the American Chemical Society*, vol. 126, no. 15, pp. 4943-50.

Suksaroj, C., Heran, M., Allegre, C. & Persin, F. 2005, 'Treatment of textile plant effluent by nanofiltration and/or reverse osmosis for water reuse', *Desalination*, vol. 178, no. 1, pp. 333-41.

Sun, L., Zhang, S., Sun, X. & He, X. 2010, 'Effect of the geometry of the anodized titania nanotube array on the performance of dye-sensitized solar cells', *Journal of nanoscience and nanotechnology*, vol. 10, no. 7, pp. 4551-61.

Sun, X., Chen, X. & Li, Y. 2002, 'Large-Scale Synthesis of Sodium and Potassium Titanate Nanobelts', *Inorganic Chemistry*, vol. 41, no. 20, pp. 4996-8.

Sun, X. & Li, Y. 2003, 'Synthesis and Characterization of Ion-Exchangeable Titanate Nanotubes', *Chemistry-A European Journal*, vol. 9, no. 10, pp. 2229-38.

Suttiponparnit, K., Jiang, J., Sahu, M., Suvachittanont, S., Charinpanitkul, T. & Biswas, P. 2011, 'Role of surface area, primary particle size, and crystal phase on titanium dioxide nanoparticle dispersion properties', *Nanoscale Res Lett*, vol. 6, no. 1, p. 27.

Sylvester, P., Westerhoff, P., Möller, T., Badruzzaman, M. & Boyd, O. 2007, 'A hybrid sorbent utilizing nanoparticles of hydrous iron oxide for arsenic removal from drinking water', *Environmental Engineering Science*, vol. 24, no. 1, pp. 104-12.

Tan, Y.N., Wong, C.L. & Mohamed, A.R. 2012, 'Hydrothermal treatment of fluorinated titanium dioxide: photocatalytic degradation of phenol', *Asia-Pacific Journal of Chemical Engineering*, vol. 7, no. 6, pp. 877-85.

Tanaka, K., Padermpole, K. & Hisanaga, T. 2000, 'Photocatalytic degradation of commercial azo dyes', *Water research*, vol. 34, no. 1, pp. 327-33.

Theron, J., Walker, J. & Cloete, T. 2008, 'Nanotechnology and water treatment: applications and emerging opportunities', *Critical reviews in microbiology*, vol. 34, no. 1, pp. 43-69.

Thiruvenkatachari, R., Vigneswaran, S. & Moon, I.S. 2008, 'A review on UV/TiO_2 photocatalytic oxidation process (Journal Review)', *Korean Journal of Chemical Engineering*, vol. 25, no. 1, pp. 64-72.

Tijing, L.D., Choi, J.-S., Lee, S., Kim, S.-H. & Shon, H.K. 2014, 'Recent progress of membrane distillation using electrospun nanofibrous membrane', *Journal of Membrane Science*, vol. 453, no. 0, pp. 435-62.

Torrades, F., Garcıa-Montano, J., Antonio García-Hortal, J., Domenech, X. & Peral, J. 2004, 'Decolorization and mineralization of commercial reactive dyes under solar light assisted photo-Fenton conditions', *Solar Energy*, vol. 77, no. 5, pp. 573-81.

Tsai, C.-C. & Teng, H. 2004, 'Regulation of the physical characteristics of titania nanotube aggregates synthesized from hydrothermal treatment', *Chemistry of Materials*, vol. 16, no. 22, pp. 4352-8.

Tupker RA, W.C., Berardesca E, Lee CH, Fartasch M, Agner T, Serup J. 1997, 'Guidelines on sodium lauryl sulfate (SLS) exposure tests. A report from the Standardization Group of the European Society of Contact Dermatitis. ', Contact Dermatitis pp. 37(2):53-69, <http://www.ncbi.nlm.nih.gov/pubmed/9285167>.

Turchi, C.S. & Ollis, D.F. 1989, 'Mixed reactant photocatalysis: intermediates and mutual rate inhibition', *Journal of Catalysis*, vol. 119, no. 2, pp. 483-96.

Turki, A., Kochkar, H., Guillard, C., Berhault, G. & Ghorbel, A. 2013, 'Effect of Na content and thermal treatment of titanate nanotubes on the photocatalytic degradation of formic acid', *Applied Catalysis B: Environmental*, vol. 138–139, no. 0, pp. 401-15.

Um, M.H., Lee, C.T. & Kumazawa, H. 2001, 'Thermal Treatment of Titanate Derivatives Synthesized by Ion-Exchange Reaction', *Journal of the American Ceramic Society*, vol. 84, no. 5, pp. 1181-3.

van Dyk, A.C. & Heyns, A.M. 1998, 'Dispersion Stability and Photo-activity of Rutile (TiO_2) Powders', *Journal of colloid and interface science*, vol. 206, no. 2, pp. 381-91.

Velez, D. & Montoro, R. 1998, 'Arsenic speciation in manufactured seafood products', *Journal of Food Protection*, vol. 61, no. 9, pp. 1240-5.

Vermeer, A., Van Riemsdijk, W. & Koopal, L. 1998, 'Adsorption of humic acid to mineral particles. 1. Specific and electrostatic interactions', *Langmuir*, vol. 14, no. 10, pp. 2810-9.

Vilar, V.J., Pinho, L.X., Pintor, A. & Boaventura, R.A. 2011, 'Treatment of textile wastewaters by solar-driven advanced oxidation processes', *Solar Energy*, vol. 85, no. 9, pp. 1927-34.

Vinu, R. & Madras, G. 2012, 'Environmental remediation by photocatalysis', *Journal of the Indian Institute of Science*, vol. 90, no. 2, pp. 189-230.

Viriya-empikul, N., Charinpanitkul, T., Sano, N., Soottitantawat, A., Kikuchi, T., Faungnawakij, K. & Tanthapanichakoon, W. 2009, 'Effect of preparation variables on morphology and anatase–brookite phase transition in sonication assisted hydrothermal reaction for synthesis of titanate nanostructures', *Materials Chemistry and Physics*, vol. 118, no. 1, pp. 254-8.

Viriya-Empikul, N., Sano, N., Charinpanitkul, T., Kikuchi, T. & Tanthapanichakoon, W. 2008, 'A step towards length control of titanate nanotubes using hydrothermal reaction with sonication pretreatment', *Nanotechnology*, vol. 19, no. 3, p. 035601.

Walling, C. 1975, 'Fenton's reagent revisited', *Accounts of Chemical Research*, vol. 8, no. 4, pp. 125-31.

Wang, B., Shi, Y. & Xue, D. 2007, 'Large aspect ratio titanate nanowire prepared by monodispersed titania submicron sphere via simple wet-chemical reactions', *Journal of Solid State Chemistry*, vol. 180, no. 3, pp. 1028-37.

Wang, B., Xue, D., Shi, Y. & Xue, F. 2008, 'Titania 1D nanostructured materials: synthesis, properties, and applications', *Nanorods, Nanotubes and Nanomaterials Research Progress*, pp. 163-201.

Wang, L., Yang, L., Li, Y., Zhang, Y., Ma, X. & Ye, Z. 2010, 'Study on adsorption mechanism of Pb (II) and Cu (II) in aqueous solution using PS-EDTA resin', *Chemical Engineering Journal*, vol. 163, no. 3, pp. 364-72.

Wang, X., Chen, X., Yoon, K., Fang, D., Hsiao, B.S. & Chu, B. 2005, 'High flux filtration medium based on nanofibrous substrate with hydrophilic nanocomposite coating', *Environmental science & technology*, vol. 39, no. 19, pp. 7684-91.

Wang, X., Zhang, K., Yang, Y., Wang, L., Zhou, Z., Zhu, M., Hsiao, B.S. & Chu, B. 2010, 'Development of hydrophilic barrier layer on nanofibrous substrate as composite membrane via a facile route', *Journal of Membrane Science*, vol. 356, no. 1, pp. 110-6.

Wang, Y. & Hong, C.-S. 2000, 'TiO_2-mediated photomineralization of 2-chlorobiphenyl: the role of O_2', *Water research*, vol. 34, no. 10, pp. 2791-7.

Wang, Y., Yu, X. & Sun, D. 2007, 'Synthesis, characterization, and photocatalytic activity of TiO_2 N_x nanocatalyst', *Journal of hazardous materials*, vol. 144, no. 1, pp. 328-33.

Watson, S., Scott, J., Beydoun, D. & Amal, R. 2005, 'Studies on the preparation of magnetic photocatalysts', *Journal of Nanoparticle Research*, vol. 7, pp. 691-705.

Wei, X., Kong, X., Wang, S., Xiang, H., Wang, J. & Chen, J. 2013, 'Removal of Heavy Metals from Electroplating Wastewater by Thin-Film Composite Nanofiltration Hollow-Fiber Membranes', *Industrial & Engineering Chemistry Research*, vol. 52, no. 49, pp. 17583-90.

Weng, C.-H. & Huang, C. 2004, 'Adsorption characteristics of Zn (II) from dilute aqueous solution by fly ash', *Colloids and Surfaces A: Physicochemical and Engineering Aspects*, vol. 247, no. 1, pp. 137-43.

Weng, L.-Q., Song, S.-H., Hodgson, S., Baker, A. & Yu, J. 2006, 'Synthesis and characterisation of nanotubular titanates and titania', *Journal of the European Ceramic Society*, vol. 26, no. 8, pp. 1405-9.

Wong, C.L., Tan, Y.N. & Mohamed, A.R. 2011, 'A review on the formation of titania nanotube photocatalysts by hydrothermal treatment', *Journal of Environmental Management*, vol. 92, no. 7, pp. 1669-80.

Wong, K., Lee, C., Low, K. & Haron, M. 2003, 'Removal of Cu and Pb by tartaric acid modified rice husk from aqueous solutions', *Chemosphere*, vol. 50, no. 1, pp. 23-8.

Wu, X., Jiang, Q.-Z., Ma, Z.-F., Fu, M. & Shangguan, W.-F. 2005, 'Synthesis of titania nanotubes by microwave irradiation', *Solid State Communications*, vol. 136, no. 9–10, pp. 513-7.

Xiao, Y., Wu, J., Yue, G., Xie, G., Lin, J. & Huang, M. 2010, 'The preparation of titania nanotubes and its application in flexible dye-sensitized solar cells', *Electrochimica Acta*, vol. 55, no. 15, pp. 4573-8.

Xiong, C., Kim, M.J. & Balkus, K.J. 2006, 'TiO2 nanofibers and core–shell structures prepared using mesoporous molecular sieves as templates', *Small*, vol. 2, no. 1, pp. 52-5.

Xiong, L., Chen, C., Chen, Q. & Ni, J. 2011, 'Adsorption of Pb (II) and Cd (II) from aqueous solutions using titanate nanotubes prepared via hydrothermal method', *Journal of Hazardous Materials*, vol. 189, no. 3, pp. 741-8.

Xu, D., Tan, X., Chen, C. & Wang, X. 2008, 'Removal of Pb (II) from aqueous solution by oxidized multiwalled carbon nanotubes', *Journal of Hazardous Materials*, vol. 154, no. 1, pp. 407-16.

Yada, M., Goto, Y., Uota, M., Torikai, T. & Watari, T. 2006, 'Layered sodium titanate nanofiber and microsphere synthesized from peroxotitanic acid solution', *Journal of the European Ceramic Society*, vol. 26, no. 4, pp. 673-8.

Yada, M., Inoue, Y., Uota, M., Torikai, T., Watari, T., Noda, I. & Hotokebuchi, T. 2008, 'Formation of sodium titanate nanotube films by hydrothermal transcription', *Chemistry of Materials*, vol. 20, no. 2, pp. 364-6.

Yan, J. & Zhou, F. 2011, 'TiO_2 nanotubes: structure optimization for solar cells', *Journal of Materials Chemistry*, vol. 21, no. 26, pp. 9406-18.

Yang, J., Jin, Z., Wang, X., Li, W., Zhang, J., Zhang, S., Guo, X. & Zhang, Z. 2003, 'Study on composition, structure and formation process of nanotube Na2Ti2O4(OH)2', *Dalton Transactions*, vol. 0, no. 20, pp. 3898-901.

Yang, K., Lin, D. & Xing, B. 2009, 'Interactions of humic acid with nanosized inorganic oxides', *Langmuir*, vol. 25, no. 6, pp. 3571-6.

Yang, Q.W., Shu, W.S., Qiu, J.W., Wang, H.B. & Lan, C.Y. 2004, 'Lead in paddy soils and rice plants and its potential health risk around Lechang Lead/Zinc Mine, Guangdong, China', *Environment International*, vol. 30, no. 7, pp. 883-9.

Yean, S., Cong, L., Yavuz, C., Mayo, J., Yu, W., Kan, A., Colvin, V. & Tomson, M. 2005, 'Effect of magnetite particle size on adsorption and desorption of arsenite and arsenate', *Journal of Materials Research*, vol. 20, no. 12, pp. 3255-64.

Ylhäinen, E.K., Nunes, M.R., Silvestre, A.J. & Monteiro, O.C. 2012, 'Synthesis of titanate nanostructures using amorphous precursor material and their adsorption/photocatalytic properties', *Journal of Materials Science*, vol. 47, no. 10, pp. 4305-12.

Yoshimura, M. & Byrappa, K. 2008, 'Hydrothermal processing of materials: past, present and future', *Journal of Materials Science*, vol. 43, no. 7, pp. 2085-103.

Yuan, Z.Y. & Su, B.L. 2004, 'Titanium oxide nanotubes, nanofibers and nanowires', *Colloids and Surfaces A: Physicochemical and Engineering Aspects*, vol. 241, no. 1, pp. 173-83.

Yuan, Z.Y., Zhang, X.B. & Su, B.L. 2004, 'Moderate hydrothermal synthesis of potassium titanate nanowires', *Applied Physics A: Materials Science & Processing*, vol. 78, no. 7, pp. 1063-6.

Zaremba, T. & Witkowska, D. 2010, 'Methods of manufacturing of potassium titanate fibres and whiskers. A review', *Materials Science-Poland*, vol. 28, no. 1, pp. 25-41.

Zaviska, F., Drogui, P., Mercier, G. & Blais, J.-F. 2009, 'Procédés d'oxydation avancée dans le traitement des eaux et des effluents industriels: Application à la dégradation des polluants réfractaires', *Revue des sciences de l'eau/Journal of Water Science*, vol. 22, no. 4, pp. 535-64.

Zhang, L. & Fang, M. 2010, 'Nanomaterials in pollution trace detection and environmental improvement', *Nano Today*, vol. 5, no. 2, pp. 128-42.

Zhang, Q., Du, Q., Hua, M., Jiao, T., Gao, F. & Pan, B. 2013, 'Sorption enhancement of lead ions from water by surface charged polystyrene-supported nano-zirconium oxide composites', *Environmental science & technology*, vol. 47, no. 12, pp. 6536-44.

Zhang, S., Niu, H., Hu, Z., Cai, Y. & Shi, Y. 2010, 'Preparation of carbon coated Fe< sub> 3</sub> O< sub> 4</sub> nanoparticles and their application for solid-phase extraction of polycyclic aromatic hydrocarbons from environmental water samples', *Journal of Chromatography A*, vol. 1217, no. 29, pp. 4757-64.

Zhang, T., Horikoshi, S., Hidaka, H., Zhao, J. & Serpone, N. 2002, 'Photocatalyzed N-demethylation and degradation of methylene blue in titania dispersions exposed to concentrated sunlight', *Solar energy materials and solar cells*, vol. 73, no. 3, pp. 287-303.

Zhang, Z., Hong, H., Zhou, J., Huang, J. & Yu, G. 2003, 'Fate and assessment of persistent organic pollutants in water and sediment from Minjiang River Estuary, Southeast China', *Chemosphere*, vol. 52, no. 9, pp. 1423-30.

Zhong, L.S., Hu, J.S., Liang, H.P., Cao, A.M., Song, W.G. & Wan, L.J. 2006, 'Self-Assembled 3D flowerlike iron oxide nanostructures and their application in water treatment', *Advanced Materials*, vol. 18, no. 18, pp. 2426-31.

Zhou, M., Yu, J., Liu, S., Zhai, P. & Huang, B. 2009, 'Spray-hydrolytic synthesis of highly photoactive mesoporous anatase nanospheres for the photocatalytic degradation of toluene in air', *Applied Catalysis B: Environmental*, vol. 89, no. 1, pp. 160-6.

Zhu, Y., Li, H., Koltypin, Y., Hacohen, Y.R. & Gedanken, A. 2001, 'Sonochemical synthesis of titania whiskers and nanotubes', *Chemical Communications*, no. 24, pp. 2616-7.

Zhu, Y., Wang, D., Jiang, L. & Jin, J. 2014, 'Recent progress in developing advanced membranes for emulsified oil/water separation', *NPG Asia Materials*, vol. 6, no. 5, p. e101.

Zhuang, G.S., Sui, G.X., Meng, H., Sun, Z.S. & Yang, R. 2007, 'Mechanical properties of potassium titanate whiskers reinforced poly(ether ether ketone) composites using different compounding processes', *Composites Science and Technology*, vol. 67, no. 6, pp. 1172-81.